Biomimetic Modeling of Superoxide Reductase

Terutaka Terence Kitagawa

A dissertation
submitted in partial fulfillment of the
requirements for the degree of:

Doctor of Philosophy

University of Washington

2007

Program Authorized to Offer Degree: Department of Chemistry

University of Washington
Graduate School

This is to certify that I have examined this copy of a doctoral dissertation by

Terutaka Terence Kitagawa

and have found that it is complete and satisfactory in all respects,
and that any and all revisions required by the final
examining committee have been made.

Chair of the Supervisory Committee:

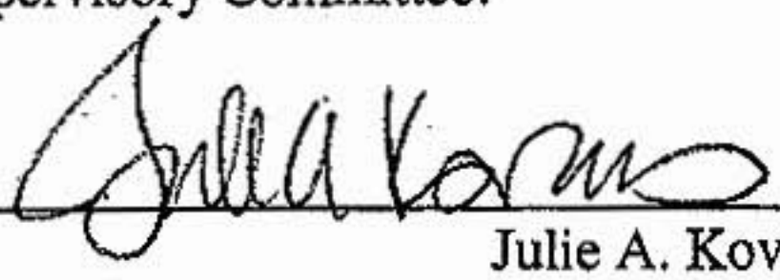

Julie A. Kovacs

Reading Committee:

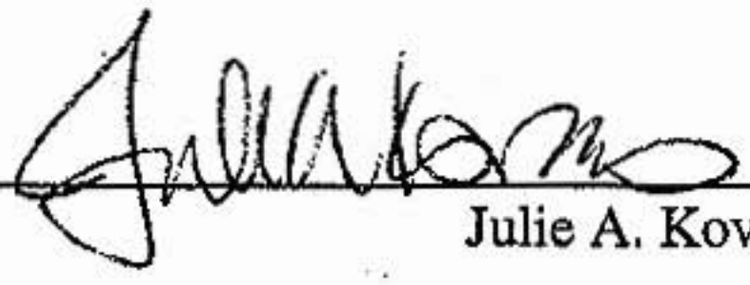

Julie A. Kovacs

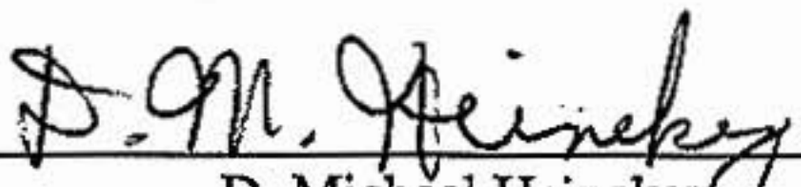

D. Michael Heinekey

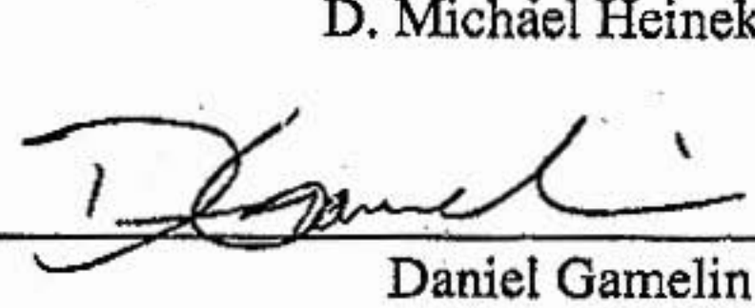

Daniel Gamelin

Date: 7/17/07

In presenting this dissertation in partial fulfillment of the requirements for the doctoral degree at the University of Washington, I agree that the Library shall make its copies freely available for inspection. I further agree that extensive copying of the dissertation is allowable only for scholarly purposes, consistent with "fair use" as prescribed in the U.S. Copyright Law. Requests for copying or reproduction of this dissertation may be referred to ProQuest Information and Learning, 300 North Zeeb Road, Ann Arbor, MI 48106-1346, 1-800-521-0600, to whom the author has granted "the right to reproduce and sell (a) copies of the manuscript in microform and/or (b) printed copies of the manuscript made from microform."

Signature 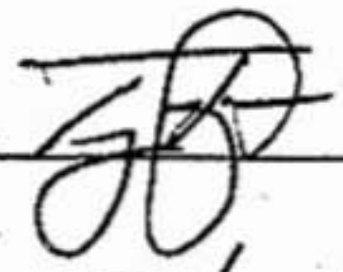

Date 07/17/2007

University of Washington

Abstract

Biomimetic Modeling of Superoxide Reductase

Terutaka Terence Kitagawa

Chairperson of the Supervisory Committee:
Professor Julie A. Kovacs
Department of Chemistry

Dioxygen is a thermodynamically superior oxidant, with the ability to be reduced to water by a four-electron reduction. During this process, toxic reactive oxygen species (ROS) are also generated. Nature uses metalloenzymes to combat this form of oxidative stress. Of particular interest to us is superoxide reductase (SOR). SOR is a non-heme thiolate-ligated metalloenzyme, consisting of a ferrous center ligated by four histidines and a cysteinate residue. It is responsible for superoxide detoxification in anaerobic and microaerophilic organisms by reducing superoxide to H_2O_2.

A novel biomimetic model of the active site of SOR, **$[Fe^{II}$cyclam-PrS$]^+$** is described in Chapter 1. This complex reacts with superoxide under protic conditions at cryogenic temperatures to form **$[Fe^{III}$cyclam-PrS(OOH)$]^+$.** This is a rare example of a high-spin Fe^{III}-OOH species, and the first reported example of a high-spin non-heme Fe^{III}-OOH containing a *trans* thiolate. The addition of acetic acid forms the acetate-bound **$[Fe^{III}$cyclam-PrS(OAc)$]^+$,** a model of the Fe^{III} resting state of SOR. The addition of cobaltocene regenerates the Fe^{II} species, completing the catalytic reduction of superoxide to hydrogen peroxide.

$[Fe^{II}(N^{Et2})N_4(tren)Cl]^+$, a synthetic analogue of $[Fe^{II}N_4(tren)S^{Me2}]^+$, is described (*vide infra*). $[Fe^{II}(N^{Et2})N_4(tren)Cl]^+$ replaces the apical thiolate ligand found in $[Fe^{II}N_4(tren)S^{Me2}]^+$ with a nitrogen. To our knowledge this is the first known aliphatic Fe-N5 complex. $[Fe^{II}(N^{Et2})N_4(tren)Cl]^+$ is a six-coordinate Fe^{II} species, lacking an open site for substrate coordination. This and other changes in the structural and electronic factors induced by the removal of the thiolate moiety most likely plays a key role in impeding this Fe^{II} center from performing superoxide reduction.

$[Fe^{II}N_4(tren)S^{Me2}]^+$ reacts with KO_2 under protic conditions, forming a metastable Fe^{III}-OOH species. $[Fe^{II}N_4(tren)S^{Me2}]^+$ also reacts with dioxygen to form $[Fe^{III}S^{Me2}N_4(tren)]_2\mu\text{-}O^{2+}$, an inert μ-oxo dimer. In an effort to stabilize this Fe^{III}-OOH species and prevent μ-oxo dimer formation, $[Fe^{II}S^{Me2}N_4(bdpa)]^+$ and $[Fe^{II}S^{Me2}N_4(bdea)]^+$ are described. These species use alkylated derivatives of tren containing no protons within the primary coordination sphere of the Fe^{II} complex. The preliminary characterization and reactivity studies with these complexes are described in this dissertation.

Table of Contents

List of Figures

List of Tables

Acknowledgements

My life has been atypical to say the least, and I must admit that I never expected to be here, writing acknowledgements to my dissertation. In retrospect, while I am extremely proud of my accomplishments in graduate school, I could not have been in this position without my family, friends, advisors and coworkers, who have all helped to mold me into the individual that I am today.

First and foremost, I would like to thank my research advisor, Julie Kovacs. I cannot express my gratitude to Julie for everything that she has done for me. My inception to graduate school was very tumultuous, and often I wondered if I had made the correct choice in my life. Julie never stopped believing in me, and was always my major support in graduate school. The lessons that Julie has taught me about science and about becoming a better person are invaluable, and I will always be indebted to her for believing in me.

I would like to also thank my undergraduate research advisor, Mahdi Abu-Omar. My professors (Dr. Gamelin, Dr. Heinekey, Dr. Goldberg, Dr. Mayer, Dr. Sasaki) have provided me with an incomparable learning experience. I also wish to thank the Kovacs group and coworkers from within the department. Namely, I would like to thank Brian Smart and Priscilla Lugo-Mas, two friends who I am eternally grateful for meeting. I could not have accomplished the the things that I have without your support and guidance.

Finally, I would like to thank my family and friends for their undying support and love, especially my father Taka and brother Norton. Somehow, someway, we have made it this far, and now life truly begins!

DEDICATION

To my mother, Yoko Kitagawa.

Chapter 1
Introduction.

Background. The advent of oxygen into the earth's atmosphere completely altered the environment for all living beings, by completely transforming it from a reducing to an oxidizing atmosphere.[1] Oxygen immediately provided benefits to living organisms, as it allowed them to increase the energy it could obtain from foodstuffs, enabled complex bio-transformations to be carried out with ease, and made possible the generation of heat and light. Oxygen unequivocally changed the evolutionary process of living beings on earth by changing selection rules and pressures. It is technically a radical species, having two electrons that are not spin-paired. This unique electronic characteristic caused dioxygen to be a very able oxidant, thermodynamically favored to accept four additional electrons until water is ultimately formed.[1,2]

However, once dioxygen is activated, the byproducts generated along this pathway are extremely reactive and have the potential to cause oxidative injury to an organism.[2] These byproducts include superoxide ($O_2^{\bullet}$), hydrogen peroxide (H_2O_2) and the extremely reactive hydroxyl radical (OH•), collectively known as the reactive oxygen species (ROS).[3] In particular, superoxide has been frequently linked to a number of often fatal disease conditions, namely increased rates of mutagenesis, Parkinson's disease, and heart disease.[4,5] In fact, superoxide is considered to be much more toxic to the health of an organism because although it is not as reactive as the other ROS, it is much more selective in its reactivity.[1-3,6] While the hydroxyl radical is much more promiscuous in attacking substrates, in many cases it often reacts with substrates which are not vital to an

organism's health, immediate or long-term. In any case it will undoubtedly react with something in its near vicinity upon its generation, perhaps something expendable. Because of these factors, understanding the chemistry of superoxide is considered imperative.

In order to combat the toxic threat of the ROS, living organisms developed enzymatic defense systems.[7] In particular, non-heme iron-containing enzymes are largely responsible for the detoxification of the ROS. Living organisms have selected iron to carry out many complex biological processes, largely because the redox potential of the Fe^{2+}/Fe^{3+} couple can easily and meticulously be tuned by simple modification of its ligand system.[8] In fact, iron is the most abundant transition metal in the human body, playing major roles in oxygen transfer and electron transport.[2,9] To date, the most described and understood enzyme for superoxide detoxification is the non-heme iron enzyme superoxide dismutase (SOD).[10,11] This enzyme is responsible for the disproportionation of superoxide to dioxygen and hydrogen peroxide via redox catalysis in *aerobic* organisms. **(Figure 1.01-a)** While H_2O_2 is a ROS and is capable of performing considerable oxidative damage, many enzymes called peroxidases exist that easily reduce hydrogen peroxide to water.[12,13]

More recently, it has been shown that another non-heme iron enzyme, superoxide reductase (SOR), is responsible for superoxide detoxification in microaerophilic and anaerobic organisms.[14-16] SOR reduces toxic superoxide radicals to hydrogen peroxide without the evolution of dioxygen, thus differentiating its function from SOD. **(Figure**

1.01-b) This unique capability of SOR makes it invaluable to the health of the anaerobic organism, which is not equipped to handle life under an oxidative atmosphere.

(a) $2O_2^- + 2H^+ \xrightleftharpoons{\textbf{SOD}} H_2O_2 + O_2$

(b) $2H^+ + e^- + O_2^- \xrightleftharpoons{\textbf{SOR}} H_2O_2$

Figure 1.01. The superoxide detoxification reactions of SOD **(a)** and SOR **(b)**.

SOR is part of a unique family of non-heme cysteinate-ligated iron enzymes. The active site of SOR has been characterized in both the "active" ferrous and "resting" ferric forms by x-ray crystallography.[15,17] So far there have been five crystal structures of SOR reported in the literature.[18-21] Each of the known species of SOR have a ferrous active site share a common N_4S active site identity, in which a ferrous center is ligated by four equatorial histidine residues and an apical cysteine residue, which is positioned *trans* to an open coordination site. This site is commonly referred to as Center II.[16,22,23] In the "resting" ferric state, the open site is occupied by a glutamate (^{47}Glu) residue. The structures of the ferrous and ferric active sites of SOR are shown in **Figure 1.02.**

In some species of SOR, a second iron center is present.[24,25] This iron center is commonly referred to as Center I, and the SOR species that it is present in are referred to as 2Fe-SOR. Center I has been characterized by x-ray crystallography as being a ferric center ligated by four cysteinate residues in a tetrahedral coordination geometry. There is a level of uncertainty that still surrounds the exact purpose of Center I. It has been

proposed to help maintain the structural integrity of Center II. It has also been suggested to play a role in electron transfer to the active site, providing the necessary electron for superoxide reduction. However, it has been recently shown in mutation studies by Kurtz and coworkers that the removal of this second Fe-center from wild-type SOR does not affect the ability of the enzyme to perform superoxide reduction.[26]

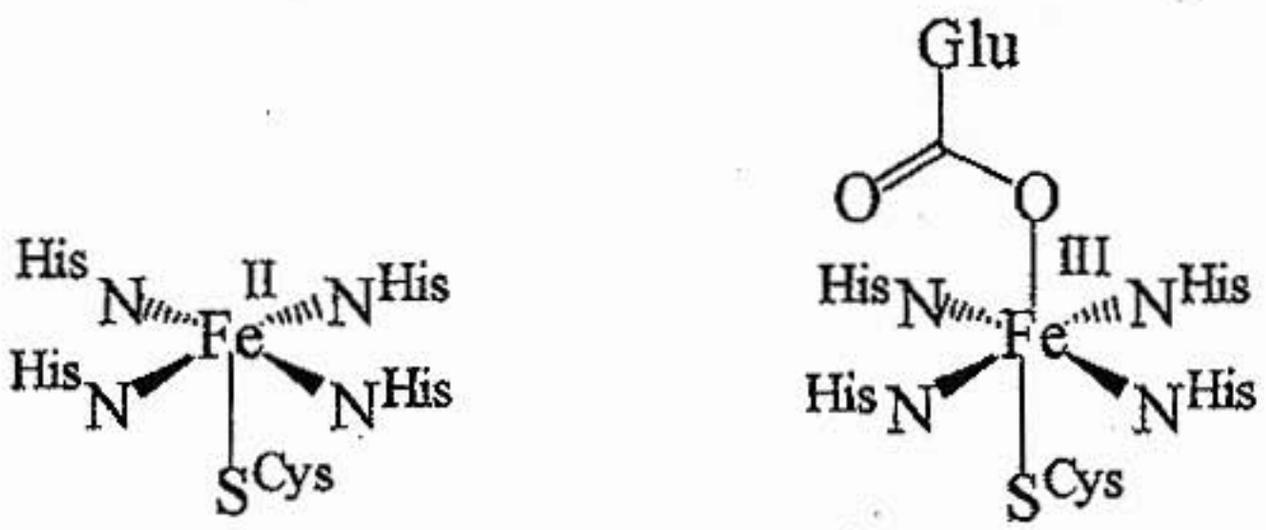

Figure 1.02. The structures of the Fe^{II} and Fe^{III} forms of the active site of SOR.

While the catalytic process of superoxide reduction by SOR has not been definitively elucidated, until recently a three step mechanism had been accepted as a general description of the catalytic process of SOR (**Figure 1.03**).[27] It has been accepted at this point that the chemistry of SOR requires two protons and an electron to complete the reduction of superoxide to H_2O_2. In this mechanism, binding of superoxide to the "active" ferrous form of SOR is naturally believed to occur at the open site *trans* to the cysteinate sulfur ligand. This is because the open site is not occupied with solvent, although the site is located at the surface of the protein, fully exposed to solvent. The "active" species reacts with superoxide in the presence of protons to form a putative ferric-(hydro)peroxo species, characterized by an intense absorption band at 590-600nm

($\varepsilon \approx 3500\ M^{-1}cm^{-1}$).[28] The origin of this intense absorption is believed to be mostly of π-type cysteinate-S^- → Fe^{III} character. The formation of this species is fast, occurring at almost diffusion-controlled rates. The addition of a second proton leads to the release of H_2O_2, causing the decomposition of the transient intermediate. Another non-heme iron-containing protein called rubrerythrin that is specific to anaerobes has been shown to have NADH-dependent peroxidase activity, which can assist the cell in removing H_2O_2 before it can aggregate to toxic levels.[29]

This process is very fast as well, and is believed to be a first order process that occurs at a rate of 40-50 s^{-1}.[28] A nearby glutamate residue then binds to the same site to form the "resting" form of the active site, which is a glutamate-bound, six-coordinate ferric complex. The absorption band at 590-600nm is also replaced by a new, less intense band at 645nm ($\varepsilon = 2000\ M^{-1}cm^{-1}$), representing a considerable red-shift in the charge transition band. Like the transient ferric-peroxo species, this band is also composed of be mostly of π-type cysteinate-S^- → Fe^{III} character. To complete the catalytic cycle of superoxide reduction, the ferric "resting" species is reduced by an electron donor, releasing the glutamate residue and regenerating the "active" species of SOR.

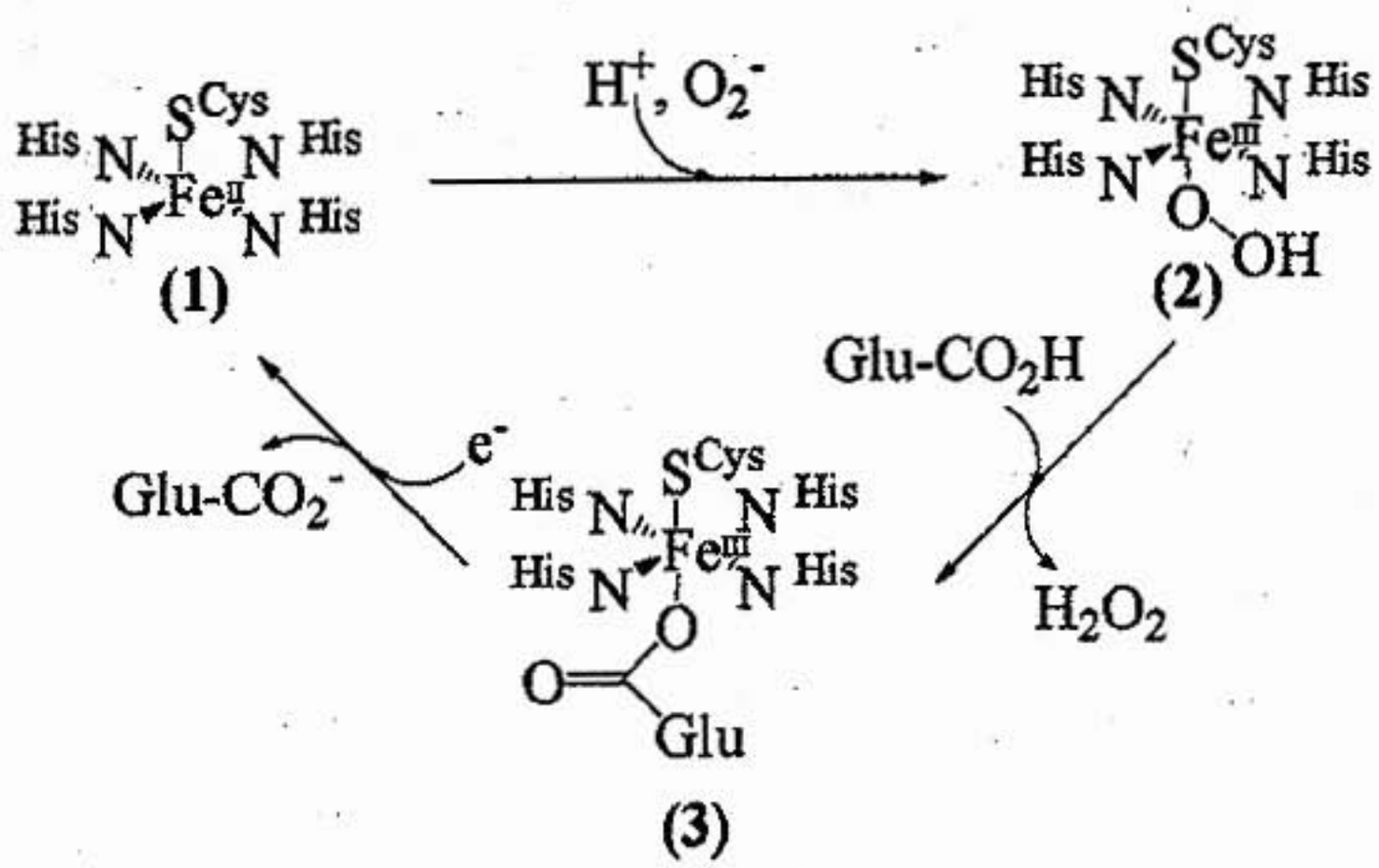

Figure 1.03. A proposed three step catalytic mechanism of superoxide reduction by SOR.

Recently the presence of a second intermediate has been proposed.[30] The two-intermediate system was initially believed to consist of a deprotonated end-on peroxo moiety and a protonated hydroperoxo moiety. However, more recently a Fe^{III}-OH species has been observed, leading to a newly proposed mechanism of SOR.[31] In this paper, the formation of a second intermediate is seen, albeit very slowly, and is characterized by resonance Raman experiments as having a pH-dependent Fe-O stretching frequency. This stretch is also isotopically-sensitive, determined from labeling experiments using H_2O and $H_2{}^{18}O$ as the solvent. The data is consistent with the formation of a Fe^{3+}-hydroxide species. The formation of this species is shown in **Figure 1.04**, which depicts solvent (water) as the second proton source, leading to the release of hydrogen peroxide and the binding of hydroxide ion.

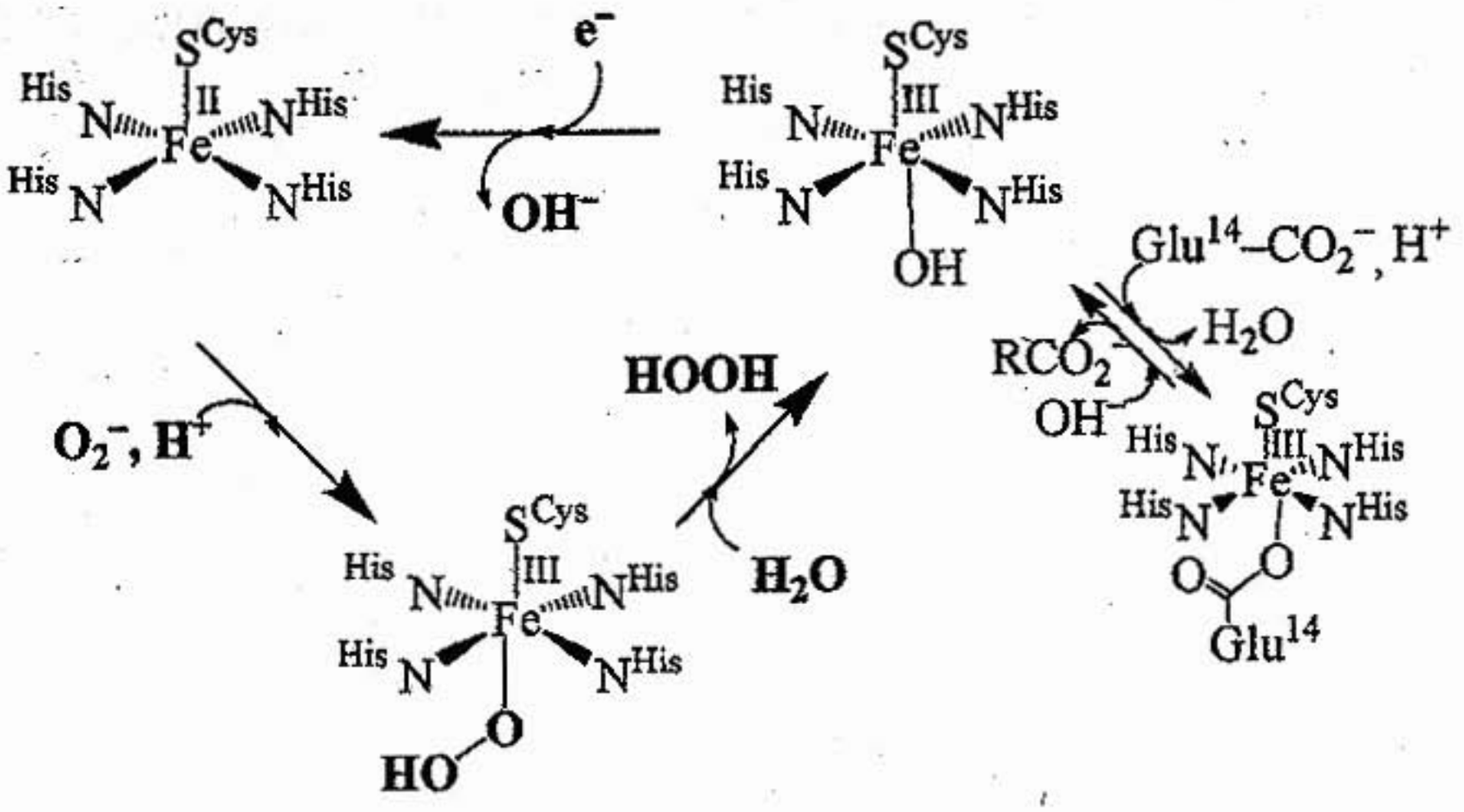

Figure 1.04. The newly proposed SOR catalytic cycle by Niviére.[30]

The use of exogenous ligands such as azide (N_3^-), cyanide (CN-) and nitric oxide (NO) to probe the SOR binding site has been reported by Johnson et al.[32,33] Johnson has shown that SOR retains its high-spin (S=5/2) state with the binding of N_3^- and NO, but becomes low-spin (S=1/2) with the binding of CN^-. In addition, it was found that CN^- inhibits SOR, while N_3^- and NO do not. These crystal structures have been reported. The data obtained from the crystal structures implies that SOR undergoes an inner-sphere electron-transfer mechanism during superoxide reduction.

The unknowns of SOR. Many unknowns still shroud the mechanism SOR catalysis, and much work needs to be done in order to understand the chemistry of SOR catalysis. For example, SOR has been shown to require two protons and one electron to perform its chemistry, yet the source of each have yet to be unambiguously identified. As stated

earlier, it is believed that the first proton is obtained from solvent, since the active site sits on the edge of the proton, fully exposed to solvent. Identifying the second proton source has been especially elusive. A highly conserved lysine residue (^{47}Lys) near the active site of all known SORs has been proposed to play some role in the second protonation step, either as a proton source or in a director role, guiding the second proton from solvent or another proton source to the active site.[19,20] Mutation studies have shown that removing this ^{47}Lys residue from the active site results in a significant loss of enzyme activity.[22]

Second, the identification of the electron donor for SOR catalysis has been proposed to be rubredoxin, a small iron-containing protein. Reduced rubredoxin (Rd) is believed to be most likely responsible for providing electrons to SOR for the reduction of superoxide to H_2O_2.[12]. Additionally, rubredoxin has been shown by Adams and coworkers to be reduced by NAD(P)H:rubredoxin oxidoreductase (NROR), another nearby protein, during times of oxidative stress. *In vitro* studies using recombinant forms of the SOR from *P. furiosus* showed that SOR, Rd and NROR must be present for SOR catalysis to occur enzymatically.[34]

Third, the role of the glutamate residue has yet to be determined. The studies by Niviére also helped to provide insight into the role of the glutamate residue as the sixth ligand of the "resting" ferric form of SOR. Research by Cabelli and coworkers studied the effects of replacing the glutamate residue (E12) of the neelaredoxin of *Archaeoglobus fulgidus* with the neutral glutamine (E12Q) or the non-coordinating valine (E12V) residues.[15] These mutated SORs were chosen to assess the effect of the bound sixth ligand (glutamate) to the ferric center of SOR. More specifically, they were chosen to

study the influence of the negative charge of glutamate, and also to test for the capacity of the glutamate residue to form H-bonds with solvent or the protein. Both mutations led to a decrease in SOR activity and increases in SOD activity of 29% and 47%, respectively. This study showed that the negatively charged ^{47}Glu residue plays an important role in directing the chemistry of SOR.

Fourth, the identity of the transient intermediate **(2)** in **Figure 1.03** is still a subject of contention. Also, the binding mode of the peroxo moiety has also been yet to be determined. A mutation study of SOR was reported by Niviére and coworkers where the ^{47}Glu residue was replaced by a non-coordinating alanine residue in order to stabilize the transient intermediate by preventing binding/displacement of the peroxo moiety by the glutamate residue.[35] When H_2O_2 was added to this mutant, resonance Raman studies identified the resulting intermediate as an iron-peroxo species. Based on the available vibrational data obtained from biomimetic N-ligated non-heme iron peroxo species, this intermediate was assigned as a side-on η^2-peroxo species. However, such a seven-coordinate side-on peroxo species was predicted to be much less stable then an end-on (hydro)peroxo species, based on DFT calculations done by Kurtz and coworkers.[24,36] Kurtz and coworkers have suggested that the peroxo moiety actually coordinates to the ferric center in a bent, end-on geometry.

Comparison with Cytochrome P450. The active site of SOR and the more well-known enzyme cytochrome P450 are strikingly similar. SOR shares the same square pyramidal

structure as cytochrome P450, with the same N_4S primary coordination environment, albeit with histidine residues in lieu of the porphyrin moiety **(Figure 1.05).**

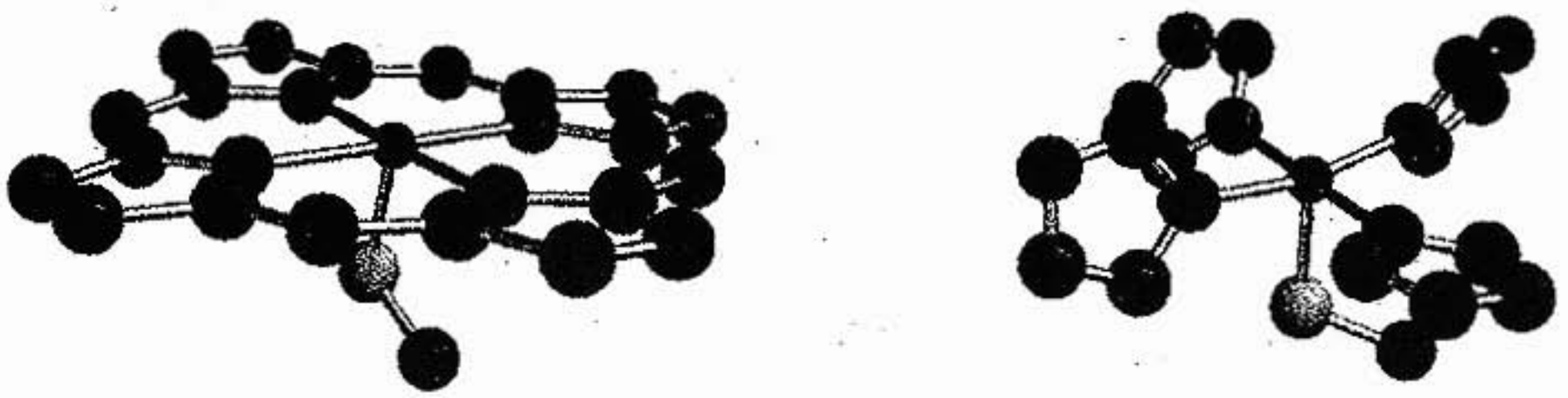

Cytochrome P450 **SOR**

Figure 1.05. The active sites of SOR and cytochrome P450.

Interestingly, SOR cleaves the Fe-O bond of its Fe^{III}-OOH intermediate to release H_2O_2, rather than cleaving the O-O bond like cytochrome P450. The main reason for the difference in the chemistry that the two enzymes perform is believed to be that the site of protonation of the second proton in the SOR catalytic cycle is at the proximal oxygen, as opposed to the distal oxygen in cytochrome P450 chemistry. This would weaken the Fe-O bond instead of the O-O bond of the peroxo species. If the O-O bond cleaved, water would be released and the Fe center would form a high-valent Fe^{IV}=O or Fe^{V}=O species, commonly referred to as Compound I.[37] SOR instead cleaves the Fe-O bond, releases H_2O_2 and forms the six-coordinate ferric "resting" species. This disparity in behavior can be explained in a couple of ways. First of all, the dinegatively-charged porphyrin ring has a highly conjugated structure that is very capable of delocalizing large amounts of positive charge, which makes it very capable of supporting the higher valent Fe^{IV}=O or Fe^{V}=O species. In contrast, the histidine ligands of SOR are not as capable as their

porphyrin counterpart at compensating for higher valent states of the iron center. SOR was therefore thought to be less likely to allow the iron center to access higher oxidation states than the ferric state. However, recently Que and coworkers described the first crystallographic characterization of a non-heme Fe^{IV}-oxo species, proving that a heme environment was not requisite to access higher oxidation states of iron.[38]

Secondly, while both enzymes are believed to go through a Fe^{III}-peroxo intermediate state, the peroxo-intermediate of cytochrome P450 has a low-spin (S=1/2) spin state, while that of SOR is believed to be a high-spin (S=5/2) species. Based on the predicted occupation of the bonding and antibonding orbital sets of Fe, it is apparent that a low-spin state of the iron center of cytochrome P450 would promote a strong Fe-O bond and a weakening of the O-O bond, favoring O-O bond cleavage. In contrast the Fe-O bond of the high-spin Fe-peroxo intermediate would have a weaker Fe-O bond and a stronger O-O bond, which in turn would favor Fe-O bond cleavage and liberation of H_2O_2.

DFT calculations and synthetic modeling of the active site of SOR has suggested that a low-spin Fe-peroxo intermediate is a possible identity for the transient intermediate observed during the catalytic process.[36,39] These descriptions of the differences in P450 and SOR chemistry are only simple explanations proposed to help to explain the differing behaviors of both enzymes. Obviously much work remains and thus one should be reticent when tempted to accept these explanations of the differing chemistries of cytochrome P450 and SOR as indisputable fact.

Biomimetic modeling. While biochemistry has helped to address the many unknowns that still surround the physical and mechanistic characteristics of this unique enzyme, techniques in this field have many limitations that either prevent or hinder the ability of the researcher to address certain issues regarding SOR. The fundamental obstacle to the direct characterization of reactive intermediates is that the kinetics of intermediate formation do not favor the aggregation of the transient intermediate species, precluding us from its detailed characterization. For example, the process of superoxide reduction by SOR occurs on an extremely fast kinetic timescale. The formation of the Fe^{III}-peroxo intermediate occurs at diffusion-controlled rates, and the liberation of hydrogen peroxide occurs at an even faster rate.[28] To establish kinetic control over such a fast reaction would naturally require performing the reaction at reduced temperatures, which in turn would require the use of non-aqueous solvent systems. However, enzymes generally are not stable in organic solvents, as their proteins quickly denature under non-aqueous solvent conditions. This is most likely due to the disruption of the H-bonding interaction of the protein backbone. The inability to establish strong kinetic control over the reaction also limits the ability of the researcher to identify transient intermediate(s) that occur during the course of the reaction. Biomimetic chemistry helps to address these issues by using small molecule mimics of the active site and its primary coordination sphere. This approach allows the researcher to study the chemistry at the active site in a much simpler manner in non-aqueous solvents, *sans* the complexities described above. Key relationships between structure, electronic character and function of metalloenzyme sites can also be more readily studied by using this approach.

Current research in biomimetic modeling. Synthetic biomimetic modeling has been used extensively in studies of non-heme metalloenzymes and also in studying the synthetic anticancer reagent bleomycin.[40] Que, Girerd, McKenzie and others have comprehensively characterized various series of nitrogen-ligated iron-peroxo complexes.[41,42] The work of these groups provided the most complete set of vibrational and spectroscopic data of synthetic non-heme iron-peroxo complexes. The spectral and vibrational data from these scientists were paramount to the interpretation of biophysical metalloenzyme data. However until recently there has been a paucity of thiolate-ligated non-heme iron model complexes to facilitate an understanding of how thiolates influence enzymatic function. The difficulties of working with thiolates in metal chemistry, such as its thermodynamic ease to be oxidized to inert disulfides or sulfenato-/sulfinato species, its propensity to reduce metals and to oligomerize make their synthesis non-trivial. Although thiolate-ligated non-heme iron complexes have been reported[38,43-48], there is still a dearth of data regarding how thiolate ligation affects iron's reactivity and its role in metalloenzymes. It should be pointed out to the reader that the majority of these complexes display limited or no reactivity with dioxygen or the ROS, and none are considered to be truly biomimetic.

Synthetic modeling of the active site of SOR. Our aspiration to synthesize a biomimetic SOR model complex stemmed from a desire to understand the larger picture, i.e. how the *trans* positioning of the thiolate affects the iron center reaction chemistry, and to understand the structural similarities and reactivity differences with respect to

cytochrome P450, etc. In order to synthesize a biomimetic SOR model complex, a "checklist" of characteristics of the desired complex was created. First of all, the complex needed to have an N_4S ligand environment, be five-coordinate, and with an open site to bind substrate. The thiolate moiety must also be tethered to the ligand system in order to control its promiscuous tendency to react with other metal centers, and prevent it from de-coordinating. Prior work by our group demonstrated this requirement.[45,46] Second, any SOR model complex must have a reversible redox couple between Fe^{2+}/Fe^{3+}. Finally the complex must be mononuclear, as thiolates can tend to bridge metal centers into binuclear complexes.[25]

Despite these challenges, in 2001, Kovacs and coworkers reported the first biomimetic model of SOR, referred to as $[Fe^{II}(S^{Me2}N_4tren)]^+$.[45,46] $[Fe^{II}(S^{Me2}N_4tren)]^+$ contains an N_4S ligand environment like that of the active site of wild-type SOR, but with the thiolate *cis* to the active site instead of *trans*. The structure of this molecule is shown in **Figure 1.06.**

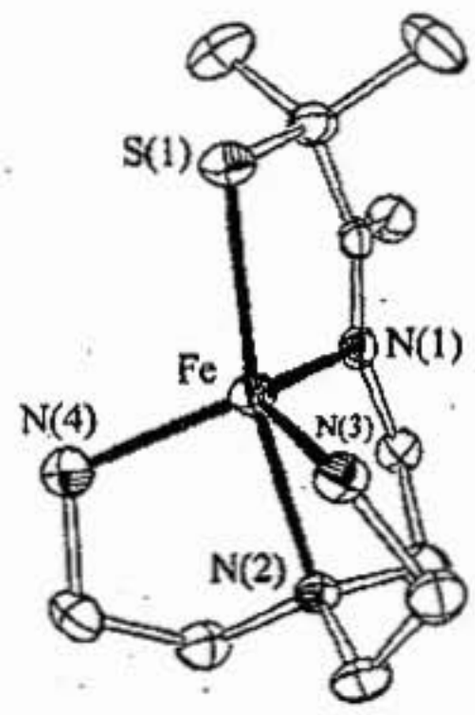

Figure 1.06. The ORTEP of $[Fe^{II}(S^{Me2}N_4tren)]^+$.

Interestingly, even with this altered positioning of the thiolate ligand with respect to the open site on the metal, $[Fe^{II}(S^{Me2}N_4tren)]^+$ was still able to reduce superoxide to hydrogen peroxide in the presence of a proton donor. The addition of superoxide to $[Fe^{II}(S^{Me2}N_4tren)]^+$ in the presence of a proton donor at low temperatures ($T \leq -78^{\circ}C$) caused the formation of a transient orange intermediate, characterized by an intense charge transfer band at 452nm ($\varepsilon = 2900$). This transient species was identified as the low-spin hydroperoxide $[Fe^{III}(S^{Me2}N_4tren)(OOH)]^+$, which was the first example of a thiolate-ligated non-heme Fe-peroxo complex reported in the literature.[45] The addition of acetic acid to this intermediate resulted in the formation of a blue species and a concurrent red shift in the absorption spectrum to afford a new band at λ=565nm (ε = 2900). This species was identified by its x-ray crystal structure as the acetate-bound $[Fe^{III}(S^{Me2}N_4tren)(OAc)]^+$, which is a model for the glutamate-bound resting state species of SOR. The formation of H_2O_2 was also verified using a catalase assay and by ^1H NMR. Finally $[Fe^{II}(S^{Me2}N_4tren)]^+$ was shown to catalytically reduce superoxide to hydrogen peroxide using cobaltocene as a sacrificial electron source.[49] Eight turnovers have been achieved in this fashion.

Remarkably, $[Fe^{II}(S^{Me2}N_4tren)]^+$ shared many similar physical traits with the wild-type SOR enzyme. Not only was $[Fe^{II}(S^{Me2}N_4tren)]^+$ able to reduce superoxide, it could do so catalytically in the presence of a sacrificial electron donor. Also, this reduction of superoxide could only be accomplished in the presence of protons. Under aprotic conditions, no reaction was observed.[50] Kovacs' work with $[Fe^{II}(S^{Me2}N_4tren)]^+$ pioneered the first synthetic analogue of SOR and also showed that the positioning of the

thiolate ligand (cis. vs. trans) did not alter the efficacy of the iron center to perform superoxide reduction. Most importantly, this work laid benchmark parameters for studying thiolate-ligated non-heme iron enzymes, especially for identifying elusive transient peroxo intermediate in SOR, as well as studying the effect of thiolate ligation on metalloenzyme function. Thiolate-ligated $[Fe^{II}(S^{Me2}N_4tren)]^+$ has been shown to activate dioxygen as well, in a rare example of a reversible of μ-oxo dimer formation.[51]

Kovacs' success demonstrated the feasiblity of using biomimetic chemistry identify probable intermediates in the SOR catalytic cycle, and their associated biophysical parameters. Once a stable, biomimetic functional model of SOR was established, other scientists began to work towards a more exacting biomimetic model of SOR, where the thiolate was *trans* to the open site of the iron center, as in wild-type SOR. In 2003 Halfen reported the synthesis of a series of *trans* thiolate-ligated Fe^{II} complexes, ligated by a tetradentate L^8Py_2 non-heme ligand system and various alkyl and aryl thiolates bound to Fe^{II} in an effort to model the structural properties of the active site of SOR.[43] These structures are shown in **Figure 1.07.** However, none of these complexes showed any reactivity with superoxide. The ferric state of these complexes was not readily accessible chemically or electrochemically; in fact only one of the complexes showed reversible electrochemical behavior, and with an extremely cathodic potential ($E_{1/2}$=+470 mV vs. SCE), explaining its robust nature under aerobic conditions. The complexes were accurate structural mimics of SOR but their inability to reduce SOR was disappointing.

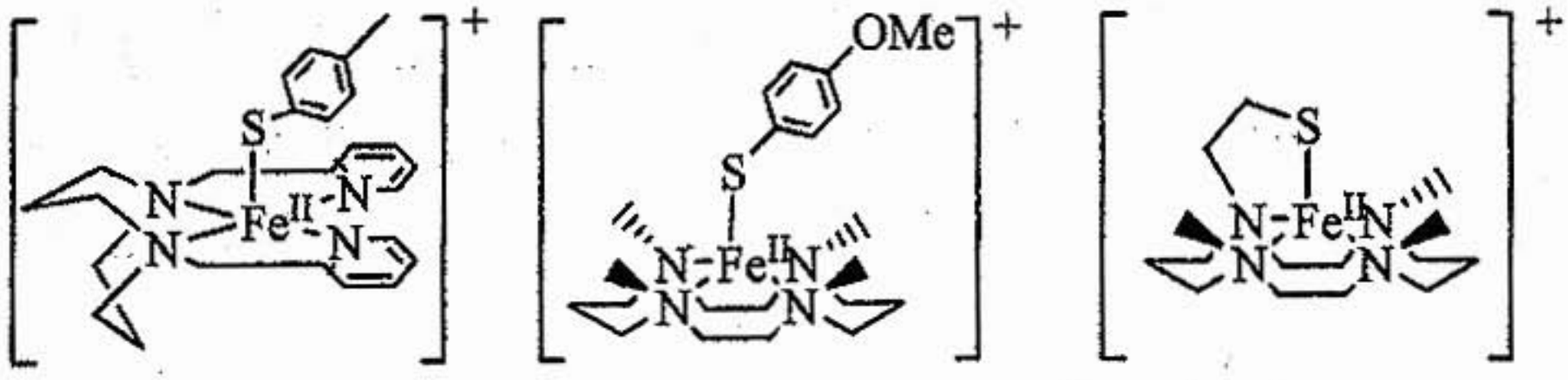

1 **2** **3**

Figure 1.07. Chemdraw structures of Halfen's SOR model complexes. Structure **1** is $[Fe^{II}(L^8Py_2)SPh]^+$, **2** is $[Fe^{II}(TMC)SPhMeO)]^+$, and **3** is $[Fe^{II}(TMCS)]^+$.

Halfen's $[Fe^{II}(L^8Py_2)SPh]^+$ system was found to structurally model the square pyramidal geometry of SOR quite well, due to its constrained nature which effectively kept the nitrogens in the equatorial plane. In 2005, Halfen and Que reported a series of complexes using Halfen's L^8Py_2 ligand system with different axial ligands occupying one of the two open axial sites on the iron center.[52] These ligands included trifluorosulfonate (triflate), benzoate, 4-methylbenzenethiolate, and pyridine N-oxide, and were selected to study the effect of the thiolate and its basicity on the metal ion spin-state, and reactivity. The reaction of these iron complexes with tBuOOH each afforded high-spin alkylperoxoiron(III) transient intermediates, characterized by charge transfer absorption bands from ~500-600nm ($\varepsilon \approx 2000\text{-}2700\ M^{-1}cm^{-1}$). The results were striking; increased basicity of the axial ligand increased the stability of the high-spin Fe-OOR intermediate, which was an effect opposite to that seen for low-spin Fe-OOR intermediates.[53] The thiolate-bound alkylperoxoiron(III) species was the longest-lived peroxo species of the series, and provided the first rationale for the presence of the axial thiolate in SOR.

These results reported by Kovacs, Halfen and Que comprised the first generation of biomimetic SOR analogues. The structural, electronic, vibrational and reactivity data obtained from these studies provided important parameters and helped to provide insight into the questions still surrounding SOR. Simultaneously, the pursuit of the next generation of biomimetic models of SOR had begun, in an effort to design a functional biomimetic model of SOR with a *trans* thiolate.

In 2004, Halfen reported the synthesis of a new ligand system that was derived from the tetraamine 1,4,8,11-tetraazacyclotetradecane, commonly known as cyclam.[54] Specifically, the ligand system contained an ethylene-linked thiolate tethered selectively to the lone secondary amine of trimethylated cyclam. Halfen also presented a crystal structure of $[Ni^{II}(TMCS)]^{+}$, showing the complex adopts a square pyramidal geometry with the thiolate occupying an axial position, mimicking the structure of SOR's active site. The structure of the corresponding Fe^{II} complex is shown in **Figure 1.08** (complex **3**) demonstrating that the thiolate is trans to the open site of the metal center. However, $[Fe^{II}(TMCS)]^{+}$ does not react with superoxide. The inability of this complex to reduce superoxide is explained by its unusually high redox potential ($E_{1/2}$ = +500mV vs. SCE). A transient intermediate assumed to be an Fe-peroxo species was obtained by reacting $[Fe^{II}(TMCS)]^{+}$ with H_2O_2 at low temperatures. Mössbauer spectroscopy later identified this transient species as an Fe^{IV}=O species, the first example of a Fe^{IV}=O species with a thiolate bound to the metal center.[38]

Very recently, Goldberg and Moënne-Loccoz reported an example of a low-spin ferric-alkylperoxo complex obtained by the addition of t-butylhydroperoxide (tBuOOH)

and cumenyl hydroperoxide (CmOOH) to the thiolate-ligated ferrous complex $[Fe^{II}([15]aneN_4)(SPh)]^+$ at low temperatures (-78°C).[39] These complexes are very similar to Halfen's but with a larger 15-member macrocycle. These reactions produced dark red transient intermediates with absorption bands at 526nm ($\varepsilon = 2150\ M^{-1}\ cm^{-1}$) and 527nm ($\varepsilon = 1650\ M^{-1}\ cm^{-1}$) respectively. Both peroxo species exhibited very short lifetimes and began to decompose within t=10 minutes. They were characterized by EPR as being low-spin Fe^{III} complexes, with g=2.20 and g=1.97, respectively. Resonance Raman analysis with a 514nm excitation wavelength showed the O-O and Fe-O stretching frequencies for the Fe^{III}-OOtBu species at 803 cm^{-1} and 612 cm^{-1}, respectively. These assignments were verified using $tBu^{18}O^{18}OH$, which caused isotopic shifts of these peaks to 757cm^{-1} and 584cm^{-1}. For the Fe^{III}-OOCm species, the O-O and Fe-O stretching frequencies appear at 795cm^{-1} and 615cm^{-1}, respectively. These frequencies were the lowest Fe-O and highest O-O stretching frequencies reported for low-spin Fe^{III}-OOR complexes. This study showed the possibility that the transient intermediate in the SOR catalytic cycle could possibly be low-spin, and also showed the effect that the axial thiolate has on weakening the Fe-O bond of the alkylperoxo intermediate, promoting Fe-O bond cleavage instead of O-O bond cleavage. The structure of this Fe^{II} complex and the method by which the Fe^{III}-OOR species is generated is shown in **Figure 1.08.**

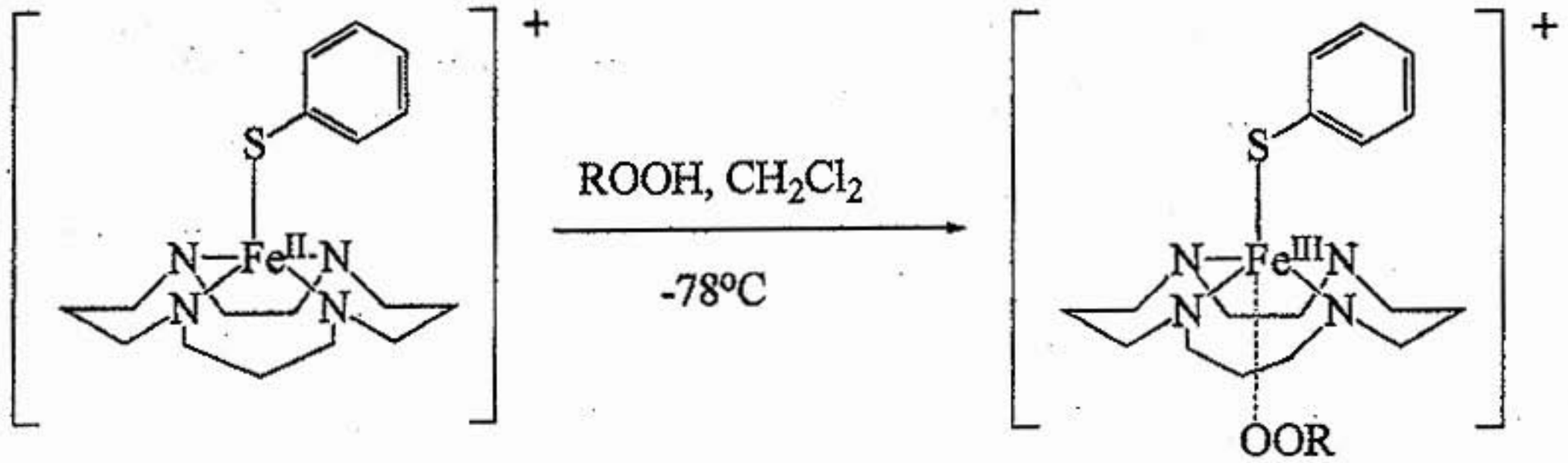

R=t-butyl(t-Bu), cumenyl(Cm)

Figure 1.08. Structure of $[Fe^{II}([15]aneN_4)(SPh)]^+$ and the reaction with alkylperoxides – generation of the Fe^{III}-OOR intermediates.[39]

Recently, our group reported the first example of a structurally relevant biomimetic model of the active site of SOR.[55] $[Fe^{II}cyclam\text{-}PrS]^+$ is described in Chapter 2, where its reaction with superoxide affords the high-spin ferric-peroxo species $[Fe^{III}cyclam\text{-}PrS(OOH)]^+$. The structure of $[Fe^{II}cyclam\text{-}PrS]^+$ is shown in **Figure 1.09** and its proposed reaction with superoxide under protic conditions is shown in **Figure 1.10.**

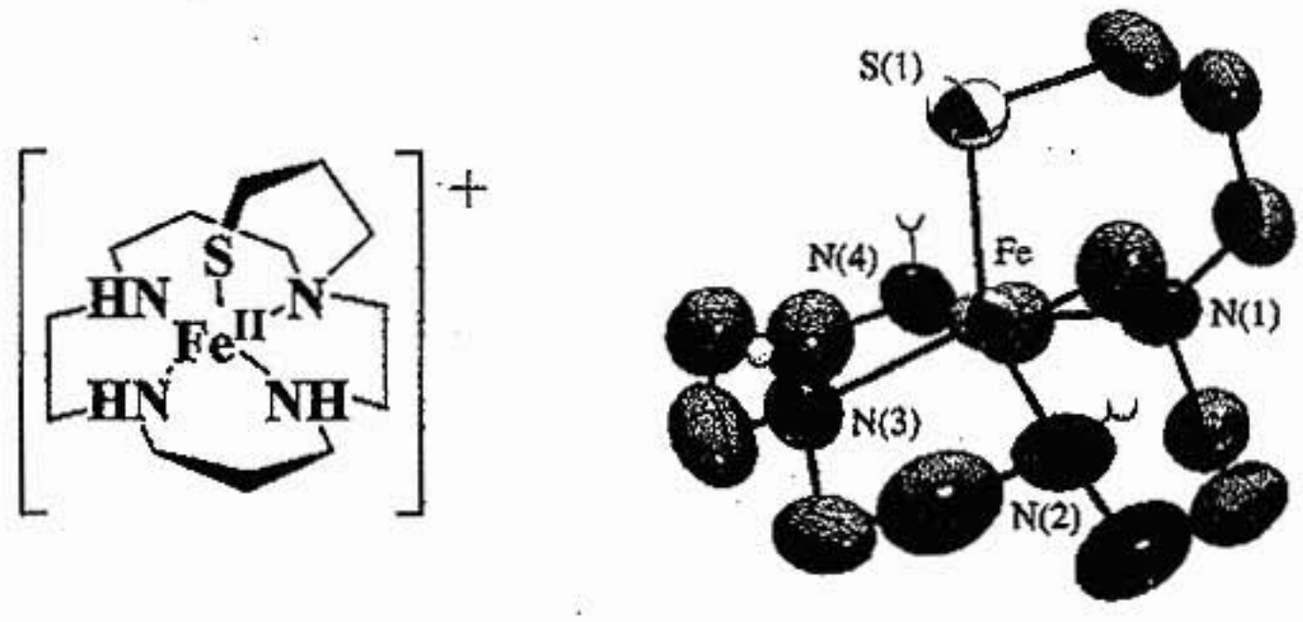

Figure 1.09. The structure and ORTEP rendering of $[Fe^{II}cyclam\text{-}PrS]^+$.

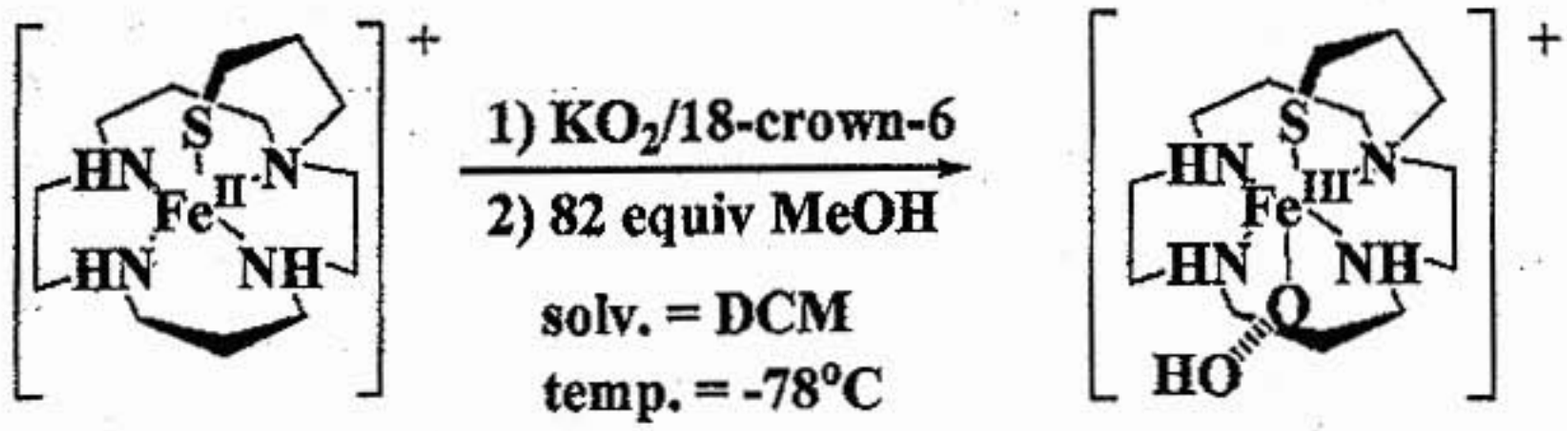

Figure 1.10. The reaction of $[Fe^{II}cyclam\text{-}PrS]^+$ with superoxide – the formation of the $[Fe^{III}cyclam\text{-}PrS(OOH)]^+$ intermediate.

This species is the first synthetic example of a thiolate–ligated high-spin Fe^{III}-OOH intermediate, and represents a very rare example of a high-spin ferric-hydroperoxo in any ligand environment. In fact, only one other example of a high-spin ferric-hydroperoxo species in a non-heme iron complex has been reported.[56] Resonance Raman vibrational data for $[Fe^{III}cyclam\text{-}PrS(OOH)]^+$, obtained in collaboration with the Solomon group at Stanford University, showed O-O and Fe-O vibrational stretches at 891 cm^{-1} and 419 cm^{-1} respectively. The O-O stretching frequency is the highest reported, and the Fe-O vibrational stretching frequency is the lowest reported, for synthetic non-heme Fe^{III}-peroxo species. These values also correspond well with the vibrational data reported for the E47 SOR mutant peroxo species[57], and are indicative of an extremely weakened Fe-O bond. This species would likely favor Fe-O bond cleavage over O-O bond cleavage. In addition, the Fe-S stretching frequency at 351 cm^{-1} proves that the thiolate remains coordinated in the transient peroxo species, and is the only Fe-S vibrational data reported for a non-heme Fe-peroxo species with a thiolate coordinated to the iron center.

The synthesis of a new $[Fe^{II}cyclam\text{-}PrS]^+$ complex and demonstration of its biomimetic character is a boon for the elucidation of the mechanism of SOR. The extensive characterization of the structure and reactivity of this complex will be discussed in the second and third chapters of this dissertation. The remainder of this dissertation will be focused on understanding the role that the thiolate plays in SOR chemistry by replacing the apical thiolate ligand in $[Fe^{II}(S^{Me2}N_4tren)]^+$ with a nitrogen. The characterization of this complex, $[Fe^{II}(N^{Et2})N_4(tren)Cl]^+$ and its reactivity is discussed in Chapter 4. Finally, the synthesis and preliminary reactivities of new novel ligands based on the well-studied tripodal tetraamine tris(2-aminoethyl)amine (tren) will be described in Chapter 5.

Chapter 1 -- Notes

(1) McCord, J. M. *Am J Med* **2000**, *108*, 652-9.

(2) McCord, J. M. *J Nutr* **2004**, *134*, 3171S-3172S.

(3) McCord, J. M. *Semin Hematol* **1998**, *35*, 5-12.

(4) Otani, H.; Umemoto, M.; Kagawa, K.; Nakamura, Y.; Omoto, K.; Tanaka, K.; Sato, T.; Nonoyama, A.; Kagawa, T. *J Surg Res* **1986**, *41*, 126-33.

(5) Fridovich, I. *Annu Rev Pharmacol Toxicol* **1983**, *23*, 239-57.

(6) Fridovich, I. *J Exp Biol* **1998**, *201*, 1203-9.

(7) Auchere, F.; Rusnak, F. *J Biol Inorg Chem* **2002**, *7*, 664-7.

(8) Pierre, J. L.; Fontecave, M. *Biometals* **1999**, *12*, 195-9.

(9) Kovacs, J. A. *Science* **2003**, *299*, 1024-5.

(10) Fridovich, I. *Annu Rev Biochem* **1995**, *64*, 97-112.

(11) Fridovich, I. *Acc. Chem. Res.* **1972**, *5*, 321-326.

(12) Jenney, F. E., Jr.; Verhagen, M. F.; Cui, X.; Adams, M. W. *Science* **1999**, *286*, 306-9.

(13) Tartaglia, L. A.; Storz, G.; Brodsky, M. H.; Lai, A.; Ames, B. N. *J Biol Chem* **1990**, *265*, 10535-40.

(14) Imlay, J. A. *J Biol Inorg Chem* **2002**, *7*, 659-63.

(15) Abreu, I. A.; Saraiva, L. M.; Soares, C. M.; Teixeira, M.; Cabelli, D. E. *J Biol Chem* **2001**, *276*, 38995-9001.

(16) Abreu, I. A.; Xavier, A. V.; LeGall, J.; Cabelli, D. E.; Teixeira, M. *J Biol Inorg Chem* **2002**, *7*, 668-74.

(17) Lombard, M.; Touati, D.; Fontecave, M.; Niviere, V. *J Biol Chem* **2000**, *275*, 27021-6.

(18) Adam, V.; Royant, A.; Niviere, V.; Molina-Heredia, F. P.; Bourgeois, D. *Structure* **2004**, *12*, 1729-40.

(19) Yeh, A. P.; Hu, Y.; Jenney, F. E., Jr.; Adams, M. W.; Rees, D. C. *Biochemistry* **2000**, *39*, 2499-508.

(20) Coelho, A. V.; Matias, P.; Fulop, V.; Thompson, A.; Gonzalez, A.; Carrondo, M. A. *J. Biol. Inorg. Chem.* **1997**, *2*, 680-689.

(21) Santos-Silva, T.; Trincao, J.; Carvalho, A. L.; Bonifacio, C.; Auchere, F.; Raleiras, P.; Moura, I.; Moura, J. J.; Romao, M. J. *J Biol Inorg Chem* **2006**, *11*, 548-58.

(22) Lombard, M.; Houee-Levin, C.; Touati, D.; Fontecave, M.; Niviere, V. *Biochemistry* **2001**, *40*, 5032-40.

(23) Coulter, E. D.; Emerson, J. P.; Jr., D. M. K.; Cabelli, D. E. *J Am Chem Soc* **2000**, *122*, 11555-11556.

(24) Kurtz, D. M., Jr. *Acc Chem Res* **2004**, *37*, 902-8.

(25) Kovacs, J. A. *Chem Rev* **2004**, *104*, 825-48.

(26) Emerson, J. P.; Cabelli, D. E.; Kurtz, D. M., Jr. *Proc Natl Acad Sci U S A* **2003**, *100*, 3802-7.

(27) Kurtz, D. M., Jr.; Coulter, E. D. *J Biol Inorg Chem* **2002**, *7*, 653-8.

(28) Kurtz, D. M., Jr.; Coulter, E. D. *Chemtracts* **2001**, 407-433.

(29) Weinberg, M. V.; Jenney, F. E., Jr.; Cui, X.; Adams, M. W. *J Bacteriol* **2004**, *186*, 7888-95.

(30) Niviere, V.; Lombard, M.; Fontecave, M.; Houee-Levin, C. *FEBS Lett* **2001**, *497*, 171-3.

(31) Mathe, C.; Niviere, V.; Mattioli, T. A. *J Am Chem Soc* **2005**, *127*, 16436-41.

(32) Clay, M. D.; Jenney, F. E., Jr.; Hagedoorn, P. L.; George, G. N.; Adams, M. W.; Johnson, M. K. *J Am Chem Soc* **2002**, *124*, 788-805.

(33) Clay, M. D.; Yang, T. C.; Jenney, F. E., Jr.; Kung, I. Y.; Cosper, C. A.; Krishnan, R.; Kurtz, D. M., Jr.; Adams, M. W.; Hoffman, B. M.; Johnson, M. K. *Biochemistry* **2006**, *45*, 427-38.

(34) Grunden, A. M.; Jenney, F. E., Jr.; Ma, K.; Ji, M.; Weinberg, M. V.; Adams, M. W. *Appl Environ Microbiol* **2005**, *71*, 1522-30.

(35) Mathe, C.; Niviere, V.; Houee-Levin, C.; Mattioli, T. A. *Biophys Chem* **2006**, *119*, 38-48.

(36) Silaghi-Dumitrescu, R.; Silaghi-Dumitrescu, I.; Coulter, E. D.; Kurtz, D. M., Jr. *Inorg Chem* **2003**, *42*, 446-56.

(37) Shaik, S.; Kumar, D.; de Visser, S. P.; Altun, A.; Thiel, W. *Chem Rev* **2005**, *105*, 2279-328.

(38) Bukowski, M. R.; Koehntop, K. D.; Stubna, A.; Bominaar, E. L.; Halfen, J. A.; Munck, E.; Nam, W.; Que, L., Jr. *Science* **2005**, *310*, 1000-2.

(39) Krishnamurthy, D.; Kasper, G. D.; Namuswe, F.; Kerber, W. D.; Narducci Sarjeant, A. A.; Moenne-Loccoz, P.; Goldberg, D. P. *J Am Chem Soc* **2006**, *128*, 14222-3.

(40) Roelfes, G.; Vrajmasu, V.; Chen, K.; Ho, R. Y.; Rohde, J. U.; Zondervan, C.; La Crois, R. M.; Schudde, E. P.; Lutz, M.; Spek, A. L.; Hage, R.; Feringa, B. L.; Munck, E.; Que, L., Jr. *Inorg Chem* **2003**, *42*, 2639-53.

(41) Hazell, A.; McKenzie, C. J.; Nielsen, L. P.; Schindler, S.; Weitzer, M. *J Chem Soc, Dalton Trans* **2002**, 310-317.

(42) Roelfes, G.; Lubben, M.; Chen, K.; Ho, R. Y.; Meetsma, A.; Genseberger, S.; Hermant, R. M.; Hage, R.; Mandal, S. K.; Young, V. G., Jr.; Zang, Y.; Kooijman, H.; Spek, A. L.; Que, L., Jr.; Feringa, B. L. *Inorg Chem* **1999**, *38*, 1929-1936.

(43) Halfen, J. A.; Moore, H. L.; Fox, D. C. *Inorg Chem* **2002**, *41*, 3935-43.

(44) Noveron, J. C.; Olmstead, M. M.; Mascharak, P. K. *J Am Chem Soc* **2001**, *123*, 3247-59.

(45) Shearer, J.; Nehring, J.; Lovell, S.; Kaminsky, W.; Kovacs, J. A. *Inorg Chem* **2001**, *40*, 5483-4.

(46) Shearer, J.; Scarrow, R. C.; Kovacs, J. A. *J Am Chem Soc* **2002**, *124*, 11709-17.

(47) Tyler, L. A.; Noveron, J. C.; Olmstead, M. M.; Mascharak, P. K. *Inorg Chem* **2003**, *42*, 5751-61.

(48) Zang, Y.; Que, L. J. *Inorg Chem* **1995**, *34*, 1030-1035.

(49) Theisen, R.

(50) Theisen, R. M.; Kovacs, J. A. *Inorg Chem* **2005**, *44*, 1169-71.

(51) Theisen, R. M.; Shearer, J.; Kaminsky, W.; Kovacs, J. A. *Inorg Chem* **2004**, *43*, 7682-90.

(52) Bukowski, M. R.; Halfen, H. L.; van den Berg, T. A.; Halfen, J. A.; Que, L., Jr. *Angew Chem Int Ed Engl* **2005**, *44*, 584-7.

(53) Kaizer, J.; Costas, M.; Que, L., Jr. *Angew Chem Int Ed Engl* **2003**, *42*, 3671-3.

(54) Halfen, J. A.; Young, V. G., Jr. *Chem Commun (Camb)* **2003**, 2894-5.

(55) Kitagawa, T.; Dey, A.; Lugo-Mas, P.; Benedict, J. B.; Kaminsky, W.; Solomon, E.; Kovacs, J. A. *J Am Chem Soc* **2006**, *128*, 14448-9.

(56) Wada, A.; Ogo, S.; Nagatomo, S.; Kitagawa, T.; Watanabe, Y.; Jitsukawa, K.; Masuda, H. *Inorg Chem* **2002**, *41*, 616-8.

(57) Mathe, C.; Mattioli, T. A.; Horner, O.; Lombard, M.; Latour, J. M.; Fontecave, M.; Niviere, V. *J Am Chem Soc* **2002**, *124*, 4966-7.

Chapter 2
$[Fe^{II}(cyclam–PrS)]^{+\cdot}$ *De novo* design of a biomimetic model of SOR.

Introduction. The design of a multidentate ligand system that could mimic the structure and N_4S composition of the SOR active site is not trivial. First, the vast majority of Fe^{II} complexes with multidentate ligands are nitrogen-ligated tetraamine and pentaamine Fe^{II} complexes, frequently with a sixth ligand occupying the open site. Very few N_4S multidentate ligand systems have been characterized, and only one has displayed biomimetic functionality.[1-5] Second, working with thiolate-bound Fe^{II} complexes has proven to be somewhat of a daunting task, due to its many synthetic obstacles caused by its propensity to oxidize to disulfides, and oligomerize to form clusters. In addition, work done by our group and others has shown the need to tether the thiolate to the ligand system to prevent the thiolate from de-coordinating, particularly when first-row transition-metals are involved.[2,6] Third, inducing the metal center to adopt the structural and electronic characteristics of the SOR active site has been shown by our group and by others to be arduous. The catalytically active ferrous of SOR is high spin (S=2), and in a square pyramidal geometry with the thiolate occupying an axial position, *trans* to the open sixth site on the iron center.

Despite these obstacles, synthesizing our target compound was still a feasible goal, once we came up with a ligand design. We hypothesized that using a saturated macrocyclic tetraamine as the basis for the ligand system would provide us with the best opportunity to obtain our target compound. The rigid nature of the macrocycle makes it a relatively weak field ligand, and also would constrain the nitrogens to become planar,

occupying the entire equatorial plane and forcing the thiolate to bind to one of the axial sites instead of an equatorial one. Tethering pendent functional groups to the nitrogens in a polyamine macrocycles has been reported previously.[7-10] The most recent example of such a ligand system has been reported by Halfen and coworkers.[11] The structure of the ligand is shown in **Figure 2.01.**

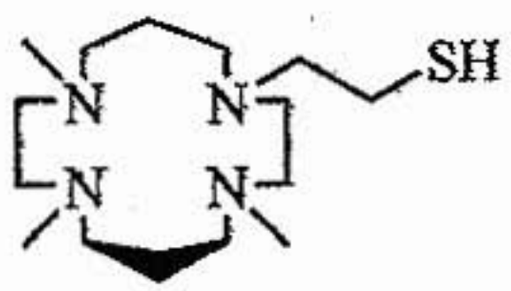

Halfen - **Me_3cyclam-S**

Kovacs - **cyclam-PrS**

Figure 2.01. The ligands from the Halfen and Kovacs SOR model complexes. The Kovacs ligand has a propylene arm tethered to the ring, compared to the ethylene arm in the Halfen ligand. Also, the amines of the Halfen ligand are permethylated.

One interesting observation about Halfen's complex is that the ligand system entails peralkylation of the amines. The resulting Fe^{II} complex has a highly cathodic electrochemical potential. Results from our laboratory agree with this as well. For example, when **bean*** and **bdep** (**Figure 2.02**), tetraalkylated topological derivatives of tren, are used in the synthesis of our model complex, $[Fe^{II}N_4{}^{(tren)}S^{(Me2)}]^+$, the resulting Fe^{II} complexes do not react with superoxide under protic or aprotic conditions.[12] In addition, both complexes display notably cathodically-shifted redox potentials ($E_{1/2}$ **(bean*)** = +410 mV and $E_{1/2}$ **(bdep?)** = +390mV vs. $E_{1/2}([Fe^{II}N_4{}^{(tren)}S^{(Me2)}]^+)$= -100 mV **vs** SCE.) Initially, the inert nature of both complexes was attributed solely to sterics, as the bulky ethyl groups appear to effectively block the open site on the Fe^{II} center.

However, it appears that peralkylation of the ligand system on all three of these complexes (**TMCS, bdep,** and **bean** ligated) has a significant effect on the electronics of the

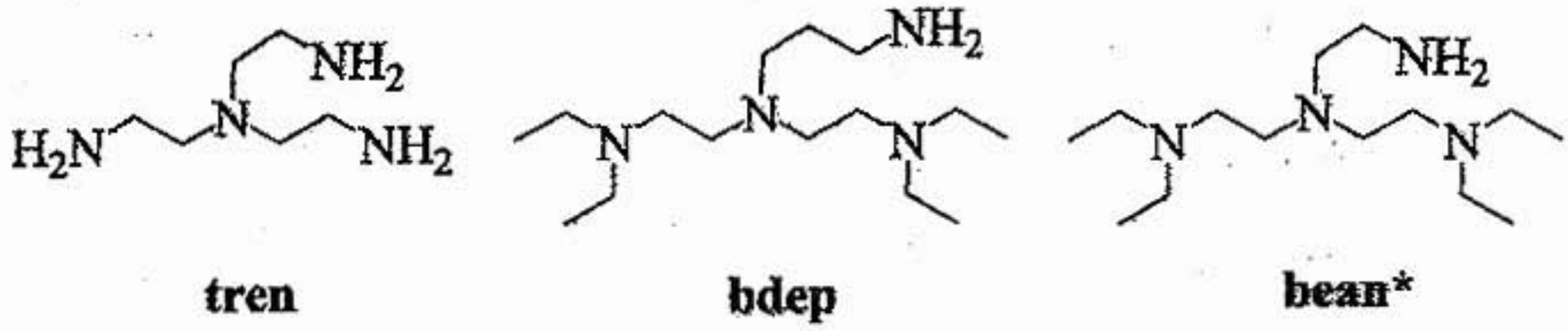

Figure 2.02. The structures of the tripodal ligand tren and the tetraalkylated derivatives bdep and bean*. The ligands bdep and bean differ by one methylene length in the arm containing the primary amine.

system. Thus, directly or indirectly, there does appear to be a significant relationship between the alkylation of the ligand system and the electronic character of the complex. Such behavior is counterintuitive to conventional thinking because alkylation of the amines on each of the ligand systems described above creates an extremely electron-rich ligand system that should also be a very good σ-donor. The higher electron density at the Fe^{II} center would theoretically decrease its Lewis acidity, and as a result, should make it more susceptible to a one-electron oxidative process, and thus should have a more negative electrochemical potential. Instead, the opposite behavior is seen in each instance.

Interestingly, it has been shown by Meyerstein and others that the ligand field of tertiary amines is considerably lowered by alkylation, compared to those induced by primary or secondary amines.[13] Also, N-alkylation of amine ligands has been shown to cause a cathodic shift in redox potential when they are ligated to a metal center,

compared to the behavior of analogous ligands that were not alkylated.[6] Based on this reasoning, it was deemed feasible that a non-alkylated analogue of the Halfen ligand would follow the reactivity precedent set by the above examples. The corresponding Fe^{II} complex should then be capable of reducing superoxide.

Experimental.

General Methods. All reactions were performed under an atmosphere of dinitrogen in a glove box or using standard Schlenk techniques, or using a custom–made solution cell equipped with a threaded glass connector sized to fit a dip probe. Reagents purchased from commercial vendors were of the highest purity available and used without further purification. THF, pentane, Et_2O, and MeCN were rigorously degassed and purified using solvent purification columns housed in a custom stainless steel cabinet, dispensed via a stainless steel schlenk-line (GlassContour). Methanol (MeOH) and ethanol (EtOH) were distilled from magnesium methoxide. ^1H NMR spectra were recorded on Bruker AV 301, Bruker AV 500, or Bruker DRX 499 FT-NMR spectrometers and are referenced to an external standard of TMS (paramagnetic compounds) or to residual protio-solvent (diamagnetic compounds). Chemical shifts are reported in ppm and coupling constants (J) are in Hz. EPR spectra were recorded on a Bruker EPX CW-EPR spectrometer operating at X-band frequency at 7 K. Cyclic voltammograms were recorded in MeCN (100 mM n-$Bu_4N(PF_6)$ solutions) on a PAR 273 potentiostat utilizing a glassy carbon working electrode, platinum auxiliary electrode, and an SCE reference electrode. Magnetic moments (solution state) were obtained using the Evans' method as modified

for super-conducting solenoids.[14,15] Temperatures were obtained using Van Geet's method.[16] Solid state magnetic measurements were obtained with polycrystalline samples in gel-caps using a Quantum Design MPMS S5 SQUID magnetometer. Ambient temperature electronic absorption spectra were recorded on a Hewlett-Packard Model 8450 spectrometer, interfaced to an IBM PC. Low temperature electronic absorption spectra were recorded using a Varian Cary 50 spectrophotometer equipped with a fiber optic cable connected to a "dip" ATR probe (C-technologies), with a custom–built two-neck solution sample holder equipped with a threaded glass connector (sized to fit the dip probe).

1,4,8-Tris(tert-butoxycarbonyl)-1,4,8,11-tetraazacyclotetradecane (3Boc-cyclam). The synthesis of 3Boc-cyclam was accomplished using a modified preparation of the initial synthesis first described by Guilard and coworkers.[17] 1,4,8,11-tetraazacyclotetradecane (cyclam) (0.100g, 0.5 mmol) was dissolved in dichloromethane (25 ml). Di-*tert*-butoxy-di-carbonate (Boc) (0.286 ml, $1.25x10^{-3}$25 m mol) was dissolved in dichloromethane (6.25 ml) and added dropwise via addition funnel over 30 minutes and allowed to stir overnight. Solvent was removed *in vacuo*, affording a white sticky residue. The residue was dissolved in hexane and insolubles were filtered. The solvent was removed *in vacuo*, affording a white foam. Column chromatography (ethyl acetate: methanol 95:5 on silica gel afforded the desired product as a white foam (0.175 g, 70%). This solid was stored at -5°C. ^{1}H-NMR (ppm in $CDCl_3$): 1.46 (s, 27H), 1.59 (bm, 2H),

1.70 (bm, 2H), 2.62 (t, *J*=4.23 Hz, 2H), 2.77 (t, *J*=5.20, 2H), 3.29-3.41 (bm, 12H). ESI-MS (M+1) calcd for $C_{10}H_{24}N_4$: 200.4; found: 201.0.

3-iodopropylthioacetate (IPTA). 3-chloropropylthioacetate (10g, 66mmol) was dissolved in 300 ml of acetone. The Finkelstein exchange reaction was performed by adding sodium iodide (30g, 200mmol) and refluxing overnight. The reaction was cooled to ambient temperature and the insoluble salts were filtered. Solvent was removed *in vacuo*, affording a red-orange solid. The solid was re-dissolved in dichloromethane (150 ml), and the insoluble white solid was filtered from the solution. Solvent was removed *in vacuo*, affording a red-orange oil, which was passed over a silica plug (95:5 hexanes/acetone) to afford the desired product as a pale yellow oil (13.65 g, yield = 85%). ^{1}H-NMR (ppm): 2.1 (m, 2H), 2.34 (s, 3H), 2.96 (t, J=6.97, 2H), 3.21 (t, *J*=6.86, 2H).

3Boc-cyclam-11-propylthioacetate (3Boc-cyclam-PrTA). (0.615 g, 1.23 mmol) and Cs_2CO_3 (0.327 g, 2.46 mmol) were dissolved in DMF (3 ml) at ambient temperature. IPTA (0.600 g, 2.5 mmol) was added dropwise while stirring. The solution was stirred for 5 days, until TLC showed product formation to be complete. Water (~100 ml) was added and the solution was extracted with ethyl acetate (3x30 ml). The organic extracts were combined and washed with brine (3x30 ml). The organic layer was dried over $MgSO_4$, filtered, and solvent was removed *in vacuo* to afford the crude product as a yellow oil. Column chromatography on silica gel (CH_2Cl_2:methanol – gradient 0-4% methanol) afforded the pure product (0.665 g, 1.08 mmol) as a pale yellow sticky residue

(yield = 88%). ^{1}H-NMR (ppm in $CDCl_3$): 1.46 (s, 27H), 1.71 (bm, 4H), 1.80 (t, *J*=7.24, 2H), 2.32 (s, 3H), 2.35-2.43 (m, 4H), 2.86 (bm, 2H), 2.83 (t, *J*=7.14, *2H*), 3.21-3.35 (bm, 12H). ESI-MS (M+1) calculated for $C_{30}H_{56}N_4O_7S$: 616.39. found: 617.7.

1-propylthioacetyl-1,4,8,11-tetraazacyclotetradecane•4HCl (cyclam-PrSAc•4HCl). The boc groups of 3Boc-cyclam-PTA were removed with 4M HCl/dioxane (30 eq.) over 24 hours. The solvent was removed by rotary evaporation. Co-evaporation with methanol afforded the pure **cyclam-PrSAc•4HCl** as an off-white solid of the tetrahydrochloride salt in quantitative yield. ^{1}H NMR (ppm in CDCl3): 1.95-2.01 (bm, 6H), 2.30 (s, 3H), 2.88 (t, J = 7.01 Hz, 2H), 3.26-3.31 (bm, 10H), 3.49-3.53 (bm, 8H). ESI-MS (M+1): calculated for $C_{13}H_{32}N_4OS$: 316.23; found: 317.4.

[Fe^{II}cyclam–PrS)]PF_6. $FeCl_2$ (0.055g, 0.433 mmol), cyclam(PrSAc)•4HCl (0.200g, 0.433 mmol), and NaOH (0.104g, 2.66 mmol) were all individually dissolved in ~2ml of MeOH and cooled to -20°C for ~30-40 min. The methanolic NaOH solution was then immediately added to the ligand solution dropwise while stirring. This solution was allowed to stir for 30 minutes at room temperature. The cold $FeCl_2$ solution was then added dropwise to the stirring ligand solution. $NaPF_6$ (0.073g, 4.33×10^{-4} mol) was then added and the solution was stirred overnight at room temperature. The pale green solution was filtered through a Celite pad and the filtrate was concentrated *in vacuo*, affording a yellow residue. This residue was redissolved in CH_2Cl_2. The solution was filtered through a Celite pad and the filtrate was concentrated *in vacuo*, affording **(3)** as a

pale yellow residue. This residue was immediately redissolved in CH_2Cl_2, filtered again through a Celite pad and concentrated *in vacuo,* affording a pale yellow residue. Coevaporation with pentane and ether afforded a dark yellow-brown solid (0.062g, yield = 30%). The solid was recrystallized by slow diffusion of ether into a CH_2Cl_2 solution, yielding colorless prisms that were not suitable for x-ray analysis. Solution magnetic moment (298 K; MeCN) μ_{eff}= 5.03 BM. Solid state magnetic moment (T=5-300 K) μ_{eff} = 4.78 BM.

[Fe^{II}cyclam–PrS)]BPh$_4$. The synthetic procedure for this salt was repeated as described for [Fe^{II}cyclam–PrS)]PF_6 above, except that $NaBPh_4$ was added in place of $NaPF_6$. The solution was filtered through a Celite pad and concentrated, affording a dark yellow residue. The residue was redissolved in THF, filtered through a Celite pad and concentrated to a minimal volume. Crystallization was accomplished by slow diffusion of pentane to afford colorless prisms suitable for x-ray analysis (0.090g, yield = 32%). Solid state magnetic moment (T= 5-300 K) μ_{eff} = 4.91 BM. $E_{1/2}$ (DMF) = +220 mV vs. SCE. ESI-MS calculated for $FeC_{13}H_{29}N_4S$: 329.1, found 329.1. Electronic absorption (MeOH): $\lambda_{max}(\varepsilon)$=299 nm (1280 L•M^{-1}cm^{-1}).

Reaction of [Fe^{II}(cyclam–PrS)](PF_6) with KO_2. Formation of [Fe^{III}(cyclam–PrS)(OOH)](PF_6) peroxide intermediate. [Fe^{II}cyclam–PrS)]PF_6 (11.1 mg, 0.024 mmol) was dissolved into CH_2Cl_2 (20 ml). To this solution was added 82 equiv of MeOH (80 uL, 2.0 mmol). The solution was injected into a custom dip probe cell under

argon and cooled to -78°C. Addition of KO_2 (100 uL of a 0.3 M solution of O_2^- solubilized in THF as the (18-crown-6)K^+ salt) caused the immediate formation of a burgundy color (530 nm). The formation of this species maximized at t=4 min. The reaction performed under the conditions described above except without exogenous methanol showed no visible sign of any reaction occurring. Electronic absorption spectrum (CH_2Cl_2): λ_{max} (ε) = 530 nm (1350). Vibrational data: 419 cm^{-1} (ν_{Fe-O}), 893 cm^{-1} (ν_{O-O}), 859 cm^{-1} ($\nu_{^{18}O-^{18}O}$), 400 cm^{-1} ($\nu_{Fe-^{18}O}$), 352 cm^{-1} (ν_{Fe-S}). EPR (collected in 1:1 CH_2Cl_2:2-methyl-THF glass, 7 K): $g_1 = 7.77$, $g_2 = 5.36$, $g_3 = 4.15$.

Amplex Red assay – peroxidase assay for H_2O_2 detection. The Amplex Red Assay kit was obtained from Invitrogen (Probes.com, Kit #A22188). The Amplex Red assay was prepared following the protocols supplied with the assay kit and published by Haugland and coworkers.[18] Fluorescent spectra were recorded using a Perkin-Elmer LS-50B Luminescence Spectrophotometer equipped with a pulsed high pressure Xenon source (Perkin Elmer Corporation, Norwalk, Connecticut). Fluorescent samples were contained and analyzed in 1 cm x 1 cm quartz cuvettes, 1.4 ml volume from Starna (Starna Inc., Atascadero, CA).

A 30mM solution of **[Fe^{II}cyclam(Pr,S)]PF_6** was prepared in a 2ml consisting of degassed acetone (1806 µl) and 82 equivalents of MeOH (194µL) and placed under an argon stream. This solution was cooled to -78°C while stirring. To this was added 1 equivalent of KO_2 solubilized in an 18-crown-6/THF solution. The solution was allowed to stir for 4-5 minutes, followed by the addition of 1 equivalent of acetic acid from an

acetone stock solution. A 93 µl aliquot ($2.8x10^{-6}$ mol, assuming 100% reduction of KO_2 has occurred) was taken from the solution and diluted in with 907 µl of 1X phosphate buffer. A 25 µl aliquot of this solution was added to an assay solution consisting of 50 µl of the Amplex Red assay and 1325 µl of 1X phosphate buffer solution. This 1.4 ml assay solution was injected into a quartz fluorescence cell, wrapped in aluminum foil and allowed to incubate at room temperature for 30 minutes. The emission at 585 nm was measured by using an excitation wavelength of 570 nm. The sample was scanned from 400-800 nm at a scan rate of 200 nm/min.

Catalytic turnover in the reaction between $[Fe^{II}$(cyclam–PrS)$](PF_6)$, KO_2, followed by HOAc, and Cp_2Co, in sequential aliquots. To a stirring solution of **$[Fe^{II}$(cyclam-PrS)$]PF_6$** (11.1 mg, 0.024 mmol) at -78 °C, in 20 mL CH_2Cl_2 (in the presence of activated 4 Å molecular sieves) was added 100 uL of a 0.3 M solution of O_2^- (solubilized in THF (as the (18-crown-6)K^+ salt) under an Ar atmosphere, followed by 82 equiv of MeOH (80 uL, 2.0 mmol). **$[Fe^{III}$(cyclam–PrS)(OO(H)$]^+$** (λ_{max}= 530 nm) forms and maximizes at t=4 min as observed by the intense burgundy color. Upon addition of 1equiv of HOAc (10 uL of a 2.4 M solution in CH_2Cl_2), **$[Fe^{III}$(cyclam–PrS)(OO(H)$]^+$** converts to a turquoise blue species **$[Fe^{III}$(cyclam–PrS)(OAc)$]^+$** (λ_{max}= 604 nm). Reduction of **$[Fe^{III}$(cyclam–PrS)(OAc)$]^+$** via the addition of 1 equiv of Cp_2Co (100 uL of a 0.24 M solution in CH_2Cl_2) regenerated **$[Fe^{II}$(cyclam-PrS)$]PF_6$** as a pale yellow solution. Using this procedure, involving the sequential delivery of reagents, five turnovers were achieved.

Resonance Raman Experiments. Resonance Raman (rR) spectra were obtained using a Princeton Instruments ST-135 back-illuminated CCD detector on a Spex 1877 CP triple monochromator with 1200, 1800, and 2400 grooves/mm holographic spectrograph gratings. Excitation was provided by a Dye Laser (Rhodamine 6G, Coherent 599) which was energized by a Coherent Innova Sabre 25/7 Ar^+ CW ion laser. The laser line, 571 nm and 600 nm (~70 mW), was chosen to coincide with the absorption of **4** and **5**, respectively. The spectral resolution was < 2 cm^{-1}. Sample concentrations were approximately 25-30 mM in Fe. The samples were either cooled to 77 K in a quartz liquid nitrogen finger dewar (Wilmad) and hand spun to minimize sample decomposition during scan collection (for obtaining the ν_{O-O}) or cooled to 190-196 K using a flow of liquid N_2 cooled, He gas in a spinner set-up.

Computational Details. All calculations were performed on dual-CPU Pentium Xeon 2.8 GHz work stations using the hybrid B3LYP functional with the Gaussian 03 package. For optimization 6-311g* basis set was used for Fe,S,N and O atoms while 6-31g* basis set was used for C and H atoms. Single point calculations were performed using tight SCF convergence criteria and a 6-311g* basis on all atoms. The Mulliken population analyses were performed using the PYMOLYZE program.

X-ray Crystallographic Structure Determination for $[Fe^{II}$(cyclam–PrS)$]BPh_4$. A clear prism cut down to 0.36 x 0.24 x 0.24 mm of **3** was mounted on a glass capillary with epoxy. Data was collected at –143°C. The crystal-to-detector distance was set to 35

mm and exposure time was 45 seconds per degree for all data sets with a scan width of 1°. The data collection was 97.8% complete to 25° in 9. A total of 59867 partial and complete reflections were collected covering the indices, h = -14 to 14, k = -10 to 12, l = -43 to 42. 7151 reflections were symmetry independent and the R_{int} = 0.0643 indicated that the data was of slightly less than average quality. Indexing and unit cell refinements indicated a monoclinic P lattice in the space group $P2_1/c$ (No. 14). The data for **3** was integrated and scaled using Denzo-hkl-SCALEPACK, and an absorption correction was performed using SORTAV. Solution by direct methods (SIR97) produced a complete heavy atom phasing model consistent with the proposed structures.[11c] All non-hydrogen atoms were refined anisotropically by full-matrix least-squares methods, while all hydrogen atoms were then located using a riding model.

Discussion.

Synthesis of 1-propylthioacetate-cyclam (cyclam-PrSAc • 4HCl). Nitrogen-donor macrocycles with four amines, commonly referred to as tetraaza-macrocycles, are commonly used in, and are available in, various ring sizes.[19-22] 1,4,8,11-tetraazacyclotetradecane (cyclam) in particular has been extensively studied.[23] Cyclam has an ideal M-N bond length of 2.07Å, and has been shown to be the ideal size for ligation to Fe^{II} and Fe^{III}.[22] The synthesis of cyclam has been reported previously[24], and is also readily available commercially.

The design of **cyclam-PrSH** began with tris-protected cyclam compounds. Two tris-protected cyclam compounds, tris(2-tertbutoxycarbonyl)cyclam (3Boc-cyclam) and

tris(trifluoroacetyl)cyclam (3TFAc-cyclam) (**Figure 2.03**) were synthesized in good yields as described in literature.[17,25] These protecting strategies were chosen because both the boc and TFAc moieties are very readily removed under ambient conditions without the use of aggressive reagents and conditions.[26]

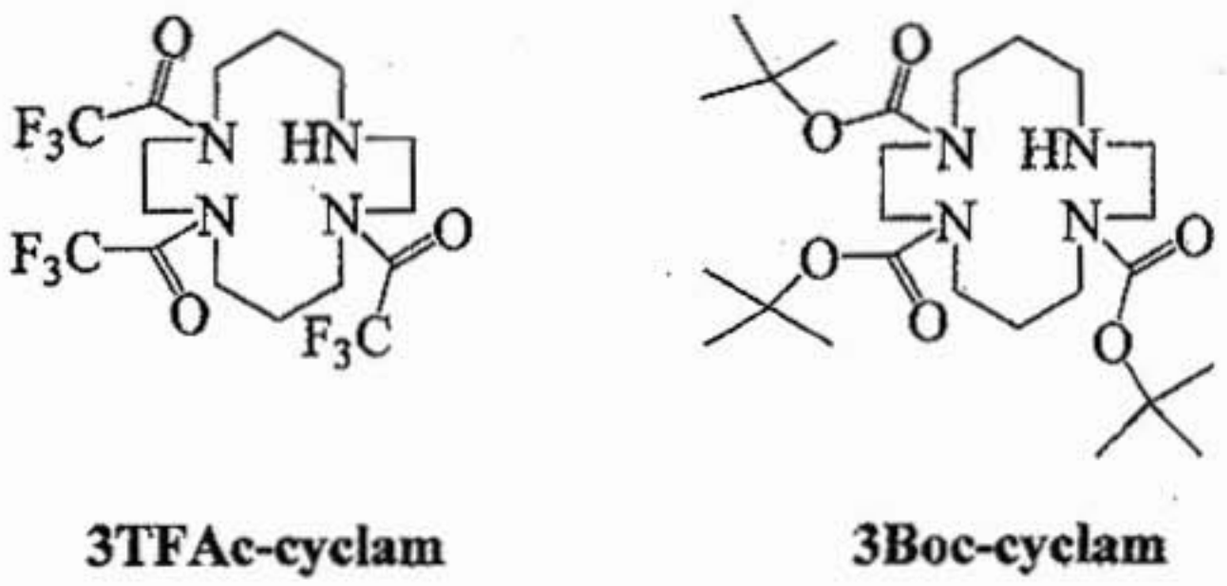

3TFAc-cyclam **3Boc-cyclam**

Figure 2.03. Structures of tris-protected cyclam compounds – precursor compounds for ligand synthesis.

Because of the susceptibility of thiols to oxidize to disulfides, a protecting group strategy was pursued to ensure the preservation of the thiol moiety until completion of the synthesis. The triphenylmethyl (trityl) group was chosen initially because of its ease of use as a protecting group and ability to be simultaneously removed with boc by trifluoroacetic acid (TFA).[26] Five trityl-protected compounds were synthesized according to literature procedures, some with minor modifications.[27-29] These and two other compounds used are shown in **Figure 2.04**.[30] In addition, direct alkylations with diiodopropane and dibromopropane were attempted in an effort to obtain a tris-protected cyclam ligand, alkylated at the free amine with a propyl halide arm. These compounds were respectively named 3Boc-cyclam-Pr,X where X=I or Br. The idea was that the

terminal halide could be displaced by potassium thioacetate, and then deprotected to afford the free thiol (**Figure 2.05**).

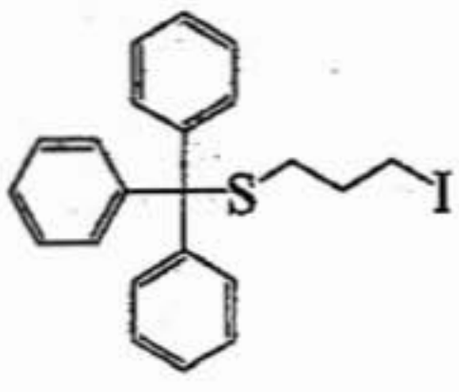

TRT-SPrI

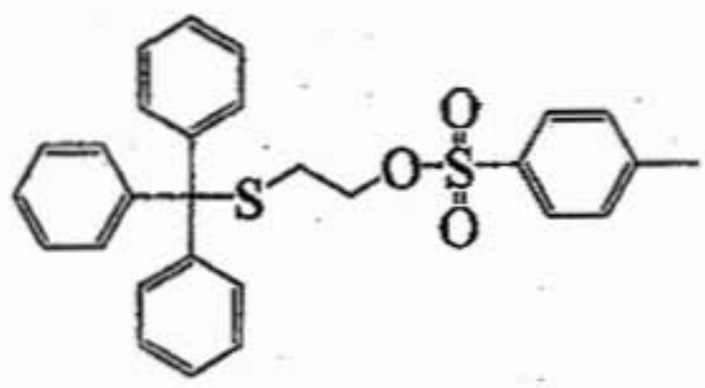

TRT-SEt-OTs

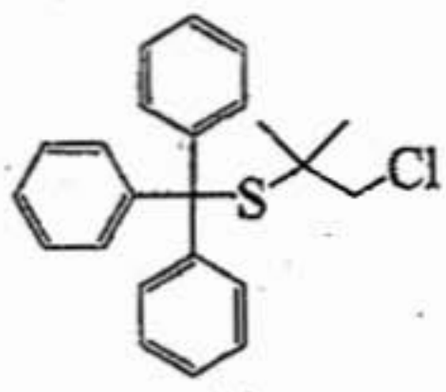

TRT-S(Me2)EtCl

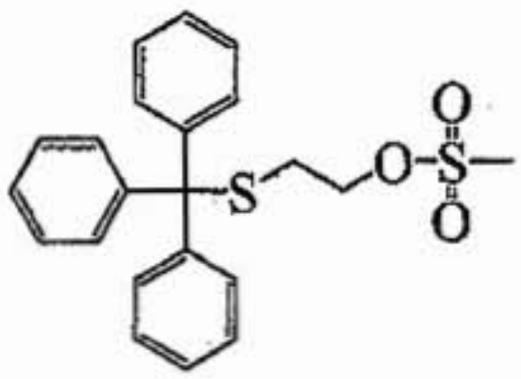

TRT-SEt-OMs

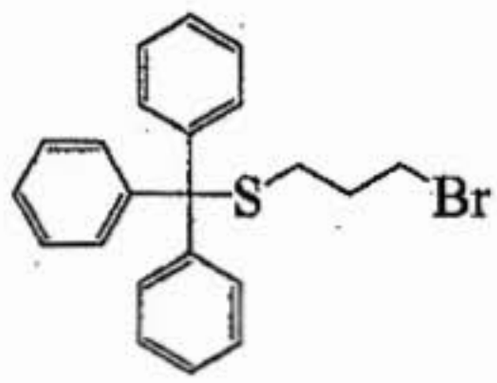

TRT-SPrBr

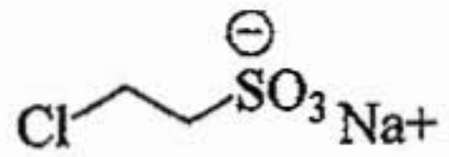

sodium 2-chloroethane sulfonate

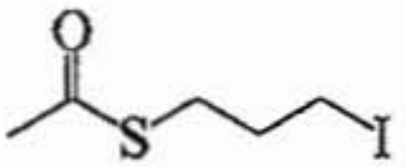

I-Pr-TA

Figure 2.04. The family of haloalkanes to be used to alkylate the tris-protected cyclam compounds. Each compound has a protected thiol moiety and a halogen or tosylate leaving group.

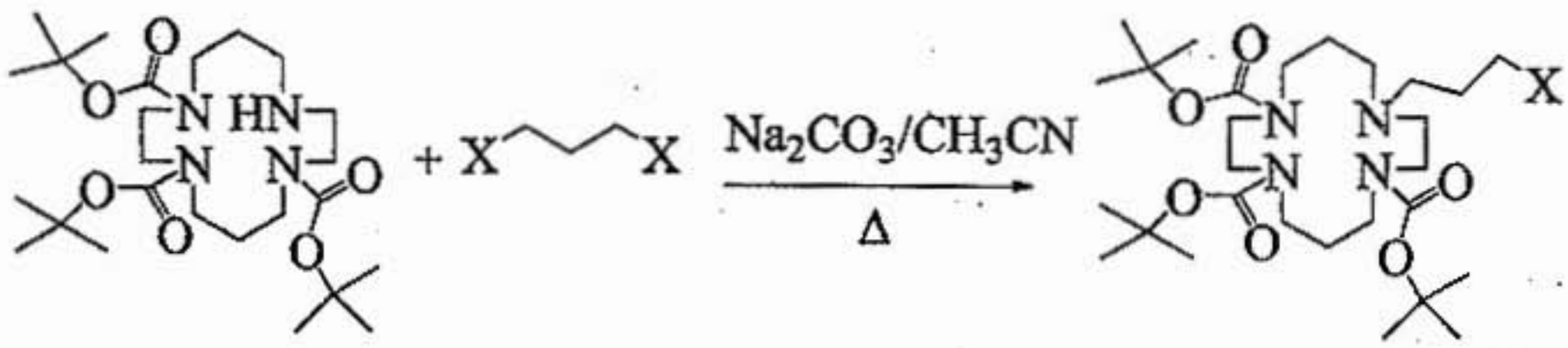

3Boc-cyclam- Pr,X
(X = Br, I)

Figure 2.05. General scheme to prepare 3Boc-cyclam-Pr,X series of compounds

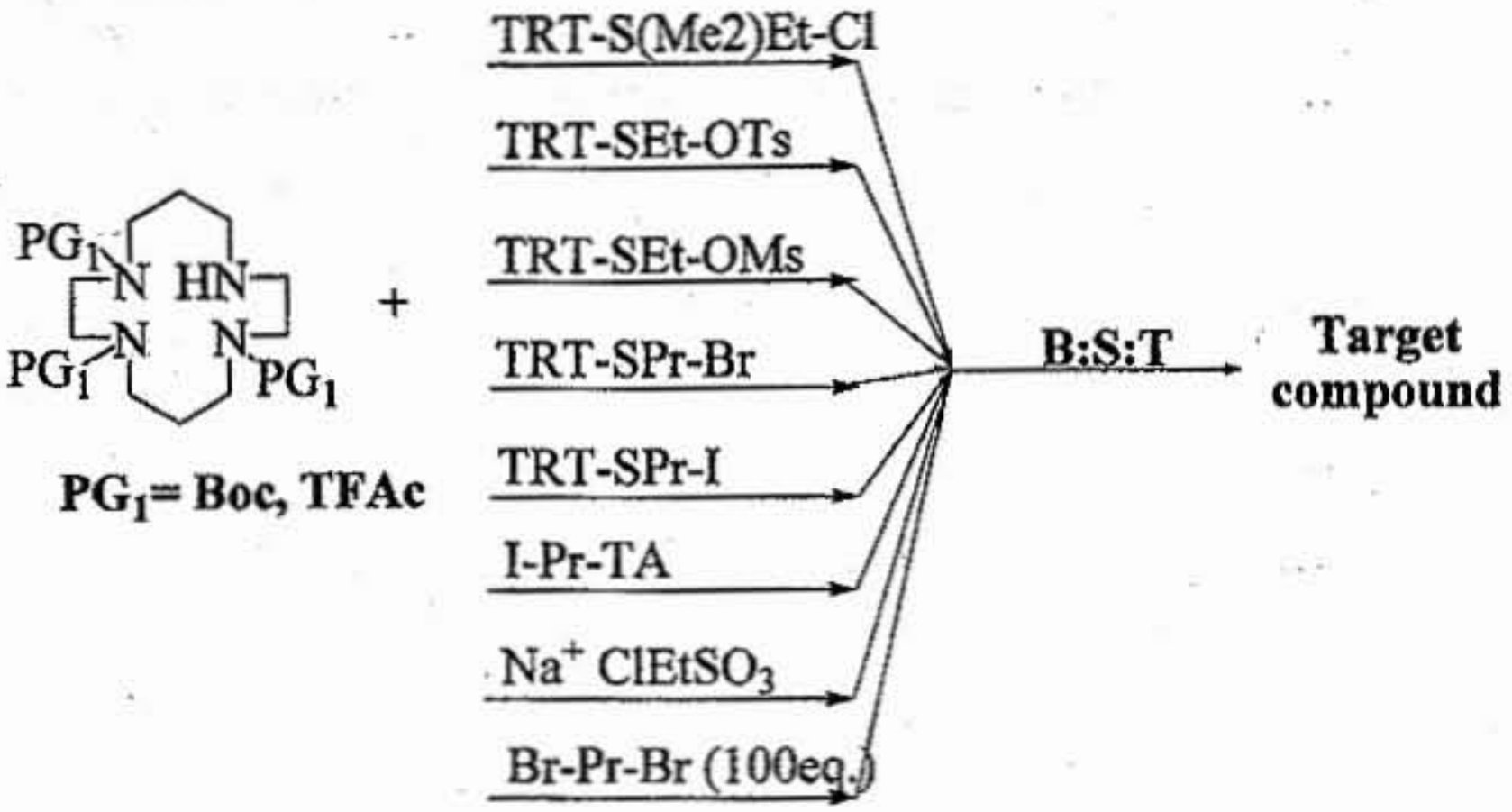

Figure 2.06. Parallel synthetic reaction scheme: reagents and conditions. The compounds used are shown in **Figures 2.03, 2.04** and **2.05.**

Each reaction was attempted under a combination of different solvent conditions (THF/CH_3CN, CH_3CN, DMF) and using different bases (Na_2CO_3, K_2CO_3, Cs_2CO_3, triethylamine (TEA), diisopropylethylamine (DIPEA)), under ambient temperature or reflux, in a parallel synthetic fashion (**Figure 2.06**). After rigorous testing, it was found that the optimal reaction conditions involved the use of I-Pr-TA as the alkylating agent, with Cs_2CO_3 in DMF at ambient temperature for ~ 72 hours. This method produced the highest yield (>90%) of the 3Boc-cyclam and the 3TFAc-cyclam – propylthioacetate (Pr, TA) compounds. While the reaction with 1,3-dibromopropane did yield the desired monomer with a terminal halide, it was not as pure or as high-yielding. The reaction with

1,3-diiodopropane afforded a complex mixture of products, most likely a mixture of starting material, the monomeric product and other oligomeric byproducts.

The protected macrocyclic thiol ligand S-3-(1,4,8,11-tetraazacyclotetradecan-1-yl)propylthioacetate tetrahydrochloride (cyclam-PrS–Ac•4HCl) was synthesized in excellent yields. The reaction scheme is shown in **Figure 2.07.** Once the ligand was prepared, it was completely stable for months under a nitrogen atmosphere.

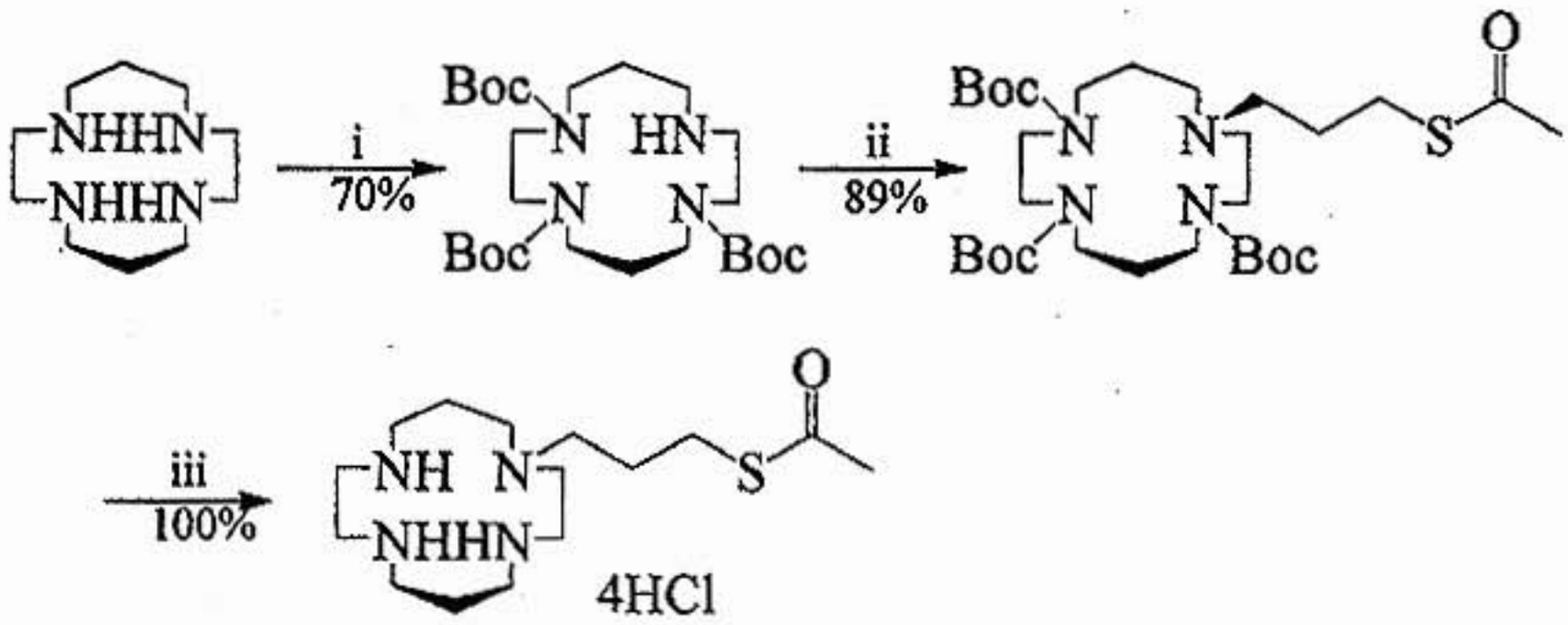

i) Boc_2O, CH_2Cl_2, RT; ii) 3-iodopropylthioacetate, Cs_2CO_3, 72 hrs.; iii) 4M HCl/dioxane.

Figure 2.07. Synthesis of cyclam-PrSAc•4HCl.

Synthesis and characterization of $[Fe^{II}$(cyclam–PrS)$]^+$. The synthesis of the Fe^{II} complex derived from our new **cyclam–PrSAc** ligand is outlined in **Figure 2.08.** The initial step involved the simultaneous deprotection of the thiol and deprotonation of the tetraammonium salt *in situ* using methanolic NaOH, followed by the addition of $FeCl_2$. This was performed by initially adding cyclam-PrSAc • 4HCl to methanol, creating a cloudy solution. Six equivalents of NaOH were added, causing the solution to go clear

for a few seconds. The precipitation of a white solid, presumably NaCl, immediately followed. The addition of $FeCl_2$ caused the solution to turn pale green. The solution was stirred overnight, affording a pale brown solution. The solution was filtered through a Celite bed in a fritted glass filter, affording a clear tannish-tinted solution. The solution was evaporated to dryness, affording a sticky brown residue, which was redissolved in CH_2Cl_2. The insolubles were filtered through a Celite bed, and the solution was evaporated to dryness. Single crystals of the iron complex **$[Fe^{II}$(cyclam–PrS)$](BPh_4)$** were grown via the slow diffusion of pentane into a THF solution at –30 °C. As shown in the ORTEP (**Figure 2.09**), the Fe^{II} center is five–coordinate, ligated by four nitrogens and an apical thiolate in a square pyramidal geometry (τ= 0.13).

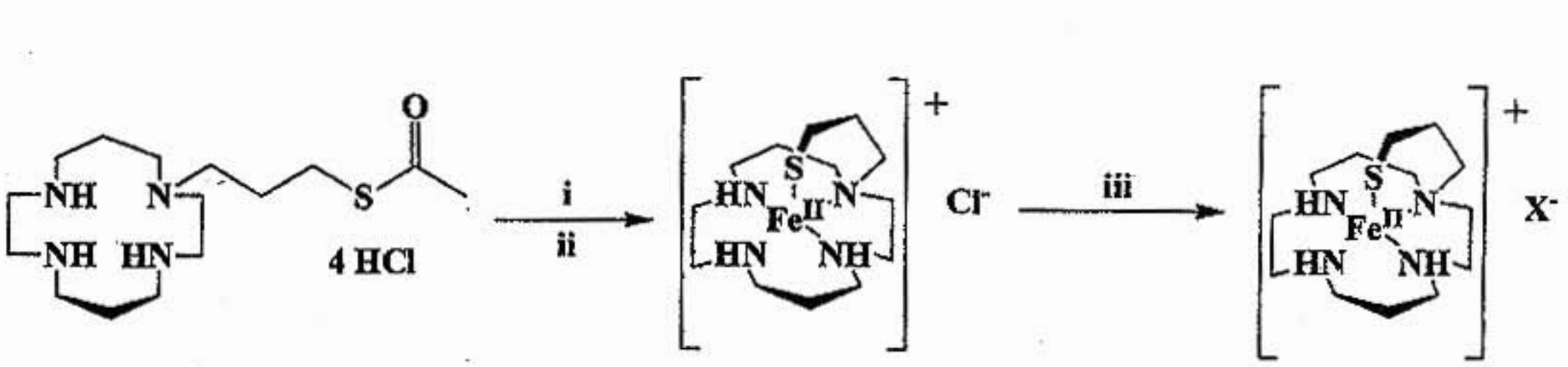

i) NaOH/MeOH; ii) $FeCl_2$, stir 24 hrs.; iii) NaX (X=PF_6, BPh_4, BF_4).

Figure 2.08. The synthesis of **$[Fe^{II}$(cyclam-PrS)$]^+$.**

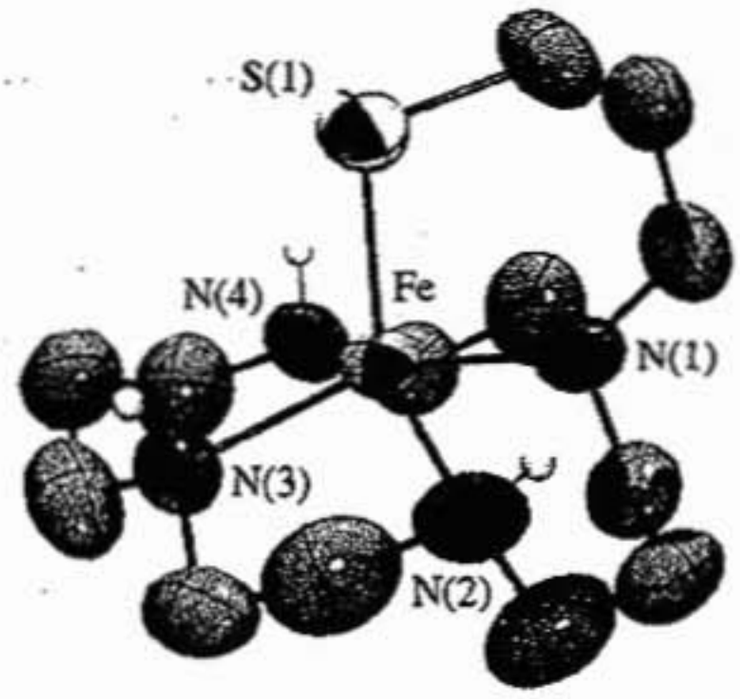

Figure 2.09. The x-ray crystal structure of **$[Fe^{II}$(cyclam–PrS)$]^+$.**

Table 2.01. Bond lengths of **$[Fe^{II}$(cyclam–PrS)$]^+$.**

Bond lengths (Å) of $[Fe^{II}$(cyclam–PrS)$]^+$ and SOR		
Bond	**$[Fe^{II}$cyclam(Pr,S)$]^+$**	**SOR *(pyr. Fur.)***
Fe(1)-N(1)	2.181 (3°N)	1.97
Fe(1)-N(2)	2.138	2.29
Fe(1)-N(3)	2.174	2.13
Fe(1)-N(4)	2.166	2.08
Fe(1)-S(1)	2.2863	2.44

As suggested by the average Fe–N bond length (2.16(2) Å), **$[Fe^{II}$(cyclam-PrS)$]^+$** is high–spin (S= 2), like the SOR active site, both in solution (μ_{eff}(MeCN)=5.03 BM) and the solid state (μ_{eff} = 4.91 BM; Figure S-9). The Fe–S bond length (2.286(1) Å) falls in the usual range for synthetic Fe^{II}–thiolate complexes but is slightly shorter than that (Fe–S= 2.4 Å) of wild-type SOR. **(Table 2.01).**

Table 2.02. The comparison of the M-L bond lengths of $[Fe^{II}(cyclam\text{-}PrS)]^+$ with the enzyme and other relevant complexes.

Bond lengths (Å) of SOR and cyclam complexes			
Bond	**$[Fe^{II}$cyclam-PrS)$]^+$**	**$[Fe^{II}TMCS]^+$**	**SOR** ***(pyr. Fur.)***
Fe(1)-N(1)	2.181 (3°N)	2.225 (3°N)	1.97
Fe(1)-N(2)	2.138	2.176	2.29
Fe(1)-N(3)	2.174	n/a	2.13
Fe(1)-N(4):	2.166	n/a	2.08
Fe(1)-S(1)	2.2863	2.297	2.44

Note: SOR bond lengths are based on Subunit A. Pyr.fur. SOR has 4 subunits (A,B,C,D).

Reactivity of $[Fe^{II}(cyclam\text{–}PrS)]^+$ with superoxide – characterization of $[Fe^{III}(cyclam\text{–}PrS)OOH]^+$. $[Fe^{II}(cyclam\text{–}PrS)]^+$ reacts with KO_2, solublized with 18-crown-6 in THF, in CH_2Cl_2 at –78 °C, after the addition of MeOH (82 equivalents) to afford a metastable intense burgundy intermediate. The absorption spectrum of this intermediate is shown in **Figure 2.10.**

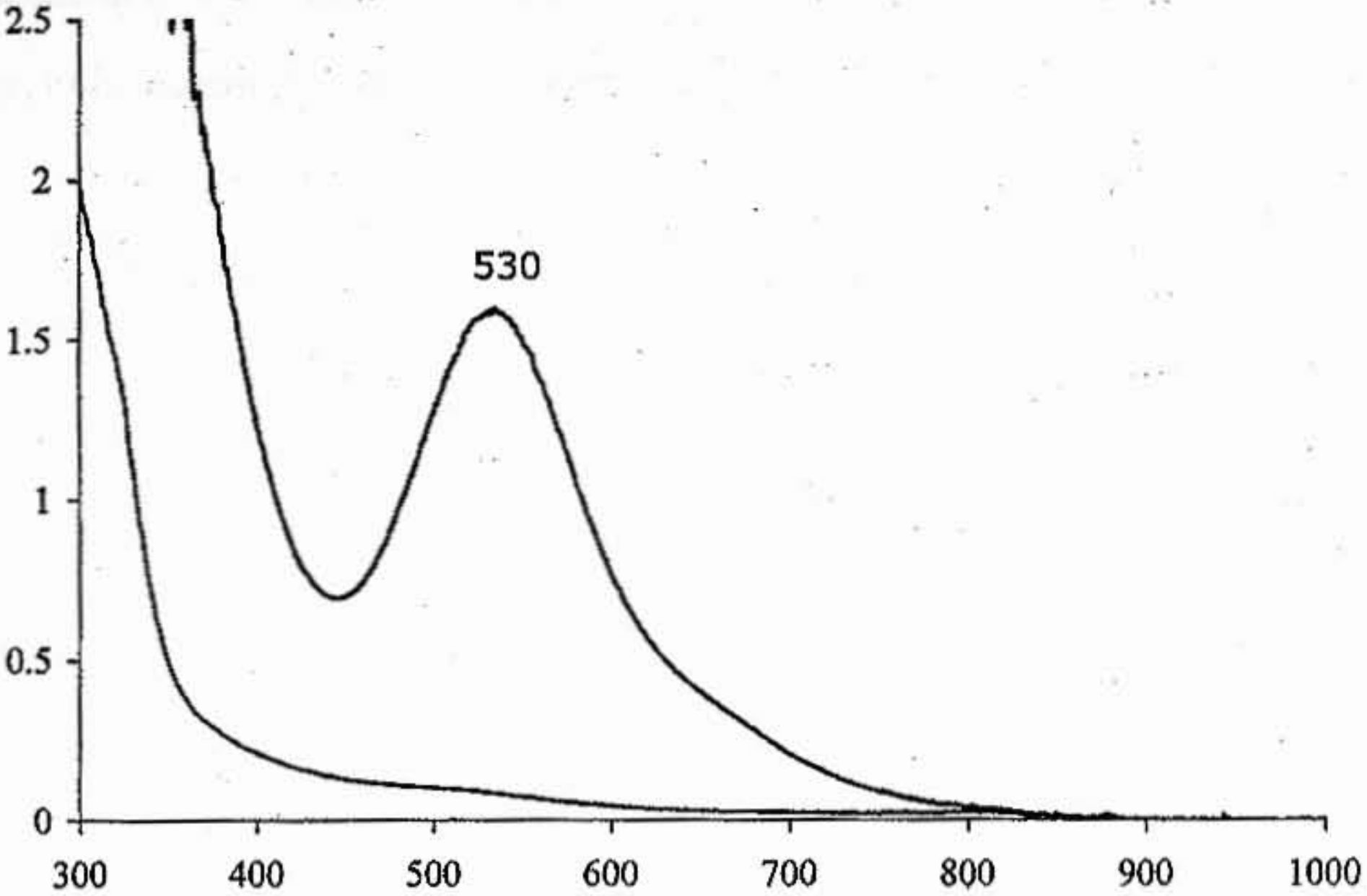

Figure 2.10. The absorption spectrum of the burgundy transient intermediate **$[Fe^{III}$(cyclam–PrS)OOH$]^+$.**

The transient intermediate **$[Fe^{III}$(cyclam–PrS)OOH$]^+$** is high-spin (g= 7.72, 5.40, 4.15), displays an absorption band at λ_{max}= 530(1350) nm, and shows ν_{O-O} , ν_{Fe-O} , and ν_{Fe-S} stretches at 891 cm^{-1} (a Fermi doublet), 419 cm^{-1}, and 352 cm^{-1} in the resonance Raman spectrum, respectively. The EPR spectrum of **$[Fe^{III}$(cyclam–PrS)OOH$]^+$** is shown in **Figure 2.11.** The ν_{O-O}, and ν_{Fe-O} peaks shift to 856 cm^{-1} and 400 cm^{-1}, respectively, upon the introduction of an isotopic label derived from $K^{18}O_2$ (50% enriched) and the Fermi doublet collapses upon the incorporation of D^+ (from MeOD). The resonance Raman data is shown in **Figure 2.12.** These data are consistent with the formation of a thiolate–ligated Fe–peroxo species, **$[Fe^{III}$(cyclam–PrS)(OOH)$]^+$**, via the

oxidative addition of superoxide to **$[Fe^{II}$(cyclam–PrS)$]^+$** in a proton–dependent mechanism. No reaction occurs without a proton source present. Also, under the conditions examined (–78°C, 82 equivalents of MeOH in a 2-MeTHF glass), O_2^- does not convert to H_2O_2 in the absence of **$[Fe^{II}$(cyclam–PrS)$]^+$**. This intermediate, **$[Fe^{III}$(cyclam–PrS)(OOH)$]^+$**, is the first example of a *trans* thiolate–ligated Fe^{III}–peroxo species. Also, it is the first example of a high-spin hydroperoxo species in a thiolate-ligated non-heme iron complex, and is only the second reported example of a high-spin Fe-hydroperoxo species.[31]

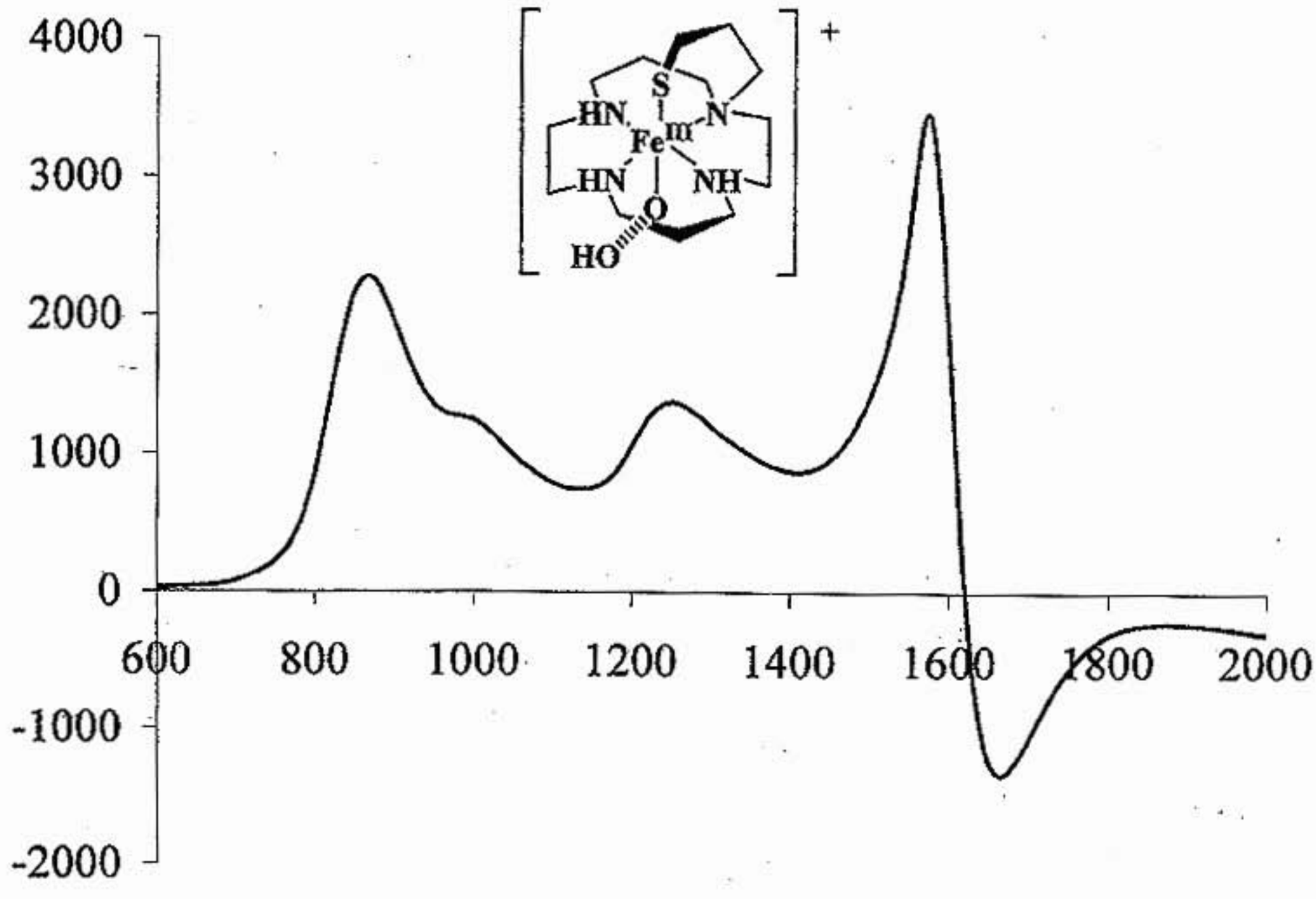

Figure 2.11. The EPR of **$[Fe^{III}$(cyclam–PrS)OOH$]^+$** in 2-MeTHF glass at -78°C. This is the high spin region. There is also an inherent small amount of a low-spin component, the identity of which will be discussed later in this chapter.

Because of the inherent appearance of a low-spin component in each reaction that was monitored by EPR, we sought to minimize the contribution by this component, by determining the optimal reaction conditions. This was done by varying the temperature, incubation time, equivalents of MeOH as a proton source, solvent medium, and concentration of **$[Fe^{II}$(cyclam-PrS)$]^+$**, and monitoring the reaction by both EPR and resonance Raman. First, although the reagent concentration for EPR experiments is typically 6-8mM, because of the low extinction coefficient of the **$[Fe^{III}$(cyclam-PrS)(OOH)$]^+$** intermediate, we were forced to use concentrations of 30mM for the resonance Raman experiments. Thus, because a direct correlation between the spin state and the Fe-O and O-O stretching frequencies of the **$[Fe^{III}$(cyclam-PrS)(OOH)$]^+$** intermediate was imperative to have, as a result the EPR experiments were also performed at 30mM concentrations of **$[Fe^{II}$(cyclam-PrS)$]^+$**. Based on this concentration, various experiments that varied the amount of MeOH to be used as a proton source were performed. Excessive use of MeOH led to increased amounts of the low-spin component being formed. However, if the amount of MeOH equivalents was limited excessively, the reaction would either take too long to complete, or the formation of **$[Fe^{III}$(cyclam-PrS)(OOH)$]^+$** would ultimately stall and thus not be able to aggregate at acceptable amounts for analysis. It was ultimately found that 82 equivalents of MeOH was the optimal amount of MeOH to maximize the formation of **$[Fe^{III}$(cyclam-PrS)(OOH]$]^+$** while keeping the amount of the low-spin component formed during this reaction to a minimum.

The reaction time was also varied between 5s-60 minutes. This set of control reactions was performed because when this reaction was monitored by UV-vis absorption spectroscopy, the band at 530nm associated with the formation of **$[Fe^{III}$(cyclam-PrS)(OOH)$]^+$** showed implicit broadening, which was thought to coincide with the formation of a second species during the reaction, possibly the low-spin component seen when the reaction was monitored by EPR. By optimizing the incubation time during which the reaction was allowed to proceed, prior to freezing the reaction tube, a balance between maximum aggregation of the **$[Fe^{III}$(cyclam-PrS)(OOH)$]^+$** and minimum formation of the low-spin component was hoped to be achieved. Select EPR spectra from this set of time control reactions are shown in **Figure 2.12.** From these experiments it was concluded that with these reagent amounts, the optimum incubation time was t=4 minutes.

It should be noted here that subtle precautions such as running each set of control experiments from a common stock solution of **$[Fe^{II}$(cyclam-PrS)$]^+$**, precooling the EPR tubes containing **$[Fe^{II}$(cyclam-PrS)$]^+$** to a temperature of –78°C, and using a minimal volume of the reaction medium (250μl) each played invaluable roles in determining the optimal conditions for this reaction to be studied by EPR and resonance Raman.

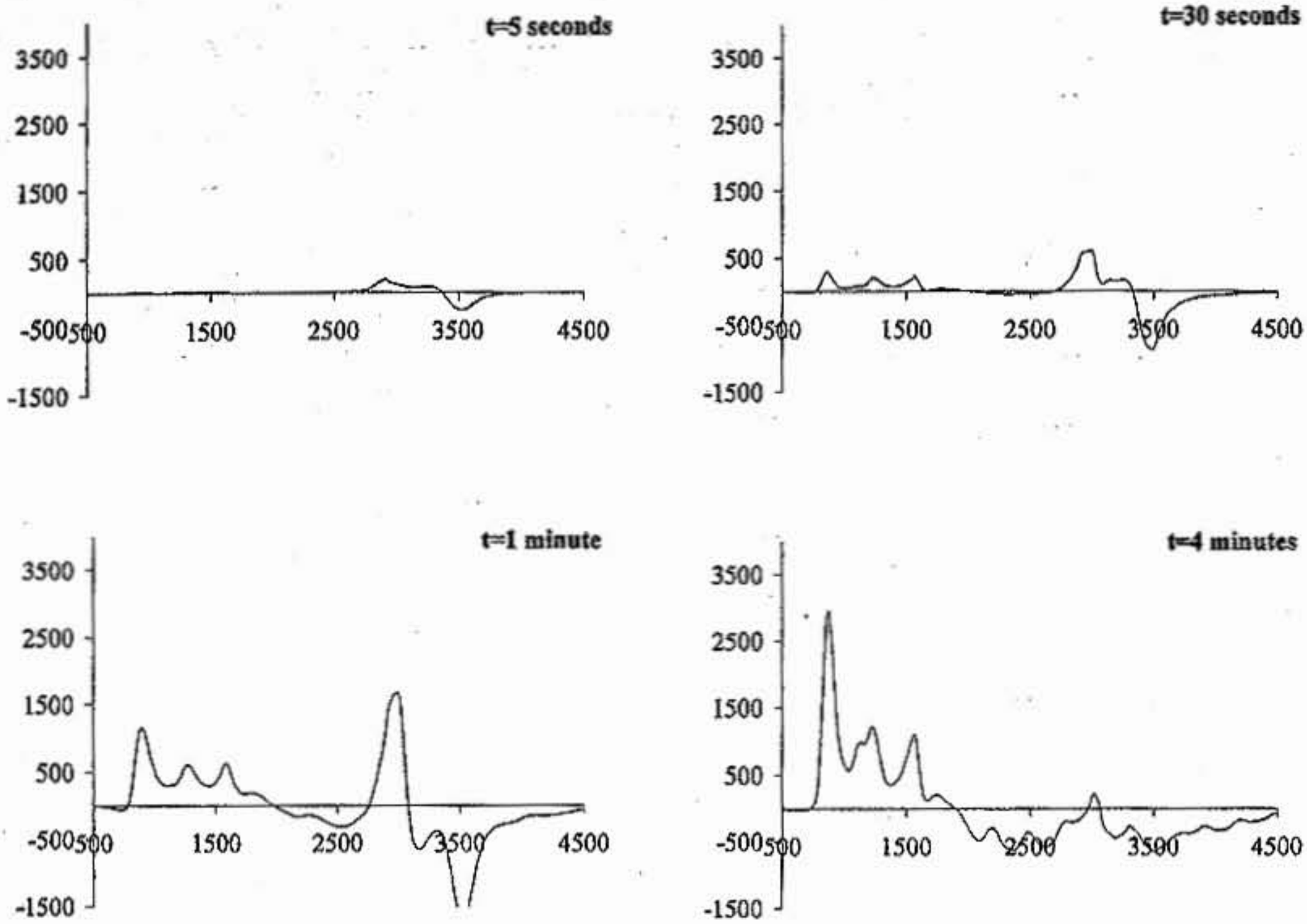

Figure 2.12. Monitoring the formation of the high-spin component (Fe^{III}-OOH) by EPR – determination of incubation time. Select plots are shown here. The incubation time is noted in the upper right corner of each plot.

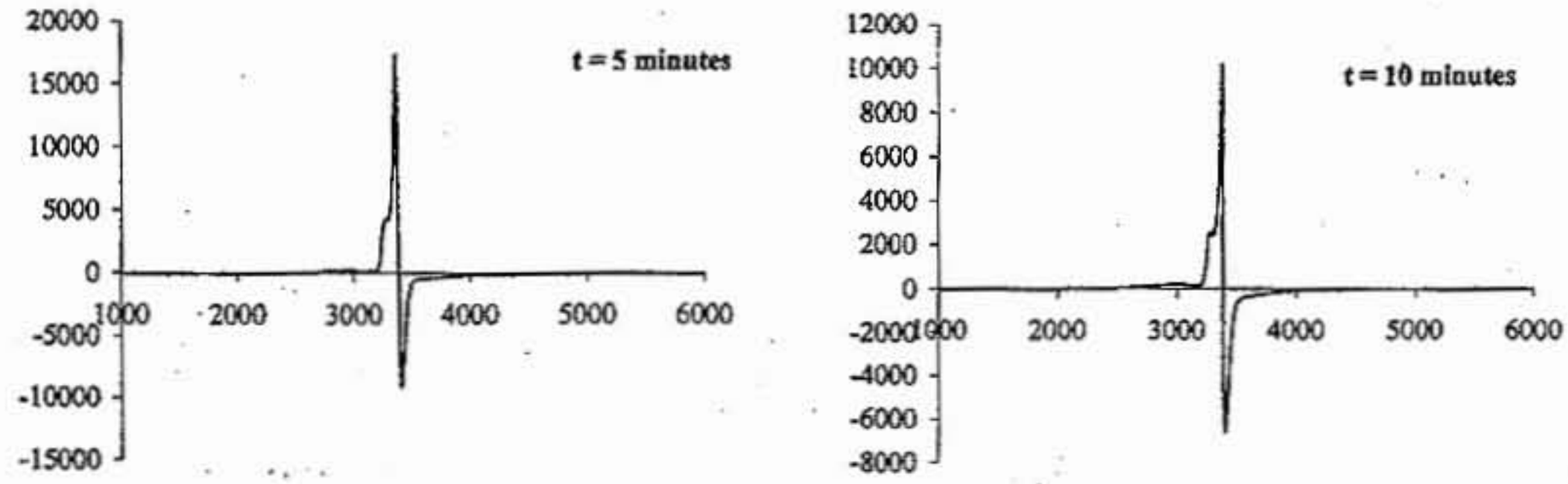

Figure 2.13. Monitoring the disappearance of the isotropic KO_2 signal in the absence of **$[Fe^{II}$(cyclam-PrS)$]^+$.** Select plots are shown here at t=5 and 10 minutes.

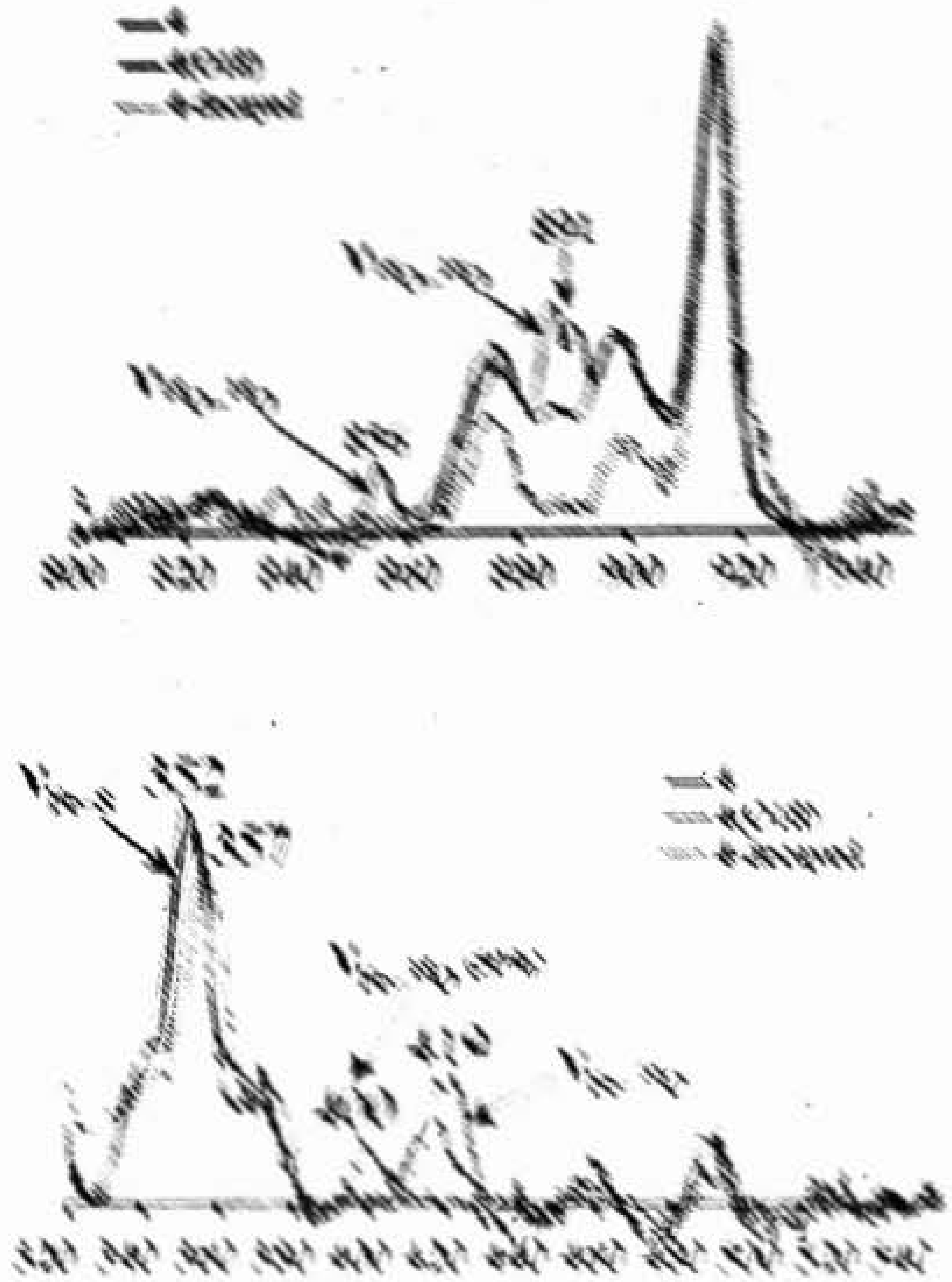

Figure 2.14. Resonance Raman spectra of $[Fe^{III}(cyclam\text{-}PrS)(OOH)]^+$. This data was collected in conjunction with Abhishek Dey and Ed Solomon (Solomon Group, Stanford University).

It is obvious from the vibrational data that the ν_{Fe-O} stretch of $[Fe^{III}(cyclam\text{-}PrS)(OOH)]^+$ (419 cm^{-1}) is unusually low, and the ν_{O-O} stretch (892 cm^{-1}) is unusually high, compared to other reported synthetic non-heme iron peroxo species.[43] However, it compares quite well with that of the only reported SOR peroxo species (ν_{Fe-O} = 438 cm^{-1} and ν_{O-O} = 850 cm^{-1}).[44] These vibrational data clearly illustrate the weakening of the Fe-O bond, and the stronger nature of the O-O bond, upon the introduction of a *trans* thiolate into the coordination sphere. This is the first direct evidence that the *trans* thiolate of

SOR plays a role in the reduction of superoxide to H_2O_2, by tuning the properties of the iron center to favor Fe-O bond cleavage over O-O bond cleavage.

Geometry optimized DFT calculations, performed by the Solomon Lab at Stanford University (Palo Alto, California), were used to estimate the most probable structure of **$[Fe^{III}$(cyclam–PrS)(OO(H)$]^+$ (Figure 2.15)**. These calculations estimated the Fe-S, Fe-O and O-O vibrations to be at 345 cm^{-1}, 400 cm^{-1} and 933 cm^{-1}, respectively. These values were found to be in good agreement with the experimental data. The corresponding calculated Fe-O and O-O frequencies for a high spin Fe^{III}-OOH complex with no thiolate ligand were predicted using **$[Fe^{III}(NH_3)_4$(OH)(OOH)$]^+$** as a model for the complex **$[Fe^{III}$(6-Me_3TPA)(OH)(OOR)]**.[34] The Fe-O and O-O stretching frequencies for **$[Fe^{III}(NH_3)_4$(OH)(OOH)$]^+$** were found to be 495 cm^{-1} and 923 cm^{-1}, thus reproducing the above mentioned experimental trend (involving a decrease in ν_{Fe-O} and an increase in ν_{O-O} upon thiolate coordination). These calculations also suggest that although the Fe-O σ bond is weakened significantly due to strong σ donation from the trans thiolate, the π-bonding between the O-O π^* orbital and the Fe^{III} center remains the same in both the trans-thiolate and trans-oxygen complexes. While both of these *trans*-positioned ligands compete for the same Fe dz^2 orbital for σ bonding, they form π bonds with different t_2 orbitals (the 3 half–occupied t_2 orbitals available in high-spin Fe^{III}). This would lead to an overall weakening of the Fe-O bond. Also, the weakening of the Fe-O σ bond leaves more electron density in the donor O-O bonding orbital which strengthens the O-O bond. Thus, our experimental observations are in good agreement with those predicted by the DFT calculations.

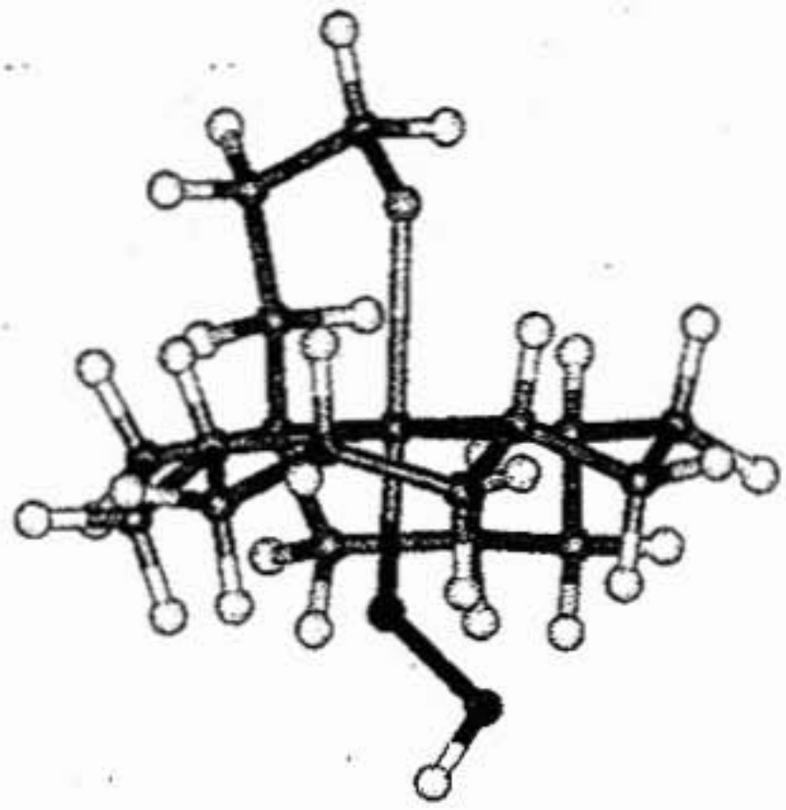

Figure 2.15. DFT geometry-optimized structure of **$[Fe^{III}$(cyclam–PrS)(OO(H)$]^+$.** Relevant distances (Å): Fe-S= 2.36, Fe-O= 1.95, Fe-N_{avg}= 2.18 and O-O= 1.44. The DFT calculations were performed by Abhishek Dey and Edward Solomon (Solomon Group, Stanford University.)

EXAFS of $[Fe^{II}$(cyclam–PrS)$]^+$ and $[Fe^{III}$(cyclam–PrS)(OOH)$]^+$. The reaction of **$[Fe^{II}$(cyclam–PrS)$]^+$** with KO_2 in the presence of MeOH formed an intermediate which we have identified as **$[Fe^{III}$(cyclam–PrS)(OOH)$]^+$.** However, because we were not able to isolate a solid crystalline stample of **$[Fe^{III}$(cyclam–PrS)(OOH)$]^+$** for x-ray crystallographic analysis, we attempted to gain physical characterization of this intermediate by using EXAFS, in a collaboration with Elena Slonkina and Britt Hedman (Stanford University). Comparisons with the **$[Fe^{II}$(cyclam–PrS)$]^+$** complex will hopefully lend insight into the electronic properties of this highly-reactive complex as related to SOR chemistry.

To begin with, a solid sample of **$[Fe^{II}$(cyclam–PrS)$]^+$** was isolated and crystallized three times from CH_2Cl_2/Et_2O. The data set for this sample was found to be well fit to a two-component first shell containing 4N and 1S.

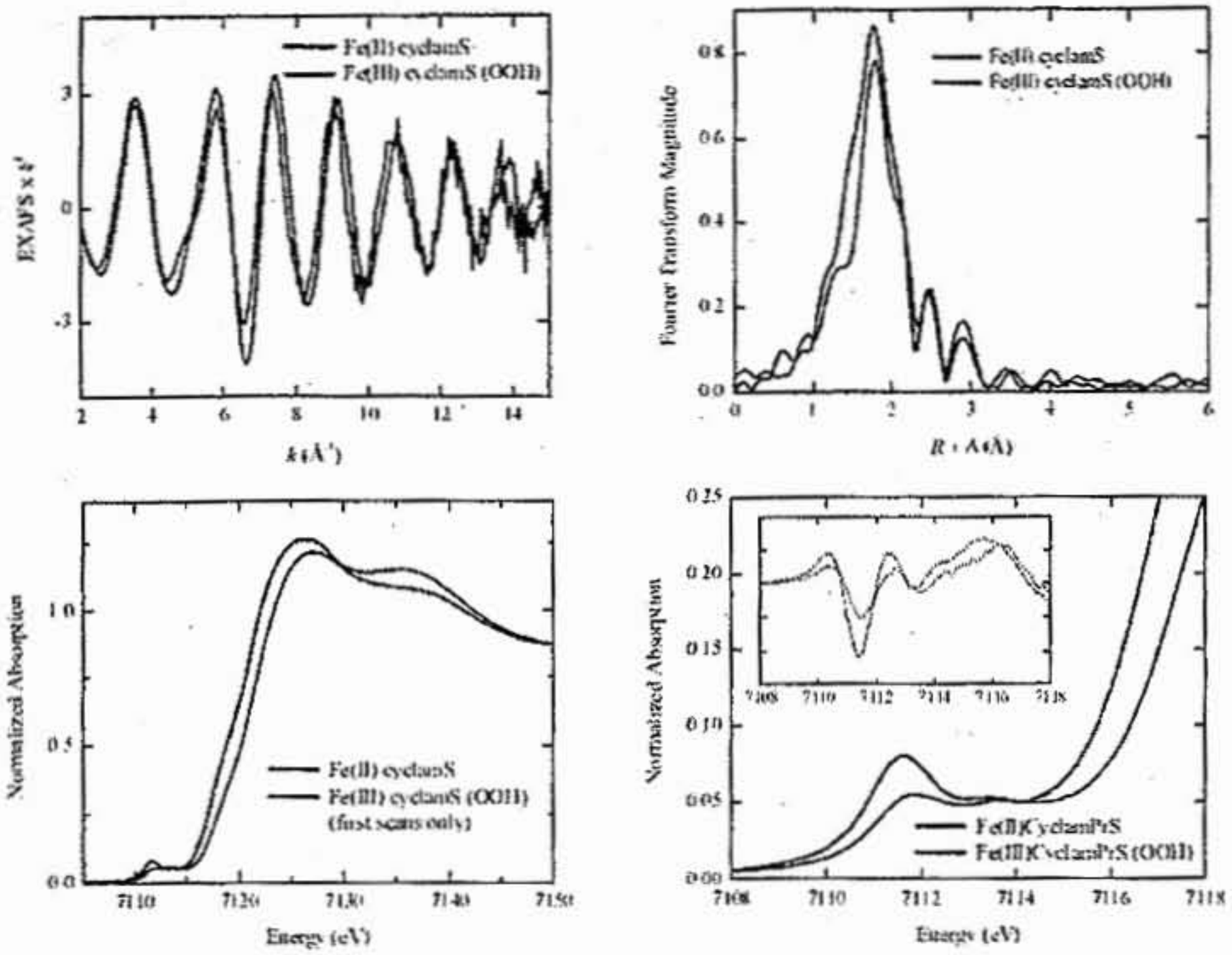

Figure 2.16. The EXAFS fits of the edge and pre-edge data collected from **$[Fe^{II}$(cyclam–PrS)$]^+$** (black) and **$[Fe^{II}$(cyclam–PrS)(OOH)$]^+$** (red). The edge and pre-edge fits for both complexes are shown here as overlay plots for ease of comparison between the Fe^{II} and Fe^{III}-OOH species, in order to illustrate the differences in coordination number and oxidation states between the two complexes. Data collected and provided by Elena Slonkina and Britt Hedman (Hedman Group, Stanford University.)

This intermediate in this case was generated in MeOH/EtOH (9:1), forming a purple solution. This purple intermediate had an obviously less intense pre-edge feature, indicating an increase in coordination number. This corresponds with the appearance of an additional atom in the first shell of this Fe^{III} intermediate's coordination sphere. Also, the pre-edge features are shifted to higher energies than those seen in the sample of **$[Fe^{II}$(cyclam–PrS)$]^+$**, which indicates an increase in the oxidation state of the sample. However, the distal oxygen was not observed. It was later concluded that this species

was actually the MeO$^-$-bound **[Fe^{III}(cyclam–PrS)](OMe)]$^+$,** which was found to be generated when the reaction with KO_2 was done in neat MeOH, as opposed to the conditions where **[Fe^{III}(cyclam–PrS)(OOH)]$^+$** formed in CH_2Cl_2 with MeOH added as a reagent (*vide infra*). The EXAFS data and fits are shown in **Figure 2.16.**

Characterization of [Fe^{III}(cyclam–PrS)OAc]$^+$ - Modeling the resting state of SOR. The addition of acetic acid (HOAc) to the metastable **[Fe^{III}(cyclam–PrS)(OOH)]$^+$** species at –78°C releases H_2O_2 and cleanly forms a new aqua blue species with an absorption band at 604 nm (ε= 1350 $M^{-1}cm^{-1}$) **(Figure 2.17).** When this reaction is monitored by EPR, the high–spin signal at g= 7.72, 5.40, 4.15 is replaced with a new low–spin signal at g= 2.37, 2.30, 1.89. The resonance Raman spectrum also changes dramatically: the ν_{O-O} and ν_{Fe-O} stretches disappear and new stretches are observed at 339, 409, and 421 cm^{-1}. **(Figure 2.18)** Additionally, the peaks associated with this species did not shift upon using $K^{18}O_2$ or ^{18}O-labeled acetic acid. This new low–spin species proved too unstable to isolate. However, this species was unambiguously identified as the acetate–bound **[Fe^{III}(cyclam–PrS)(OAc)]$^+$** using ESI mass spectrometry (M+1 = 387.3).[35] This species serves as a model for the glutamate–bound SOR resting **state.**

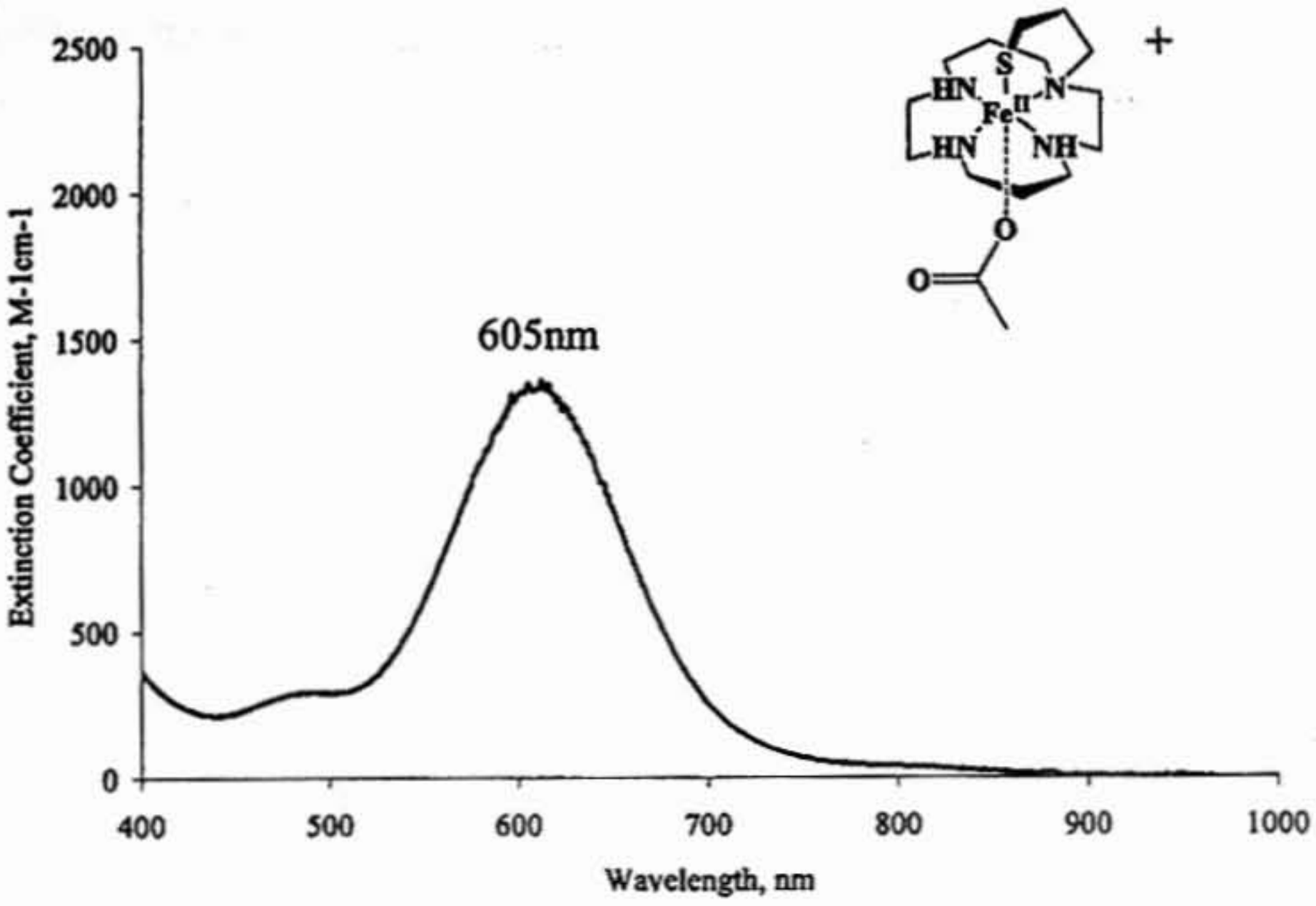

Figure 2.17. The absorption spectrum of the aqua blue species $[Fe^{III}(cyclam–PrS)OAc]^+$, formed by the addition of HOAc to the metastable $[Fe^{III}(cyclam–PrS)(OO(H)]^+$ species at –78°C.

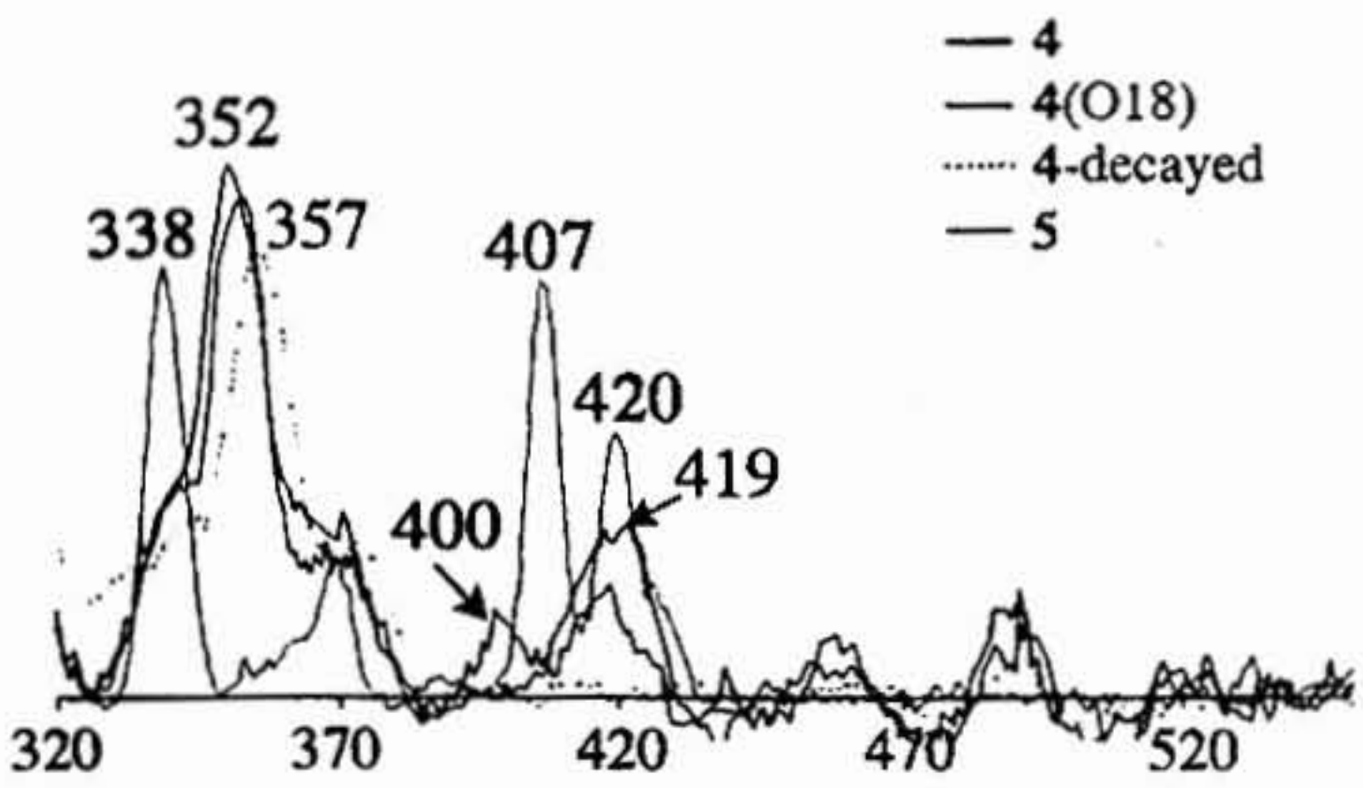

Figure 2.18. The resonance Raman spectra of $[Fe^{III}(cyclam–PrS)(OOH)]^+$ (black) and decay product $[Fe^{III}(cyclam–PrS)(OMe)]^+$ (dotted black). The data for $[Fe^{III}(cyclam–PrS)(OOH)]^+$ was collected using 571 nm excitation @193 K, and the data for the $[Fe^{III}(cyclam–PrS)(OAc)]^+$ (green) was collected using 600nm excitation @77K.

Catalytic turnover of $[Fe^{II}(cyclam–PrS)]^+$. In order to demonstrate the ability of **$[Fe^{II}(cyclam–PrS)]^+$** to act as a biomimetic catalyst, a sacrificial reductant, cobaltocene (Cp_2Co), was added to **$[Fe^{III}(cyclam–PrS)(OAc)]^+$** at low temperatures (–78°C) in order to regenerate reduced **$[Fe^{II}(cyclam–PrS)]^+$**. Subsequent addition of another stoichiometric equivalent of O_2^- regenerates the peroxide intermediate, which releases H_2O_2 upon the addition of another stoichiometric equivalent of HOAc, thereby completing the catalytic turnover, and demonstrating that reduction of O_2^- by **$[Fe^{III}(cyclam–PrS)(OOH)]^+$** is catalytic. Five clean turnovers have been achieved in this biomimetic cycle. The data for the catalytic cycle is shown in **Figure 2.19.**[36]

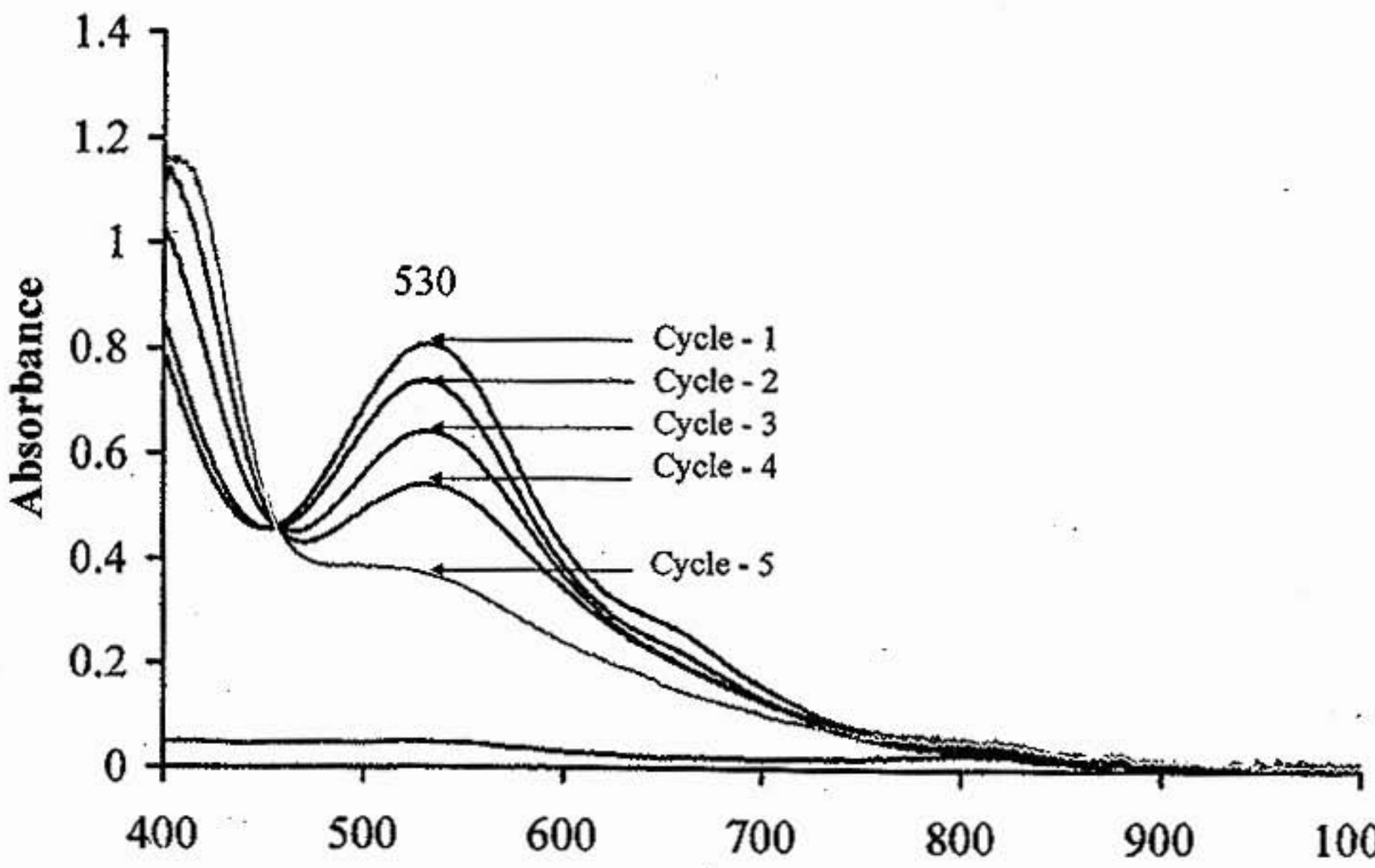

Figure 2.19. The catalytic turnover of **$[Fe^{II}(cyclam–PrS)]^+$**. Cobaltocene was used as a sacrificial reducing agent, providing the electron used to complete the cycle.

Detection of H_2O_2. In order to test for the formation of H_2O_2 during the reaction of $[Fe^{II}(cyclam–PrS)]^+$ with O_2^-, Amplex Red©, a colorimetric peroxidase assay, was used. Amplex Red is an assay that uses a reagent, 10-acetyl-3,7-dihydroxyphenoxazine as a colorimetric indicator. In the presence of horseradish peroxidase, the Amplex Red reagent reacts with H_2O_2 with a 1:1 stoichiometry to produce the resorufin molecule.[18] This reaction is shown in **Figure 2.17.** The resorufin molecule is highly fluorescent, and can be detected and quantified by its emission wavelength at λ_{em}= 585 nm (λ_{ex}= 570 nm). Alternatively, resorufin formation can also be monitored by UV-vis absorption spectroscopy by measuring its absorption band at λ_{max} = 570 nm.

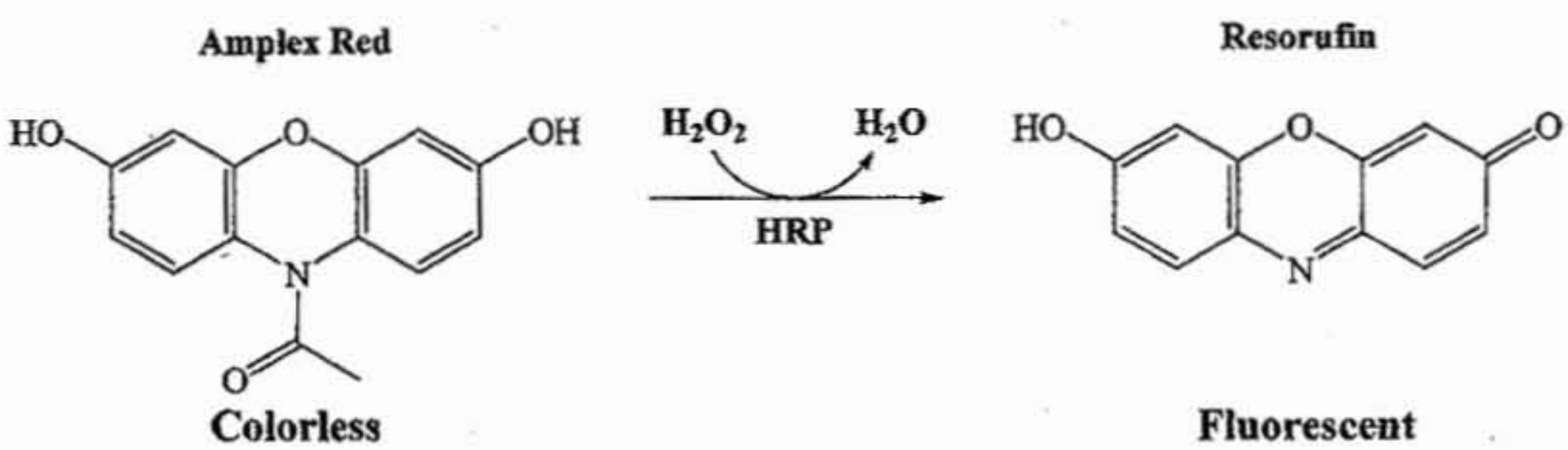

Figure 2.20. Formation of fluorescent resorufin indicator by the reaction of Amplex Red and H_2O_2.

A caveat to using enzymatic assays is that they are usually only effective in water. Non-aqueous solvents do not necessarily destroy the enzyme *per se*, but often denature the protein H-bonding backbone of the enzyme, causing the loss of most, if not all, enzymatic activity, rendering the enzyme and assay useless.[37,38] This was tested and shown independently in our lab, using solvents such as methanol, THF, DMF, acetonitrile,

and isopropanol. However, **$[Fe^{III}$(cyclam–PrS)(OOH)$]^+$** is a very thermodynamically unstable intermediate, and the reactions with this complex must be done in solvents that can be cooled to extremely reduced temperatures, ideally $\leq$-78°C, in order to slow the decomposition process of **$[Fe^{III}$(cyclam–PrS)(OOH)$]^+$**. Additionally, under aqueous conditions, superoxide ion will undergo spontaneous disproportionation to form H_2O_2 and O_2 as the ultimate products.[39] Since H_2O_2 is also a product of this reaction, a number of control experiments are required in order to determine if the source of H_2O_2 formed during the reaction was from the spontaneous disproportionation of superoxide ion, or if its formation was metal-mediated.

However, it was found that dichloromethane and acetone could be used in conjunction with the Amplex Red peroxidase assay, provided that the ultimate concentration of the organic solvent in the assay was kept to a minimum. Dichloromethane was the first solvent tried of the two and surprisingly showed promise, despite its nature as one of the more aggressive organic solvents. It was reasoned that because the dichloromethane/water mixture in the assay was biphasic, the H_2O_2 formed during the reaction was extracted into the aqueous layer as soon as the reaction aliquot was added to the assay mixture, while simultaneously keeping the assay free of any dichloromethane, due to its hydrophobic nature. However, the efficacy of the enzyme was still lowered substantially, leading to the desire for a solvent that was less aggressive towards the enzyme. Acetone has also surprisingly been shown in several instances to co-exist with peroxidase enzymes in assays, with minimal denaturing of the enzyme, provided the concentration of acetone in the assay was kept to a minimum.[40] The

reaction between **$[Fe^{II}(cyclam–PrS)]^+$** and superoxide was then performed under an argon atmosphere in acetone at -78°C (acetone/CO_2), and MeOH was used as the proton source. After the intermediate formation was complete (monitored by UV-vis absorption), 1 equivalent of acetic acid was added, forming the **$[Fe^{III}(cyclam–PrS)(OAc)]^+$** species and completing the reduction of $O_2^{\cdot}$ to H_2O_2. An aliquot of this sample was then extracted and injected into a quartz fluorescence cell containing a standardized amount of the Amplex Red assay. It should be noted that the Amplex Red assay is extremely photosensitive, so the reaction was carefully performed in the dark, and the reaction cell and the fluorescence cell was generously covered with aluminum foil. The formation of the resorufin product was seen in the fluorescence spectrum, and was indicative of H_2O_2 formation during this reaction. **(Figure 2.21)**

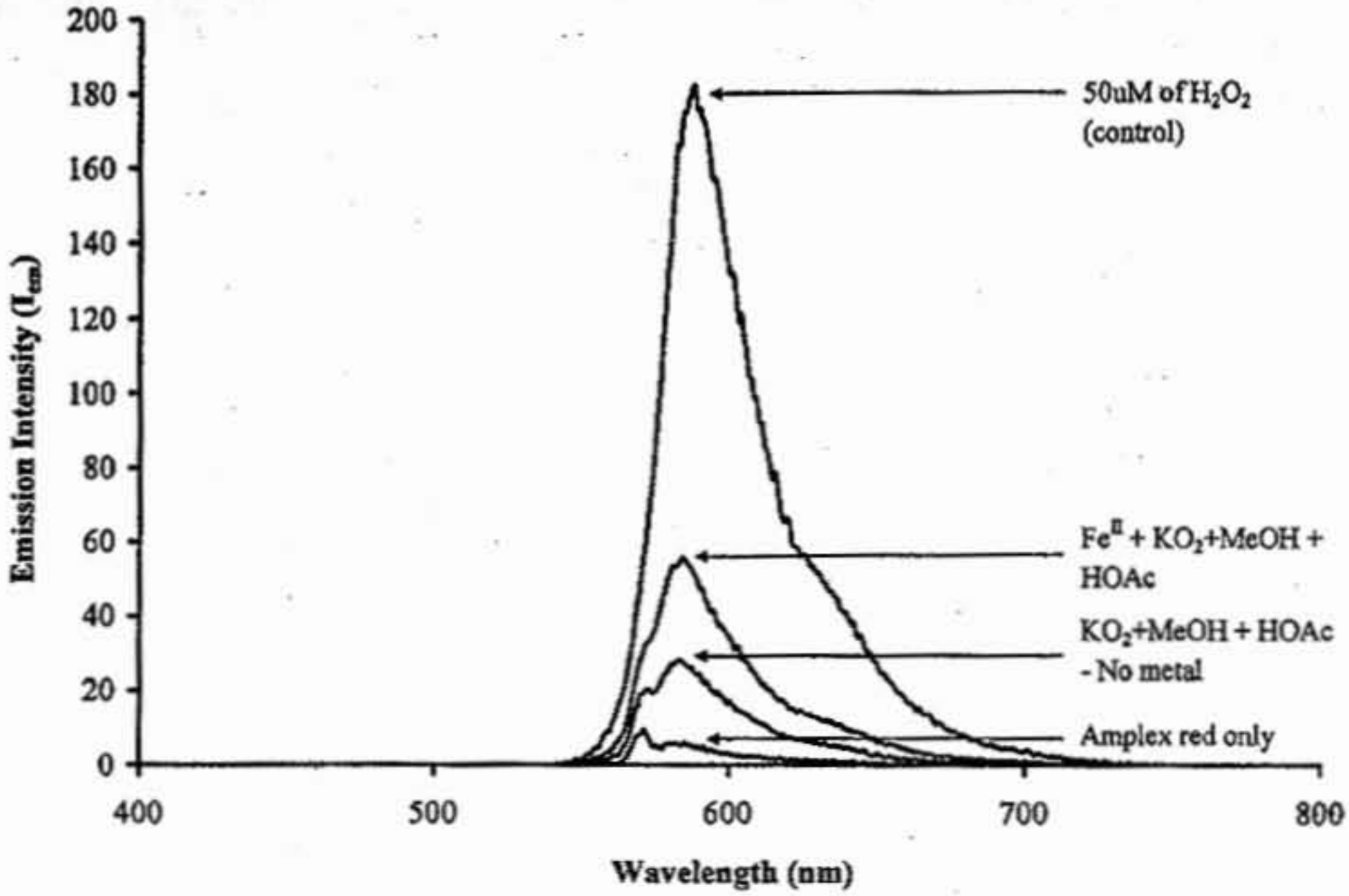

Figure 2.21. Amplex Red Assay and relevant control experiments. The control experiments consist of the 1X phosphate buffer, the assay, KO_2 + MeOH + assay with no metal, and 1 equiv of H_2O_2 + assay.

In order to verify that the H_2O_2 formed during this reaction was indeed metal-mediated and not a result of spontaneous disproportionation of superoxide, several control experiments were performed. First, the reaction was repeated, sans the **$[Fe^{II}$(cyclam–PrS)$]^+$** complex. The Amplex Red assay activity was also analyzed in a sample containing the identical amount of acetone, in order to roughly estimate the denaturing effect that the requisite amount of acetone had on the enzyme. Isolated samples of the assay and the 1X phosphate buffer solution used in the assay were also analyzed. The results clearly show that the majority of the activity seen by the Amplex Red assay was due to the metal-mediated reduction of superoxide to H_2O_2. **(Figure 2.21)** This shows qualitatively that the **$[Fe^{II}$(cyclam–PrS)$]^+$** complex is able to perform SOR

chemistry. The reaction was estimated to have an efficacy of roughly 30%. An exact quantification of the amount of H_2O_2 produced by this reaction has not yet been established, and should be the target of future work.

Identifying the low-spin component formed during the formation of $[Fe^{III}$(cyclam–PrS)OOH$]^+$. In the EPR spectrum of each sample of **$[Fe^{III}$cyclam-PrS(OOH)$]^+$** performed in aprotic solvents (i.e. 2-MeTHF, DCM, etc.), there was noticeably always a small amount of low-spin component present, along with the high spin component that we identified initially as the **$[Fe^{III}$cyclam-PrS(OOH)$]^+$** species **(Figure 2.22)**. This low-spin component was characterized as having g-values of g=2.26, 2.11, 1.91.

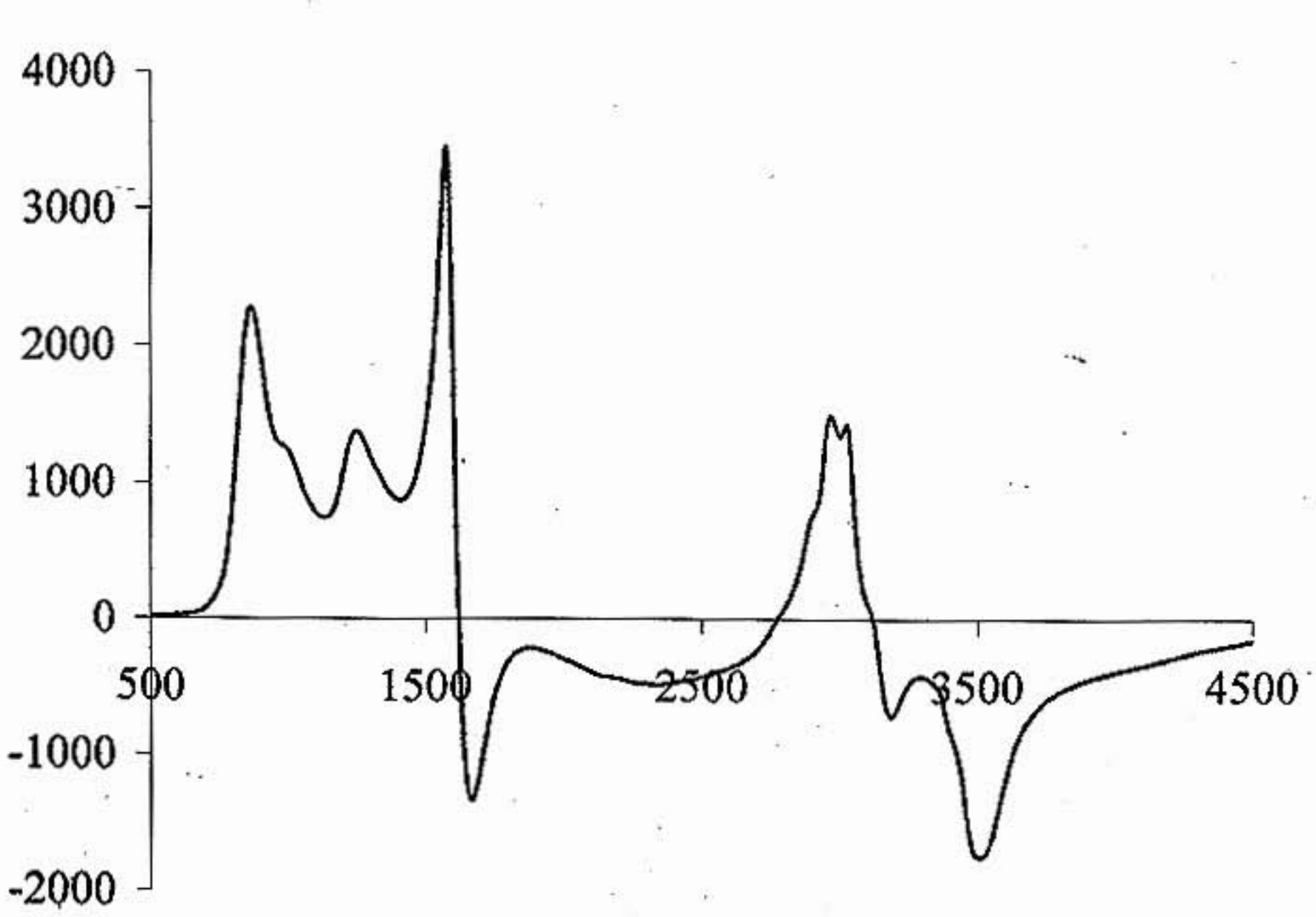

Figure 2.22. The EPR of **$[Fe^{III}$(cyclam–PrS)OOH$]^+$** in 2-MeTHF glass. This is the full spectrum of the experiment shown in **Figure 2.11**, showing both the low-spin and high-spin components that are formed during the reaction.

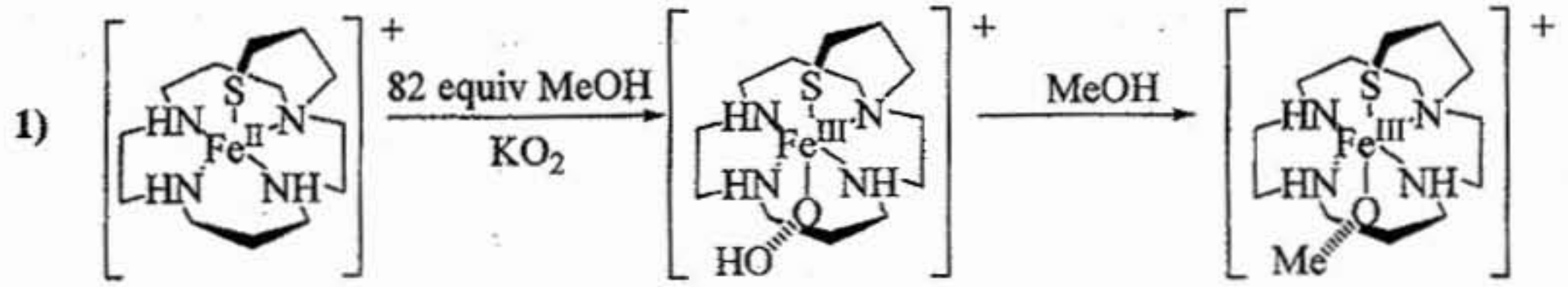

Figure 2.23. Possible identities of the low-spin component seen in the reaction of **$[Fe^{II}$(cyclam–PrS)$]^+$** with KO_2 and MeOH.

Our working hypothesis led us to three possible identities for this low-spin species. These possibilities are shown in **Figure 2.23**, and included **$[Fe^{III}$cyclam-PrS(OMe)$]^+$**, generated after the release of H_2O_2 from **$[Fe^{III}$cyclam-PrS(OOH)$]^+$**, **$[Fe^{III}$cyclam-PrS$]^{2+}$**, also formed after the release of H_2O_2 from the **$[Fe^{III}$cyclam-PrS(OOH)$]^+$** intermediate, or **$[Fe^{III}$cyclam-PrS(MeOH)$]^{2+}$**, also be formed after the release of H_2O_2 from the **$[Fe^{III}$cyclam-PrS(OOH)$]^+$** intermediate.

In order to test for the presence of these species, preliminary absorption experiments were done, in an effort to generate and identify these species *in situ* based on their λ_{max}. To generate these oxidized species, ferrocenium hexafluorophosphate

($FeCp_2PF_6$), a common chemical oxidant, was used. Ferrocenium was added to **$[Fe^{III}$cyclam-PrS$]^+$** both in the absence and presence of MeOH, and both in the absence and presence of base, in order to generate five–coordinate, methanol– and methoxide–bound species.

The first experiment led to the formation of a blue species, with a λ_{max}=558nm, shown in **Figure 2.24.** Notably, the reaction required a second equivalent of $FeCp_2PF_6$ to push it to completion. After no further change in the absorbance was observed, the reaction was deemed complete. This species was preliminarily identified as the methanol-bound **$[Fe^{III}$cyclam-PrS(MeOH)$]^{2+}$** species.

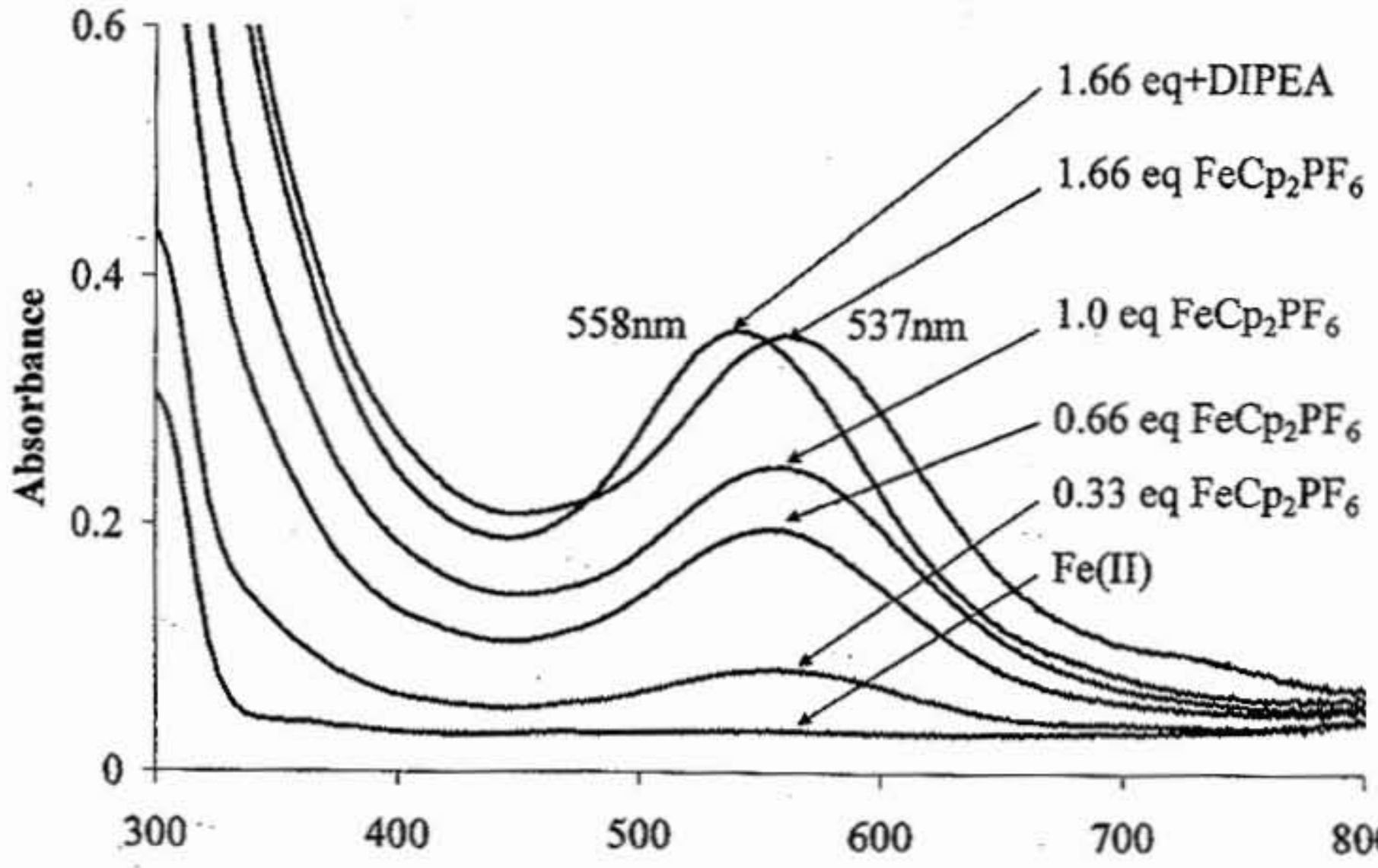

Figure 2.24. The reaction of **$[Fe^{II}$cyclam-PrS$]^+$** and $FeCp_2PF_6$ in MeOH. The reaction was followed by the addition of DIPEA (Hünig's Base).

One equivalent of Hünig's base (diisopropylethylamine – DIPEA) was then added, leading to the immediate formation of a maroon species and a corresponding blue shift of 20nm to a new λ_{max} = 538nm. The formation of both species with the respective observed blue shift is shown in **Figure 2.24.** This species was preliminarily identified as the methoxide-bound **[Fe^{III}cyclam-PrS(OMe)]$^{+}$** species.

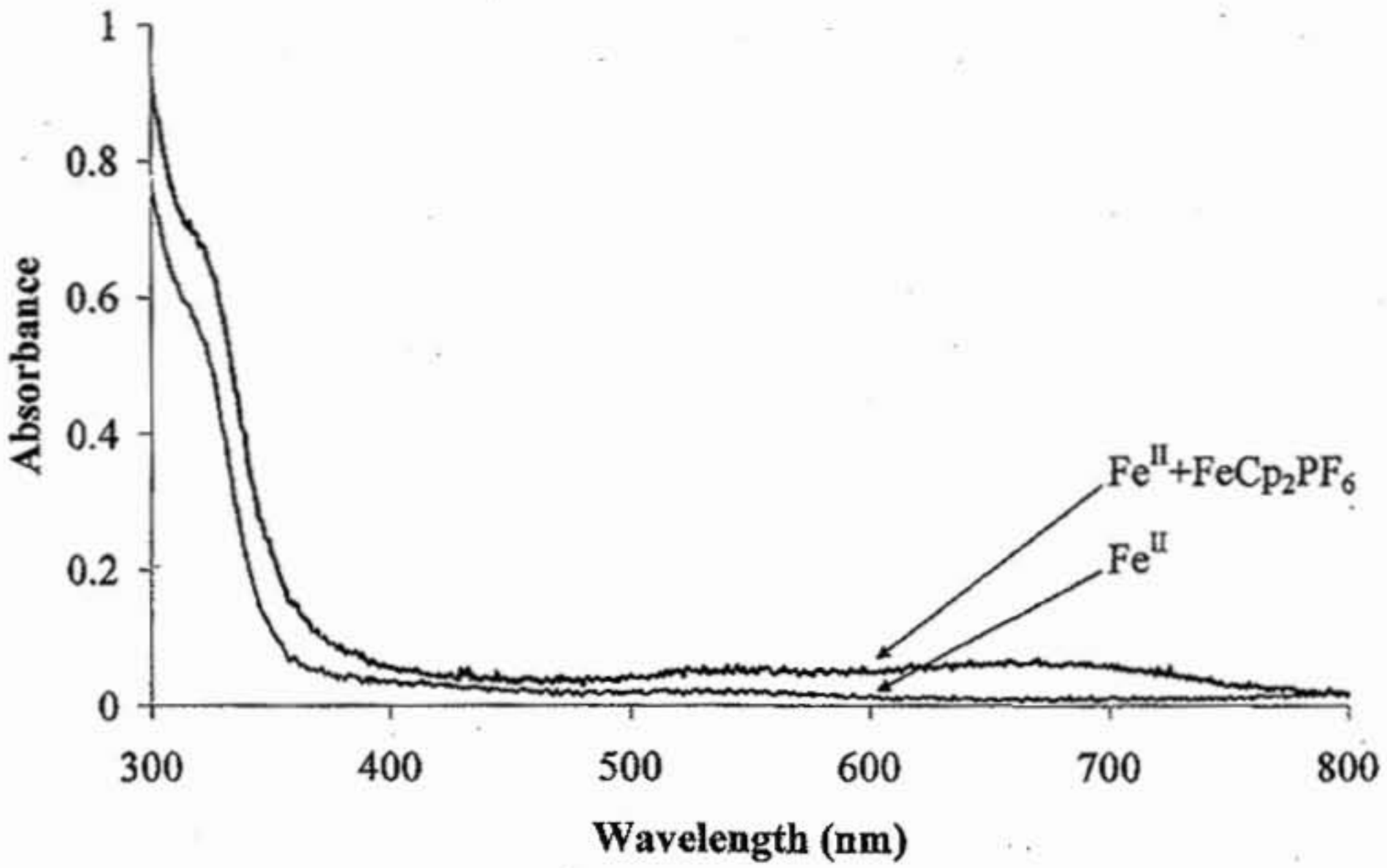

Figure 2.25. The reaction of **[Fe^{II}cyclam(Pr-S)]$^{+}$** and $FeCp_2PF_6$ in DCM @ -80°C.

This reaction was repeated in CH_2Cl_2 **(Figure 2.25)**, but no reaction was observed, even with the addition of excess $FeCp_2PF_6$. In order to explain this, it was reasoned that going from a five-coordinate, monocationic Fe^{II} species to a five-coordinate, dicationic Fe^{III} species was not thermodynamically favorable, and would probably require the presence of a stronger oxidant. CH_2Cl_2 is also a non-coordinating solvent, which left the

reaction completely absent of a possible sixth ligand. There are relatively few examples of five-coordinate Fe^{III} species, as the Fe^{III} center prefers to be six-coordinate.[41] Thus, this species could not be generated under these conditions.

These reactions were also studied by EPR. **$[Fe^{III}$cyclam-PrS(OMe)$]^+$**, generated from the addition of $FeCp_2PF_6$ and DIPEA to **$[Fe^{II}$cyclam-PrS$]^+$** in MeOH **(Figure 2.26)**, was found to yield a low-spin species (g=2.25, g=2.14, g=1.89), which corresponded nicely with that of the low-spin component seen during the reduction of superoxide by **$[Fe^{II}$cyclam-PrS$]^+$**. From this, it was concluded that the low-spin component was due to **$[Fe^{III}$cyclam-PrS(OMe)$]^+$**. This was a significant result because it showed the extreme lability of the Fe-O bond and the higher pKa of the proximal peroxo oxygen compared to other peroxos, as well as the distal peroxo oxygen. Most likely, the *trans* positioning of the thiolate is responsible. The high-spin state of the **$[Fe^{III}$cyclam-PrS(OOH)$]^+$** species undoubtedly contributes to the weakening of the Fe-O bond. This is undoubtedly influenced by the *trans* positioning of the thiolate as well, because while this reaction occurs with **$[Fe^{III}N_4$(tren)$S^{Me}(OOH)^2]^+$**, it does so on a much slower timescale, as opposed to the first four minutes of the reaction with **$[Fe^{III}$cyclam-PrS(OOH)$]^+$**.

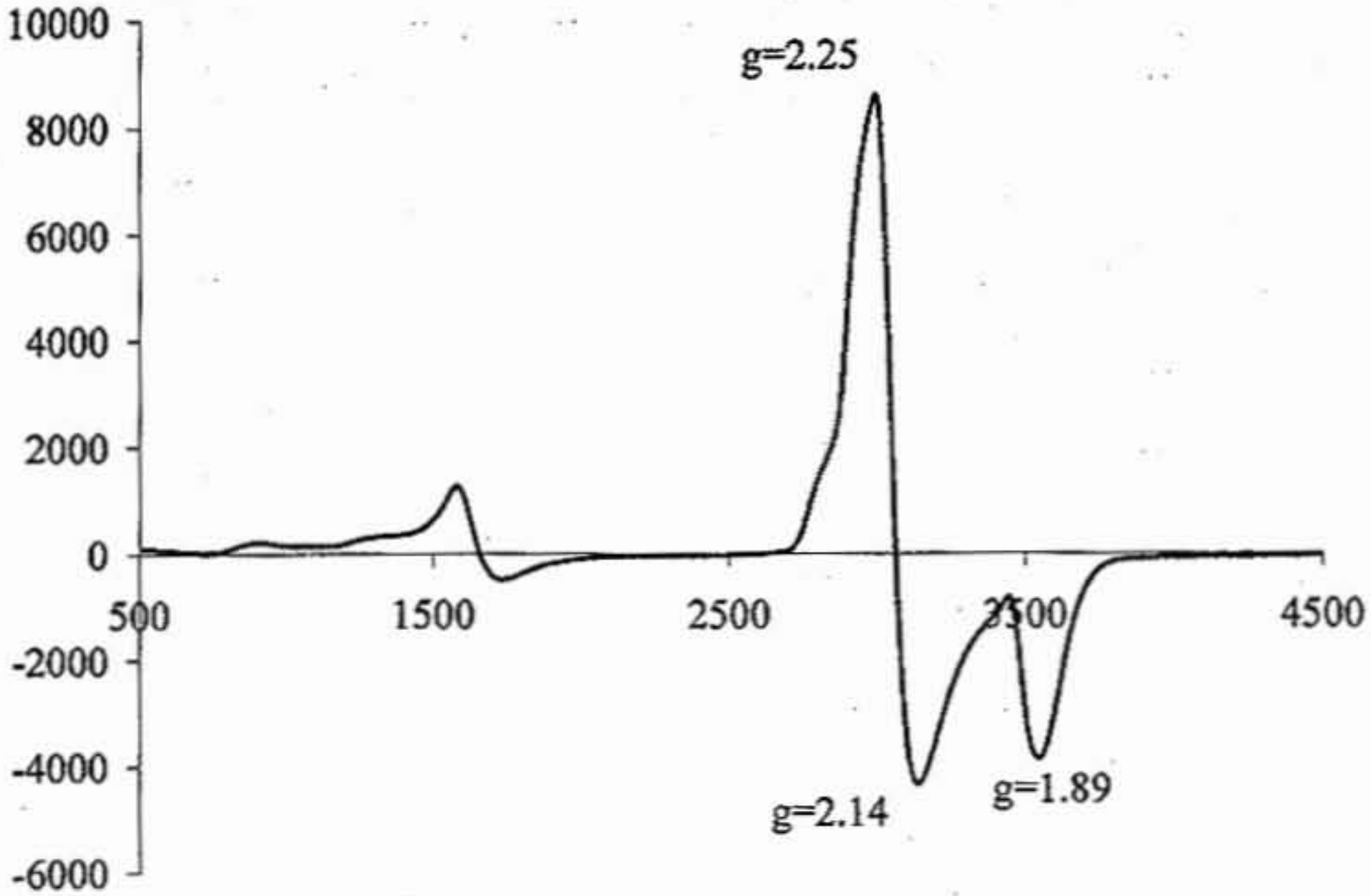

Figure 2.26. The EPR spectrum of the reaction between **[Fe^{II}cyclam-PrS]$^+$**, Hunig's base and $FeCp_2PF_6$ in MeOH/EtOH (9:1).

Alternative proton sources. The use of alternative proton sources in the reduction of O_2^- by **[Fe^{II}cyclam-PrS]$^+$** was explored. This was done because when this reaction was studied by EPR, there was always a small amount of a low-spin component, presumably the methoxide-bound **[Fe^{III}cyclam-PrS(OMe)]$^+$**, in each experiment, the formation of which was discussed earlier. The inherent problem with using methanol as a proton source is that its conjugate base is the methoxide ion (MeO^-), which is strongly nucleophilic. The presence of MeO^- could possibly displace the peroxo moiety from the metal, forming the more thermodynamically favorable MeO^--bound Fe^{III} species. Undoubtedly, the use of methanol has some destabilizing effect on the transient

[Fe^{III}cyclam-PrS(OOH)]$^+$ species. Thus, we sought to use alternative proton sources that could possibly avert this issue.

The reactive and highly unstable nature of the **[Fe^{III}cyclam-PrS(OOH)]$^+$** requires the use of aprotic organic solvents that can be cooled to cryogenic temperatures (≤-78°C). Low temperatures are necessary in order to aggregate a significant amount of the hydroperoxo intermediate for characterization. In addition, solubility issues also govern the solvent choice for these reactions. Avoiding the use of solvents that do not fit these criteria limits the solvent choices to acetonitrile, dichloromethane and THF, which are readily available in our lab and rigorously dried.

Another drawback caused by working in solvents such as acetonitrile, dichloromethane and THF is that measured pKas of acids are naturally reported in water, and the pKas reported in organic solvents is limited to DMSO and DMF. The acids were thus initially chosen based on having neutral, weakly or non-coordinating conjugated bases. Diisopropylethylammonium tetrafluoroborate (DIPEA • HBF_4), ammonium hexafluorophosphate (NH_4PF_6), hexafluoroisopropyl alcohol (HFI), and phenol were chosen based on these criteria. The structures of these acids are shown in **Figure 2.27**.

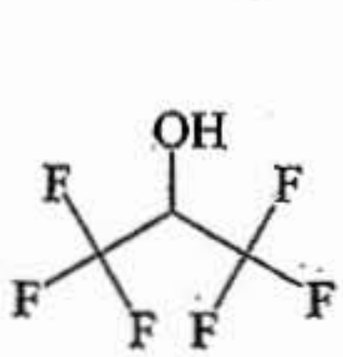

hexafluoroisopropanol

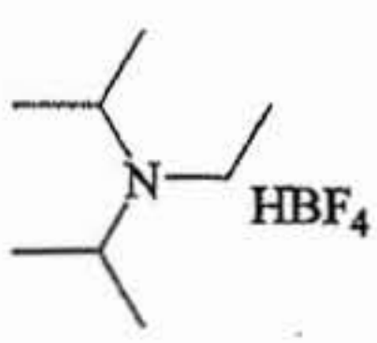

Diisopropylethylammonium tetrafluoroborate

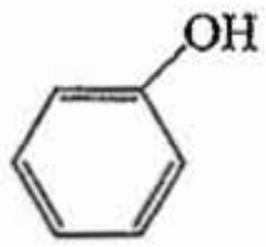

phenol

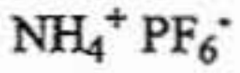

ammonium hexafluorophosphate

Figure 2.27. Alternative proton sources to use in the SOR catalytic cycle.

Diisopropylethylammonium tetrafluoroborate (DIPEA • HBF_4) was synthesized by first dissolving diisopropylethylamine (DIPEA – Hünig's base) in dry ether. The addition of HBF_4 caused the immediate deposition of the ammonium salt, which was then filtered out of solution and dried under vacuum. The addition of 1 equivalent of DIPEA • HBF_4 to **[Fe^{II}cyclam-PrS]$^+$** + KO_2 in CH_3CN caused the formation of a purple species, with an broad absorption band at λ_{max} = 540nm. The spectrum is shown in **Figure 2.28.** The addition of a second equivalent of DIPEA • HBF_4 caused this band to maximize. However, this band was very broad and not as well-defined as that seen when methanol was used as the proton source and the equivalents were controlled. The lack of a distinct sharp band led to the assumption that a mixture of species was present.

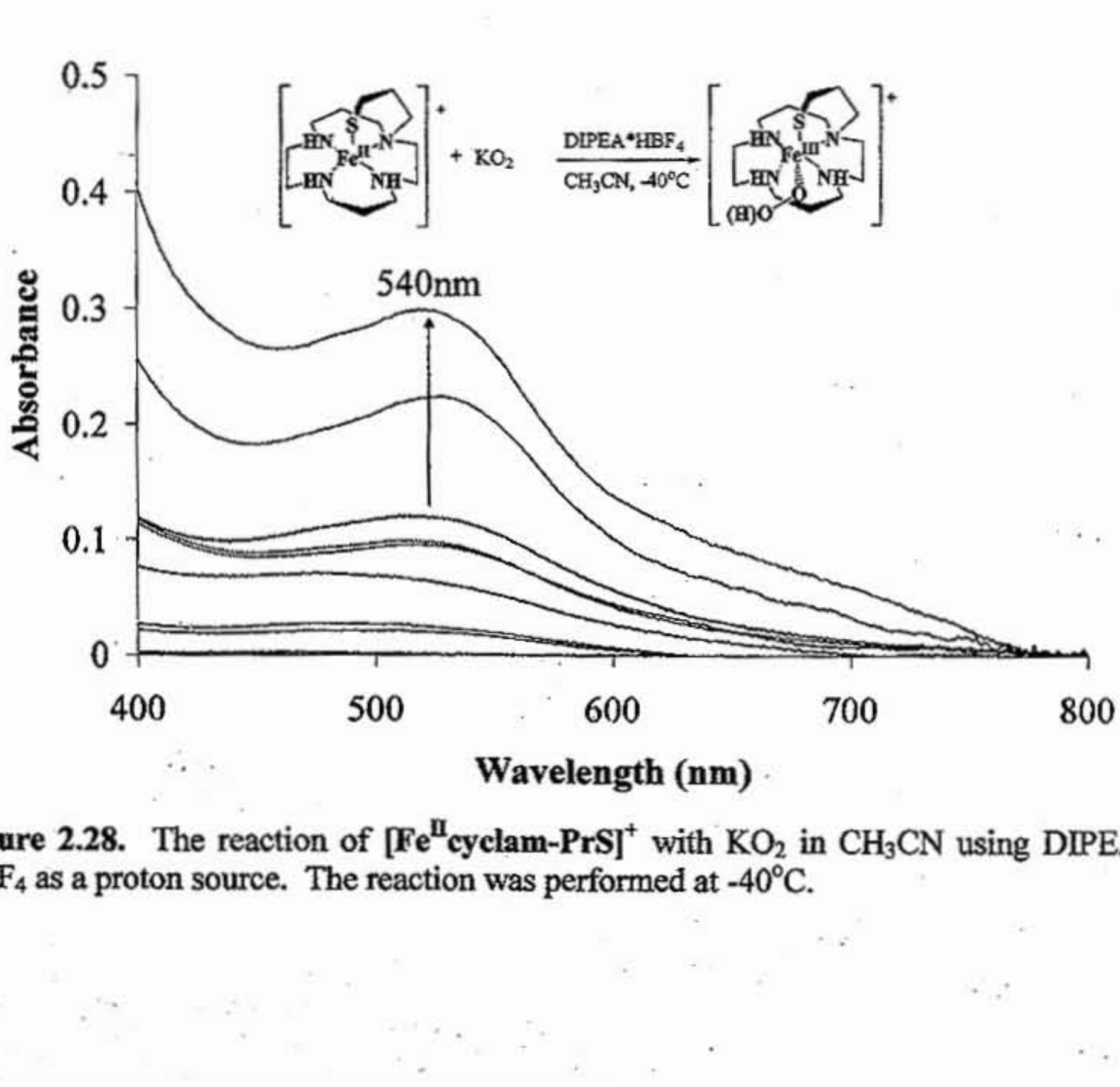

Figure 2.28. The reaction of **[Fe^{II}cyclam-PrS]$^+$** with KO_2 in CH_3CN using DIPEA • HBF_4 as a proton source. The reaction was performed at -40°C.

The above reaction was repeated in methanol (prior to the observation of the low-spin methoxide-bound component in the EPR.) The addition of 1 equivalent of DIPEA • HBF_4 to **$[Fe^{II}$cyclam-PrS$]^+$** + KO_2 in CH_3CN caused the formation of a purple species, with a broad absorption band at λ_{max} = 543nm. The spectrum is shown in **Figure 2.29.** Due to the broad character of this band and its estimated λ_{max} = 540 nm, it was assumed that this species was not purely the peroxo-bound **$[Fe^{III}$cyclam-PrS(OOH)$]^+$** species, and that that the methoxide-bound species was also present. The reaction was not pursued beyond this point.

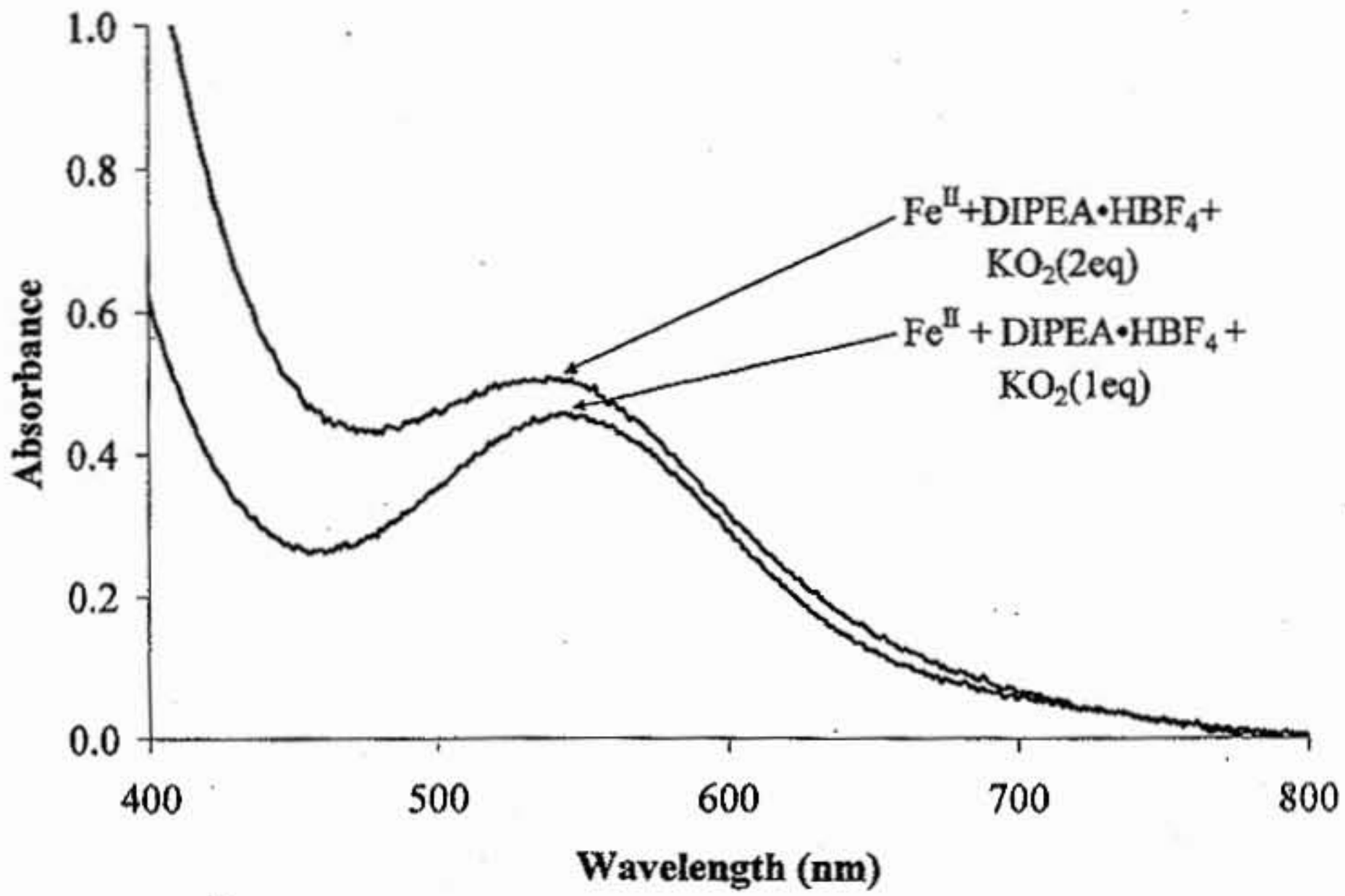

Figure 2.29. The reaction of **$[Fe^{II}$cyclam-PrS$]^+$** with KO_2 in MeOH using DIPEA • HBF_4 as a proton source. The reaction was performed at -78°C.

NH_4PF_6 was the next acid tested. Due to solubility issues, the reaction was performed in THF at -78°C. The addition of 1 equivalent of NH_4PF_6 caused the slow

formation of a very faint sky blue solution, with a very weak band at 613nm. The addition of 2 equivalents of NH_4PF_6 caused this band to intensify and blue shift to a new broad band at 583nm. This data is shown in **Figure 2.30**. The spectrum was not clearly that of a single species in solution, so the use of NH_4PF_6 was not pursued beyond this point.

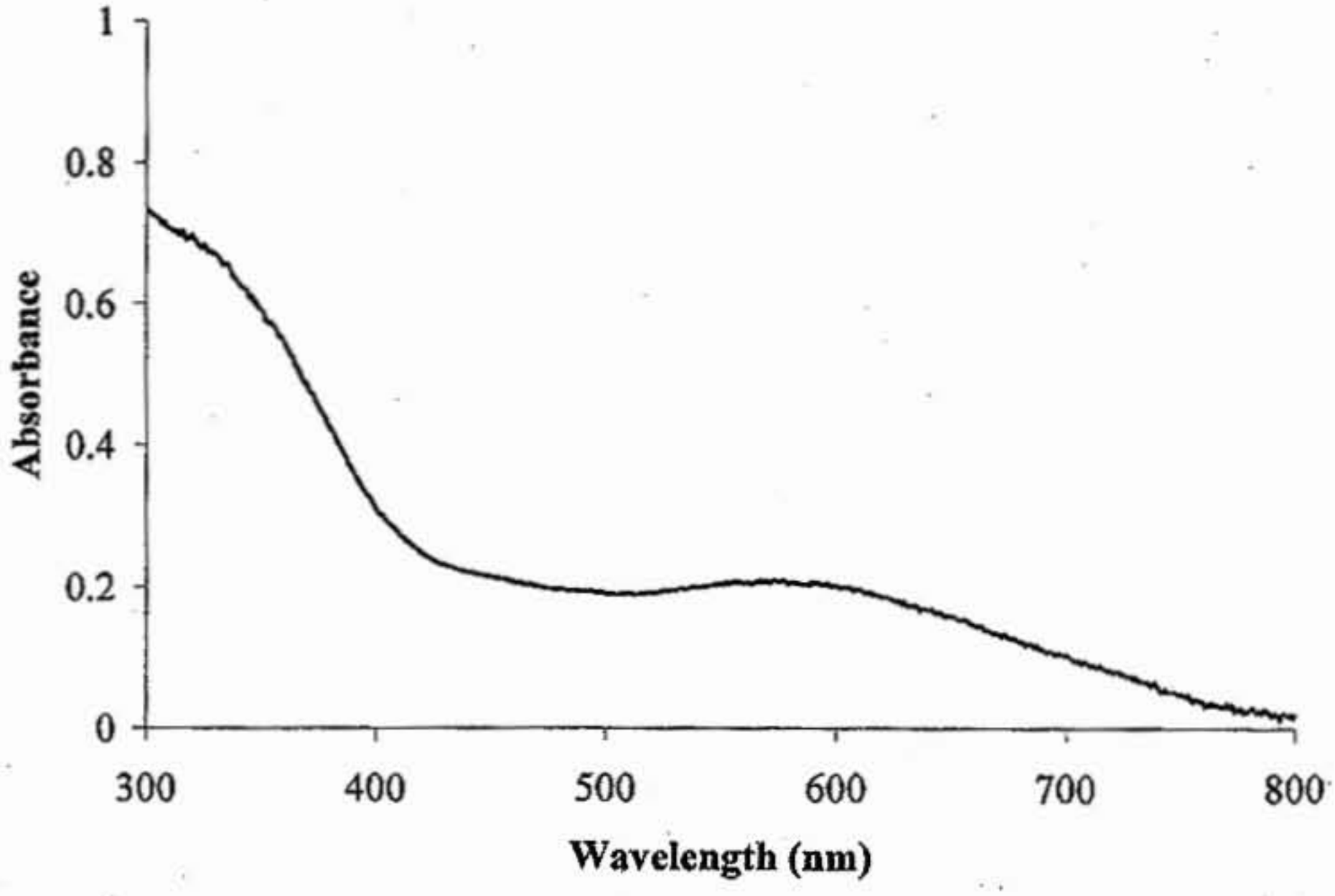

Figure 2.30. The reaction of $[Fe^{II}$**cyclam-PrS**$]^+$ with KO_2 in CH_2Cl_2 using NH_4PF_6 as a proton source. The reaction was performed at -78°C.

Hexafluoroisopropanol (HFI) was then tested as a proton source in dichloromethane and acetonitrile. The results were interesting, as the presence of at least three distinct species was observed. The addition of 1 equivalent of HFI in dichloromethane caused the initial formation of a band at 530 nm. The addition of another equivalent of HFI caused the red shift of this band to 561nm, accompanied by a

strong increase in intensity of the band. Upon warming, this band red shifted to 571nm and began to lose its intensity. After 30 minutes the band lost much of its intensity and red shifted again to 607nm. This data is shown in **Figure 2.31**.

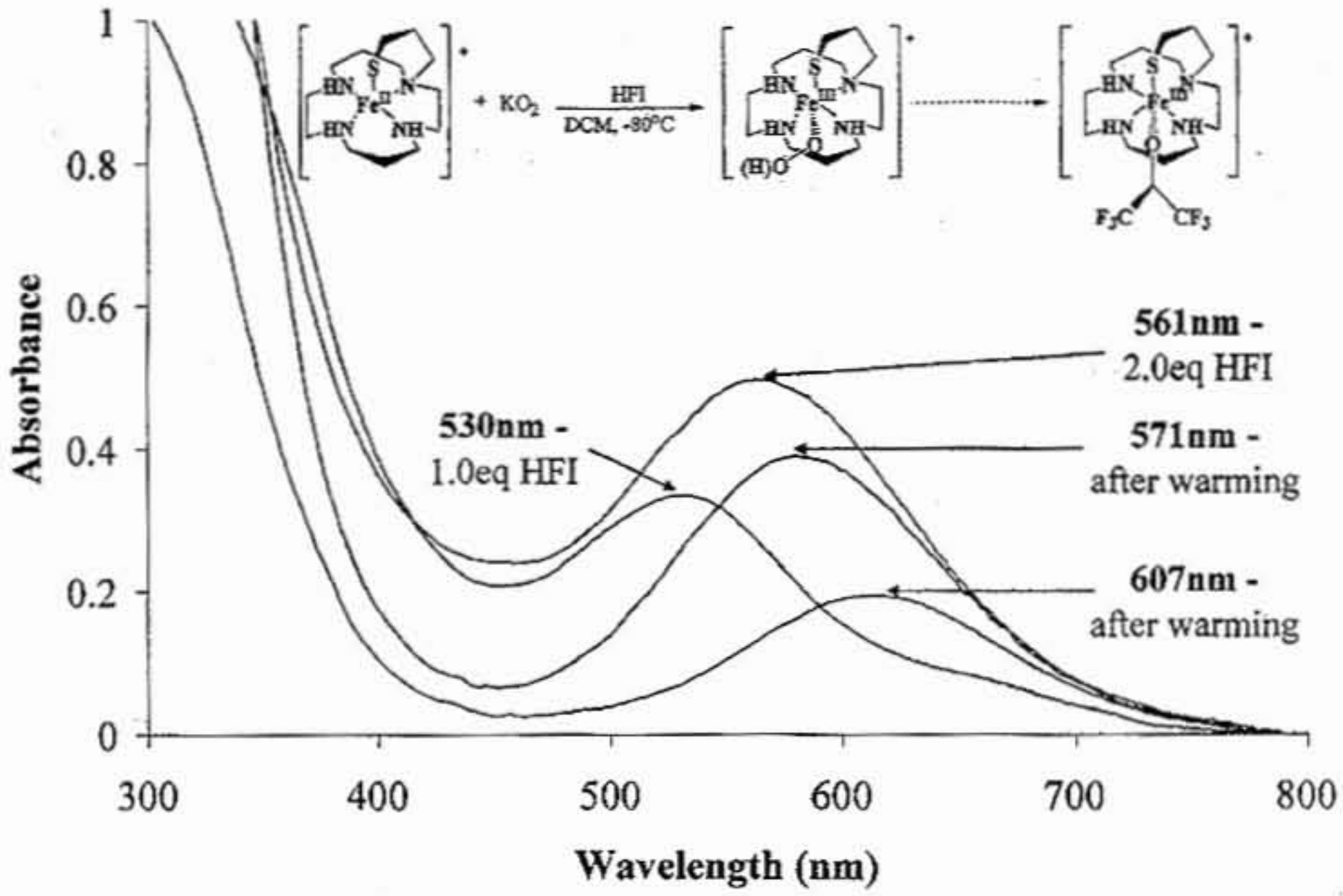

Figure 2.31. The reaction of $[Fe^{II}cyclam\text{-}PrS]^+$ with KO_2 in CH_2Cl_2 using HFI as a proton source. The reaction was performed at -78°C.

This experiment was repeated in acetonitrile at -40°C. The addition of 1 equivalent of HFI to this solution caused the slow growth of a weak absorption band at 500 nm. The addition of another equivalent of HFI caused the growth and subsequent red shift of this band to 561 nm. Upon warming, this band red shifted to an ultimate wavelength of 577 nm, and also lost much of its intensity.

The experiment using phenol as the proton source was done in CH_2Cl_2 at -78°C. The addition of 0.2 equivalents of phenol caused the immediate color change of the colorless **[Fe^{II}cyclam-PrS]$^+$** + O_2^- solution to a purple color, synonymous with the appearance of an absorption band at 522 nm. After the addition of 0.6 equivalents of phenol, the absorption band gradually red shifted to 527 nm and became much broader and asymmetric. After 1 equivalent of phenol was added, the solution attained a very intense purple color and also formed a new absorption band at 560nm, notably extremely broad and intense. Excess phenol was then added, but no further change was observed. The spectrum of this experiment is shown in **Figure 2.32.**

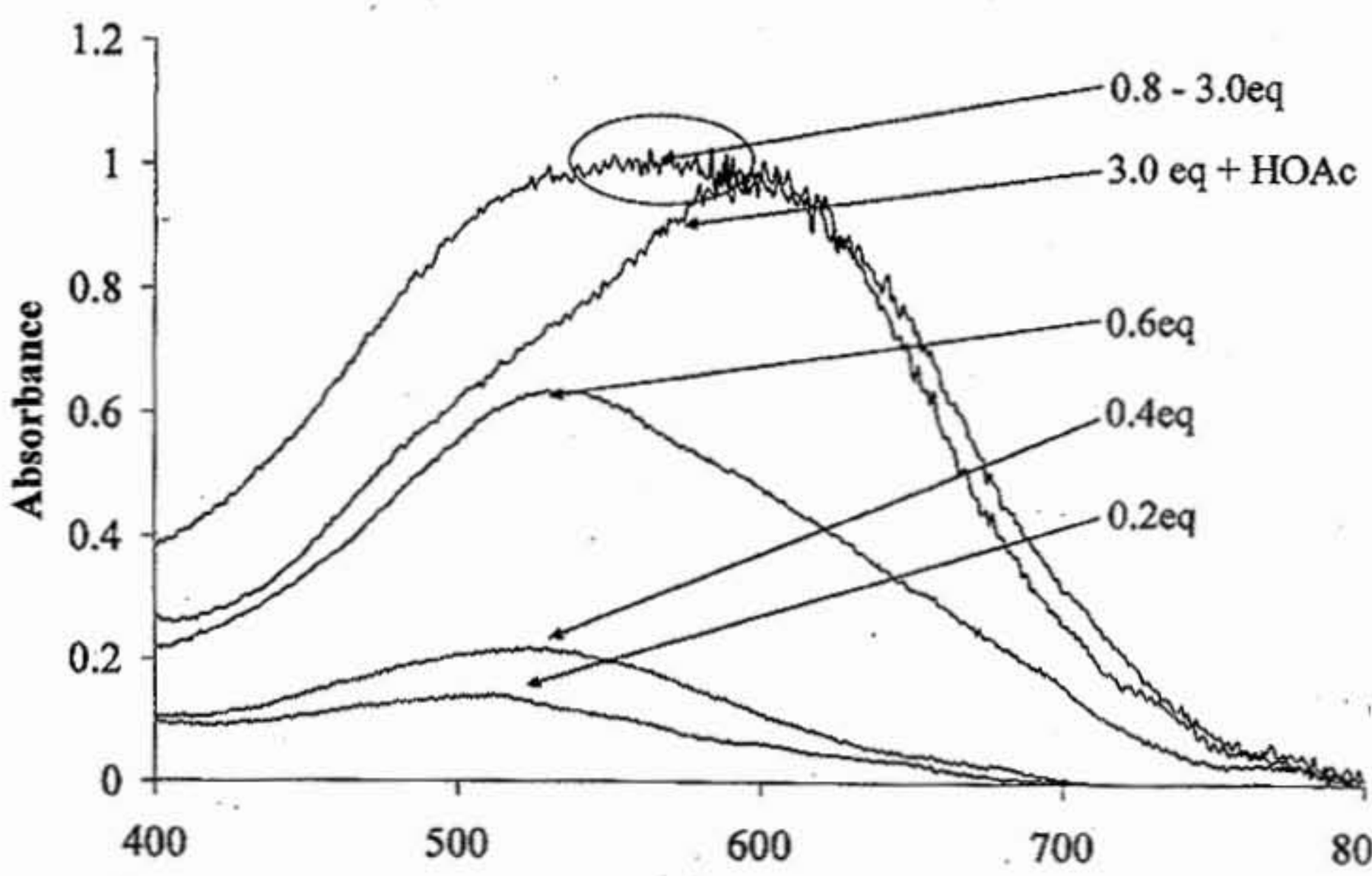

Figure 2.32. The reaction of **[Fe^{II}cyclam-PrS]$^+$** with KO_2 in CH_2Cl_2 using phenol as a proton source. The reaction was performed at -78°C.

Based on these results, methanol has surprisingly thus far been shown to provide the cleanest absorption data for the formation of the **$[Fe^{III}$cyclam-PrS(OOH)$]^+$** intermediate. One explanation for these results is the possible formation of a new species, a five-coordinate **$[Fe^{III}$cyclam-PrS$]^{2+}$** complex, in the absence of a coordinating anion. Because of the weakly or non-coordinating nature of each of the conjugate bases of these acids, this is indeed a distinct possibility. Although five-coordinate non-heme Fe^{III} complexes exist, they are not commonly found.[41] They have been shown to be generally unstable and thermodynamically favor binding a sixth ligand due to its dicationic state and increased Lewis acidity. The broad absorption bands seen in each experimental spectrum also possibly indicates the presence of multiple species in solution, possibly from the **$[Fe^{III}$cyclam-PrS(OOH)$]^+$** species, and the five-coordinate **$[Fe^{III}$cyclam-PrS$]^{2+}$** species. Further experiments, especially EPR, should be performed in an effort to isolate clean **$[Fe^{III}$cyclam-PrS(OOH)$]^+$** and **$[Fe^{III}$cyclam-PrS$]^{2+}$** samples.

Exogenous ligand binding. The binding of exogenous ligands such as azide (N_3^-) and cyanide (CN^-) to SOR has been studied extensively.[42,43] CN^- has been shown to deactivate the active site of SOR, preventing it from completing its catalytic cycle. CN^- is a strong-field ligand, and changes the SOR active site to a low-spin state. The stability of the low-spin state and the strength of the CN^- ligand as a π-acceptor ligand *trans* to the thiolate ligand, which is a strong π-donor ligand, greatly stabilizes this form of the enzyme once bound. Additionally, exogenous ligand binding studies with CN^- and N_3^- have been important to establishing that the catalysis of SOR proceeds via an inner

sphere mechanism. Kovacs' $[Fe^{II}S^{Me2}N_4{}^{tren}]^+$ complex also has been shown to bind the CN^-, N_3^- and acetate (OAc^-) ligands when oxidized to the Fe^{III} form, replicating the behavior seen with SOR. Additionally, the $[Fe^{III}S^{Me2}N_4{}^{tren}(OAc)]^+$ complex provides a structurally relevant model complex of the glutamate-bound "resting" state of SOR.

Based on these precedents, similar binding studies were performed with the $[Fe^{II}$**cyclam-PrS**$]^+$ complex, in an effort to replicate the substrate binding of SOR. The CN^-, N_3^- and OAc^- ligands were used in conjunction with a chemical oxidant, $FeCp_2PF_6$, in an effort to isolate and study these oxidized Fe^{III} species.

The use of tetraethylammonium cyanide (NEt_4CN) as a cyanide source to test for substrate binding to the metal center of the oxidized derivative of $[Fe^{II}$**cyclam-PrS**$]^+$ was studied in dichloromethane at -78°C. The results are shown in **Figure 2.33.** The addition of 1 equivalent of $FeCp_2PF_6$, followed by the addition of 1 equivalent of NEt_4CN, led to the formation of an aqua blue species, characterized by a new absorption band at 623 nm and a weaker feature at 483 nm. Upon warming, the band at 623 nm increased in intensity slightly, while the band at 483 nm has broadened slightly.

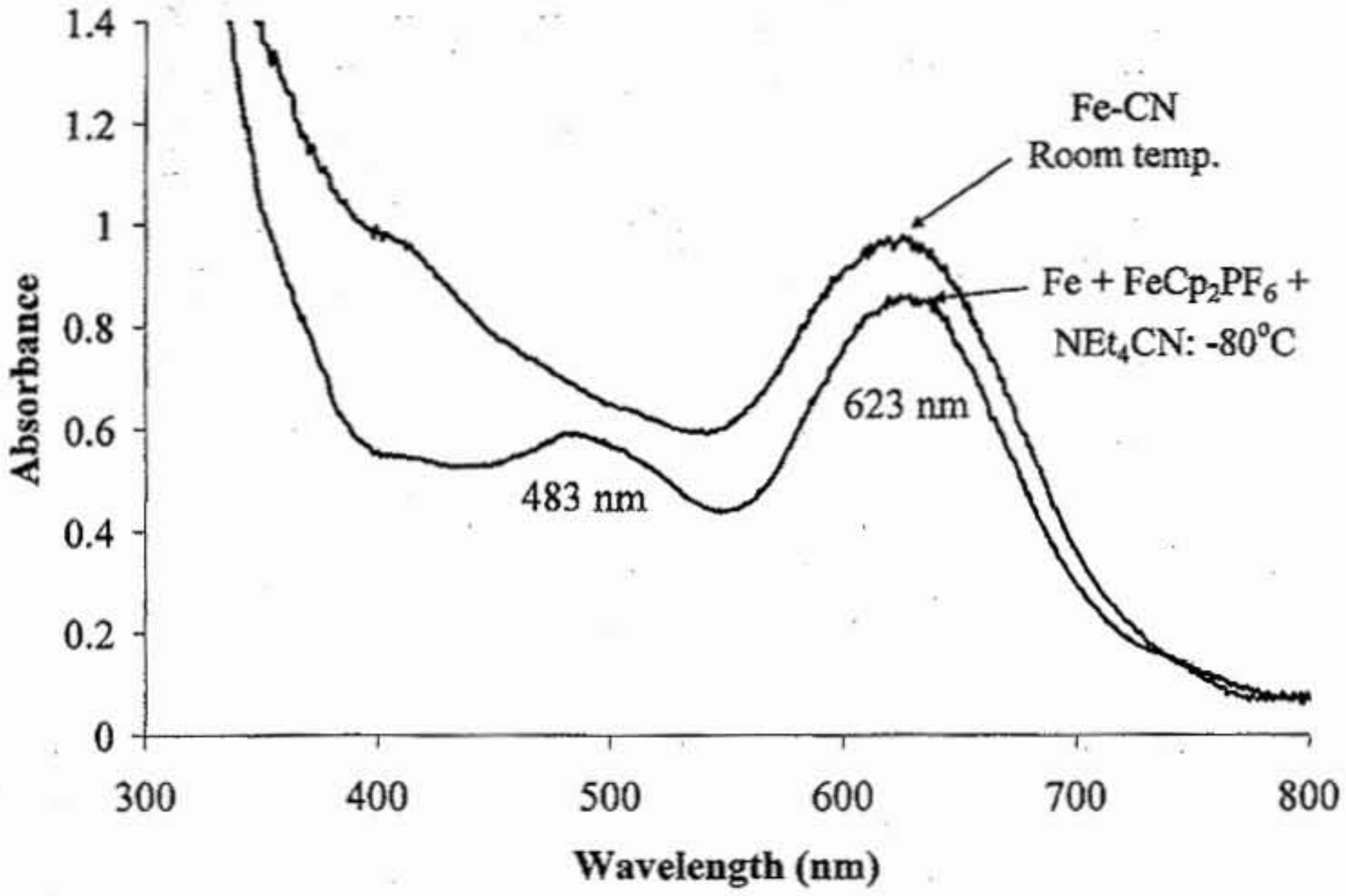

Figure 2.33. The reaction of **[Fe^{II}cyclam-PrS]$^+$** with $FeCpPF_6$ in CH_2Cl_2, followed by the addition of NEt_4CN as a cyanide source. The reaction was performed at -78°C.

Because the color of the solution of **[Fe^{III}cyclam-PrS(CN)]$^+$** kept its intensity at ambient temperature, an attempt to isolate the complex as a stable Fe^{III} complex was made. The solution was dried *in vacuo* and triturated with ether and pentane, affording a dark blue solid. Attempts to obtain an x-ray quality crystal were not successful. The solid obtained was analyzed by IR spectroscopy. The spectrum is shown here in **Figure 2.34.**

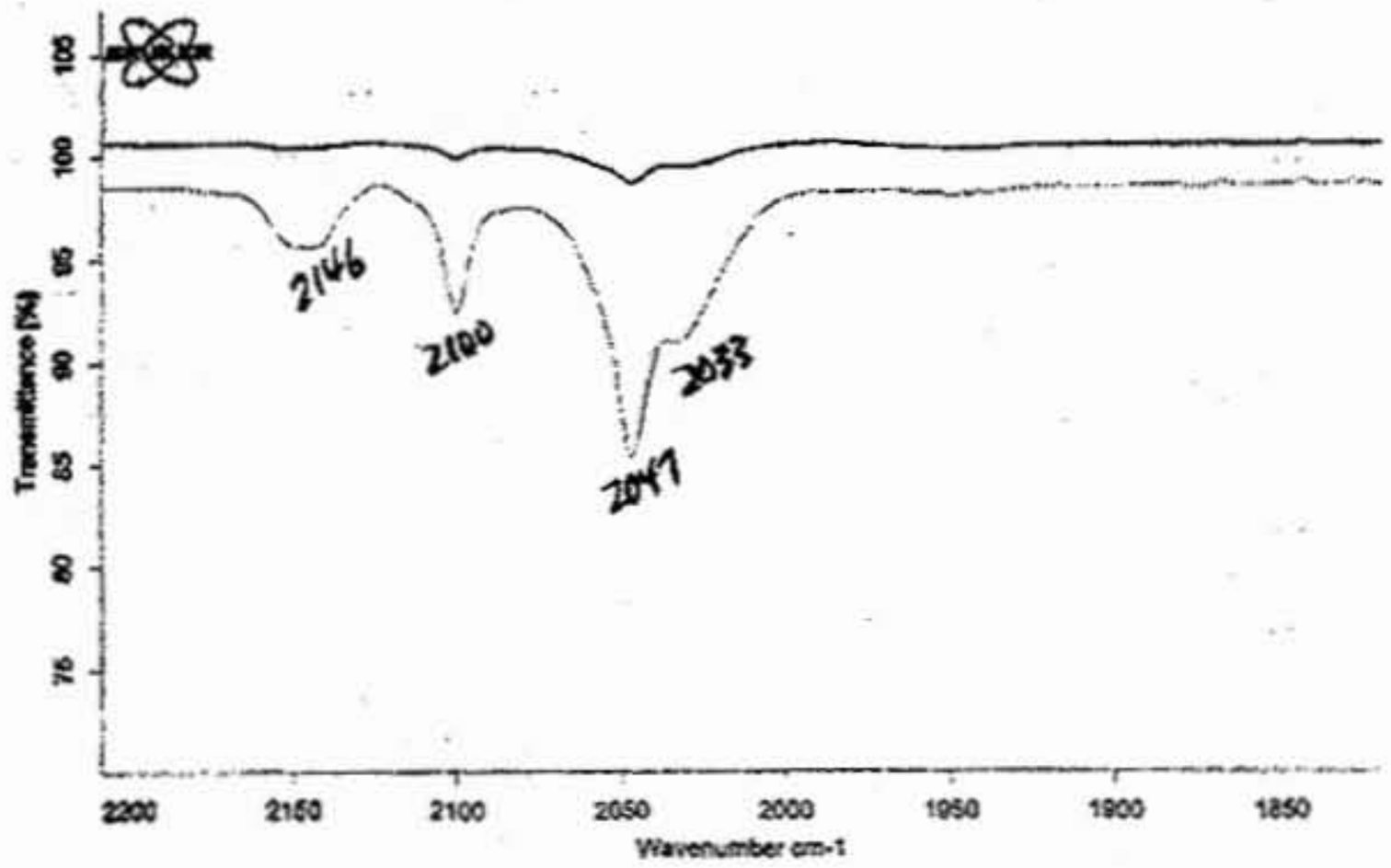

Figure 2.34. The IR spectrum of **[Fe^{III}cyclam-PrS(CN)]$^{+}$.** The sample was analyzed as a KBr pellet.

The reaction with tetramethylammonium acetate (NMe_4OAc), $FeCp_2PF_6$ and **[Fe^{II}cyclam-PrS]$^{+}$** was studied under the same experimental conditions. The importance of this study was two-fold; not only was exogenous ligand binding being tested, but the independent synthesis of the **[Fe^{III}cyclam-PrS(OAc)]$^{+}$** complex was necessary in order to verify that it was indeed the final product of the reduction of superoxide by **[Fe^{II}cyclam-PrS]$^{+}$,** followed by the addition of acetic acid. The formation of the aqua blue species with an absorption band at 600nm confirmed that this was indeed the species being formed during the catalytic cycle of **[Fe^{II}cyclam-PrS]$^{+}$.** The results are shown here in **Figure 2.35.**

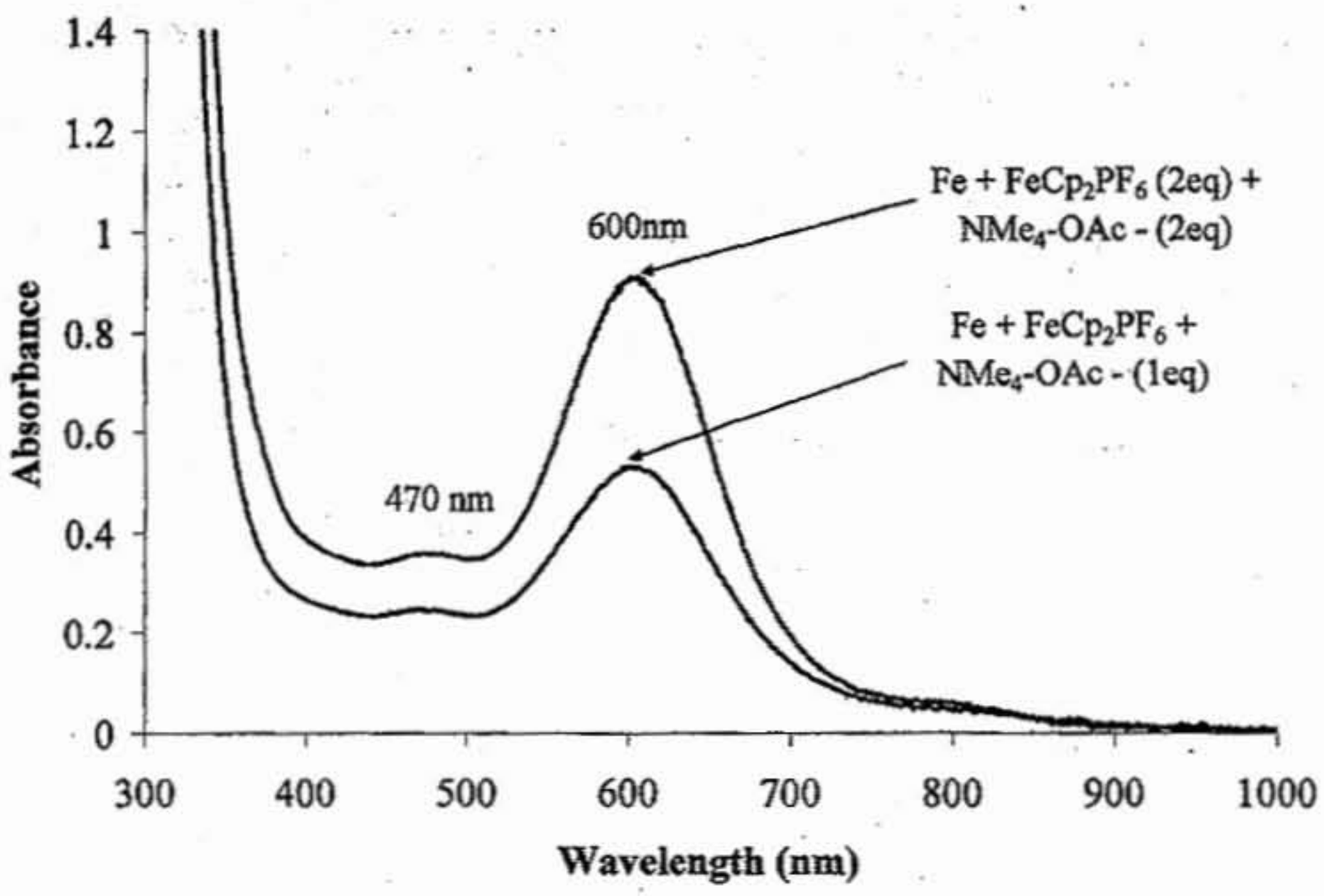

Figure 2.35. The reaction of **[Fe^{II}cyclam-PrS]$^+$** with $FeCpPF_6$ in CH_2Cl_2, followed by the addition of NEt_4OAc as an acetate source. The reaction was performed at -78°C.

Finally, the reaction was repeated with tetra-n-butylammonium azide (NBu_4N_3) to see if N_3^- could bind to the open site of the oxidized Fe^{III} center as well. Upon the addition of NBu_4N_3 to the reaction, the color became a deep green color and showed a new absorption band at 608nm. The absorption spectrum of this species is shown in **Figure 2.36.**

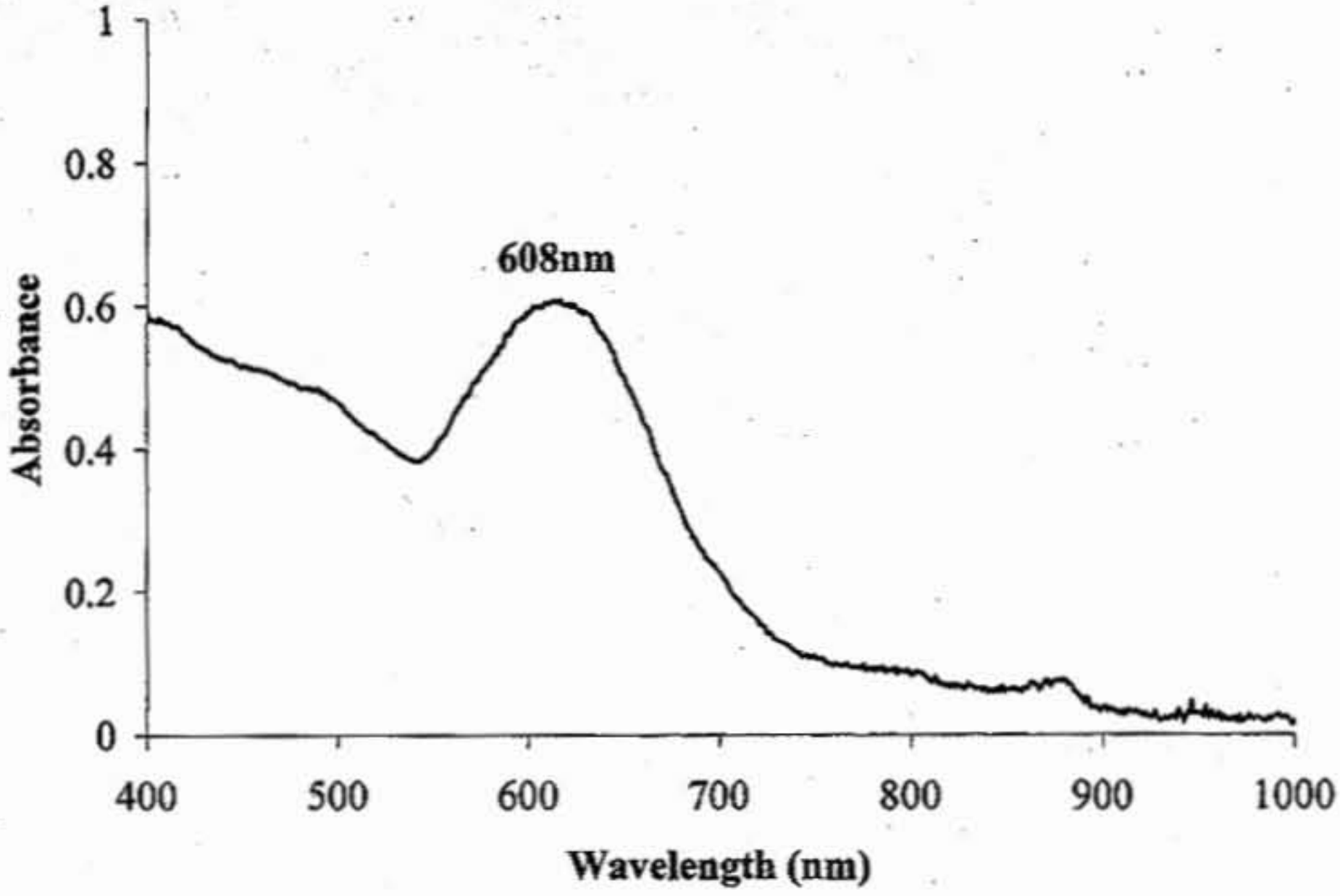

Figure 2.36. The reaction of **[Fe^{II}cyclam-PrS]$^+$** with $FeCpPF_6$ in CH_2Cl_2, followed by the addition of NBu_4N_3. The reaction was performed at -78°C.

To test if NO could bind to the Fe center, 1 equivalent of NO gas was vacuum transferred to a frozen solution of **[Fe^{II}cyclam-PrS]$^+$** in CH_3CN. The solution was slowly warmed to ambient temperature under a nitrogen atmosphere and allowed to stir overnight. The solution immediately turned from colorless to a dark red-brown color. The solution was then filtered through a Celite bed, evaporated to dryness, and redissolved in CH_2Cl_2. The resulting solution was filtered again, and the solution was concentrated *in vacuo*. The concentrated solution was layered with pentane, causing the deposition of dark brown crystals suitable for x-ray analysis. The resulting crystal structure is shown in **Figure 2.37.**

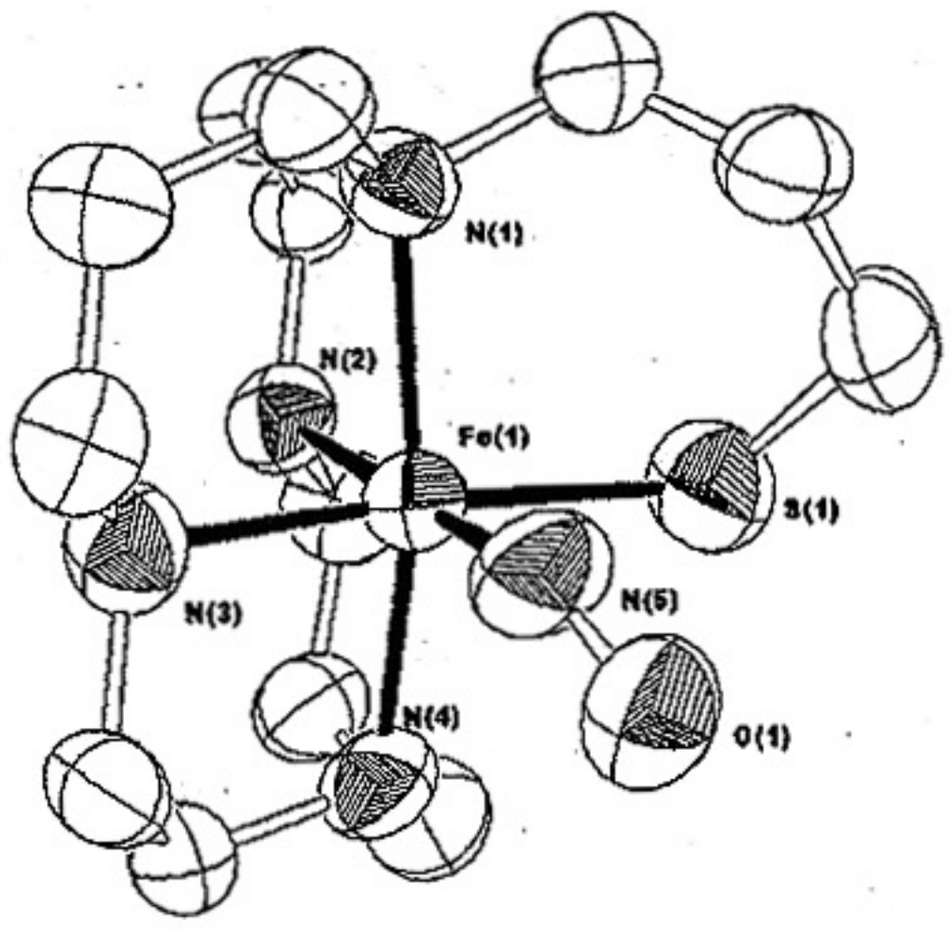

Figure 2.37. The x-ray crystal structure of **[Fe^{III}cyclam-PrS(NO)]$^{+}$.** The complex is six-coordinate, with the NO binding *cis* to the thiolate moiety. The NO has bound in a bent geometry, indicating that the complex is most likely in the Fe^{III} oxidation state.

Bond Lengths. The cyclam ligand system has remarkably rearranged itself to accommodate the NO ligand to bind *cis* to the thiolate moiety as opposed to *trans*. In order determine if this was proceeding via the *trans* isomer, this reaction was studied by UV-vis absorption spectroscopy at low temperatures. NO(g) was bubbled into a solution of **[Fe^{II}cyclam-PrS]$^{+}$** in CH_2Cl_2 at -78°C. The solution immediately turned a burgundy color, and showed the appearance of an absorption band at 518 nm. The solution was then warmed to ambient temperature, causing the loss of the absorption band at 518 nm. Upon warming, there was no discernable absorption band remaining in the visible region of the absorption spectrum. The absorption spectra for these experiments are shown together here in **Figure 2.38.**

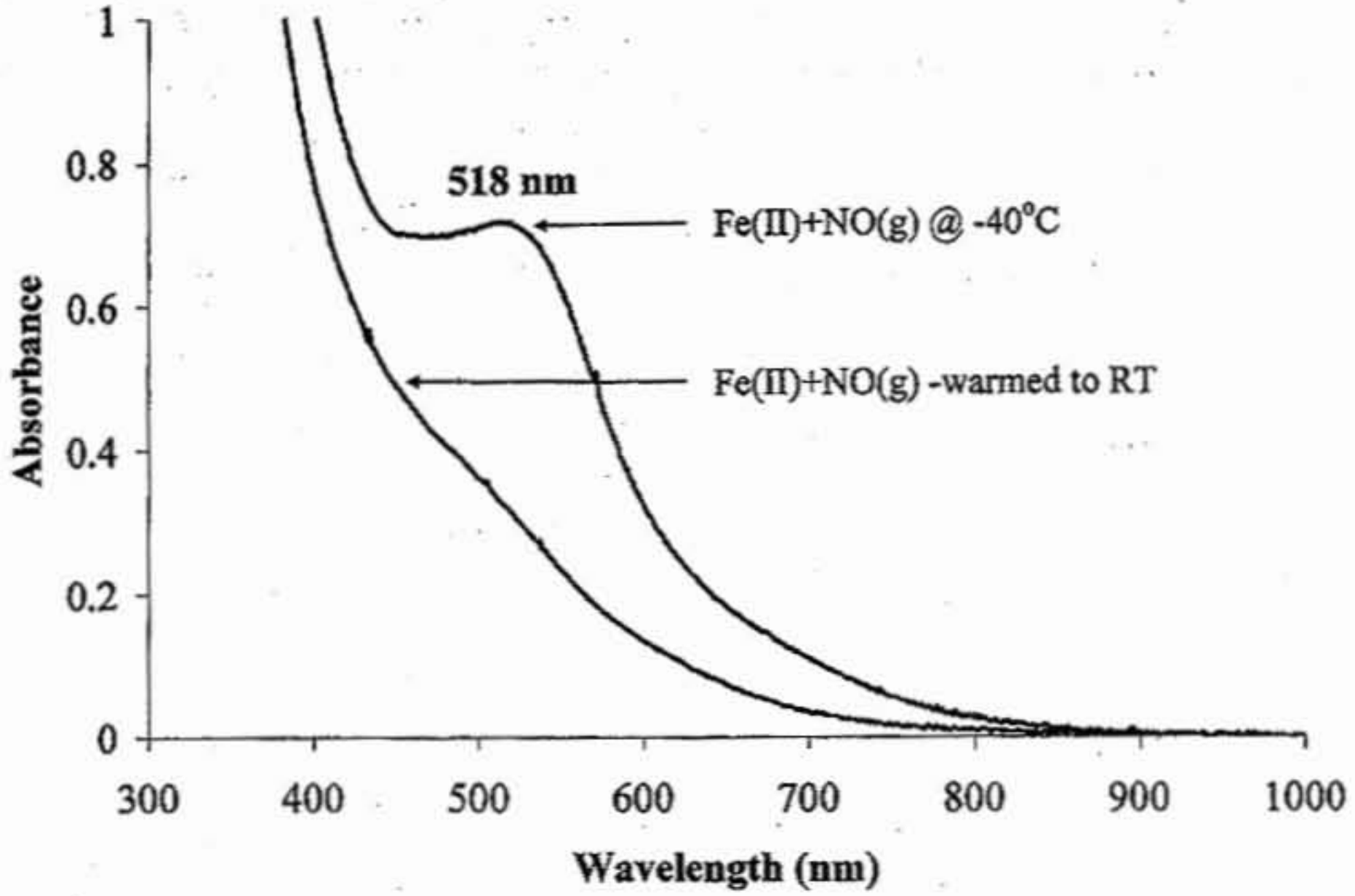

Figure 2.38. The reaction of **[Fe^{II}(cyclam-PrS)]$^+$** with NO(g) in CH_3CN. The reaction was initialized at -40°C, and the peak at 518 nm was allowed to maximize. After the band maximized in intensity, the solution was gradually warmed to room temperature.

The reason for doing these experiments was to probe if there was an intermediate species initially formed after the addition of NO to **[Fe^{II}(cyclam-PrS)]$^+$,** prior to rearrangement. It was believed that the NO molecule initially bound *trans* to the thiolate moiety on the Fe^{III} center, but that because of the significant *trans* effect of the thiolate, the macrocycle eventually underwent rearrangement to the *cis* configuration. In other words, there is a kinetically favored product, and a thermodynamically favored product that are both formed during the course of this reaction. This observation emphasizes the strong influence that the *trans* thiolate plays in SOR chemistry, particularly during substrate release.

Conclusion. The synthesis and physical characterization of **$[Fe^{II}$(cyclam-PrS)$]^+$**, a novel biomimetic analogue of SOR has been described. This complex is a five-coordinate Fe^{II} species that reacts with O_2^- in the presence of protons to form a metastable Fe^{III}-OOH species. This transient intermediate, **$[Fe^{III}$(cyclam-PrS)(OOH)$]^+$**, is an extremely rare example of a high-spin Fe^{III}-hydroperoxo species, and is the first reported example of a non-heme ferric peroxo intermediate with a thiolate ligated trans to the peroxo moiety. **$[Fe^{III}$(cyclam-PrS)(OOH)$]^+$** gives valuable synthetic insight into the identity of the transient Fe-peroxo intermediate seen during the catalytic reduction of superoxide by SOR. Additionally, the vibrational data collected from **$[Fe^{III}$(cyclam-PrS)(OOH)$]^+$** shows extremely weak Fe-O bond stretching frequencies, and strong O-O stretching frequencies, both of which were uncharacteristic of reported synthetic non-heme Fe-peroxo species. This helps to explain the preference of SOR to cleave the bond between the Fe center and the proximal oxygen, rather than cleaving the O-O bond, thus favoring release of H_2O_2 over formation of high-valent Fe^{IV}=O or Fe^{V}=O species, a la cytochrome P450 chemistry. Thus, despite the structural similarities between the heme-containing cytochrome P450 and the active site of the non-heme metalloenzyme SOR, we have gained significant insight into the effects that the subtle physical and electronic differences between the two active sites have on their respective chemistries. Additionally, from a synthetic standpoint, we have shown that the simple topological variation of an additional methylene group in the tethered alkyl arm containing the thiolate moiety, as well as the avoidance of permethylation of the macrocyclic amines, causes significant change in the chemistry of the metal center by possibly playing a role

in altering the electronic (redox potential) and physical nature (sterics) of the metal center, allowing it to reduce superoxide, and thus mimicking SOR chemistry.

The binding of exogenous ligands to the Fe^{III} center of **$[Fe^{II}$(cyclam-PrS)$]^+$** upon oxidation has unequivocally shown the ability of the Fe^{III} center to bind a sixth ligand, implying an inner-sphere mechanism of superoxide reduction by **$[Fe^{III}$(cyclam-PrS)(OOH)$]^+$.** Additionally, it has been shown that while the positioning of the thiolate moiety (*cis* versus *trans*) does not prevent the reduction of superoxide by the Fe center from occurring, it does indeed play a role in dictating the thermodynamic and kinetic stability of the **$[Fe^{III}$(cyclam-PrS)(OOH)$]^+$** species, as opposed to that of the *cis*-thiolate SOR model $[Fe^{II}N_4{}^{(tren)}S^{(Me2)}]^+$ by favoring fast dissociation of H_2O_2 by the Fe center, even at cryogenic temperatures. Kinetic studies of the catalytic reduction of superoxide by the *trans*-thiolate model **$[Fe^{II}$(cyclam-PrS)$]^+$** aimed at determining the reaction mechanism is now possible and would provide valuable insight into the effect of the thiolate positioning versus the peroxo moiety. Additionally, the rare example of **$[Fe^{II}$(cyclam-PrS)$]^+$** as a truly biomimetic synthetic model complex is a marvel and will undoubtedly help to illustrate the truly rich chemistry that the cysteinate residue provides in nature.

Chapter 2 – Notes

(1) Krishnamurthy, D.; Kasper, G. D.; Namuswe, F.; Kerber, W. D.; Narducci Sarjeant, A. A.; Moenne-Loccoz, P.; Goldberg, D. P. *J Am Chem Soc* **2006**, *128*, 14222-3.

(2) Fiedler, A. T.; Halfen, H. L.; Halfen, J. A.; Brunold, T. C. *J Am Chem Soc* **2005**, *127*, 1675-89.

(3) Shearer, J.; Scarrow, R. C.; Kovacs, J. A. *J Am Chem Soc* **2002**, *124*, 11709-17.

(4) Halfen, J. A.; Moore, H. L.; Fox, D. C. *Inorg Chem* **2002**, *41*, 3935-43.

(5) Zang, Y.; Que, L. J. *Inorg Chem* **1995**, *34*, 1030-1035.

(6) Kovacs *unpublished results.* **2006**.

(7) Szulbinski, W. S.; Busch, D. H. *Inorg Chim Acta* **1995**, *234*, 143-148.

(8) Serres, R. G.; Grapperhaus, C. A.; Bothe, E.; Bill, E.; Weyhermuller, T.; Neese, F.; Wieghardt, K. *J Am Chem Soc* **2004**, *126*, 5138-53.

(9) Stolarczyk, K.; Bilewicz, R.; Siegfried, L.; Kaden, T. *Inorg Chim Acta* **2003**, *00*, 1-6.

(10) Pallavicini, P. S.; Perotti, A.; Poggi, A.; Seghi, B.; Fabbrizzi, L. *J Am Chem Soc* **1987**, *109*, 5139-5144.

(11) Halfen, J. A.; Young, V. G., Jr. *Chem Commun (Camb)* **2003**, 2894-5.

(12) Theisen, R. M.; Shearer, J.; Kaminsky, W.; Kovacs, J. A. *Inorg Chem* **2004**, *43*, 7682-90.

(13) Meyerstein, D. *Coordination Chemistry Reviews* **1999**, *185-186*, 141-147.

(14) Live, D. H.; Chan, S. I. *Anal Chem* **1970**, *42*, 791-792.

(15) Evans, D. A. *J Am Chem Soc* **1959**, 2003-2005.

(16) Van Geet, A. L. *Anal Chem* **1968**, *40*, 2227-2229.

(17) Brandès, S.; C., G.; Denat, F.; Pullumbi, P.; Guilard, R. *Bull. Chim. de France* **1996**, *133*, 65-73.

(18) Zhou, M.; Diwu, Z.; Panchuk-Voloshina, N.; Haugland, R. P. *Anal Biochem* **1997**, *253*, 162-8.

(19) Baran, Y.; Yilmaz, I. *Transition Metal Chem* **2001**, *26*, 36-38.

(20) Chantson, T. E.; Hancock, R. D. *Inorg Chim Acta* **1995**, *230*, 165-167.

(21) Hodges, K. D.; Wollman, R. G.; Barefield, E. K.; Hendrickson, D. N. *Inorg Chem* **1977**, *16*, 2746-2751.

(22) Martin, L. Y.; DeHayes, L. J.; Zompa, L. J.; Busch, D. H. *J Am Chem Soc* **1974**, 4046-4048.

(23) Liang, X.; Sadler, P. J. *Chem Soc Rev* **2004**, *33*, 246-66.

(24) Barefield, E. K.; Wagner, F.; Herlinger, A. W.; Dahl, A. R. *Inorg Syntheses*, 220-225.

(25) Yang, W.; Giandomenico, C. M.; Sartori, M.; Moore, D. *Tetrahedron Letters* **2003**, *44*, 2481-2483.

(26) Greene, W. T.; Wuts, P. G. M. *Protective Groups in Organic Synthesis*; 3 ed.; Wiley-Interscience, 2003.

(27) Maltese, M. *J Org Chem* **2001**, *66*, 7615-25.

(28) Okubo, H.; Feng, F.; Nakano, D.; Hirata, T.; Yamaguchi, M.; Miyashita, T. *Tetrahedron* **1999**, *55*, 14855-14864.

(29) Trujillo, D. A.; McMahon, W. A. J.; Lyle, R. E. *J Am Chem Soc* **1987**, *52*, 2932-2933.

(30) Gil, L.; Han, Y.; Opas, E. E.; Rodan, G. A.; Ruel, R.; Seedor, J. G.; Tyler, P. C.; Young, R. N. *Bioorg Med Chem* **1999**, *7*, 901-19.

(31) Wada, A.; Ogo, S.; Nagatomo, S.; Kitagawa, T.; Watanabe, Y.; Jitsukawa, K.; Masuda, H. *Inorg Chem* **2002**, *41*, 616-8.

(32) Roelfes, G.; Vrajmasu, V.; Chen, K.; Ho, R. Y.; Rohde, J. U.; Zondervan, C.; La Crois, R. M.; Schudde, E. P.; Lutz, M.; Spek, A. L.; Hage, R.; Feringa, B. L.; Munck, E.; Que, L., Jr. *Inorg Chem* **2003**, *42*, 2639-53.

(33) Mathe, C.; Mattioli, T. A.; Horner, O.; Lombard, M.; Latour, J. M.; Fontecave, M.; Niviere, V. *J Am Chem Soc* **2002**, *124*, 4966-7.

(34) Kitagawa, T.; Dey, A.; Lugo-Mas, P.; Benedict, J. B.; Kaminsky, W.; Solomon, E.; Kovacs, J. A. *J Am Chem Soc* **2006**, *128*, 14448-9.

(35) *Supplemental information.*

(36) Lugo-Mas, P. *Data obtained by and used with permission.*

(37) Gupta, M. N.; Roy, I. *Eur. J. Biochem* **2004**, *271*, 2573-2583.

(38) Klibanov, A. M. *Trends Biotechnol.* **1997**, *15*, 97-101.

(39) Sawyer, D. T.; Valentine, J. S. *Acc Chem Res* **1981**, *14*, 393-400.

(40) Santagostini, L.; Gullotti, M.; Monzani, E.; Casella, L.; Dillinger, R.; Tuczek, F. *Chem. Eur. J.* **2000**, *6*, 519-522.

(41) Lanznaster, M.; Hratchian, H. P.; Heeg, M. J.; Hryhorczuk, L. M.; McGarvey, B. R.; Schlegel, H. B.; Verani, C. N. *Inorg Chem* **2006**, *45*, 955-7.

(42) Yang, T. C.; McNaughton, R. L.; Clay, M. D.; Jenney, F. E., Jr.; Krishnan, R.; Kurtz, D. M., Jr.; Adams, M. W.; Johnson, M. K.; Hoffman, B. M. *J Am Chem Soc* **2006**, *128*, 16566-78.

(43) Clay, M. D.; Yang, T. C.; Jenney, F. E., Jr.; Kung, I. Y.; Cosper, C. A.; Krishnan, R.; Kurtz, D. M., Jr.; Adams, M. W.; Hoffman, B. M.; Johnson, M. K. *Biochemistry* **2006**, *45*, 427-38.

Chapter 3
Exploring the behavior of $[Fe^{II}(cyclam\text{-}PrS)]^+$

Introduction. The successful synthesis of $[Fe^{II}(cyclam\text{-}PrS)]^+$ as a biomimetic model of the active site of SOR was a significant result. Because of its structural similarities with important enzymes such as cytochrome P450, it was desireable to fully explore its reactivity. Specifically, we sought to see if it could activate dioxygen and hydrogen peroxide (H_2O_2) and mimic the reactivity of cytochrome P450 by modeling the intermediate Fe^{III}-peroxo species known as Compound I, either through the dioxygen pathway, or through reaction with H_2O_2, also known as the "shunt" pathway. In addition, we desired to use exogenous ligand binding as a means to understand if there was a direct *trans* effect that the thiolate has on the ligand bound opposite to it along the apical axis, as well as to try and find stable Fe^{III} analogues of $[Fe^{II}(cyclam\text{-}PrS)]^+$.

Dioxygen. Current research involving the mechanisms of heme and non-heme Fe-containing monoxygenase enzymes suggests that the interaction of dioxygen and iron is actually very diverse and multiple mechanisms are most likely involved. Indeed, oxygen atom transfer, oxidative dehydrogenation and non-radical hydroxylations are only a few of many possible reaction pathways that these Fe-peroxo species can proceed through. Understanding these interactions, their respective oxidation mechanisms, and how nature tunes the iron centers of these enzymes to perform their specific chemistry remains a highly desired goal of both biologists and chemists. Enzymes such as bacterial catechol dioxygenases, lipoxygenases, isopenicillin N-synthase (IPNS), and various other

enzymes have non-heme Fe centers that activate dioxygen, forming reactive intermediate Fe-peroxo species that are able to perform specific and complex biotransformations.[1] Many of these complexes described also are powerful oxidants, showing the ability to specifically oxidize substrates such as olefins and hydrocarbons by means of epoxidations, hydroxylations, and H-atom abstraction.[2] Synthetic bioinspired iron-containing complexes and the natural antitumor drug bleomycin, among others, have also been extensively studied. Amazingly, it was shown recently by Nam, *et al* that a simple non-heme Fe^{II} complex, $\mathbf{[Fe^{II}(TMC)(CF_3SO_3)_2]}$ reacts with dioxygen, activating the O-O bond to produce a transient Fe^{IV}=O species, providing the first example of a non-heme Fe complex activating dioxygen, and directly accessing the Fe^{IV} oxidation state.[1] Of particular interest to our group is the heme-containing enzyme cytochrome P450, because of its structural similarities with SOR.

Cytochrome P450 is known to react with dioxygen to form a transient Fe^{III}-peroxo intermediate, commonly known as Compound I.[3] The major difference between cytochrome P450 and SOR lies in the highly conjugated heme environment that exists in cytochrome P450. SOR is ligated by a more flexible nitrogen ligand system composed of histidine residues, but its ligand environment does not possess the level of conjugation as that of the heme moiety. These subtle differences between the two enzymes are proposed to play a major role in governing the type of chemistry done by each enzyme (i.e. O-O bond cleavage vs. Fe-O bond cleavage).

Hydrogen peroxide (H_2O_2). The reaction of Fe-containing complexes with H_2O_2 has been studied to a great extent. The reaction of ferrous centers with H_2O_2 has been shown to lead to the formation of hydroxyl radicals (Fenton chemistry) and a ferryl (Fe^{IV}) species.[4] The reaction of Fe^{III} porphyrins leads to the formation of Fe-oxo species (Fe^{IV}=O and Fe^{V}=O). The use of H_2O_2 in heme chemistry as an alternative to oxidative pathways involving dioxygen is commonly known as the "shunt pathway". It has been frequently used to generate the Fe^{III}-peroxo species of cytochrome P450 in order to study substrate hydroxylation. It provides a simple pathway to study the reactivity of the intermediate peroxo species without requiring NADP(H) regeneration, additional proteins, or rate-limiting electron-transfer pathways.

Thus, from a synthetic standpoint, H_2O_2 is often used favorably as an exogenous oxidant. The complex Fe^{III}-EDTA is the most studied complex of the non-heme complexes that react with H_2O_2. It has been shown to act as a catalase at elevated pH levels, and at physiological pH levels, it has been shown to catalyze the Haber-Weiss reaction.[5] More recently Que, Girerd, McKenzie and others have extensively characterized a series of non-heme Fe-peroxo complexes, which have also been shown to bind in different modes (i.e. end-on *versus* side-on).[6,7] In each case, the reaction of excess H_2O_2 with Fe^{II} and Fe^{III} centers has led to the formation of transient colored intermediates, identified as low-spin Fe^{III}-OOH species. The addition of base to these hydroperoxo species led to the formation of a new high-spin Fe^{III}-OO species, bound in a side-on η^2 configuration. The presence of both species is implicit in the mechanisms of bleomycin and cytochrome P450.

The use of H_2O_2 in these studies has produced an invaluable set of benchmark parameters, consisting of vibrational, mass spectrometry, and spectroscopic data, used to characterize identify the different binding modes of the peroxo moiety to an Fe center and allowing for the identification of the peroxo-to-iron charge transition band in the absorption spectrum. Probing these bands with resonance Raman allowed for the identification of the O-O and Fe-O stretches that are present in the Fe-peroxo species. Studying these species led to the observation that O-O bond weakening occurs in low-spin Fe-OOH complexes, as well as strong Fe-O bonds, which explains why low-spin Fe-OOH species such as those in cytochrome P450 prefer to cleave at the O-O bond and form high-valent Fe-oxo species, rather than at the Fe-O bond. Many of these complexes described are also powerful oxidants, showing the ability to specifically oxidize substrates such as olefins and hydrocarbons by means of epoxidations, hydroxylations, and H-atom abstraction.

H_2O_2 has also been used in shunt pathways involving biological systems to model reactivities of iron-containing metalloenzymes. The E47-mutant of SOR reported by Niviere and coworkers has been shown to react with H_2O_2 to form the side-on Fe-peroxo species that they report as the putative intermediate in the SOR-catalyzed reduction of superoxide to H_2O_2.

Two-electron oxidants. More recently, non-heme iron complexes have been shown to form stable $Fe^{IV}=O$ complexes when reacted with two-electron oxidants such as MCPBA, iodosylbenzene and peracetic acid. It was originally thought that only heme-containing

iron complexes could support oxidation states higher than Fe^{III}. Revolutionary work by Que allowed for the crystallographic characterization of the first non-heme Fe^{IV}=O species, providing the first direct structural evidence of these species.[6] Non-heme Fe^{IV}=O species have also been shown to be potent, non-promiscuous oxidants, capable of performing olefin epoxidation, hydroxylation and H-atom abstractions, in mechanisms similar to cytochrome P450.[8-10] Que has also recently reported the first Fe^{IV}=O species with a thiolate coordinated to the Fe center.[11]

Thiolates have been shown to play an important role in tuning the redox potential of the metal center, lowering it into a range where it can activate the O-O bond of dioxygen.[12] Recently our $[Fe^{II}S^{Me2}N_4{}^{tren}]^+$ complex has been shown to react with dioxygen, forming the thermodynamically favorable μ-oxo dimer complex $[Fe^{III}S^{Me2}N_4{}^{tren}]_2(\mu\text{-}O)$.[13] It has been proposed that dioxygen can also oxidize a synthetic model to a high-valent perferryl (Fe^{IV}=O) state.[14] Remarkably, Que and Halfen recently published the first synthetic example of a thiolate-ligated Fe^{IV}=O complex, providing the first direct correlation between both P450 and SOR enzymes.[11] However, generating this complex required the use of *m*CPBA, a two-electron, single oxygen donor. The complex $[Fe^{II}TMCS]^+$ was inert to O_2 and required the use of an exogenous oxidant in order to access higher oxidation states. Because of these structural similarities, we decided to examine the reactivity of $[Fe^{II}(cyclam\text{-}PrS)]^+$ with dioxygen. The ability to somewhat control the kinetic and thermodynamic aspects of the reactions with $[Fe^{II}(cyclam\text{-}PrS)]^+$ should allow the closer analysis of the oxidative chemistry, as well as a direct synthetic correlation between structure and function of the two enzymes P450 and SOR. Stable

thiolate-bound Fe complexes are not trivial to synthesize, and preliminary reactivity studies indicate that the reactivity of $[Fe^{II}(cyclam\text{-}PrS)]^+$ is very diverse. In conjunction with $[Fe^{II}S^{Me2}N_4{}^{tren}]^+$, much can be learned about the effect of thiolates on Fe oxidation chemistry.

The reactivity of $[Fe^{II}(cyclam\text{-}PrS)]^+$ with dioxygen. The reaction of $[Fe^{II}(cyclam\text{-}PrS)]^+$ with dioxygen was studied in various solvents in order to determine the optimal conditions for experimentation, and to study the effect of coordinating vs non-coordinating solvent and the different reactivities under protic and aprotic conditions. First, the reaction between $[Fe^{II}(cyclam\text{-}PrS)]^+$ and dioxygen was studied in dichloromethane at -78°C and is shown in **Figure 3.01.** A dry source of dioxygen from an oxygen tank was streamed into a pre-cooled solution of the $[Fe^{II}(cyclam\text{-}PrS)]^+$ in dichloromethane. The immediate formation of a band at 530 nm (ε = 1210 $M^{-1}cm^{-1}$) was observed, in conjunction with a color change to a pink-purple color. The reaction appeared to be complete at this point. When this reaction was performed at ambient temperature, the deep pink-purple color of the solution lasted for about a minute before the color began to bleach, indicating that this species had a noticeably longer lifetime than the $[Fe^{III}(cyclam\text{-}PrS)(OOH)]^+$ intermediate formed from the reaction with superoxide..

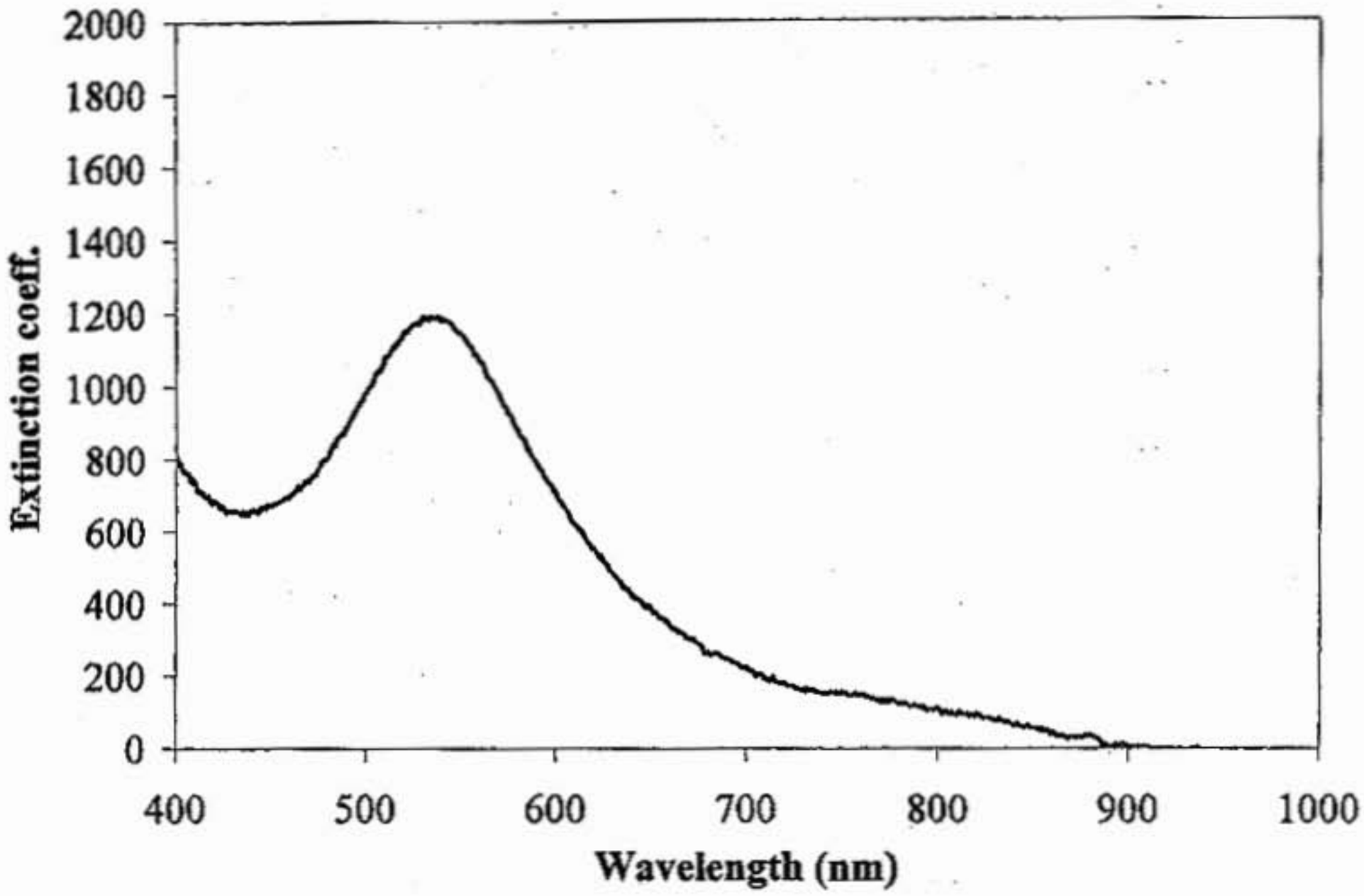

Figure 3.01. The reaction between **[Fe^{II}(cyclam-PrS)]$^+$** and dioxygen in dichloromethane at -78°C.

This reaction was then monitored by EPR. Using a CH_2Cl_2/2-MeTHF glass (1:1), the reaction was ran at [Fe^{II}] = 30mM, in order to have a direct correlation with the EPR data gathered for the reaction between **[Fe^{II}(cyclam-PrS)]$^+$** and superoxide (*vide supra*). The results are shown here in **Figure 3.02.** The addition of dry dioxygen to a pre-cooled solution of **[Fe^{II}(cyclam-PrS)]$^+$** in CH_2Cl_2/2-MeTHF led to the formation of high-spin and low-spin components. Interestingly, the signal intensities of these components are much lower than those obtained from the reaction of **[Fe^{II}(cyclam-PrS)]$^+$** and KO_2, under the same conditions.

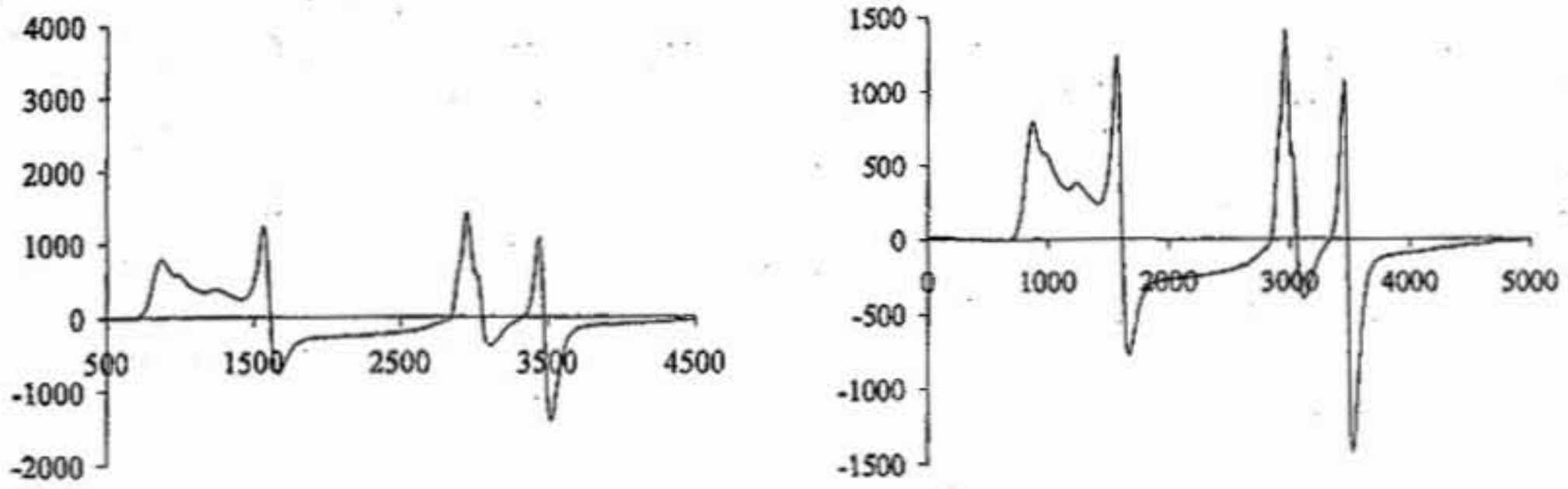

Figure 3.02. The EPR spectrum of the reaction between **[Fe^{II}(cyclam-PrS)]$^+$** and dioxygen under aprotic conditions (CH_2Cl_2: 2-MeTHF). The left plot is scaled identically to that of **[Fe^{III}(cyclam-PrS)(OOH)]$^+$ (Figure 2.19,** *vide supra*) in order to compare the relative signal intensities between the two experiments. The right plot is scaled to enhance the signal.

The reaction with **[Fe^{II}(cyclam-PrS)]$^+$** with dioxygen was then studied in acetonitrile by electronic absorption spectroscopy. Upon the injection of dry dioxygen into a pre-cooled solution of **[Fe^{II}(cyclam-PrS)]$^+$** in acetonitrile, the immediate formation of a band at 532 nm (ε = 1410 $M^{-1}cm^{-1}$) was observed, in conjunction with a color change to maroon. The reaction was complete within the first 5 minutes after the injection of dioxygen into the system. The color began to bleach soon after, and the color was bleached within 15 minutes even at low temperatures. The absorption spectrum is shown in **Figure 3.03.**

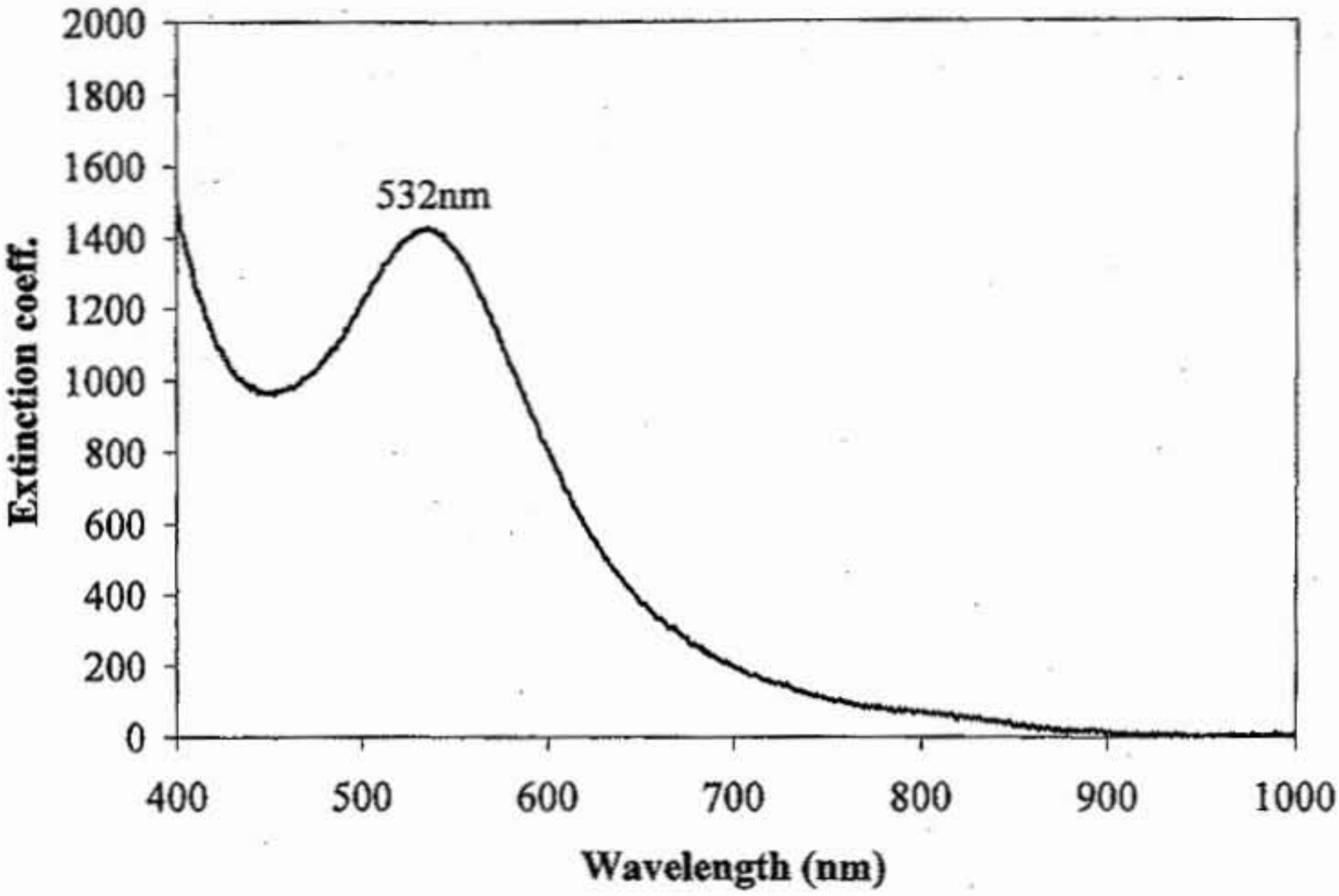

Figure 3.03. The reaction between $[Fe^{II}(cyclam\text{-}PrS)]^+$ and dioxygen in acetonitrile at -40°C.

Finally the reaction between $[Fe^{II}(cyclam\text{-}PrS)]^+$ and dioxygen was studied in methanol, in order to characterize its behavior in protic solvents. Upon the injection of dry dioxygen into a pre–cooled solution of $[Fe^{II}(cyclam\text{-}PrS)]^+$ in MeOH, the immediate formation of a band at 542 nm (ε = 620 $M^{-1}cm^{-1}$) was observed, in conjunction with a color change to a deep purple color. The reaction was complete within the first minute after the injection of dioxygen into the system. The color lingered for a couple of minutes at low temperatures before it began to bleach. The decomposition of the colored solution was complete within 15 minutes. The absorption spectrum is shown in **Figure 3.04.**

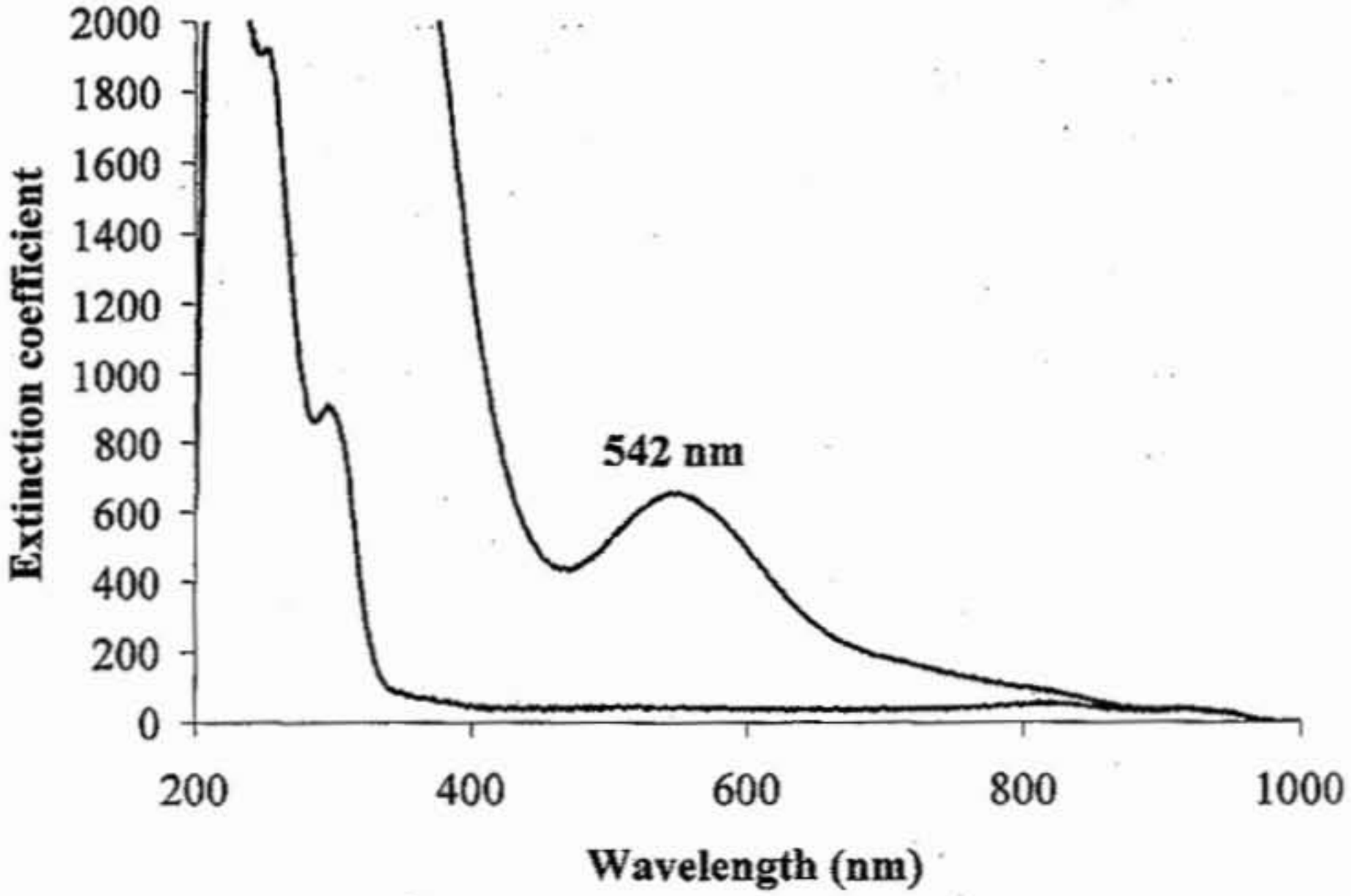

Figure 3.04. The reaction between $[Fe^{II}(cyclam\text{-}PrS)]^+$ and dioxygen in methanol at -80°C.

This reaction was then monitored by EPR. Using a CH_2Cl_2/2-MeTHF glass (1:1), the reaction was performed with $[Fe^{II}]$ = 30mM, in order to have a direct correlation with the EPR data gathered for the reaction between $[Fe^{II}(cyclam\text{-}PrS)]^+$ and KO_2 (*vide supra*). The results are shown here in **Figure 3.05.** The addition of dry dioxygen to a precooled solution of $[Fe^{II}(cyclam\text{-}PrS)]^+$ in MeOH/EtOH (9:1) also led to the formation of high-spin and low-spin components, characterized by their respective g-values. (g = 6.81, 5.53, 4.30 (high-spin) and g = 2.26, 2.13, 1.90 (low-spin)). Remarkably the signal intensities of these components are even lower than those obtained from the reaction of $[Fe^{II}(cyclam\text{-}PrS)]^+$ and dioxygen under aprotic conditions. Based on the intensity of the high-spin signal, the amount of the high-spin component generated under these

conditions is approximately 10% of the **[Fe^{III}(cyclam-PrS)(OOH)]$^+$** species. It is tempting to label both of the species generated from the addition of dioxygen to **[Fe^{II}(cyclam-PrS)]$^+$** as possibly being EPR silent, and the generation of an Fe^{IV}=O or bis-μ-oxo/peroxo species remains a possibility. However, preliminary resonance Raman experiments did not show obvious Fe-O or O-O stretching bands, even with isotopic labeling studies using $^{18}O_2$. Unfortunately at this point these experiments are far from conclusive, and no speculation can be made as to the identity of these species without further investigation.

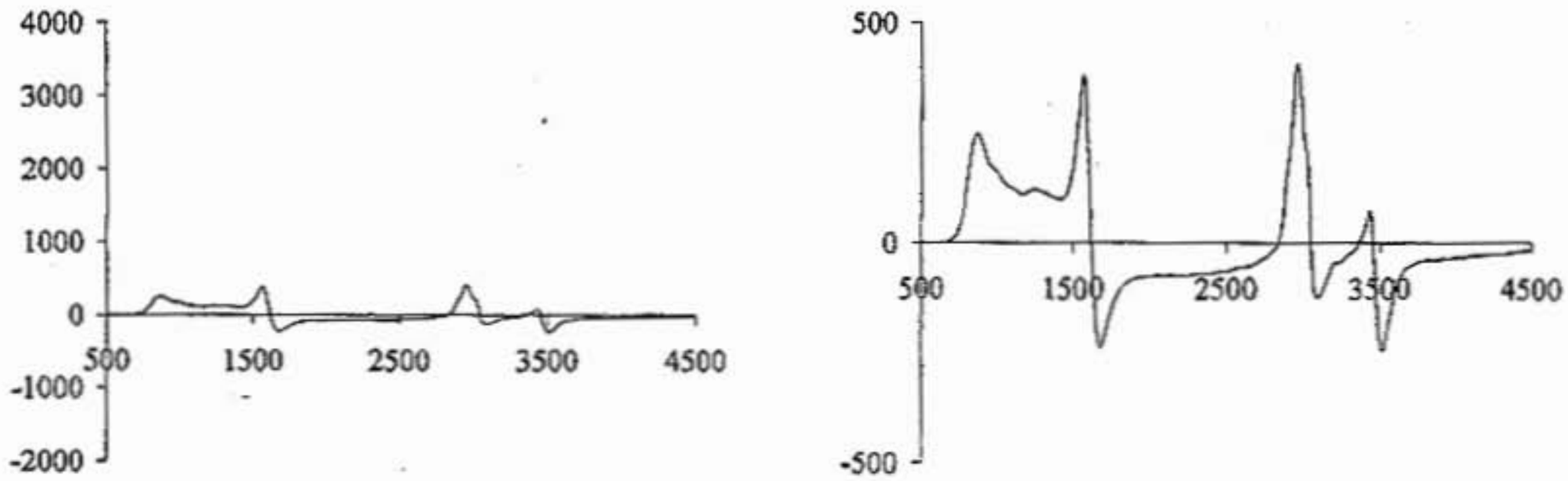

Figure 3.05. The EPR spectrum of the reaction between **[Fe^{II}(cyclam-PrS)]$^+$** and dioxygen under protic conditions (MeOH:EtOH). The left plot is scaled identically to that of **[Fe^{III}(cyclam-PrS)(OOH)]$^+$ (Figure 2.19,** *vide supra*) in order to compare the relative signal intensities between the two experiments. The right plot is scaled to enhance the signal.

H_2O_2 chemistry. In order to probe the reactivity of **[Fe^{II}(cyclam-PrS)]$^+$** with H_2O_2, experiments were run under aprotic and protic conditions. Generating the **[Fe^{III}(cyclam-PrS)(OOH)]$^+$** species by the addition of H_2O_2 instead of KO_2, via the "shunt" pathway, would allow for an easier, faster and cleaner method of generating and studying this intermediate. The issues that arise with the use of KO_2 such as solubility and secondary

disproportionation reactions in the presence of protons would be avoided. The first reaction was performed in THF at -78°C. The addition of 2.0 equivalents of H_2O_2 to a cooled solution of **$[Fe^{II}$(cyclam-PrS)$]^+$** caused the immediate formation of a transient purple intermediate species, with a λ_{max}=520nm. The absorption spectrum is shown below in **Figure 3.06.**

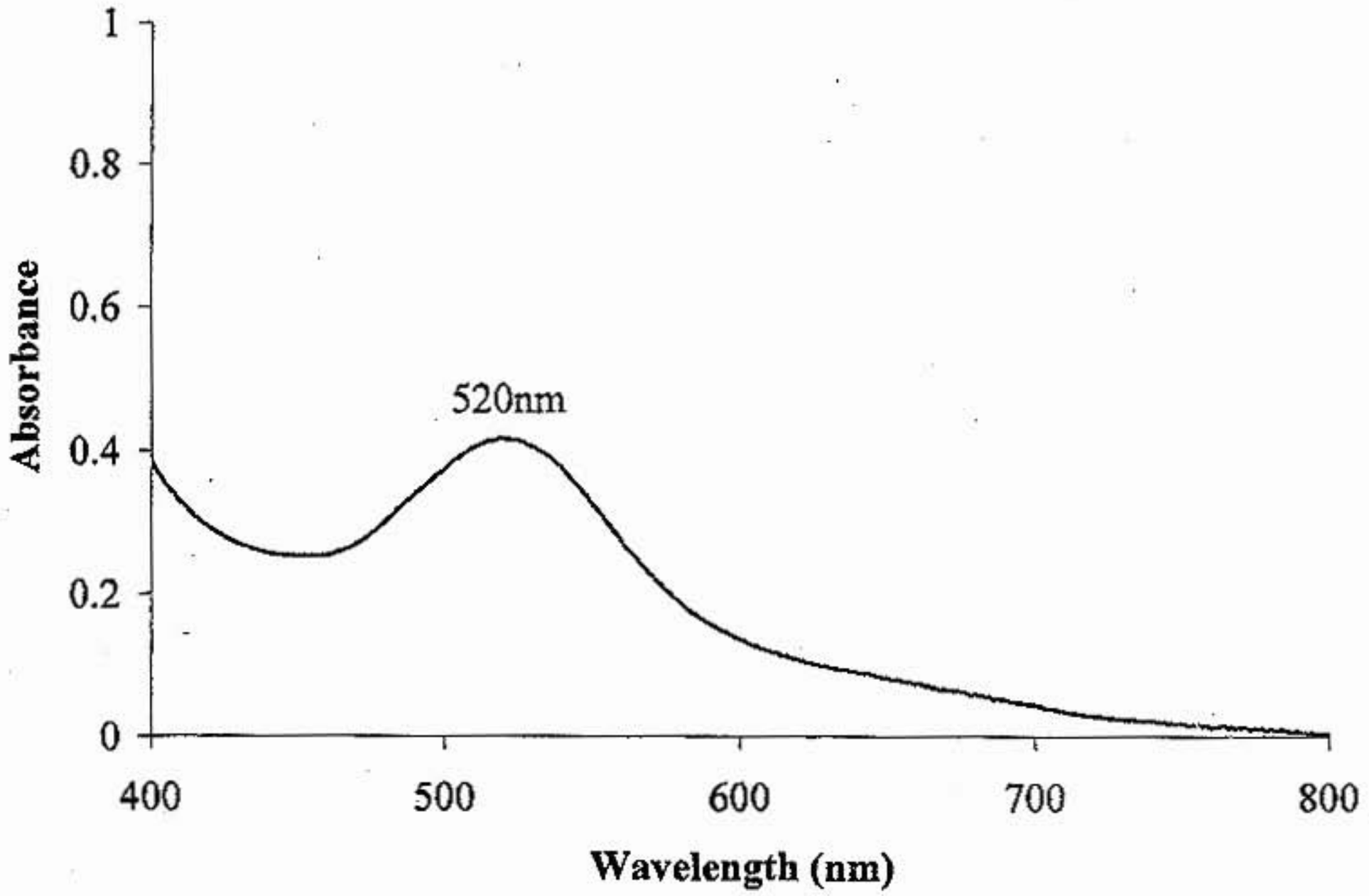

Figure 3.06. The reaction between **$[Fe^{II}$(cyclam-PrS)$]^+$** and H_2O_2 in THF at -78°C. (λ_{max}=520nm).

In order to identify this transient intermediate, this species was generated in 2-MeTHF and studied by EPR. The results indicate the formation of a new high-spin species with g=7.68, 5.37, and 4.13. These values are almost identical to those obtained

from the high-spin species generated from the reaction of $[Fe^{II}(cyclam\text{-}PrS)]^+$ and KO_2 (g= 7.72, 5.40, 4.15). The EPR spectrum is shown in **Figure 3.07.**

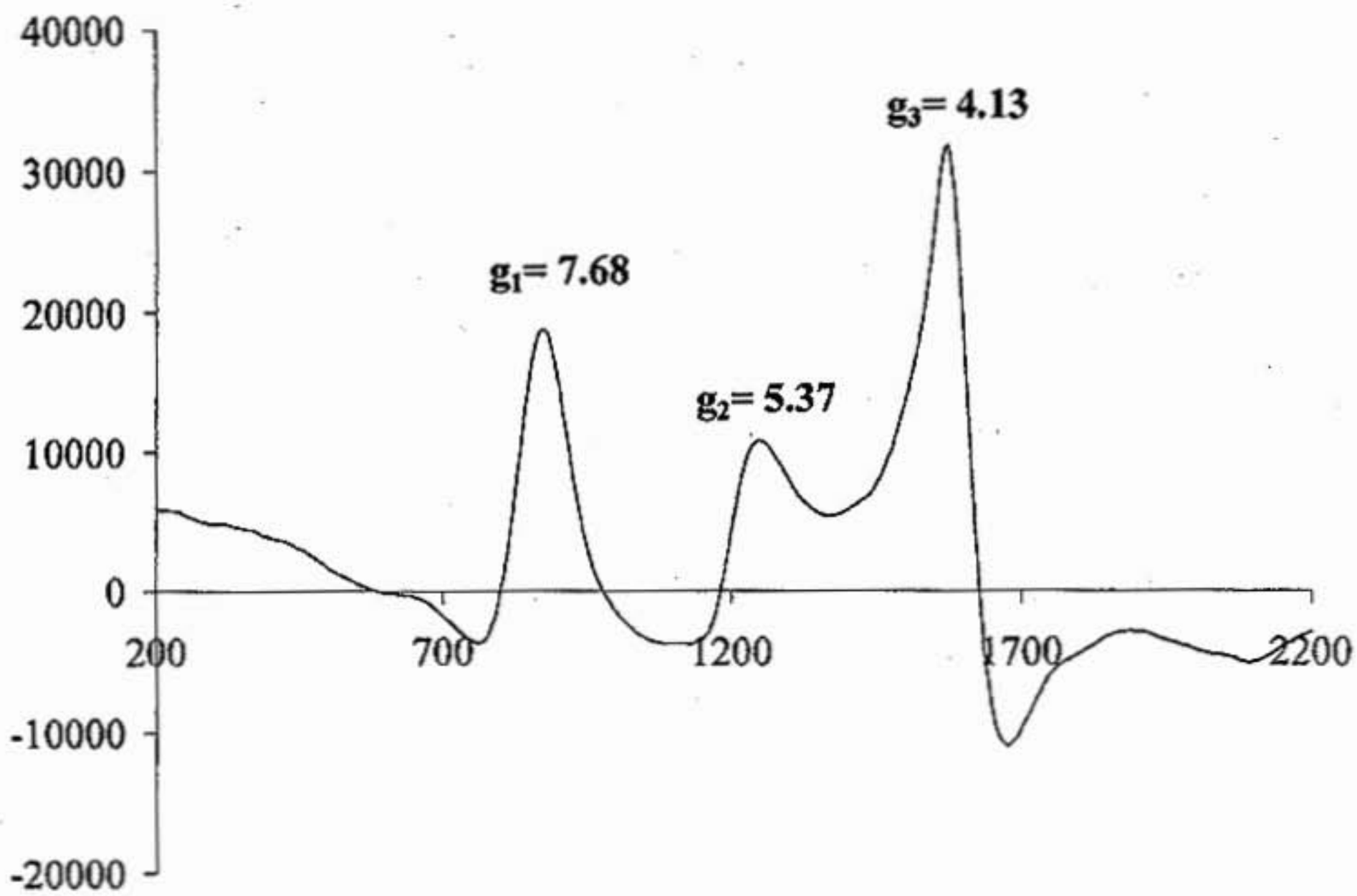

Figure 3.07. The reaction between $[Fe^{II}(cyclam\text{-}PrS)]^+$ and H_2O_2 in 2-MeTHF glass, monitored by EPR. The experiment was initiated at -78°C and allowed to develop for approximately 30 seconds before quenching at 77 K.

The reaction was then performed in MeOH (at -78°C), to study the effect of performing the shunt reaction under protic conditions. The addition of 2.0 equivalents of H_2O_2 to a cooled solution of $[Fe^{II}(cyclam\text{-}PrS)]^+$ caused the immediate formation of a different transient purple intermediate species, with a λ_{max}=544nm. The absorption spectrum of which is shown below in **Figure 3.08.**

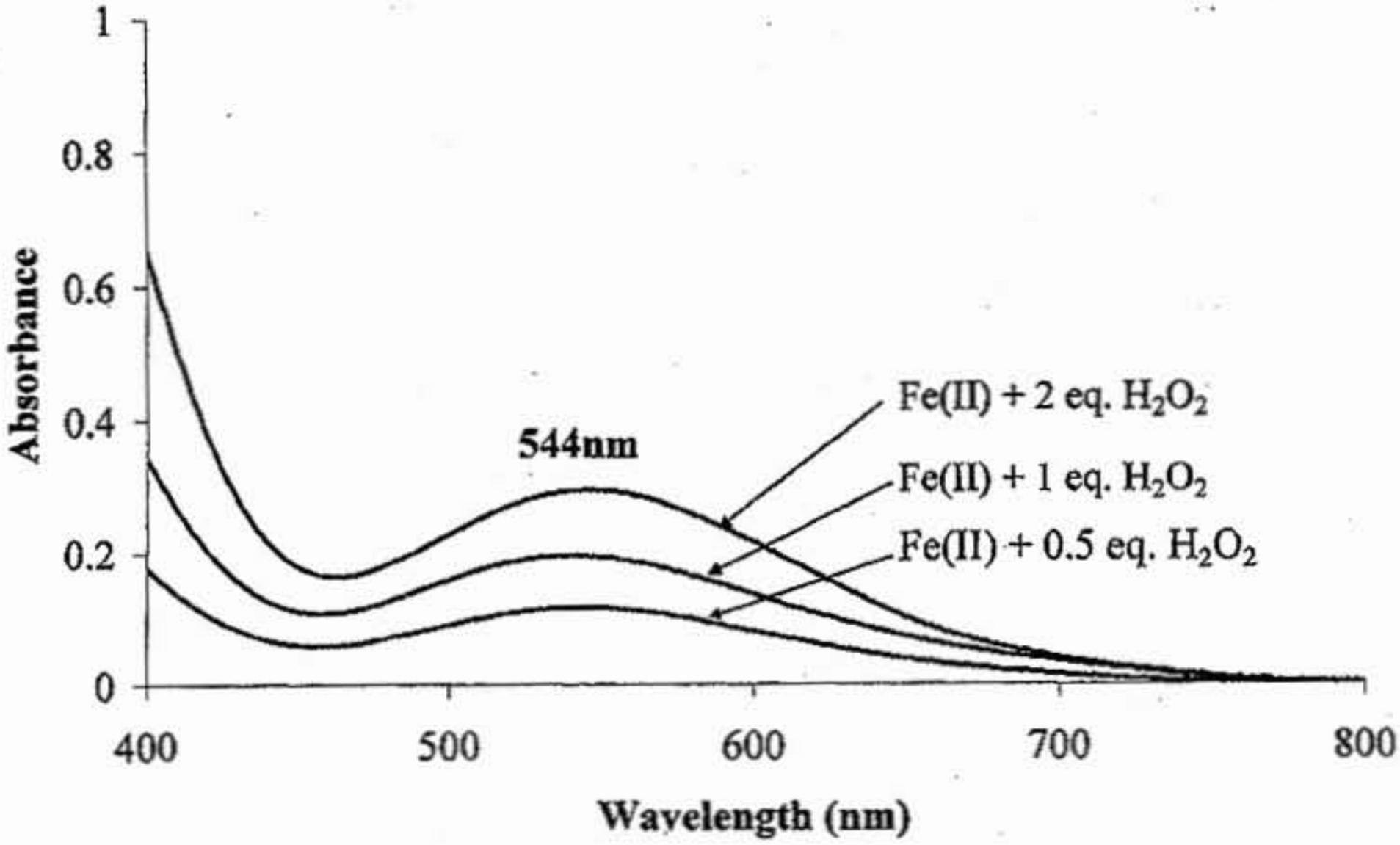

Figure 3.08. The reaction between **[Fe^{II}(cyclam-PrS)]$^+$** and H_2O_2 in MeOH at -78°C.

It appears based on the absorption data that this species could be the Fe^{III}-OMe bound species seen when the reaction with KO_2 is performed in MeOH. However, a clean EPR spectrum of this species could not be obtained and should be the target of future work.

Aqueous chemistry. The reactivity of the vast majority of non-heme iron complexes are studied in organic solvents. While there are examples of metalloporphyrin chemistry performed under aqueous conditions, the study of analogous non-heme iron complexes under similar conditions has not been pursued extensively.[15] Aqueous chemistry is desirable because it is green and biologically relevant. This is especially important when

studying SOR, because the chemistry of this enzymes is pH-dependent. Studying the chemistry of our model complexes in water would allow us to buffer the solutions that the experiments are performed in, providing direct insight into the relationship between pH and SOR chemistry.

However, because our intermediates are extremely thermodynamically unstable, controlling the formation of the intermediate **$[Fe^{III}(cyclam\text{-}PrS)(OOH)]^+$** by cooling the reaction to subzero temperatures becomes a necessity. This becomes a liability when working with water. Based on this, a mixture of isopropanol and water (H_2O:iPrOH = 70:30) was used for each reaction, allowing the solution to be cooled to a minimum of -30°C without freezing. This mixture also can allow for accurate pH buffering to be performed as well, which is similar to conditions adapted by Nam and coworkers (H_2O: CH_3CN = 3:1).[15]

Preliminary reactions were performed to study the reactions of **$[Fe^{II}(cyclam\text{-}PrS)]^+$** and KO_2, O_2 and H_2O_2 at ~ -15°C to -20°C in aqueous solutions. Because the solvent mixture was very viscous at reduced temperatures, solubility because an issue when working with KO_2 and O_2. However, a transient purple intermediate immediately formed when H_2O_2 was added to **$[Fe^{II}(cyclam\text{-}PrS)]^+$**. This species has an absorption band at 523 nm and the absorption spectrum is shown here in **Figure 3.09.** This species is very similar in appearance to the species generated during the reaction between **$[Fe^{II}(cyclam\text{-}PrS)]^+$** and H_2O_2 in THF. EPR data needs to be acquired in order to assist in the identification of this species.

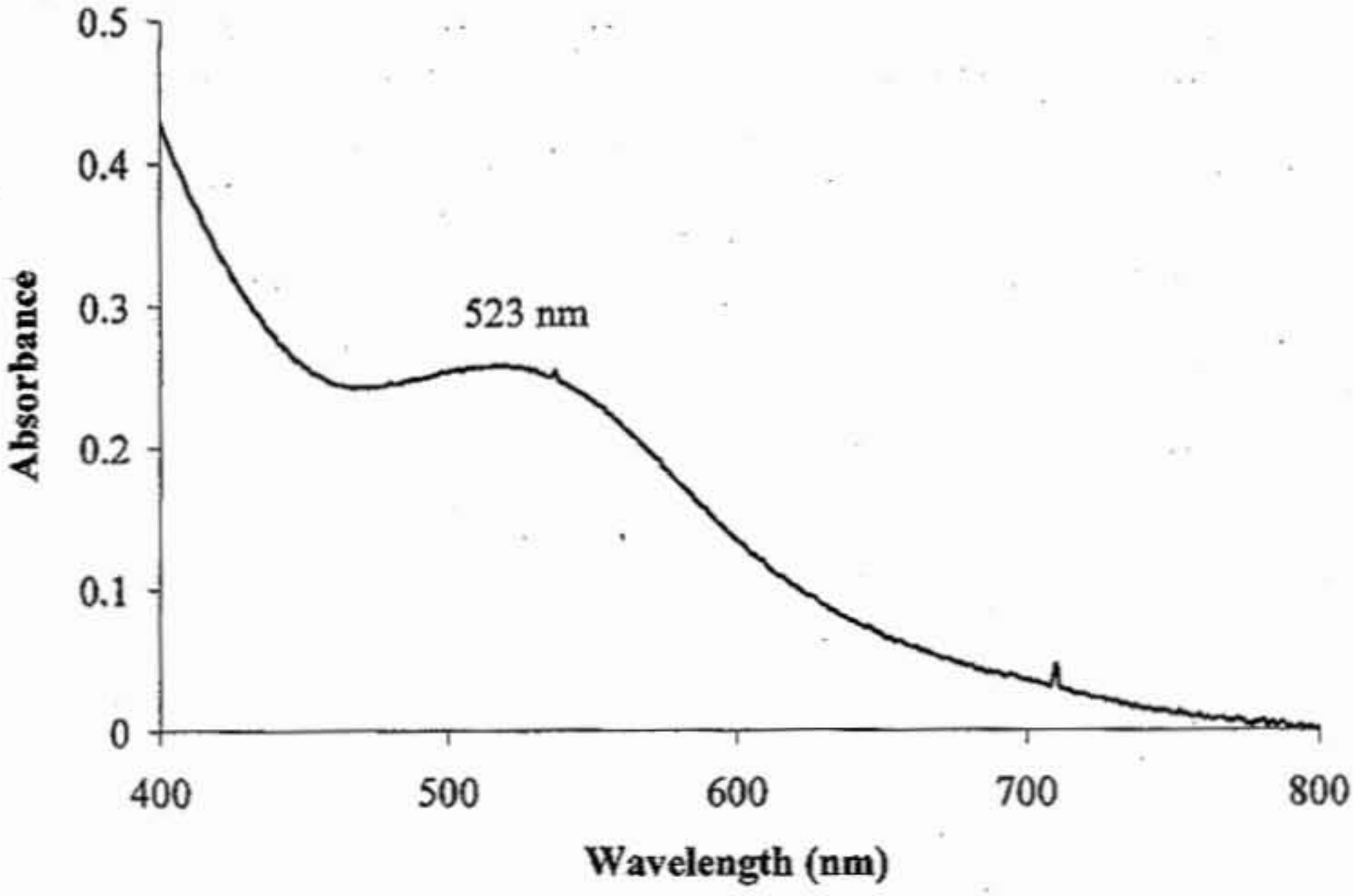

Figure 3.09. The reaction between $[Fe^{II}(cyclam\text{-}PrS)]^+$ and H_2O_2 in H_2O-iPrOH (70:30) at -15°C.

Reaction with *m*CPBA. High valent Fe^{IV}=O species have been implicated as the main oxidizing species in the mechanisms of heme- and non-heme iron enzymes which are capable of performing complex biotransformations.[16] Recently, Fe^{IV}=O species have been physically and spectroscopically characterized, and much has been reported about the reactivities of metalloenzymes and biomimetic models.[11,17] In particular, the $[Fe^{IV}TMCS(O)]^+$ complex has been characterized via EXAFS, providing the first insight into a thiolate-containing non-heme Fe^{IV} complex.[11] Additionally, this species was shown to undergo hydrogen-atom abstraction (one-electron oxidation) as opposed to oxygen-atom transfer to PPh_3 (two-electron oxidation), which its non-thiolate containing counterpart $[Fe^{IV}(TMC)(OTf)]^{2+}$ is capable of doing, providing important insight into

the effect that introducing a thiolate ligand into the coordination sphere of an Fe^{IV} complex has on its ability to perform specific chemical transformations.

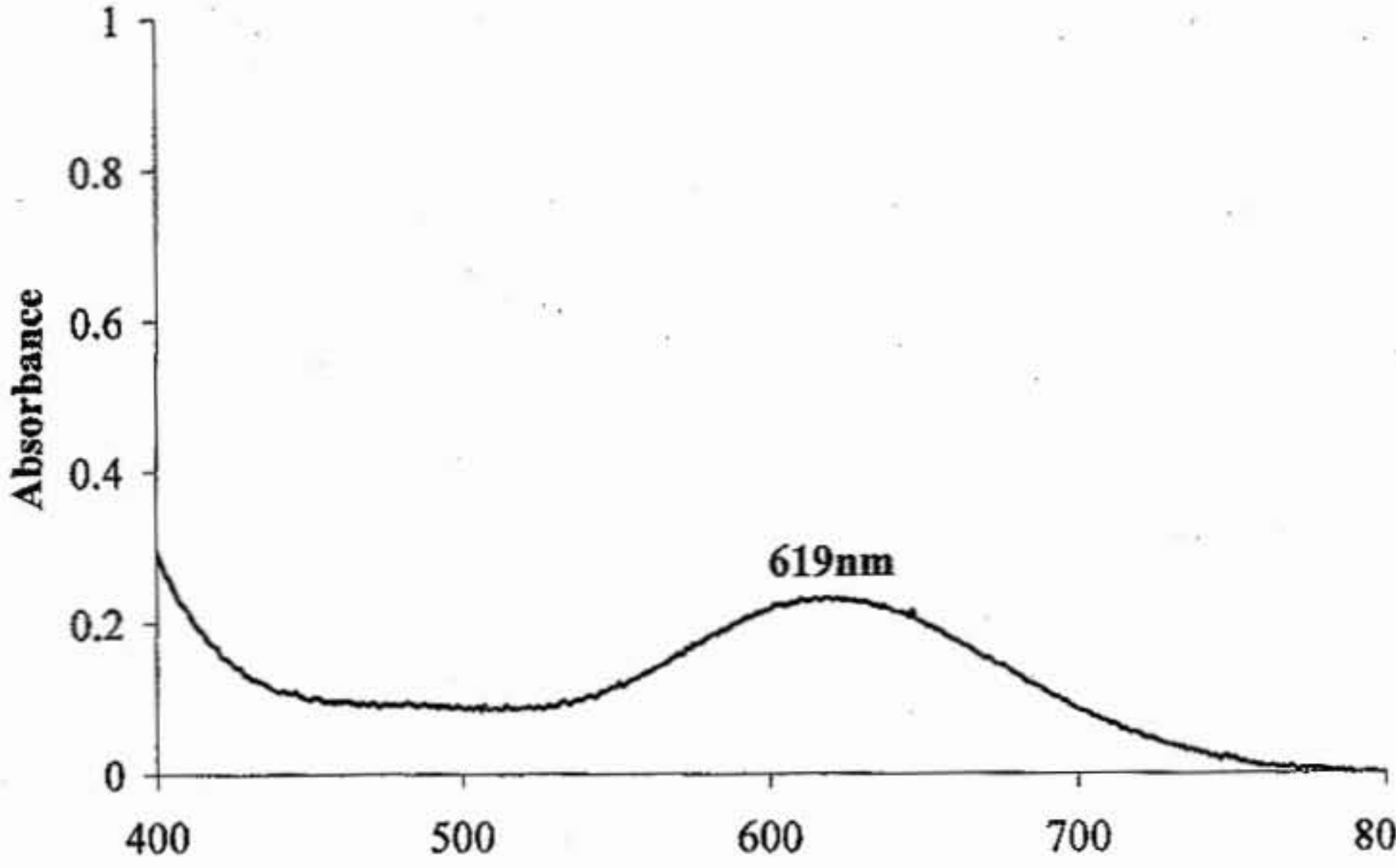

Figure 3.10. The reaction between **$[Fe^{II}$(cyclam-PrS)$]^+$** and *m*CPBA in CH_3CN at -40°C.

The reaction of 0.5 equivalents of *m*CPBA with **$[Fe^{II}$(cyclam-PrS)$]^+$** at -40°C in CH_3CN caused the instantaneous formation of an aqua blue transient intermediate, characterized by an absorption band at 619 nm. It was found that additional *m*CPBA beyond 0.5 equivalents caused the decomposition of this species, and the bleaching of the color. This species was stable for about 20 minutes at this temperature before the intensity of the absorption band began to lower, most likely due to decomposition. The absorption spectrum of this reaction is shown below in **Figure 3.10.** The identity of this

complex remains to be seen. It is possible that this is an Fe^{IV}=O species, but we also cannot rule out the possibility of this aqua-colored intermediate being an Fe^{III} species either, produced via an Fe^{IV} intermediate. Obtaining Mössbauer and EPR data is imperative to identifying this complex and its mechanism of formation, and should be collected on this reaction in the future.

Exogenous ligand binding – studying the effect of the *trans* thiolate. The binding of exogenous ligands such as azide (N_3^-) and cyanide (CN^-) to SOR has been studied extensively. Previously in Chapter 2, the experimental binding of N_3^-, CN^- and the acetate (OAc^-) ligand to the **$[Fe^{II}$(cyclam-PrS)$]^+$** complex in the presence of the one-electron oxidant $FeCp_2PF_6$ was described in detail. The difference in the energies of the respective charge transfer bands in the absorption spectra appeared to follow a trend; the "harder" the ligand, the higher the energy of its respective charge transition. Resonance Raman studies have shown that the origin of the charge transfer band at 608 nm for the **$[Fe^{III}$(cyclam-PrS)(OAc)$]^+$** complex stems almost completely from the Fe-S interaction, most likely from S(π)→Fe(π) charge transfer. By observing the extreme blue shift of the absorption band of from 608 nm (OAc^--bound) to 564 (CN^--bound), it can be postulated that the positioning of a π-acceptor CN^- ligand *trans* to the π-donor Fe-S has a synergistic effect, increasing the energy of the transition between the Fe^{III} center and the thiolate ligand. To probe this effect, a series of binding experiments with several halides (X–= F-, I-) were performed. These halides have similar electronic character, all of them being anionic-ligands with the same valence electron count, but differ in the context of hard-

soft ligands. The increase in the atomic size of each of the halogens and the respective differences in their electronegativities provides different levels of interaction with the Fe^{III} center, which would lead to a direct probe of the *trans* effect they have on the Fe^{III} center and the *trans*-ligated thiolate ligand.

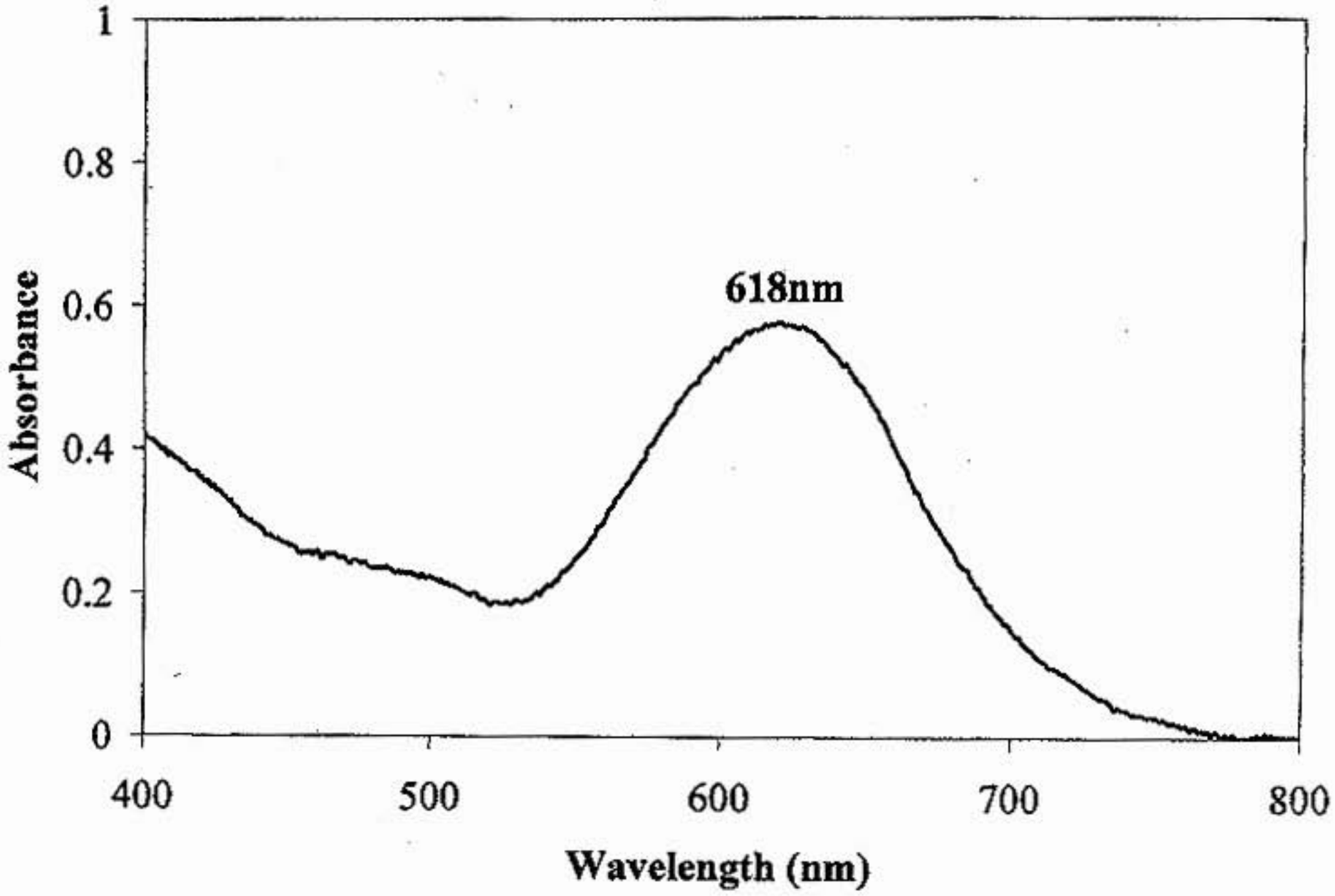

Figure 3.11. The binding reaction between **$[Fe^{II}$(cyclam-PrS)$]^+$** and NEt_4I in the presence of $FeCp_2PF_6$ in CH_2Cl_2 at -78°C.

The reactions were performed in rigorously dried dichloromethane at -78°C. The solution of **$[Fe^{II}$(cyclam-PrS)$]^+$** was pre-cooled to -78°C and 1 equivalent of $FeCp_2PF_6$ was added to the while stirring. The first experiment involved the binding of I^-, which was accomplished by adding 1 equivalent of NEt_4I from a pre-made stock solution. The solution immediately turned green-blue and the UV-vis analysis showed the appearance

of an intense absorption band in the visible region at 618 nm. This species was stable for about 30 minutes at -78°C before the color began to bleach. The absorption spectrum is shown in **Figure 3.11.**

The next reaction was between $[Fe^{II}(cyclam\text{-}PrS)]^+$ and NBu_4F in the presence of $FeCp_2PF_6$ in CH_2Cl_2 at -78°C. The immediate formation of a deep violet species was observed, characterized by an intense absorption band at 543 nm. This species was much less stable than that obtained by the addition of NEt_4I, as it began to decompose after 10 minutes. The absorption spectrum is shown here in **Figure 3.12.**

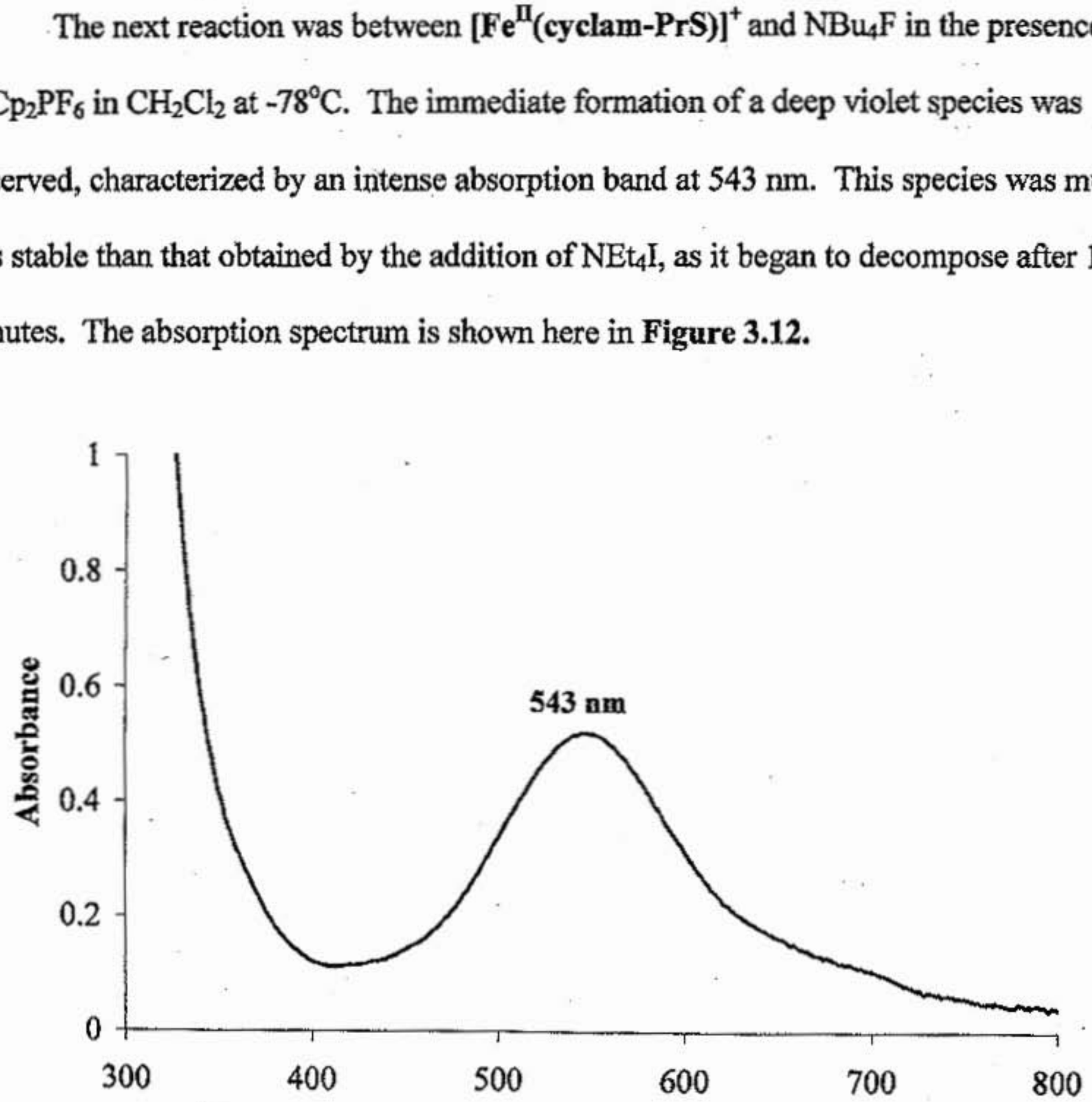

Figure 3.12. The reaction between $[Fe^{II}(cyclam\text{-}PrS)]^+$ and NBu_4F in CH_2Cl_2 at -78°C.

Conclusion. **$[Fe^{II}(cyclam\text{-}PrS)]^+$** has shown diverse reactivity with biorelevant oxidants such as dioxygen and H_2O_2, forming transient intermediates reminiscent of the **$[Fe^{III}(cyclam\text{-}PrS)(OOH)]^+$** species obtained via reaction with KO_2 in the presence of protons. It appears that based on the absorption data and the g-values obtained by EPR, the species obtained in the reaction between **$[Fe^{II}(cyclam\text{-}PrS)]^+$** and H_2O_2 in THF or Me-THF is also **$[Fe^{III}(cyclam\text{-}PrS)(OOH)]^+$**, identical to the species obtained in the SOR reaction. This successfully mimics the "shunt" mechanism that is often used by synthetic chemists to generate Fe^{III}-OOH species. This method has also been used successfully by Niviere *et al* to model the Fe^{III}-OOH intermediate in SOR. It provides an alternative method to generating our **$[Fe^{III}(cyclam\text{-}PrS)(OOH)]^+$** without the issues of solubility or secondary disproportionation reactions seen with KO_2. This will undoubtedly allow for easier generation and characterization of **$[Fe^{III}(cyclam\text{-}PrS)(OOH)]^+$** and should be pursued in future experiments.

Because of its structural similarity with cytochrome P450, the reactivity between **$[Fe^{II}(cyclam\text{-}PrS)]^+$** and *m*CPBA has also been explored, in an effort to access the high-valent Fe^{IV}=O species and to see if a synthetic model of Compound I in the cytochrome P450 catalytic cycle can be produced. The addition of *m*CPBA to **$[Fe^{II}(cyclam\text{-}PrS)]^+$** caused the formation of an aqua blue species, weakly colored with an absorption band at 619 nm. It is not yet understood what this species is. Mössbauer spectroscopy and resonance Raman, along with EPR spectroscopy, would help to identify the nature of this species.

Finally, because almost all of the exogenous ligands tested for binding to the oxidized Fe^{III} form (generated *in situ*) have very similar characteristic intensities and a single absorption band in the visible region, a pragmatic comparison can be made based on the λ_{max} positioning. In order of increasing energy of the major absorption bands, the exogenous ligands follow the order: $\mathbf{I^- < OAc^- < N_3^- < F^- < OMe^- < OOH^- < NO^-}$. In general, it appears that smaller, harder ligands have increasing σ-interaction with the Fe center, a direct result of the presence of the *trans* thiolate being present across from the open site of the Fe center.

Chapter 3 – Notes

(1) Costas, M.; Mehn, M. P.; Jensen, M. P.; Que, L., Jr. *Chem Rev* **2004**, *104*, 939-86.

(2) Selke, M.; Sisemore, M. F.; Ho, R. Y. N.; Wertz, D. L.; Valentine, J. S. *Journal of Molecular Catalysis A: Chemical* **1997**, *117*, 71-82.

(3) Montellano, P. R. O. d.; Voss, J. J. D. *Nat. Prod. Re.* **2002**, *19*, 477-493.

(4) Mathe, C.; Mattioli, T. A.; Horner, O.; Lombard, M.; Latour, J. M.; Fontecave, M.; Niviere, V. *J Am Chem Soc* **2002**, *124*, 4966-7.

(5) Kehrer, J. P. *Toxicology* **2000**, *149*, 43-50.

(6) Roelfes, G.; Vrajmasu, V.; Chen, K.; Ho, R. Y.; Rohde, J. U.; Zondervan, C.; La Crois, R. M.; Schudde, E. P.; Lutz, M.; Spek, A. L.; Hage, R.; Feringa, B. L.; Munck, E.; Que, L., Jr. *Inorg Chem* **2003**, *42*, 2639-53.

(7) Hazell, A.; McKenzie, C. J.; Nielsen, L. P.; Schindler, S.; Weitzer, M. *J Chem Soc, Dalton Trans* **2002**, 310-317.

(8) Jensen, M. P.; Lange, S. J.; Mehn, M. P.; Que, E. L.; Que, L., Jr. *J Am Chem Soc* **2003**, *125*, 2113-28.

(9) van den Berg, T. A.; de Boer, J. W.; Browne, W. R.; Roelfes, G.; Feringa, B. L. *Chem Commun (Camb)* **2004**, 2550-1.

(10) Lim, M. H.; Rohde, J. U.; Stubna, A.; Bukowski, M. R.; Costas, M.; Ho, R. Y.; Munck, E.; Nam, W.; Que, L., Jr. *Proc Natl Acad Sci U S A* **2003**, *100*, 3665-70.

(11) Bukowski, M. R.; Koehntop, K. D.; Stubna, A.; Bominaar, E. L.; Halfen, J. A.; Munck, E.; Nam, W.; Que, L., Jr. *Science* **2005**, *310*, 1000-2.

(12) Brines, L. M.; Kovacs, J. A. *Eur. J. Inorg. Chem* **2007**, 29-38.

(13) Theisen, R. M.; Shearer, J.; Kaminsky, W.; Kovacs, J. A. *Inorg Chem* **2004**, *43*, 7682-90.

(14) Kim, S. O.; Sastri, C. V.; Seo, M. S.; Kim, J.; Nam, W. *J Am Chem Soc* **2005**, *127*, 4178-9.

(15) Sastri, C. V.; Sook Seo, M.; Joo Park, M.; Mook Kim, K.; Nam, W. *Chem Commun (Camb)* **2005**, 1405-7.

(16) Makris, T. M.; von Koenig, K.; Schlichting, I.; Sligar, S. G. *J Inorg Biochem* **2006**, *100*, 507-18.

(17) de Visser, S. P. *J Am Chem Soc* **2006**, *128*, 9813-24.

Chapter 4
$[Fe^{II}(N^{EtS})N_4(tren)Cl]^+$: a non-thiolate containing analogue of $[Fe^{II}N_4(tren)S^{Me2}]^+$

Introduction. The interest in studying Fe complexes with such nitrogen-rich ligand systems also stems from structural similarities with many histidine-ligated iron-containing enzymes, such as the intradiol-cleaving catechol dioxygenases, Rieske dioxygenases, and isopenicillin N-synthase, among various other enzymes containing nitrogen-rich ligand environments.[1] Bleomycin (BLM), a natural product used in antitumor therapy, chelates via five nitrogens to an Fe^{II} center. The interesting characteristic that each of these species share is that they react with dioxygen to form a highly reactive Fe^{III}-(hydro)peroxo species.

Biomimetic modeling has played a large role in understanding the chemistry of each of the histidine-ligated metalloenzymes. Que, Girerd and McKenzie have reported the most comprehensive set of data pertaining to Fe-N_5 complexes.[2-10] The respective Fe^{II} complexes have been shown to react with H_2O_2 to form Fe^{III}-OOH intermediates. These systems have been used successfully to model BLM and the activated bleomycin species (aBLM), which has been characterized as a low-spin Fe^{III}-hydroperoxo intermediate. Interestingly, each has shown the ability of the hydroperoxo moiety to be deprotonated by mild bases to form a side-on Fe^{III}-peroxo species. The addition of a proton donor causes the regeneration of the end-on Fe^{III}-OOH species. The work of these groups has led to the direct observation of these metastable intermediates, allowing for very detailed characterization of each binding mode and providing the most detailed and complete set of benchmark parameters to study the mechanism of H_2O_2 activation by a

non-heme iron center. The ability to observe these peroxo intermediates also demonstrated the different possible coordination modes of the peroxo moiety to the iron center, i.e. η^2-side-on peroxo versus η^1-end-on hydroperoxo. An example of this reversible protonation is shown here in **Figure 4.01.**

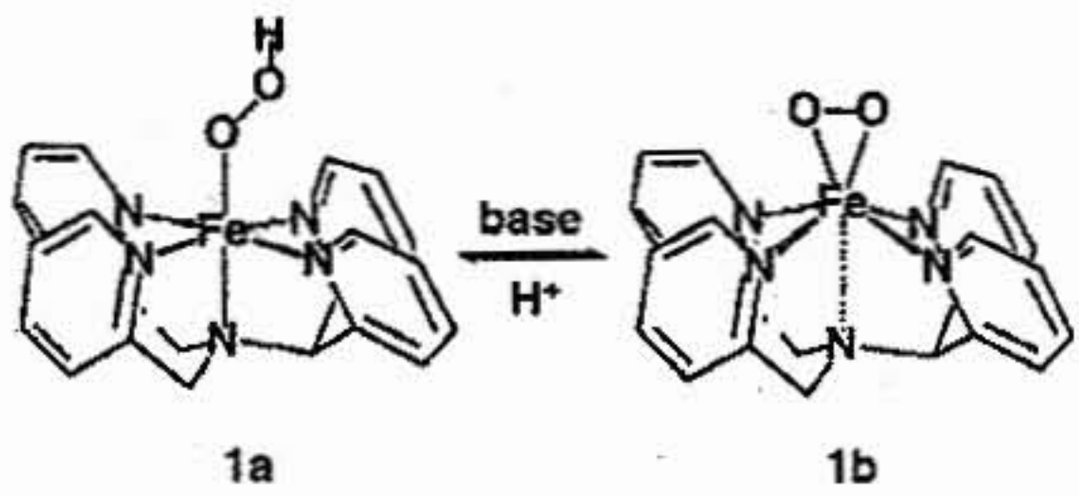

Figure 4.01. The acid-base interconversion between end-on bound **$[Fe(N4Py)OOH]^{2+}$ (1a) and $[Fe(N4Py)O_2]^{+}$ (1b).** Figure is adapted from Que et al, reference 19.

More recently, nitrogen-ligated non-heme Fe^{II} complexes have shown the ability to be oxidized to higher-valent Fe^{IV}=O and Fe^{V}=O species.[11] Oxoiron(IV) and oxoiron(V) species are invoked as reactive intermediates in the chemistries of both the heme-containing enzyme cytochrome P450 and non-heme iron enzymes.[12] Que and coworkers have been successful in stabilizing and isolating these metastable species and have reported solid state parameters of these species from x-ray crystallography.[11] These complexes each share a nitrogen-rich ligand environment, meticulously tuned to support and stabilize the higher oxidation states.

Recently a new class of non-heme iron enzymes ligated by cysteinate residues has emerged. These enzymes consist of nitrile hydratase, peptide deformylase and superoxide reductase (SOR).[13] In particular, SOR has become a very important research

target because of its structural similarity with the heme-containing iron enzyme cytochrome P450. The active sites of both enzymes are very similarly structured, but perform drastically different chemistry (*vide infra*).

Biomimetic modeling has also played an invaluable role in understanding the effect of the thiolate ligand with respect to its presence and positioning. The thiolate-containing Kovacs SOR model complexes, $[Fe^{II}N_4(tren)S^{Me2}]^+$ and $[Fe^{II}cyclam(PrS)]^+$ have been shown to activate superoxide.[14-19] Additionally, they have been shown to activate dioxygen, leading to O-O bond cleavage in the former complex. Kovacs and Mascharak have also characterized an extensive set of thiolate-ligated non-heme iron complexes, shown to be very air-sensitive.[14,18]

Understanding how each ligand environment participates in substrate activation, and the effect that the *trans*-cysteinate residue has on the metal-mediated chemistry are currently the focus of many scientists. In particular, a unique property of these cysteinate-ligated Fe complexes is that they possess drastically different spectroscopic properties relative to other enzymes containing only histidines. For example, the charge transfer transition from the sulfur to the Fe^{III} center causes the formation of intensely colored species. This unique property allows for easier and better spectroscopic analysis of the complexes relative to their histidine-only containing counterparts.

Studying the effects of thiolate ligation. The chemistry of non-heme iron-containing enzymes containing an N_5-ligand system is well-documented in the literature and provides a plethora of benchmark parameters allow the assignment of spectroscopically

observed intermediates. Additionally, the structure and chemistry of the thiolate-ligated Kovacs $[Fe^{II}N_4(tren)S^{Me2}]^+$ model has also been thoroughly described.[16-18] Thus, an obvious research target would be to synthesize a structurally analogous model of $[Fe^{II}N_4(tren)S^{Me2}]^+$, containing an apical nitrogen ligand in lieu of the thiolate ligand. In order to do so, the thioketone reagent was replaced by diethylaminoacetone (DEAA). The use of this reagent would allow us to follow the synthetic pathway for the $[Fe^{II}N_4(tren)S^{Me2}]^+$ model, while providing us with an analogous nitrogen-containing analogue of the thiolate-ligated $[Fe^{II}N_4(tren)S^{Me2}]^+$ model. This complex, referred to as $[Fe^{II}(N^{Et2})N_4(tren)Cl]^+$, is, to the best of our knowledge, the first aliphatic non-heme N_5-ligated complex characterized. By having a direct analog to the well-studied thiolate-ligated $[Fe^{II}N_4(tren)S^{Me2}]^+$ model, determining the effect of thiolate-ligation to the Fe^{II} center is more direct.

Experimental Section.

General Methods. Unless otherwise noted, all reactions were performed under an inert atmosphere of dinitrogen or argon in a drybox or using standard Schlenk techniques. Reagents purchased from commercial vendors were of the highest purity available and were used without further purification. Acetonitrile and dichloromethane were dried over CaH_2. Methanol was dried over $Na/CaH_2/I_2$. Pentane and tetrahydrofuran were dried over sodium benzophenone ketyl. Tetra-n-butyl (PF_6) was recrystallized three times in ethanol and dried under reduced pressure for 48 hours. KCl was recrystallized three

times in deionized water/acetone and dried under reduced pressure for 48 hours. Water was purified using a MilliQ purification system.

Physical Methods. NMR spectra were recorded using Bruker DRX-499, DPX-200, AF-301, or AC-200 spectrometers. ^{1}H-NMR spectra were referenced to either TMS or residual proton peaks in the deuterated solvent and chemical shifts are reported in ppm. Cyclic voltammograms were recorded on a Princeton Applied Research Model 273 potentiostat with a glassy carbon working electrode, a platinum wire counter electrode, and a saturated calomel electrode (SCE) reference electrode. Electrochemical experiments were performed in acetonitrile and methanol (100mM tetra-n-butyl (PF_6) solutions) and water (100mM KCl solutions). IR spectra were recorded on a Perkin-Elmer 1720 FT-IR spectrometer as KBr pellets. Electronic absorption spectra were recorded on a Hewlett-Packard model 8452A diode array spectrophotometer and a Varian Cary 50 spectrophotometer. Electrospray mass spectra were recorded on a Bruker Esquire Liquid Chromatograph - Ion Trap Mass Spectrometer.

$[Fe^{II}(N^{Et2})N_4(tren)Cl]PF_6$. A solution of tren (0.584 g, 0.004 mol) was dissolved in 10 ml of dry methanol, followed by the addition of diethylaminoacetone (0.532 g, 0.004 mol). This solution was allowed to stir for 10 minutes. $Fe^{II}Cl_2$ (0.504 g, 0.004 mol) was dissolved in 5 ml of dry methanol and added to the ligand mixture dropwise, immediately producing a yellow precipitate. $NaPF_6$ (1.34 g, 0.008 mol) was added and the reaction mixture was allowed to stir overnight. The precipitate was filtered and washed with

methanol to yield 0.612 g (31%) of $[Fe^{II}(N^{Et2})N_4(tren)Cl]PF_6$ as a pale yellow solid. Yellow needle-like crystals were obtained by slow diffusion of diethyl ether into an acetonitrile solution.

1) **Preparation of $[Fe^{III}(N^{Et2})N_4(tren)](PF_6)_2$.** The oxidized Fe^{III} complex was prepared by two methods. The first method was done using ferrocenium hexafluorophosphate in order to chemically oxidize the Fe^{II} intermediate to the Fe^{III} form. The second method involved the direct preparation from $FeCl_3$.

a) $[Fe^{II}(N^{Et2})N_4(tren)Cl]PF_6$ (0.400 g, $6.63x10^{-4}$ mol) was dissolved in 20 ml of acetonitrile. To this solution was added ferrocenium hexafluorophosphate (0.220 g, $6.63x10^{-4}$ mol). Solution was allowed to stir overnight, yielding a deep purple solution. The solvent was removed and the solid was washed with diethyl ether until the solvent ran clear, indicating the removal of the ferrocene byproduct. The solid was then dissolved in a minimal amount of acetonitrile and precipitated with diethyl ether, affording 0.250 g (62.6%) of a dark purple solid. Electronic Absorption λ_{max} nm (ε cm^{-1} M^{-1}): 564 (2129) in acetonitrile, 570 (2100) in methanol.

b) The ligand mixture was prepared as previously described. A solution of tren (0.584 g, 0.004 mol) was dissolved in 10 ml of dry methanol, followed by the addition of diethylaminoacetone (0.532 g, 0.004 mol). This solution was allowed to stir for 10 minutes. $FeCl_3$ (0.649 g, 0.004 mol) was dissolved in 10 ml of methanol and added dropwise to the ligand

mixture. The solution was allowed to stir overnight, yielding a purple solution. The solution was filtered through bed of Celite in a glass frit. The solvent was removed under reduced pressure, yielding 0.987 g (50%) of a deep purple solid (0.987 g, 0.002 mol) with identical absorption properties.

X-ray Crystallographic Structure Determination.

$[Fe^{II}(N^{Et2})N_4(tren)Cl]PF_6$. A birefringent yellow crystal prism of **$[Fe^{II}(N^{Et2})N_4(tren)Cl]PF_6$** was cut down to 0.24 x 0.12 x 0.12 mm, submerged in oil and mounted on a glass capillary. Data was collected at ambient temperature (23°C). The crystal-to-detector distance was 30mm and the exposure time was 15 seconds per degree for all sets with a scan width of 1.8°. Data collection was 98.6% complete to 24.71o in 9. A total of 20518 partial and complete reflections were collected covering the indices, h = -15 to 16, k = -21 to 21, l = -10 to 10. 3472 reflections were symmetry independent and the Rint = 0.116 indicating that the data was of less than average quality. Indexing and unit cell refinement indicated an orthorhombic P lattice in the space group $Pna2_1$. The data was integrated and scaled using hkl-SCALEPACK. Solutions by direct methods (SIR97) produced a complete heavy atom phasing model consistent with the proposed structure. All hydrogen atoms were located using a riding model, and all non-hydrogen atoms were refined anisotropically by full-matrix least-squares.

$[Fe^{III}(N^{Et2})N_4(tren)NO_3]NO_3$. A light-purple prism, size 0.40 x 0.34 x 0.05 mm was mounted on a glass capillary with oil. Data was collected at -143°C with one set of exposure. Crystal-to-detector distance was 30 mm and exposure time was 40 seconds per degree for all sets. The scan width was 1°. Data collection was 85.5 % complete to 20.8° in 9. A total of 25078 partial and complete reflections were collected covering the indices, h = -10 to 10, k = -24 to 25, l = -7 to 7. 1781 reflections were symmetry independent and the R_{int} = 0.1000 indicated that the data was of slightly less than average quality (0.07). Indexing and unit cell refinement indicated a monoclinic C lattice. The space group was found to be C c (non-centrosymmetric). The data was integrated and scaled using hkl-SCALEPACK. Solution by direct methods (SIR97) produced a complete heavy atom phasing model consistent with the proposed structure. All hydrogen atoms were located using a riding model. All non-hydrogen atoms were refined anisotropically by full-matrix least-squares.

Synthesis and characterization of $[Fe^{II}(N^{Et2})N_4(tren)Cl]^+$. The preparation of this complex involves a modified procedure based on general methods used in the Kovacs group to prepare a variety of Schiff-base complexes.[16] The reaction scheme is shown in **Figure 4.02**.

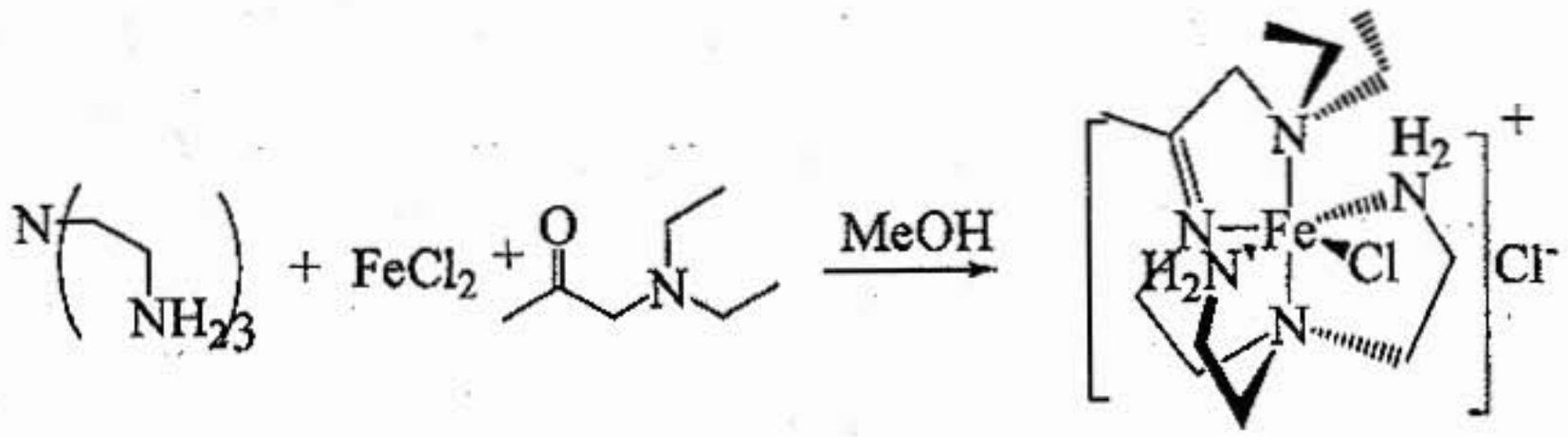

Figure 4.02. The synthesis of $[Fe^{II}(N^{Et2})N_4(tren)Cl]^+PF_6^-$.

The preparation of the metal complex involved the mixing of tris-(2-aminoethyl)amine (tren) with DEAA in methanol and allowing the reaction mixture to stir at ambient temperature. The Schiff-base condensation between tren and DEAA leads to the formation of a pentadentate ligand system. $FeCl_2$ was then dissolved in methanol and added dropwise to the ligand solution while stirring. Immediately, a pale yellow solid precipitated from the solution. The addition of $NaPF_6$ causes the further deposition of a pale yellow solid, which was crystallographically characterized as the monocationic six-coordinate species $[Fe^{II}(N^{Et2})N_4(tren)Cl]^+$. This complex was found to be completely soluble in acetonitrile, slightly less soluble in methanol, and sparingly soluble in dichloromethane. Additionally, it was found to be fairly robust under aerobic conditions. As a solid, it was stable for 24 hours under an aerobic atmosphere before

slow decomposition to a brown solid began to be observed, most likely rust and other iron-containing and ligand decomposition byproducts.

X-ray quality pale yellow needles of $[Fe^{II}(N^{Et2})N_4(tren)Cl]^+$ were obtained after slow diffusion of ether/acetonitrile (~10:1) over a three week period. The ORTEP is shown in **Figure 4.03.**

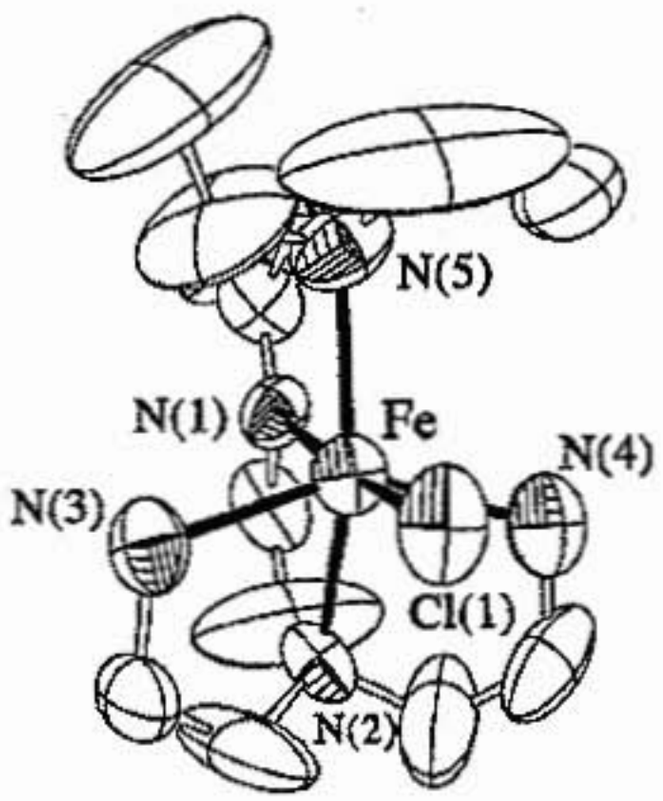

Figure 4.03. The ORTEP diagram of crystallographically characterized $[Fe^{II}(N^{Et2})N_4(tren)Cl]^+$. The large ellipsoids on the bis-ethylated apical amine denote a high amount of disorder at the site.

Notably, the ferrous species is a six-coordinate monocationic complex in a distorted octahedral geometry, with chloride bound to the inner sphere. Comparatively, the $[Fe^{II}S^{Me2}N_4(tren)]^+$ model complex is five-coordinate in a distorted trigonal bipyramidal geometry. The presence of the sixth ligand can be attributed to the lower electron donating ability and the increased electronegativity of the apical nitrogen, as opposed to the apical thiolate ligand. This would increase the Lewis acidity of the iron center, thus explaining its higher affinity for a sixth ligand. This is not unexpected, as Fe^{II}-N_5 complexes characterized thus far in the literature also have a sixth ligand in the

open site, which is either a charged counterion or neutral solvent molecule.[5,11,20,21] Finally the large ellipsoids of the ethyl groups attached to the apical nitrogen indicate a large degree of disorder, caused by collecting the data at ambient, as opposed to low temperatures. A phase change observed upon cooling precluded the collection of X-ray data at the preferred lower temperatures. Table 4.01 shows significant bond lengths and bond angles for this complex.

Table 4.01. Selected bond lengths and bond angles of **$[Fe^{II}(N^{Et2})N_4(tren)Cl]PF_6$.** The ORTEP is shown in **Figure 4.03** for reference.

Bond lengths (Å)		**Bond angles (deg)**	
Fe-N(1)	2.131	N(1)-Fe(1)-N(3)	97.8
Fe-N(2)	2.267	N(1)-Fe(1)-N(4)	92.5
Fe-N(3)	2.215	N(3)-Fe(1)-N(4)	148.2
Fe-N(4)	2.232	N(1)-Fe(1)-N(2)	77.2
Fe-N(5)	2.293	N(3)-Fe(1)-N(2)	76.7
N(1)-C(7) (C=N)	**1.234**	N(4)-Fe(1)-N(1)	76.4
		N(1)-Fe(1)-N(5)	75.1
		N(3)-Fe(1)-N(5)	107.0
		N(4)-Fe(1)-N(5)	104.7
		N(2)-Fe(1)-N(5)	152.3

The Fe-N(5) bond length is 2.293Å, which is slightly shorter than the Fe-S bond length of $[Fe^{II}S^{Me2}N_4(tren)]^+$ (2.329 Å). This makes sense based on the differences in N versus S covalent radii. The Fe-N(1) bond length is 2.131 Å, which is slightly longer than the normal range for Fe^{II}-imine bond lengths.[16,22] The trans effect of the bound anionic chloride ligand most likely causes this bond elongation. The average Fe-N bond length is 2.23 Å, which is indicative of a high spin Fe^{II} complex.[10] The presence of the

anionic chloride ligand and the weak ligand field are most likely responsible for the spin state being high spin (S=2).[20,21] The C=N bond of the ligand backbone at the site of the Schiff base condensation has a bond length of 1.234 Å, and will be the subject of discussion (*vide supra*).

Electrochemical studies on this complex were performed in dry acetonitrile, using tetra-n-butylammonium hexafluorophosphate (NBu_4PF_6) as the supporting electrolyte. A reversible one-electron oxidation wave was observed, with $E_{1/2}$ = +303 mV vs. SCE, shown here in **Figure 4.04**.

Figure 4.04. Cyclic voltammogram of $[Fe^{II}(N^{Et2})N_4(tren)Cl]^+ PF_6^-$. The experiment was performed using a Pt electrode in CH_3CN, with NBu_4PF as the supporting electrolyte.

Replacement of the thiolate sulfur with an amine causes the redox potential to shift cathodically by +403 mV vs. SCE. This indicates that, in contrast to the thiolate-ligated complex, the Fe^{III} state is not readily accessible under aerobic or other mild oxidative conditions in an aliphatic nitrogen environment. This result helps to clarify the necessity of the thiolate ligand of SOR, because it appears that the lack of a thiolate ligand is placing the complex out of the range where superoxide reduction can occur.

The anodic shift in the redox potential also corresponds nicely with the data from the characterization of other selected non-heme Fe-N_5 systems in literature. The redox potentials of these selected non-heme Fe-N5 complexes are shown in **Table 4.02.**

Table 4.02. The electrochemical data for selected pentadentate N_5 systems and comparison with the pH-dependent redox potentials of superoxide reduction.

Complex	**Solvent**	**$E_{1/2}$(mV) vs SCE**
$[(N_4Py)Fe(CH_3CN)](ClO_4)_2$[20]	CH_3CN	+1010
$[Fe(Py5)CH_3CN]](ClO_4)_2$	CH_3CN	+1210
$[Fe^{II}(tpmen)Cl]PF_6$	CH_3CN	+670
$[L_5{}^3Fe^{II}Cl]\ PF_6$	CH_3CN	+605
$[Fe^{II}(N^{Et2})N_4(tren)Cl]^+$	CH_3CN	+303

$O_2^- + 2H^+ + e^-$	$\overset{pH=14}{\rightleftharpoons}$	H_2O_2	H_2O	-40
$HO_2 + e^- + H^+$	$\overset{pH=0}{\rightleftharpoons}$	H_2O_2	H_2O	+1127
$HO_2 + e^- + H^+$	$\overset{pH=7}{\rightleftharpoons}$	H_2O_2	H_2O	+860

All of the ligand systems of the other complexes mentioned in Table 4.02 above are pyridine-based, which help to stabilize the ferrous species.[20-24] These results clearly show that the use of an aliphatic N_5 ligand system instead of a pyridine-based ligand system allows for the Fe^{III} state to be somewhat more accessible. Also, the reversibility of the Fe^{II}/Fe^{III} redox couple allows for redox chemistry to occur, as in the wild-type SOR

enzyme. The occupation of the open site by a chloride ligand in the Fe^{II} complex most likely causes strong inhibition of inner-sphere oxidative addition of substrates, such as dioxygen, superoxide, and H_2O_2.[21]

The increased Lewis acidity of the apical amine in $[Fe^{II}(N^{Et2})N_4(tren)Cl]^+$ most likely plays a large role in causing the chloride ligand to occupy the open coordination site. The increase in Lewis acidity is caused by the higher electronegativity of nitrogen compared to sulfur.

Synthesis of oxidized $[Fe^{III}(N^{Et2})N_4(tren)]^{2+}$. $[Fe^{III}(N^{Et2})N_4(tren)]^{2+}$ was prepared via the chemical oxidation of $[Fe^{II}(N^{Et2})N_4(tren)Cl]^+$ using ferrocenium hexafluorophosphate (**Figure 4.05**).

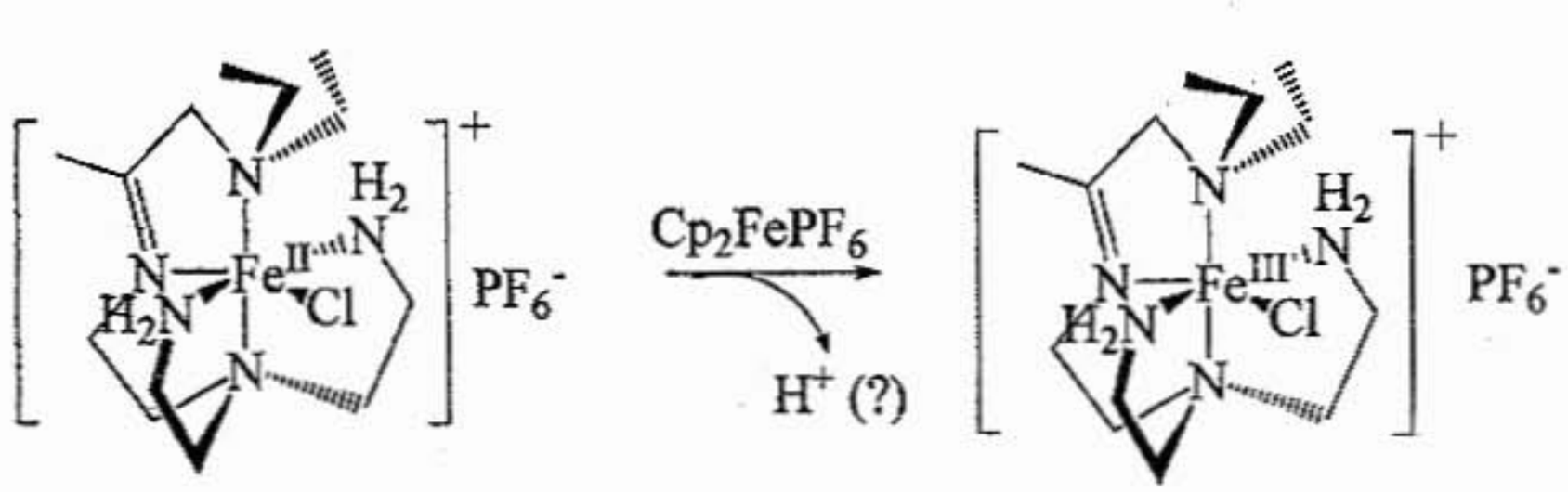

Figure 4.05. The preparation of $[Fe^{III}(N^{Et2})N_4(tren)]^+$ via chemical oxidation of $[Fe^{II}(N^{Et2})N_4(tren)]^+$ with $FeCp_2PF_6$.

$[Fe^{III}(N^{Et2})N_4(tren)]^+$ was also synthesized directly from Fe^{III} sources, i.e. $FeCl_3$, $Fe(NO_3)_3 \cdot 9H_2O$, and $Fe(ClO_4)_3 \cdot H_2O$. The general synthetic pathway is shown in **Figure 4.06.**

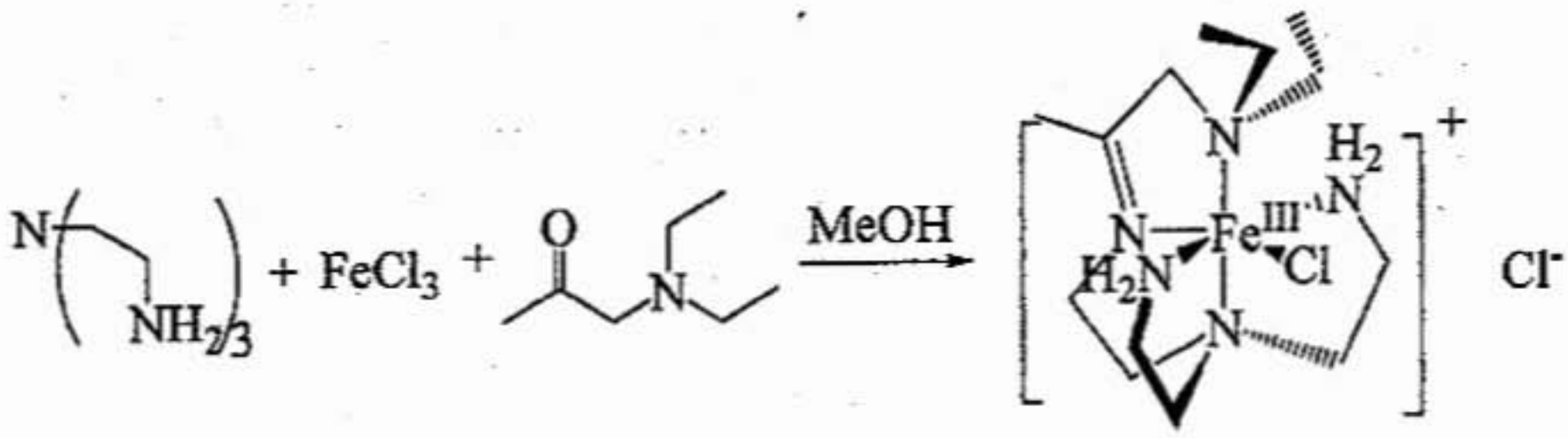

Figure 4.06. The synthesis of $[Fe^{III}(N^{Et2})N_4(tren)]^+$ via $FeCl_3$.

$[Fe^{III}(N^{Et2})N_4(tren)]^+$ was found to be completely soluble in acetonitrile, slightly less soluble in methanol, and sparingly soluble in dichloromethane. It is intensely colored purple and displays an intense absorption band at 564 nm in acetonitrile (ε = 2129 M^{-1} cm^{-1}), as shown in **Figure 4.07**. It is surprising to see such an intense low-energy charge transfer band in the visible region for $[Fe^{III}(N^{Et2})N_4(tren)]^+$, because ferric amine complexes typically tend to be fairly weakly colored. Because the origin of this intense color was unknown and unique for this complex, we began to speculate about the nature of this species.

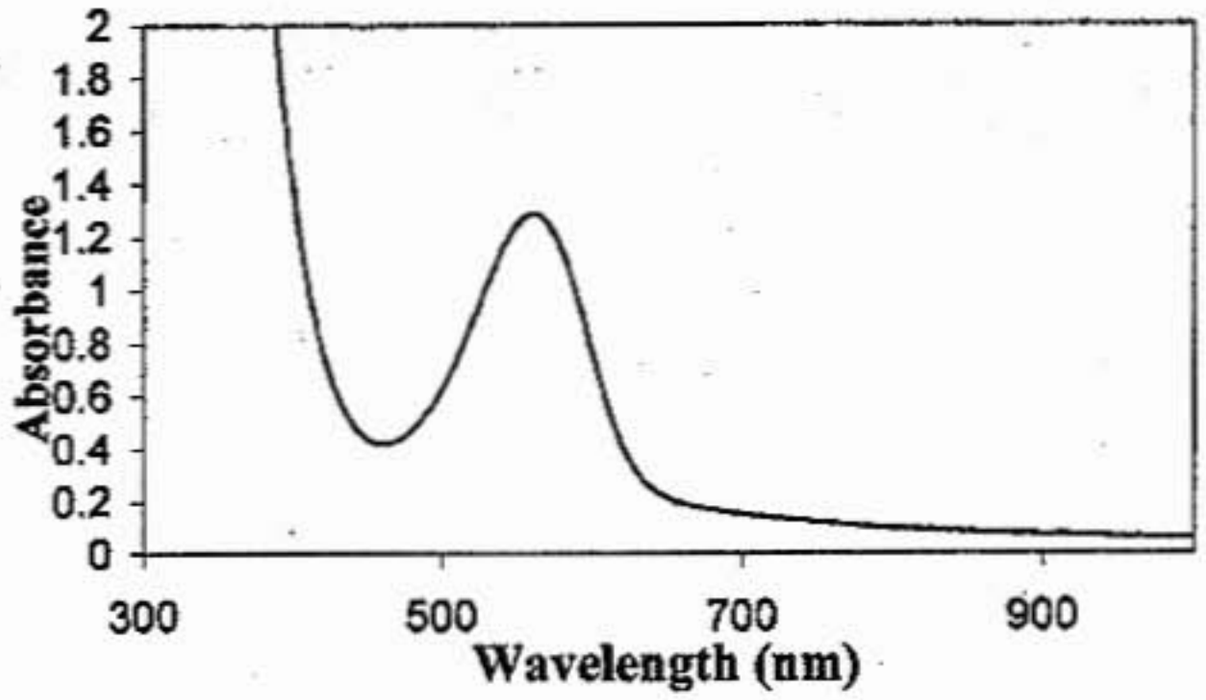

Figure 4.07. Absorption spectrum of $[Fe^{III}(N^{Et2})N_4(tren)]^+$.

Four possible identities of the intensely colored Fe^{III} complex were proposed, shown in **Figure 4.08.** The first possibility would be the formation of a solvent-bound tricationic Fe^{III} species **(A).** However, there are very few examples of tricationic ferric complexes in literature, and those that exist are also very short-lived. Thus, the probability of our complex being tricationic is not supported strongly by literature precedence.

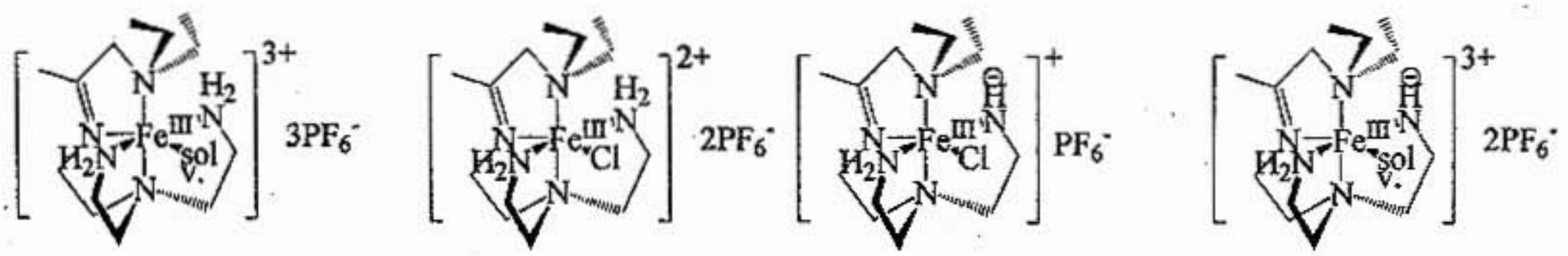

Figure 4.08. Possible structures for $[Fe^{III}(N^{Et2})N_4(tren)]^+$.

The second possibility would be a chloride-bound dicationic species **(B).** The third and fourth possibilities are the spontaneous loss of a proton from the tren ligand

upon oxidation to the ferric species to afford the chloride-bound (**C**) or the solvent-bound (**D**). This can be rationalized by the fact that the higher electron affinity of the ferric state draws electron density away from the ligand system, thereby decreasing the pKa of the protons, leading to the facile loss of a proton, which would then provide electrons for π-backbonding to the Fe^{III} center. There is precedence for such a mechanism in the literature.[25] Wieghardt prepared a bis(1,4,7-triazacyclononane) Fe^{III} complex which also displayed an intense deep blue LMCT at pH>10.[25] In the pH range 2-10, a dramatic color change to from deep blue to orange was witnessed. This color change was found to be completely reversible with the systematic addition of base and acid. This reaction is shown in **Figure 4.09.**

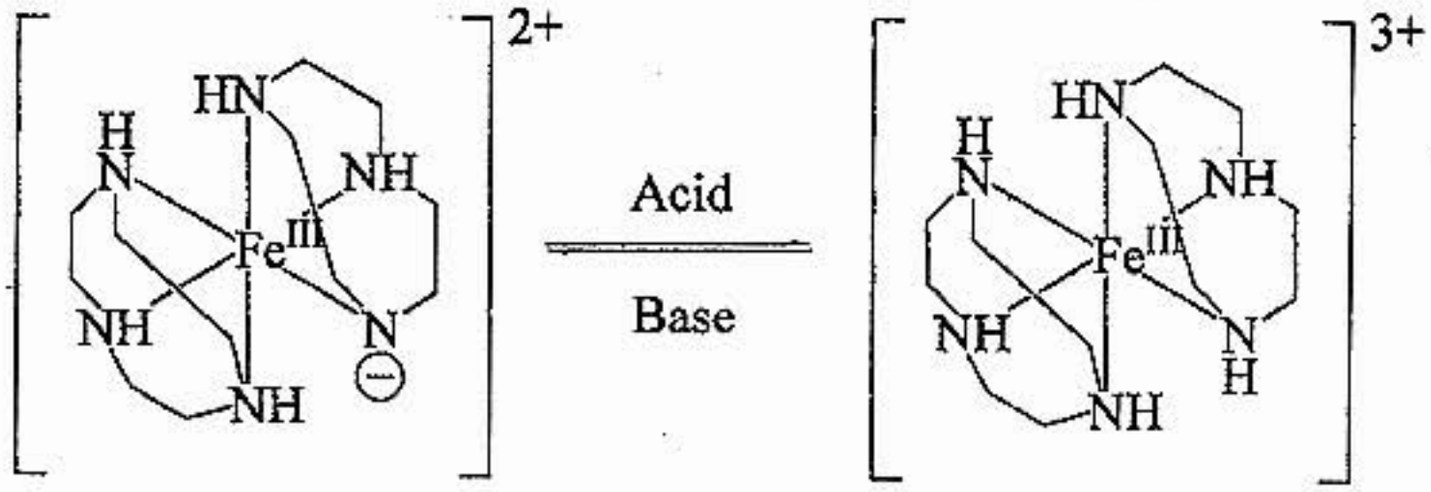

Colored: λmax = 542 nm Colorless

Figure 4.09. The reversible protonation/deprotonation of Wieghardt's amido complex $[Fe^{III}(tacn)_2]^{2+/3+}$.

A similar qualitative study was performed to see if the systematic addition of acid and base to $[Fe^{III}(N^{Et2})N_4(tren)]^+$ would lead to the observation of a similar reversible color change. Using tetrafluoroboric acid (HBF_4) and sodium methoxide in dichloromethane, approximate stoichiometric amounts of the respective acid and base

were added and the electronic absorption spectra were recorded, shown here in **Figure 4.10**. The reversibility of the color change by the addition of base and acid is apparent. Thus the qualitative analysis of this complex indicates a dependence on the pH of the solution.

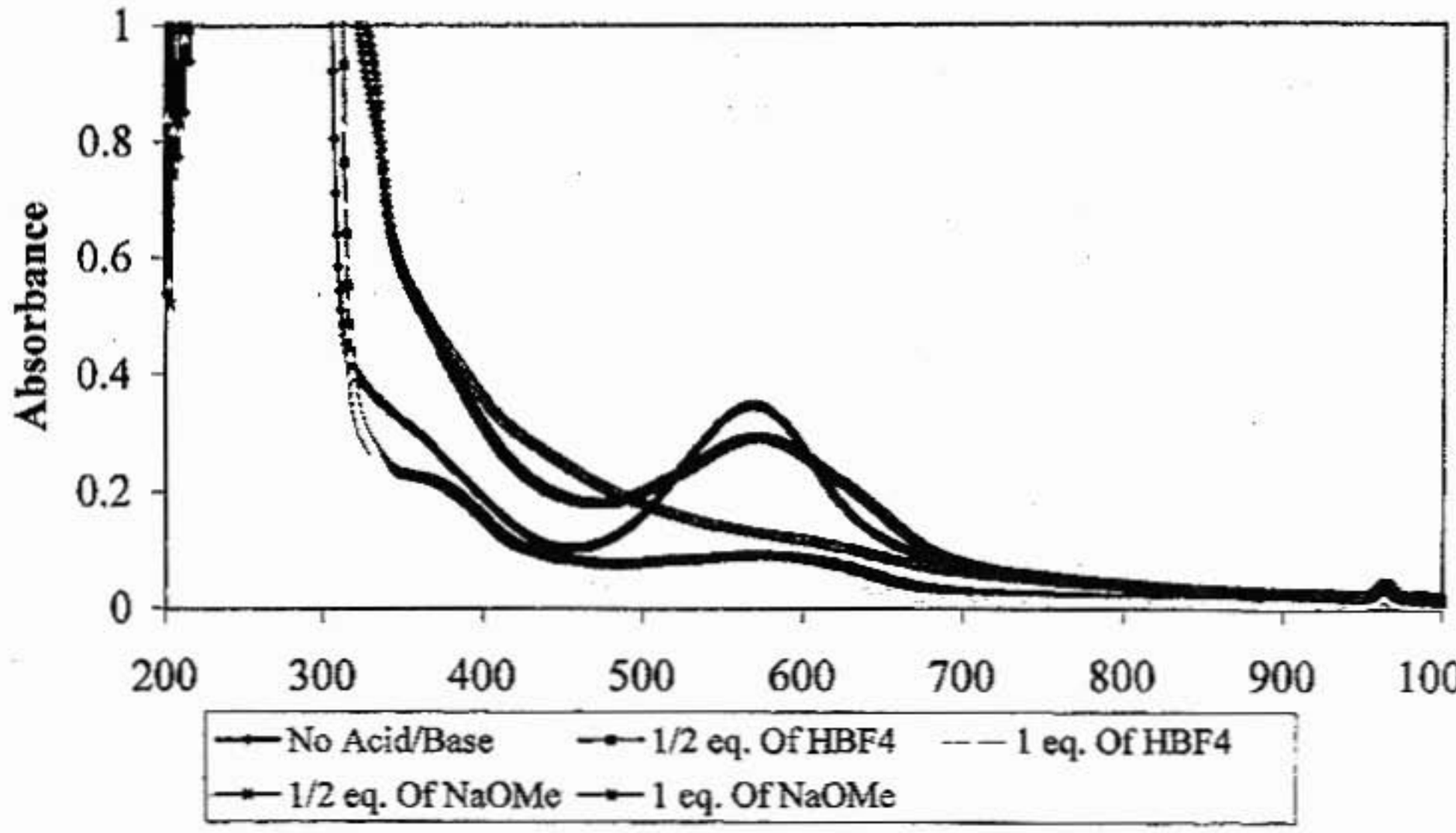

Figure 4.10. Absorption spectrum of reversible protonation-deprotonation of $[Fe^{III}(N^{Et2})N_4(tren)]^{+/2+}$.

These results led us to favor the formation of complex **(C)** or **(D)** from the oxidation of $[Fe^{III}(N^{Et2})N_4(tren)]^{+}$. A breakthrough in the elucidation of the identity of the ferric species occurred when the x-ray structure of the nitrate-bound salt $[Fe^{III}(N^{Et2})N_4(tren)NO_3]NO_3$ was obtained, via slow diffusion of ether into a methanolic solution of $[Fe^{III}(N^{Et2})N_4(tren)NO_3]NO_3$. The x-ray crystal structure is shown in **Figure 4.11,** and selected bond lengths are shown in **Table 4.03**.

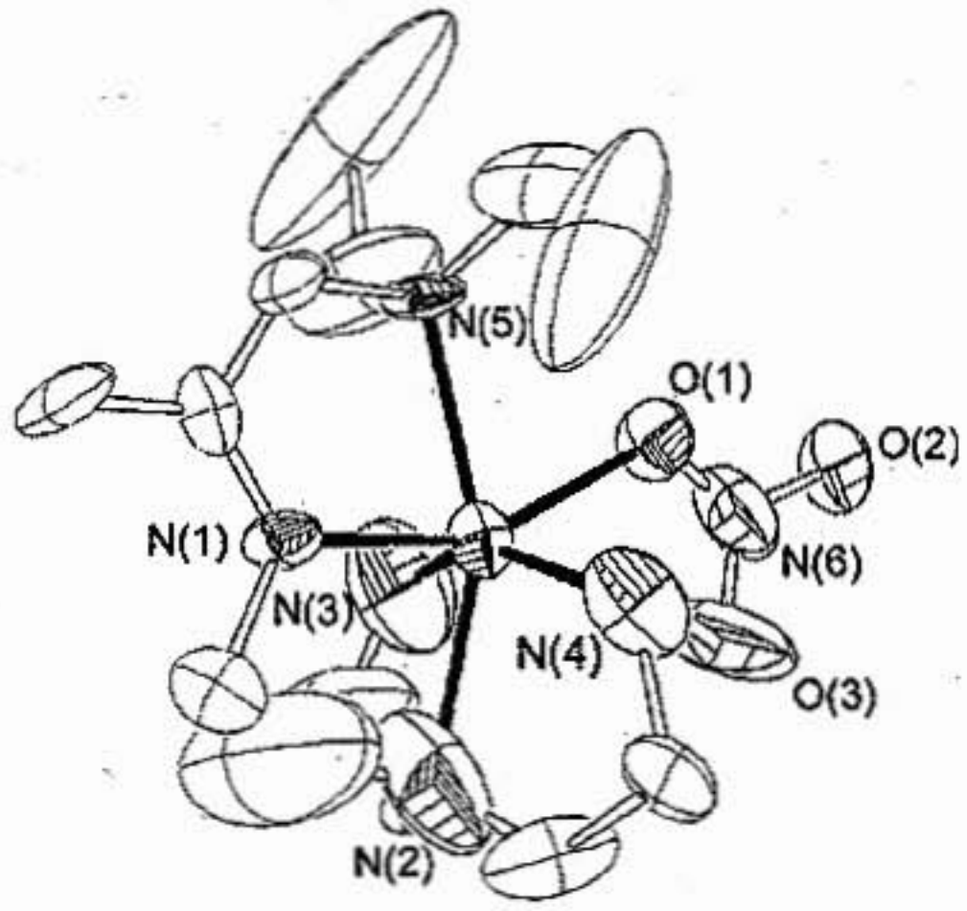

Figure 4.11. ORTEP of $[Fe^{III}(N^{Et2})N_4(tren)(NO_3)]^+$.

Table 4.03. Selected bond lengths $[Fe^{III}(N^{Et2})N_4(tren)NO_3]NO_3$. The ORTEP is shown in **Figure 4.11** for reference.

Bond lengths (Å)		**Bond angles (deg)**	
Fe-N(1)	2.124	N(1)-Fe(1)-N(3)	100.2
Fe-N(2)	2.27	N(1)-Fe(1)-N(4)	101.2
Fe-N(3)	2.089	N(3)-Fe(1)-N(4)	145.0
Fe-N(4)	2.1	N(1)-Fe(1)-N(2)	80.8
Fe-N(5)	2.334	N(3)-Fe(1)-N(2)	81.8
N(1)-C(7) (C=N)	2.189	N(4)-Fe(1)-N(1)	101.2
	1.35	N(1)-Fe(1)-N(5)	76.6
		N(3)-Fe(1)-N(5)	111.1
		N(4)-Fe(1)-N(5)	100.7
		N(2)-Fe(1)-N(5)	155.6

Interestingly, this is a dicationic salt, with one nitrate ion bound to the inner sphere, and a second nitrate ion present as an outer sphere counterion. Additionally, the bond length of the Fe-N(1) bond, which is the Fe-imine bond, showed considerable contraction, coincident with the C=N bond length being lengthened to 1.35 Å. This seems to imply that deprotonation has occurred at the β-carbon of the imine bond. The electron density formed by this deprotonation can then be delocalized into the imine bond, which can then π-backbond into the π*-antibonding orbitals of the Fe^{III} center, resulting in an intense color. This explanation is more feasible when considering the difference in relative pKas of a neutral primary amine versus a β-carbon of an imine bond. In fact, examples of spontaneous deprotonations occurring at a neutral amine bound to a metal-center are not common (Wieghardt's system being of course an exception).

It should also be noted that the apical nitrogens are tertiary and also maintain extremely long bond lengths for Fe-N bonds (Fe(1)-N(2): 2.27Å, Fe(1)-N(5): 2.334Å). These effects are most likely due to the sterically hindered nature of the tertiary amines. Finally, from the Fe-N bond lengths of this species, it appears that this is a high-spin (S=5/2) ferric species.

In order to determine the spin–state of the ferric complex, SQUID analysis was performed on a solid sample of $[Fe^{III}(N^{Et2})N_4(tren)Cl]PF_6$. The SQUID data was collected from 300K-4K. The μ_{eff} (B) versus temperature (K) plot is shown in **Figure 4.12**. The data shows that at temperatures higher than 50K, this species is intermediate spin, with the μ_{eff}=3.68. Around 50K, this species undergoes a spin crossover to a lower

spin state. This data is in direct contrast with the data obtained from the x-ray crystal data, as the longer Fe-N bond lengths are more typical of a high-spin Fe^{III} species. Since these results are contradictory, this experiment should be repeated in future work.

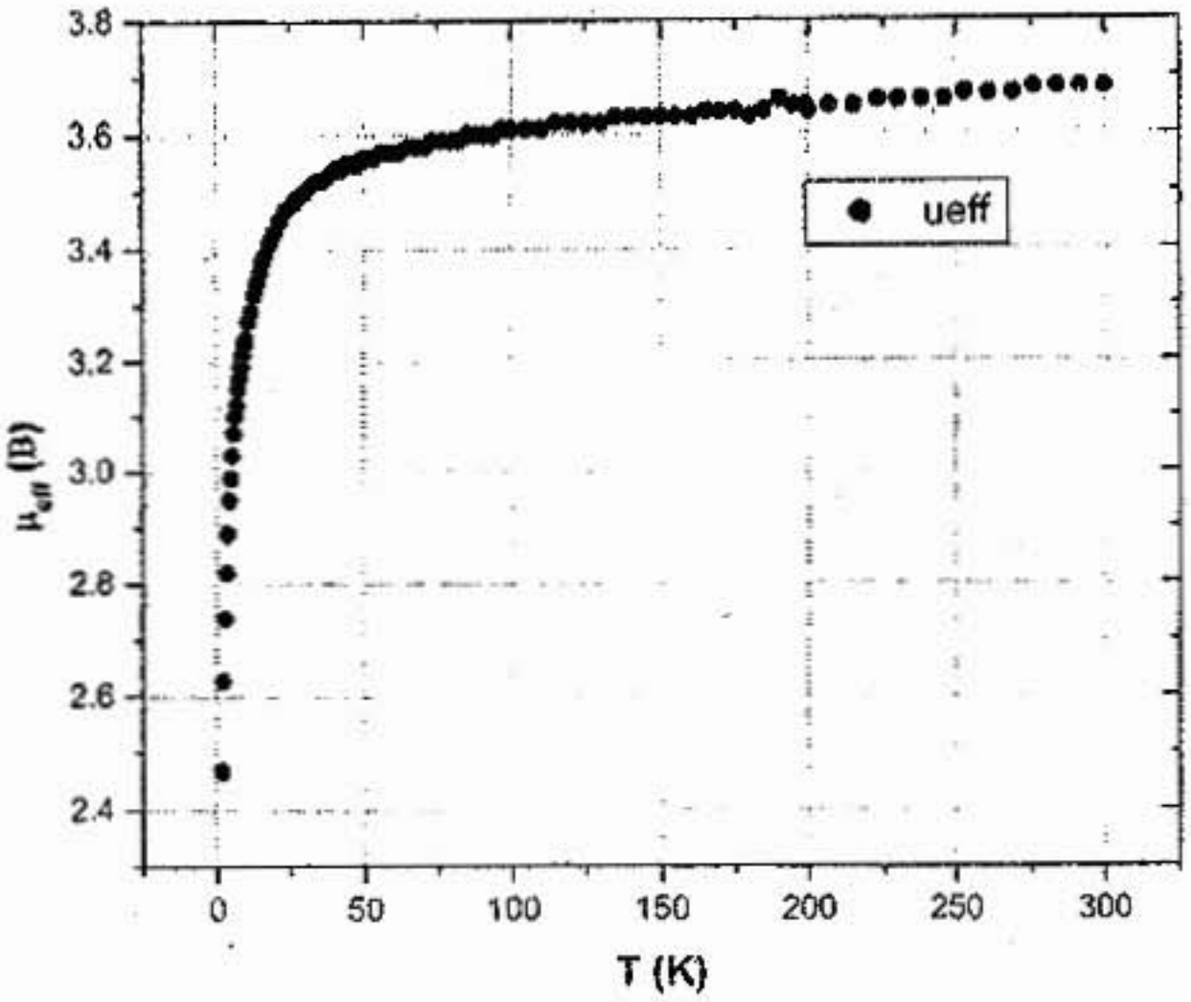

Figure 4.12. SQUID analysis of $[Fe^{III}(N^{Et2})N_4(tren)Cl]PF_6$. This is the μ_{eff} (B) versus temperature (K) plot. The SQUID data was collected from 300K-4K.

Infrared (IR) spectroscopy of the $[Fe^{II}(N^{Et2})N_4(tren)Cl]^+$ and the $[Fe^{III}(N^{Et2})N_4(tren)Cl]^+$ salts were taken in order to confirm the presence of the C=N imine stretches, and to also compare them with each other to monitor a possible weakening of the C=N bond due to the proposed deprotonation that could be occurring at the β-C of the C=N bond. The Fe-N stretching frequencies occur at less than 400 cm^{-1}, so IR can not be used to identify possible changes in the Fe-N(1) bond strength if one of the primary amines is being spontaneously deprotonated upon oxidation of the metal center.

From the analysis of the data, it appears that the C=N bond in $[Fe^{II}(N^{Et2})N_4(tren)Cl]^+$ is present at 1601 cm^{-1}. However, in the $[Fe^{III}(N^{Et2})N_4(tren)Cl]^+$

spectrum, this peak has completely disappeared. A possible peak for the C=N stretch could be at 1444cm^{-1}. Although this is out of the reported range of C=N bonds in inorganic complexes,[26] because the C=N bond should theoretically be weakened due to electron delocalization from the deprotonated β-carbon of the imine, this is not an unreasonable location for the C=N stretch. Both spectra are shown here in **Figure 4.13** and **Figure 4.14** respectively.

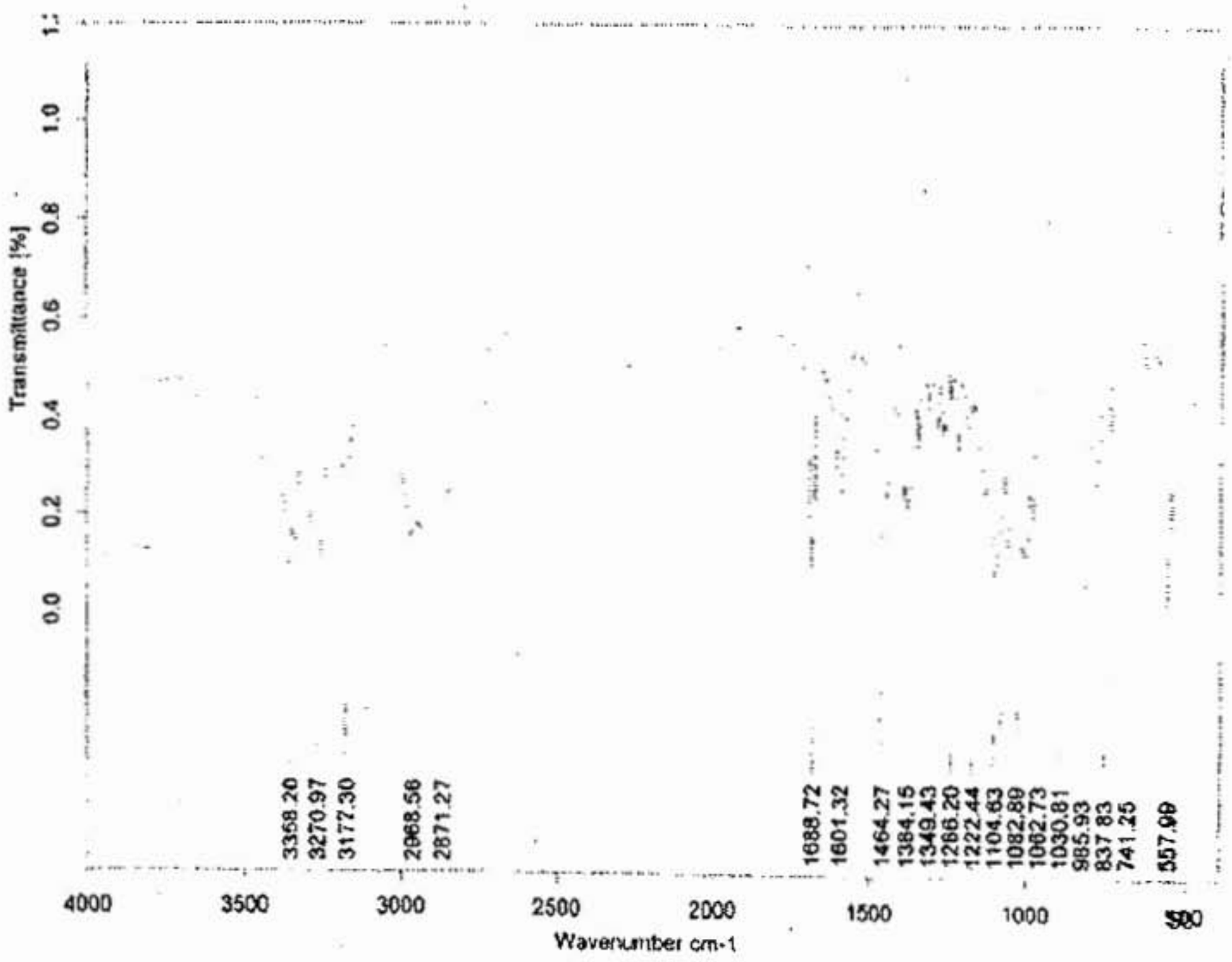

Figure 4.13. The IR spectrum of $[Fe^{II}(N^{Et2})N_4(tren)Cl]^+PF_6^-$.

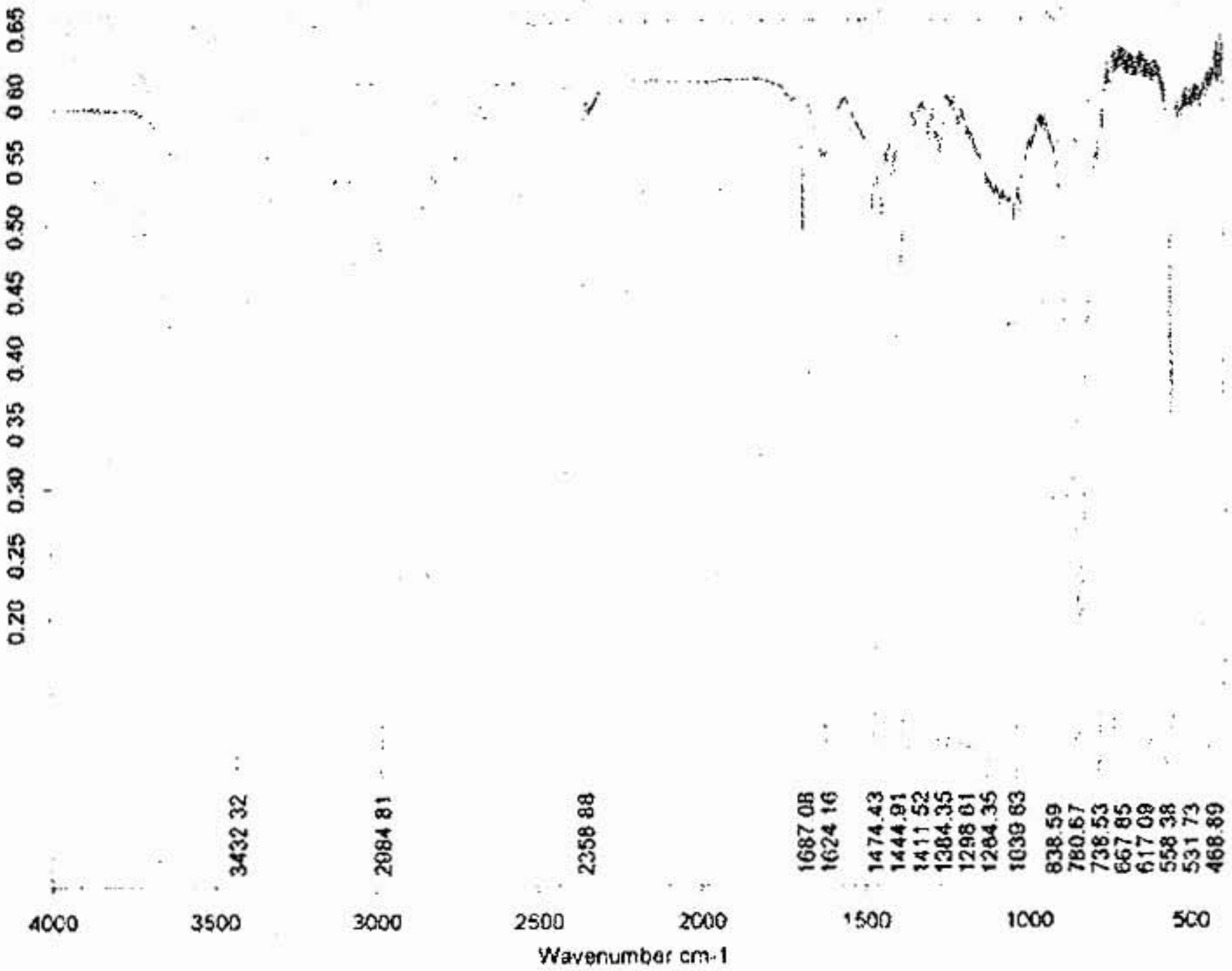

Figure 4.14. The IR spectrum of $[Fe^{III}(N^{Et2})N_4(tren)Cl]^+PF_6^-$.

Reactivity of $[Fe^{II}(N^{Et2})N_4(tren)Cl]^+$. The $[Fe^{II}(N^{Et2})N_4(tren)Cl]^+$ complex did not show any obvious reactivity with substrates such as O_2, KO_2, H_2O_2, and NaOCl. Most likely the cause of this is the chloride ligand, which occupies the open site of the Fe^{II} center. The redox potential (+303mV vs. SCE) and the reversibility of the redox process suggests that $[Fe^{II}(N^{Et2})N_4(tren)Cl]^+$ should at least be in the range of oxidation by NaOCl and H_2O_2. The lack of reactivity suggests that the chloride ion bound to the Fe center is inhibiting this reaction. In order to abstract the chloride ion from the Fe center, $AgPF_6$ was added in a stoichiometric amount. $AgPF_6$ is often used to remove a chloride ion from a metal center, causing the precipitation of AgCl. The addition of $AgPF_6$ to a

MeCN solution containing $[Fe^{II}(N^{Et2})N_4(tren)Cl]^+$ caused the immediate deposition of a white solid, presumably the AgCl salt. However, the pale yellow solution immediately turned purple, and after a few minutes, the solution bleached. It appears that Ag^+ ion could be oxidizing the Fe^{II} center in a secondary reaction, causing the formation of an unstable solvent-bound Fe^{III} species. Because a stable five-coordinate or solvent-bound six-coordinate Fe^{II} species was unable to be isolated via this method, no further experimentation was performed.

Conclusion. Nitrogen-ligated Fe^{II} complexes are common in nature. Biomimetic modeling have shown these complexes to have very anodic redox potentials, stabilizing them in the Fe^{II} state. However, more recently they have been shown to form relatively stable species in both the Fe^{III} and Fe^{IV} oxidation states, appearing to contradict this. These oxidized species have the ability to perform oxidative chemistry of substrates, such as olefins and hydrocarbons. These Fe centers are activated by oxygen, H_2O_2, or two-electron oxidants such as iodosylbenzene and *m*CPBA, forming reactive Fe^{III}-peroxo or Fe^{IV}-oxo species which are potent oxidants that are capable of functionalizing alkanes and olefins. These nitrogen-ligated enzymes, however, are not capable of performing superoxide reduction. The main difference between SOR and these nitrogen-ligated complexes is the presence of a cysteinate sulfur bound to the Fe site of SOR.

Replacing the thiolate ligand of $[Fe^{II}N_4(tren)(S^{Me2})]^+$ with an amine led to the formation of a new six-coordinate species $[Fe^{II}(N^{Et2})N_4(tren)Cl]^+$. The six-coordinate nature of this complex is not unexpected, as other Fe-N_5 complexes in literature are also

six-coordinate. This effect can be explained by the following effects. First, the thiolate ligand is a strong σ-donor and also is electron-rich in its filled π-orbitals. In contrast, the tertiary amine ligand is a poor σ-donor, mostly due to steric effects. It does not have π electrons available for bonding either. Also, nitrogen is more of a "hard" ligand than sulfur, and is more electronegative. The combination of these effects leads to an overall electron deficiency at the Fe center. Consequently, the increased Lewis acidity of the Fe center favors the binding of a sixth ligand to compensate for this. These observations also are in good agreement with the electrochemistry of $[Fe^{II}(N^{Et2})N_4(tren)Cl]^+$. The substitution of the thiolate ligand with the amine ligand causes a significant anodic shift in the redox potential, from -100mV to +303mV (versus SCE). These observations are consistent with other Fe^{II}-N_5 biomimetic model complexes in the literature.[1,10,20,21,23,24] In general these complexes also prefer to be high-spin, with extremely cathodic redox potentials. However, it is not yet understood why these complexes can form stable Fe^{IV}-oxo species, which is unexpected with respect to their highly cathodic redox potentials. Recently Que has shown that a thiolate-ligated Fe-complex in an N_4S ligand environment, similar to SOR, can form a transient Fe^{IV}-oxo species, capable of substrate oxidation.[27] However, at this point this result is more of the exception than the rule. In general, this type of high-valent non-heme Fe chemistry appears to be more favorable and controlled by Fe-N_5 complexes without a thiolate in the coordination sphere.

All in all, it is clear that the thiolate ligand plays an important role in tuning the electrochemical properties of the Fe center. The presence of the thiolate enables the Fe center to remain five-coordinate, keeping an open site for substrate binding. It also plays

a noticeable role in tuning the redox potential of the Fe center into range where it can perform the one-electron reduction of superoxide to H_2O_2. The removal of the thiolate from the coordination sphere of $[Fe^{II}(S^{Me2})N_4(tren)]^+$ causes significant changes to occur in the electronic and structural characteristics of the metal complex. This most likely contributes to altering the biological purpose of non-heme Fe enzymes with similar reactive sites.

Chapter 4 – Notes

(1) Que, L., Jr.; Ho, R. Y. *Chem Rev* **1996,** *96*, 2607-2624.

(2) Bernal, I.; Jensen, I. M.; Jensen, K. B.; McKenzie, C. J.; Toftlund, H.; Tuchagues, J.-P. *J. Chem. Soc. Dalton Trans.* **1995**, 3667-3675.

(3) Dubois, G.; Murphy, A.; Stack, T. D. *Org Lett* **2003**, *5*, 2469-72.

(4) Guajardo, R. J.; Chavez, F.; Farinas, E. T.; Mascharak, P. K. *J. Am. Chem. Soc.* **1995**, *117*, 3883-3884.

(5) Hazell, A.; McKenzie, C. J.; Nielsen, L. P.; Schindler, S.; Weitzer, M. *J. Chem. Soc. Dalton Trans.* **2002**, 310-317.

(6) Ho, R. Y. N.; Roelfes, G.; Feringa, B. L.; Que, L. J. *J. Am. Chem. Soc.* **1999**, *121*, 264-265.

(7) Ho, R. Y. N.; Roelfes, G.; Hermant, R.; Hage, R.; Feringa, B. L.; Que, L. J. *Chem. Comm.* **1999**, 2161-2162.

(8) Koehntop, K. D.; Rohde, J. U.; Costas, M.; Que, L., Jr. *Dalton Trans* **2004**, 3191-8.

(9) Park, M. J.; Lee, J.; Suh, Y.; Kim, J.; Nam, W. *J Am Chem Soc* **2006**, *128*, 2630-4.

(10) Simaan, A. J.; Banse, F.; Girerd, J. J.; Wieghardt, K.; Bill, E. *Inorg Chem* **2001**, *40*, 6538-40.

(11) Klinker, E. J.; Kaizer, J.; Brennessel, W. W.; Woodrum, N. L.; Cramer, C. J.; Que, L., Jr. *Angew Chem Int Ed Engl* **2005**, *44*, 3690-4.

(12) Shaik, S.; Kumar, D.; de Visser, S. P.; Altun, A.; Thiel, W. *Chem Rev* **2005**, *105*, 2279-328.

(13) Kovacs, J. A. *Chem Rev* **2004**, *104*, 825-48.

(14) Kitagawa, T.; Dey, A.; Lugo-Mas, P.; Benedict, J. B.; Kaminsky, W.; Solomon, E.; Kovacs, J. A. *J Am Chem Soc* **2006**, *128*, 14448-9.

(15) Kovacs, J. A. *Science* **2003**, *299*, 1024-5.

(16) Shearer, J.; Scarrow, R. C.; Kovacs, J. A. *J Am Chem Soc* **2002**, *124*, 11709-17.

(17) Theisen, R. M.; Kovacs, J. A. *Inorg Chem* **2005**, *44*, 1169-71.

(18) Theisen, R. M.; Shearer, J.; Kaminsky, W.; Kovacs, J. A. *Inorg Chem* **2004**, *43*, 7682-90.

(19) MacBeth, C. E.; Golombek, A. P.; Young, V. G., Jr.; Yang, C.; Kuczera, K.; Hendrich, M. P.; Borovik, A. S. *Science* **2000**, *289*, 938-41.

(20) Roelfes, G.; Vrajmasu, V.; Chen, K.; Ho, R. Y.; Rohde, J. U.; Zondervan, C.; La Crois, R. M.; Schudde, E. P.; Lutz, M.; Spek, A. L.; Hage, R.; Feringa, B. L.; Munck, E.; Que, L., Jr. *Inorg Chem* **2003**, *42*, 2639-53.

(21) Roelfes, G.; Lubben, M.; Chen, K.; Ho, R. Y.; Meetsma, A.; Genseberger, S.; Hermant, R. M.; Hage, R.; Mandal, S. K.; Young, V. G., Jr.; Zang, Y.; Kooijman, H.; Spek, A. L.; Que, L., Jr.; Feringa, B. L. *Inorg Chem* **1999**, *38*, 1929-1936.

(22) Patra, A. K.; Afshar, R.; Olmstead, M. M.; Mascharak, P. K. *Angew Chem Int Ed Engl* **2002**, *41*, 2512-5.

(23) Balland, V.; Banse, F.; Anxolabehere-Mallart, E.; Ghiladi, M.; Mattioli, T. A.; Philouze, C.; Blondin, G.; Girerd, J. J. *Inorg Chem* **2003**, *42*, 2470-7.

(24) Rowland, J. M.; Olmstead, M.; Mascharak, P. K. *Inorg Chem* **2001**, *40*, 2810-7.

(25) Pohl, K.; Wieghardt, K.; Wolfgang, K.; Steenken, S. *Inorg Chem* **1988**, *27*, 440-447.

(26) Gagné, R. R.; Ingle, D. M.; Lisensky, G. C. *Inorg Chem* **1981**, *20*, 1991-1993.

(27) Bukowski, M. R.; Koehntop, K. D.; Stubna, A.; Bominaar, E. L.; Halfen, J. A.; Munck, E.; Nam, W.; Que, L., Jr. *Science* **2005**, *310*, 1000-2.

Chapter 5
Towards the Design of Asymmetric Tripodal Polyamine Ligands

Introduction. The effort to create novel bulky aliphatic tren-derivatives was undertaken in order to determine the proton source during the SOR catalytic cycle, to stabilize the Fe^{III}-peroxo species, and also to prevent μ-oxo dimer formation. Steric bulk is commonly used as a dimerization deterrent.[1,2] Additionally, protons on the ligand system have been known to cause decomposition of peroxo/hydroperoxo species.[3] The pentadentate ligand system employed in our $[Fe^{II}S^{Me2}N_4(tren)]^+$ model complex relies on imine formation via a Schiff base condensation between tris-2-aminoethyl-amine (tren) and the thioketone. Upon imine formation, there are two remaining free amines that bind to the metal center. These free amines could possibly be a source of protons needed during the reduction of superoxide or dioxygen for SOR or cytochrome P450 chemistry.

Previous work by Theisen *et al* described the formation of the μ-oxo dimer $[Fe^{III}S^{Me2}N_4(tren)]_2\mu\text{-}O^{2+}$ upon the exposure of $[Fe^{II}S^{Me2}N_4(tren)]^+$ to dioxygen (**Figure 5.01**).[4] In an attempt to stabilize the mononuclear species and prevent μ-oxo dimer formation, a bulkier tren-derived ligand, N-(2-aminoethyl)-N-(2-diethylaminoethyl)-N', N'-(diethylethane-1,2-diamine) (**tren***) was synthesized by Shearer (**Figure 5.01**).

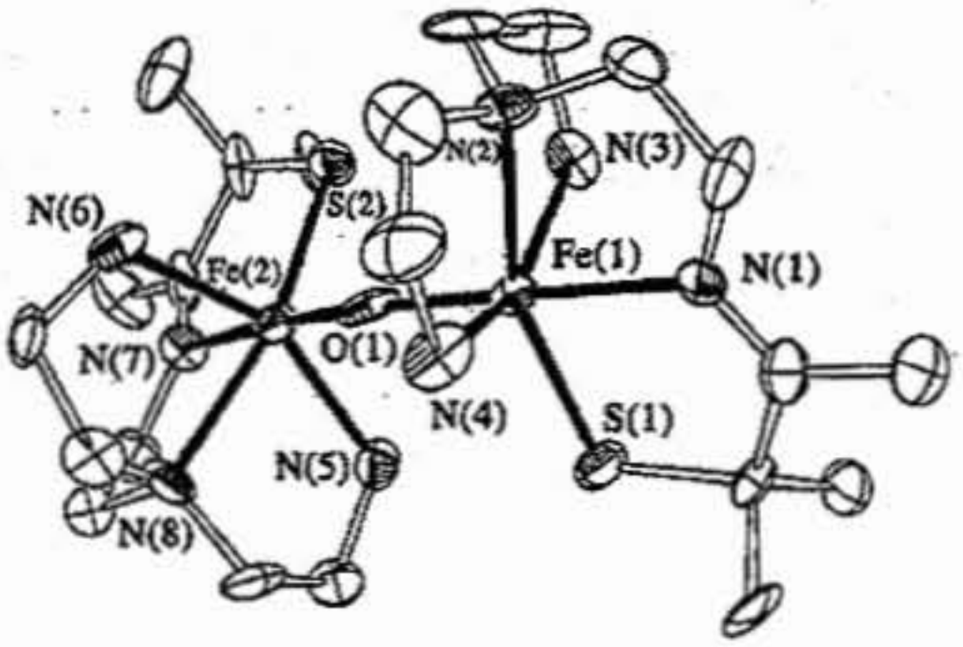

Figure 5.01. The x-ray crystal structure of $[Fe^{III}S^{Me2}N_4(tren)]_2\mu\text{-}O^{2+}$.

This tren* ligand incorporates ethyl groups on two of the amine nitrogens of tren, effectively protecting two of the amines and removing these amines from consideration as a possible proton source. Use of this ligand afforded the ferrous complex $[Fe^{II}S^{Me2}N_4(tren^*)]^+$, shown in **Figure 5.02.**

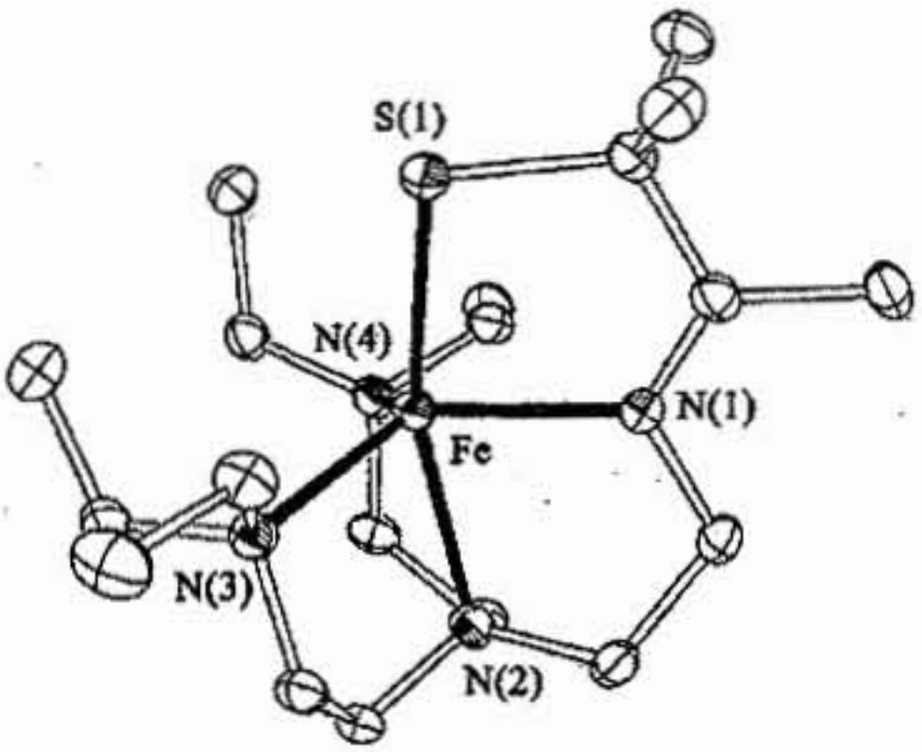

Figure 5.02. The x-ray crystal structure of $[Fe^{II}S^{Me2}N_4(tren^*)]^+$. N(3) and N(4) are the tetraethylated tertiary amines.[4]

Surprisingly, this complex did not react readily with O_2. Attempts to produce the ferric version of $[Fe^{II}S^{Me2}N_4(\mathbf{tren^*})]^+$ using various Fe^{III} sources and chemical oxidants repeatedly failed, yielding only unidentifiable products, most likely rust compounds and disulfides formed from dissociated ligand. Electrochemical studies showed that the oxidation of this complex is irreversible, with an oxidation potential of +410 mV vs. SCE, supporting indications that the ferric state is not readily accessible. Additionally, the ORTEP of the ferrous complex shows atypically elongated Fe-N bond lengths for a high-spin Fe^{II} amine complex.[5] The tertiary amines of **tren*** are much more electron-rich than their primary amine counterparts, so it was initially expected that this would lead to stronger σ-bonding interactions between the ligand and metal. However, it appears that the sterically hindered ethyl groups are actually responsible for the Fe-N bond elongation. This is most likely due to the highly bulky and contiguous character of the ethyl groups on the equatorial amines. Such an effect from sterics has been observed many times and is not completely unexpected.[6]

These results led to the design of three novel ligand systems, each varying by steric or topological factors, shown below in **Figure 5.03**. By using these ligands, we are hoping to prevent μ-oxo dimer formation, while simultaneously stabilizing the Fe^{III}-OOH species.

Experimental Section

General Methods. Unless otherwise noted, all reactions were performed under an inert atmosphere of dinitrogen or argon in a drybox or using standard Schlenk techniques. Reagents purchased from commercial vendors were of the highest purity available and were used without further purification. Acetonitrile and dichloromethane were dried over CaH_2. Methanol was dried over $Na/CaH_2/I_2$. Pentane and tetrahydrofuran were dried over sodium benzophenone ketyl. Tetra-n-butyl (PF_6) was recrystallized three times in ethanol and dried under reduced pressure for 48 hours. KCl was recrystallized three times in deionized water/acetone and dried under reduced pressure for 48 hours. Water was purified using a MilliQ purification system.

Physical Methods. NMR spectra were recorded using Bruker DRX-499, DPX-200, AF-301, or AC-200 spectrometers. ^{1}H-NMR spectra were referenced to either TMS or residual proton peaks in the deuterated solvent and chemical shifts are reported in ppm. Cyclic voltammograms were recorded on a Princeton Applied Research Model 273 potentiostat with a glassy carbon working electrode, a platinum wire counter electrode, and a saturated calomel electrode (SCE) reference electrode. Electrochemical experiments were performed in acetonitrile and methanol (100mM tetra-n-butyl (PF_6) solutions) and water (100mM KCl solutions). IR spectra were recorded on a Perkin-Elmer 1720 FT-IR spectrometer as KBr pellets. Electronic absorption spectra were recorded on a Hewlett-Packard model 8452A diode array spectrophotometer and a Varian

Cary 50 spectrophotometer. Electrospray mass spectra were recorded on a Bruker Esquire Liquid Chromatograph - Ion Trap Mass Spectrometer.

Preparation of tris(2-dimethylaminoethyl)amine (Me_6-tren). Formic acid (90%) (53.5 ml, 1.05 mol) was cooled to 0 °C. To this solution was added tris(2-aminoethylamine) (tren) (10.5 g, 0.070 mol) dropwise. Formaldehyde (37%) (37.4 ml, 0.46 mol) was added and solution was allowed to warm to room temperature. Solution was then allowed to reflux overnight. The next day the solution was cooled to room temperature and made alkaline with saturated NaOH. Product was extracted with dichloromethane (3x25 ml). Extract was dried over $MgSO_4$ and solvent was removed via rotary evaporation, affording a musky-smelling, dark orange oil (13.74g, 85.7%). 301 MHz 1H NMR ($CDCl_3$): 2.60 – 2.50 (t, 6H, $(CH_3)_2NCH_2CH_2N$), 2.38 – 2.28 (t, 6H, $(CH_3)_2NCH_2CH_2N$), 2.15 (s, 18H, $(CH_3)_2N$).

Preparation of *N, N, N', N'*-tetramethyldiethylenetriamine (TMDA). Me_6-tren (6.88 g, 0.030 mol) was solubilized in pentane (120 ml) and cooled to –78°C. To this was added n-BuLi (1.6 M in hexanes) (18.7 ml, 0.030 mol) dropwise. Upon completion of addition, the solution was stirred at 0°C for 1 hour, followed by 3 hours at ambient temperature. The reaction was quenched with saturated NaOH (150 ml) and organic layer was separated. Residual product was extracted with dichloromethane (3x25 ml). Organic layers were combined, dried over $MgSO_4$ and solvent was removed via rotary evaporation, affording a yellow oil (3.1 g, 65%). 301 MHz ^{1}H NMR ($CDCl_3$): 2.75 - 2.65

(t, 4H, $(CH_3)_2NCH_2CH_2N$), 2.45 – 2.35 (t, 4H, $(CH_3)_2NCH_2CH_2N$), 2.25 (s, 12H, $(CH_3)_2N$).

Preparation of bis-(2-dimethylamino-ethyl)-cyanamide (TMDA-CN). TMDA (3.98g, 0.025 mol) dissolved in THF was cooled to 0°C. To this was added HCl(aq) (37%) (2.5ml, 0.025 mol) dropwise. Vigorous fuming was immediately seen. Upon completion of HCl addition, the solution was allowed to stir for several minutes until fuming subsided. Subsequently an aqueous solution of KCN (1.63 g, 0.025 mol) in 10 ml of water was added dropwise. Formaldehyde (37%) (0.025 mol, 2.03 ml) was then added dropwise. The reaction mixture was then warmed to ambient temperature and allowed to stir overnight. The next day the reaction mixture was extracted with dichloromethane (3x25 ml) and the combined extracts were dried over $MgSO_4$ and solvent was removed via rotary evaporation, yielding 3.47g (70%) of a yellow oil. 301 MHz ^{1}H NMR ($CDCl_3$): 3.85 (s, 2H, NCH_2CN), 2.75 – 2.70 (t, 4H, $(CH_3)_2NCH_2CH_2N$), 2.50 - 2.45 (t, 4H, $(CH_3)_2NCH_2$ CH_2N), 2.25 (s, 12H, $(CH_3)_2NCH_2CH_2N$).

Preparation of Bis-(2-dimethylamino-ethyl)amine (TMDA). Lithium aluminum hydride (0.600g , 0.016 mol) was suspended under argon in 20 ml of dry THF. The suspension was cooled to –5°C. To this suspension was added dropwise H_2SO_4 (0.815g, 0.008 mol) and the solution was stirred at 0°C for 1 hour. The reaction mixture was allowed to warm to ambient temperature. TMDA-CN (0.950g, 0.005 mol) was dissolved in 5 ml of dry THF and added dropwise with an addition funnel at a rate such that the

solvent did not start to boil. The reaction mixture stirred at ambient temperature overnight. The next day the residual lithium aluminum hydride was hydrolyzed with an excess of isopropanol, followed by an excess of cold water. The reaction was filtered and the solid residue was washed several times with methanol. The solvent was removed and the residue was washed with 30 ml of 25% NaOH and extracted with dichloromethane (3x25 ml). The extracts were combined, dried over $MgSO_4$ and solvent was removed via rotary evaporation, affording 0.465 g (46%) of a pale yellow oil. 301 MHz ^{1}H NMR ($CDCl_3$): 2.85 – 2.75 (t, 2H, $NCH_2CH_2NH_2$), 2.70 - 2.60 (t, 4H, $(CH_3)_2NCH_2CH_2N$)), 2.60-2.50 (t, 2H, $NCH_2CH_2NH_2$), 2.45-2.35 (t, 4H, $(CH_3)_2NCH_2CH_2N$)), 2.25 (s, 12H; $(CH_3)_2NCH_2CH_2N$). Electrospray Mass Spec. (ESI-MS): Calculated: 203. Found: 204 (positive ion mode).

Preparation of Bis-(2-dimethylaminopropyl)amine (bdpa). To a flask was added n-(3-bromopropyl)phthalimide (8.45 g, 0.031 mol). The flask was then placed under nitrogen and heated to 180°C. A needle was added to vent. To this was added TMDA (5.0 g, 0.031 mol) dropwise. The solution immediately turned dark brown and gas was seen evolving. The reaction mixture was allowed to stir for 2 hours and was then cooled to ambient temperature. Upon cooling, the solution formed a dark brown solid with a black oil visible on the surface. 50 ml of HCl (37%) was added and the solution refluxed overnight. The next day a dark brown liquid was seen, along with a precipitate. The reaction mixture was filtered and the solvent was removed under reduced pressure. The compound was redissolved in CH_2Cl_2 and was washed with saturated NaOH. The

compound was extracted with dichloromethane (3x25 ml). The extracts were combined, dried over $MgSO_4$ and solvent was removed via rotary evaporation, affording 1.468 g (21.9%) of a dark brown oil. 301 MHz ^{1}H NMR ($CDCl_3$): 2.95 - 2.85 (t, 2H, $NCH_2CH_2CH_2NH_2$), 2.80 - 2.65(m, 2H, $NCH_2CH_2CH_2NH_2$), 2.5 - 2.50 (t, 2H, $NCH_2CH_2CH_2NH_2$), 2.5 - 2.38 (t, 4H, $(CH_3)_2NCH_2CH_2N$), 2.20 - 2.10 (t, 4H, $(CH_3)_2NCH_2CH_2N$), 2.08 (s, 12H, $(CH_3)_2NCH_2CH_2N$), 1.85 - 1.70 (broad peak, 2H, $NCH_2CH_2CH_2NH_2$).

Preparation of Bis-(2-diethylaminoethyl)-3-aminopropylphthalimide. This is a modified preparation derived from Spiccia *et. al.* To a flask charged with 120 ml of dry acetonitrile was added sodium carbonate (3.29 g, $7.77x10^{-3}$ mol). To this suspension was added N, N, N', N'-tetraethyldiethylenetriamine (Et_4-DTA) (0.600 ml, $2.32x10^{-3}$ mol.) While stirring, n-(3-bromopropyl)phthalimide (0.622 g, $2.32x10^{-3}$ mol) was added. The reaction mixture was placed under nitrogen and allowed to reflux for 3 days. The reaction mixture was then cooled to ambient temperature and solvent was removed via rotary evaporation, affording an orange oil. The oil was dissolved into 1M HCl and excess n-(3-bromopropyl)phthalimide was filtered. The solution was made alkaline by the addition of 1M KOH and the product was extracted with ethyl acetate (6x25 ml). KOH was added in between extractions in order to keep the solution alkaline. The combined extracts were dried over $MgSO_4$ and solvent was removed via rotary evaporation, affording 0.607g (65%) of an orange oil. 301 MHz ^{1}H NMR ($CDCl_3$):

Electrospray Mass Spec. (ESI-MS): Calculated: 402.5. Found: 403.5 (positive ion mode).

Preparation of bis-(2-diethylamino-ethyl)(3-aminopropyl)amine (bdea). Bis-(2-diethylaminoethyl)-3-aminopropylphthalimide (0.607 g, $1.51x10^{-3}$ mol) was dissolved in 50 ml of 5M HCl. The reaction mixture was allowed to reflux for 72 hours and allowed to cool to ambient temperature. The reaction mixture was then placed in the freezer for 24 hours in order to precipitate the phthalic acid byproduct. The reaction mixture was then filtered and made alkaline by the addition of KOH. The product was extracted with ethyl acetate (6x25 ml). The combined extracts were dried over $MgSO_4$ and the solvent was removed via rotary evaporation, yielding 0.308g (75%) of a yellow oil. 301 MHz ^{1}H NMR ($CDCl_3$): 3.90 – 3.60 (broad peak, 2H, $NCH_2CH_2CH_2\mathit{NH_2}$), 3.10 – 2.95 (t, 2H, $NCH_2CH_2\mathit{CH_2}NH_2$), 2.85-2.75 (m, 8H, $NCH_2\mathit{CH_2}CH_2NH_2$), 2.70 – 2.50 (t, 2H, $N\mathit{CH_2}CH_2CH_2NH_2$), 2.65 – 2.45 (m, $-N(CH_2CH_3)_2$), 1.75 – 1.65 (t, 4H, $(CH_3CH_2)_2NCH_2\mathit{CH_2}N$), 1.30 – 1.20 (t, 4H, $(CH_3CH_2)_2N\mathit{CH_2}CH_2N$), 1.15 – 0.95 (t, 12H, $\mathit{CH_3}CH_2)_2NCH_2CH_2N$). Electrospray Mass Spec. (ESI-MS): Calculated: 272.5. Found: 273.5 (positive ion mode).

Preparation of $[Fe^{II}S^{Me2}N_4(bdpa)](PF_6)_2$. This method is a modified version of a previously described method by Kovacs. 3-mercapto-3-methyl-2-butanone (0.043 g, $3.68x10^{-4}$ mol) and bdpa (0.100 g, $3.68x10^{-4}$ mol) were dissolved in 10 ml of methanol. To this was added NaOMe (0.020g, $3.68x10^{-4}$ mol) and the solution was cooled to -30 °C.

$FeCl_2$ (0.047 g, $3.68x10^{-4}$ mol) was dissolved in 5 ml of methanol and cooled to -30 °C. The $FeCl_2$ solution was then added dropwise to the ligand mixture and allowed to stir overnight at ambient temperature. $NaPF_6$ (0.062 g, $3.68x10^{-4}$ mol) was added to the reaction mixture and allowed to stir for 1 hour and the resulting precipitate was filtered through a bed of Celite. The solvent was removed under reduced pressure and the brown precipitate was redissolved in acetonitrile, filtered through a bed of Celite and concentrated to ~5ml. Diethyl ether (30 ml) was layered on top of this solution and was allowed to sit for 7 days, yielding 0.030 g of a pale yellow precipitate. X-ray quality pale yellow crystals were obtained from the same reaction flask.

Preparation of $[Fe^{III}S^{Me2}N_4(bdea)]$ $(2PF_6)$. This method is a modified version of a previously described method by Kovacs. 3-mercapto-3-methyl-2-butanone (0.029 g, $2.47x10^{-4}$ mol) and bdea (0.050 g, $2.47x10^{-4}$ mol) were dissolved in 10 ml of methanol. To this was added NaOMe (0.064 g, $2.47x10^{-4}$ mol) and the solution was cooled to -30°C. $FeCl_2$ (0.031 g, $2.47x10^{-4}$ mol) was dissolved in 5 ml of methanol and cooled to -30°C. The $FeCl_2$ solution was then added dropwise to the ligand mixture and allowed to stir overnight at ambient temperature. Ferrocenium hexafluorophosphate (0.082 g, $2.47x10^{-4}$ mol) was added to the reaction mixture and allowed to stir overnight. An insoluble precipitate formed, presumably the disulfide byproduct that was seen previously with the tren* complex.[4]

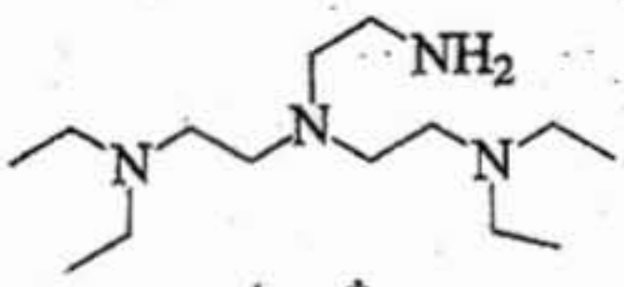

tren*

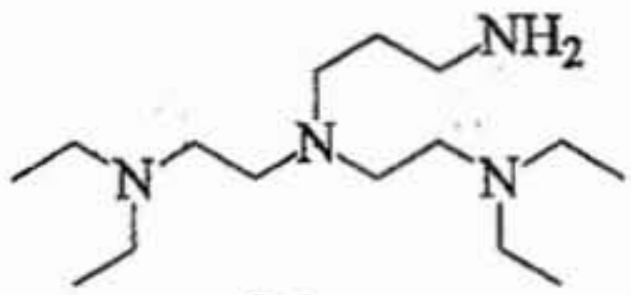

bdep

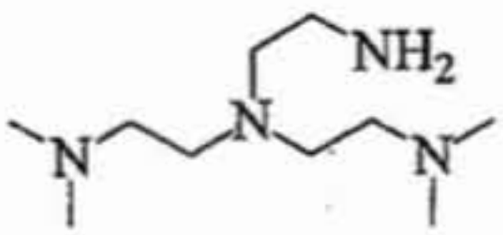

bdea

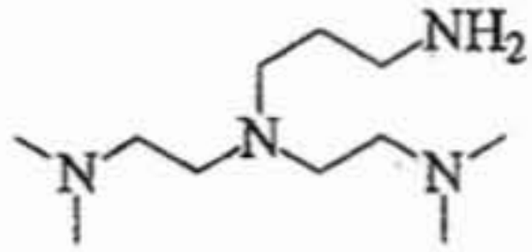

bdpa

Figure 5.03. The ligand structures of the tetraalkylated tren-derived ligands. The ligand **bdep** is a topological variant of **tren***, containing a propylene arm attached to the primary amine as opposed to the ethylene arm of **tren***.

Discussion. The ligand **bdep** is a topological variant of **tren***, varying by one methylene unit in the arm attached to the free amine. The methylated ligands **bdea** and **bdpa** also vary from one another by one methylene length in the arm possessing the free amine. Because of the structural similarities between these ligands, a parallel synthetic pathway was developed to synthesize these ligands from common intermediates. The synthetic route to **bdep** is shown in **Figure 5.04.** **bdep** is synthesized using a modified Gabriel synthetic pathway adapted from Spiccia et. al[7], followed by base workup to yield the free amine. Tetraethyldiethylenetriamine reacts with the phthalimide compound in an S_N2-type alkylation reaction. Although this appears to be a simple S_N2 addition, the addition of base and heat to drive the reaction forward was found to be an integral part of driving the reaction to completion. There was also no observed alkylation at the tertiary amine positions. Using n-(3-bromopropyl)phthalimide or n-(2-bromoethyl)phthalimide to

synthesize **bdep** and **tren*** provides a simplified way to introduce an alkyl arm containing an amino moiety to the tren-based ligand without the use of toxic cyanide reagents in the presence of fuming acid (H_2SO_4).

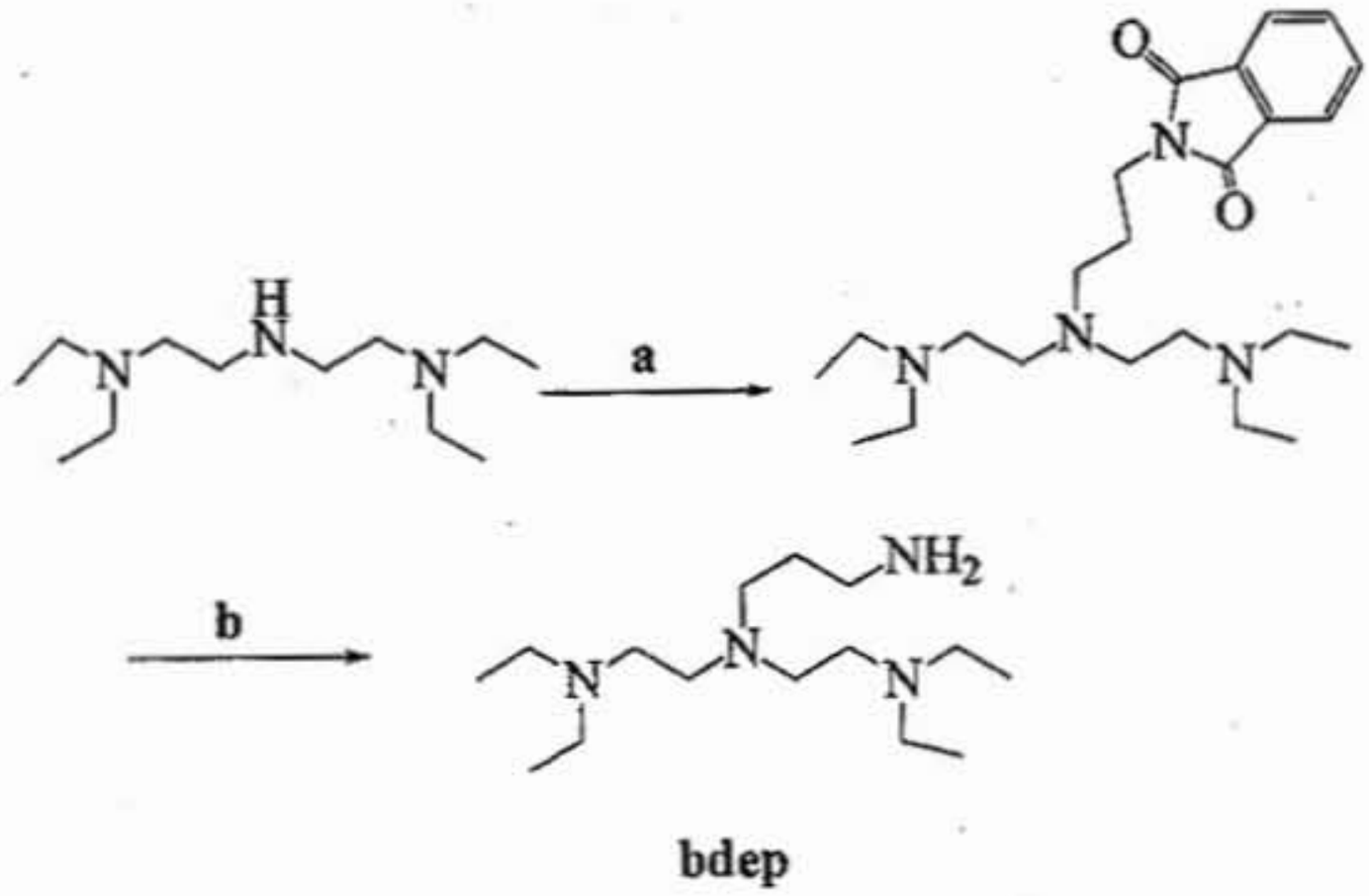

bdep

a) n-(3-bromopropyl)phthalimide, K_2CO_3, CH_3CN, Δ; b) 5M HCl, Δ, KOH workup

Figure 5.04. The synthesis of the tetraethylated tren derivative **bdep.**

The pathway to the methylated **bdea** and **bdpa** ligands (**Figure 5.05**) begins with the formic acid/formaldehyde methylation of tren, affording the hexamethylated tren.[8] One equivalent of butyllithium is then added to remove an arm from the hexamethylated tren, affording the intermediate **TMDA**.[9] From here, **bdpa** is synthesized using a modified Gabriel synthesis under neat conditions (**Figure 5.05**, Path c).[10] **bdea** is synthesized via cyanomethylation of **TMDA**, followed by reduction with lithium aluminum hydride (**Figure 5.05**, Path d-e).[11] Both products are musky-smelling oils that were stored in a drybox for extended time periods (2-3 months) without decomposition.

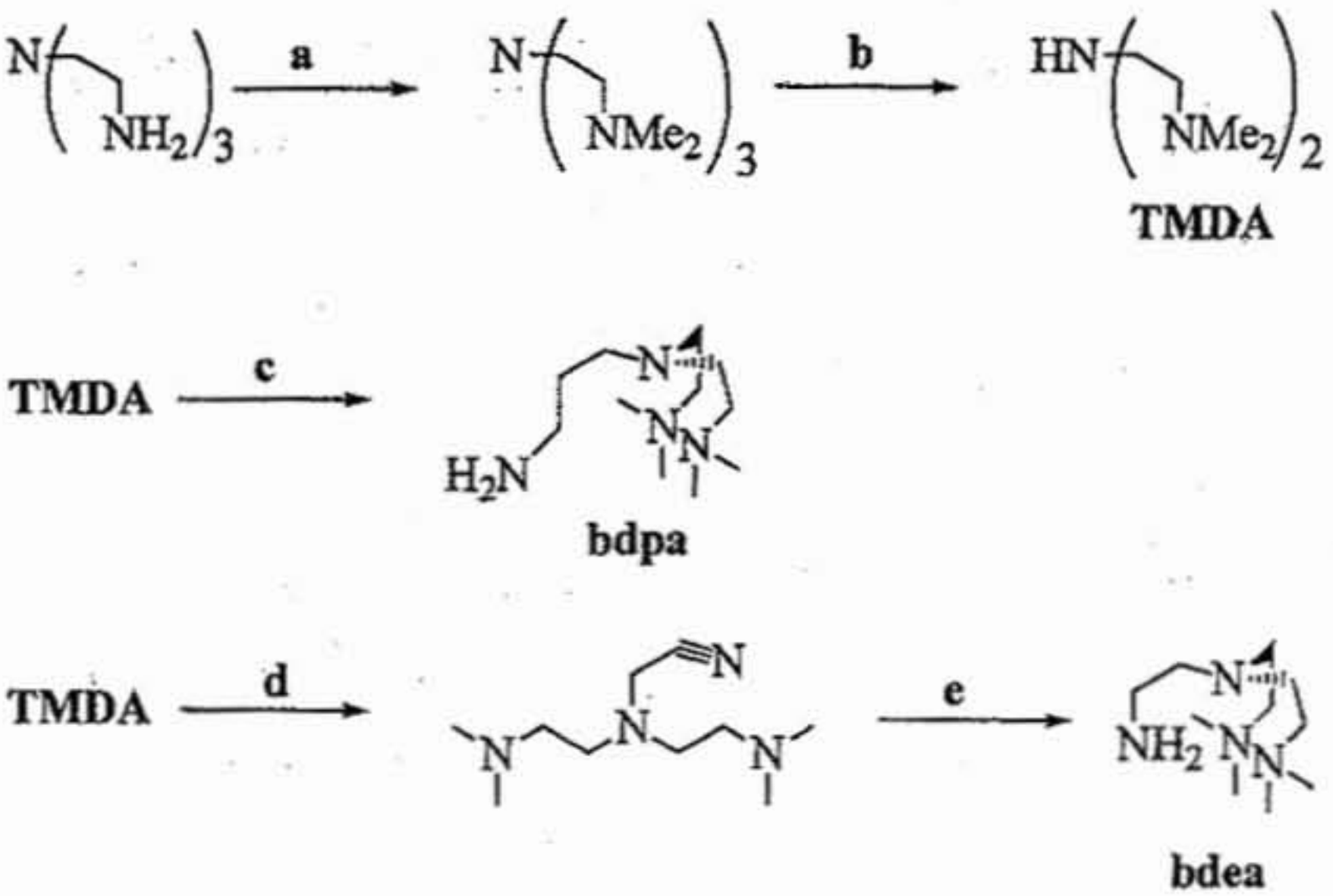

a) formic acid, formaldehyde, Δ; b) BuLi, pentane, -78°C (1 hr), 0°C (1 hr), NaOH workup; c) n-(3-bromopropyl)phthalimide; 10M HCl; d) HCl, KCN, CH_2O; e) $LiAlH_4$.

Figure 5.05. The parallel synthesis of **bdea** and **bdpa.**

Discussion. The synthesis of $[Fe^{II}S^{Me2}N_4(bdea)]^+$ is shown in **Figure 5.06.** $[Fe^{II}S^{Me2}N_4(bdea)]^+$ is a pale yellow solid with a featureless absorption spectrum. When this species was exposed to air, no visible reaction was observed, meaning that either it is completely stable under aerobic conditions, or the oxidation of the Fe^{II} species leads to ligand dissociation and ultimately complex decomposition. Attempts to oxidize this complex via chemical oxidation using $FeCp_2PF_6$ were unsuccessful, only producing an insoluble organic compound, similar to observations made by Theisen.[4] No reaction was observed when KO_2 was added to a solution of $[Fe^{II}S^{Me2}N_4(bdea)]^+$, under protic or aprotic conditions. Because this complex did not display any visible reactivity, no further characterization was pursued beyond this point.

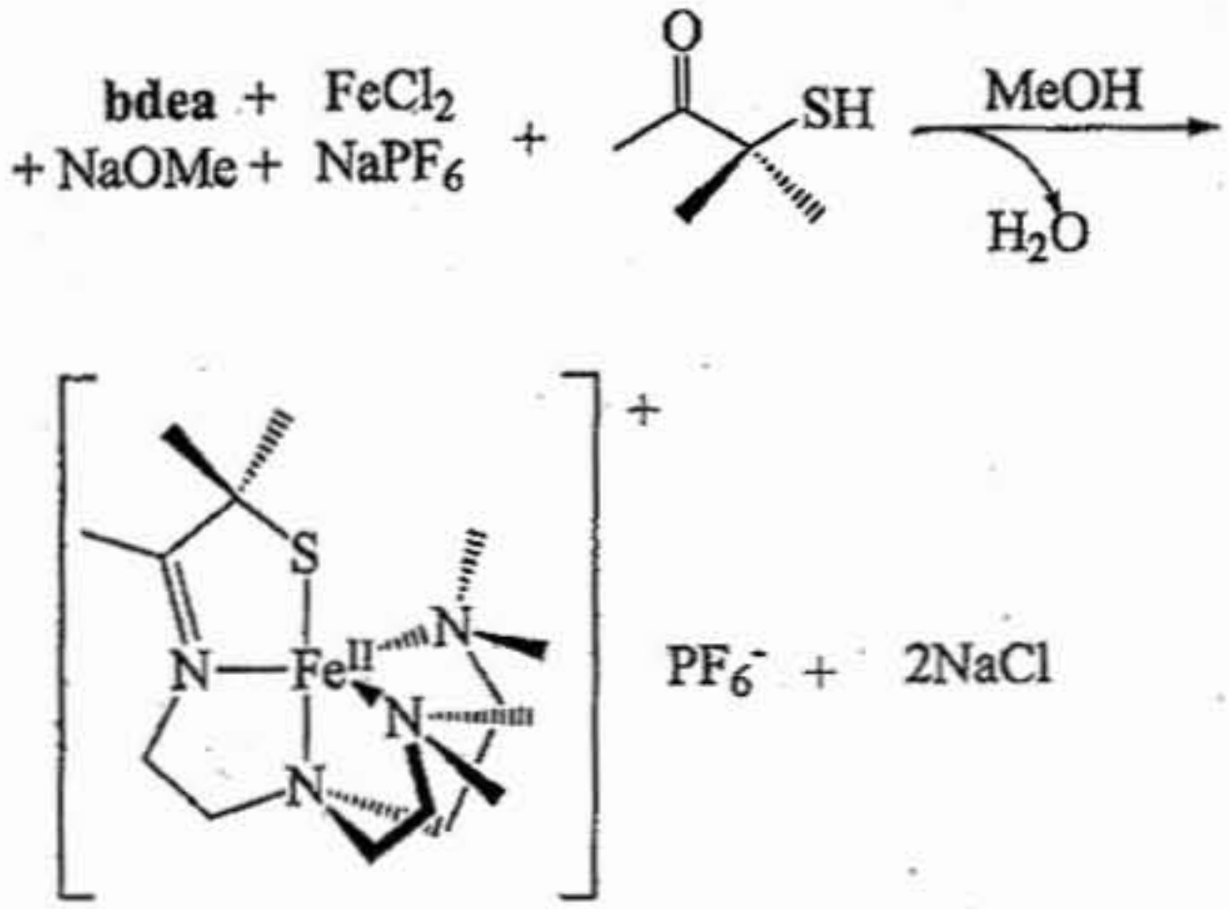

$[Fe^{II}(S^{Me2}bdea)]^+$

Figure 5.06. The synthesis of $[Fe^{II}S^{Me2}N_4(bdea)]^+$. The general synthesis of all the metal complexes in this chapter follow this preparatory scheme. For simplicity, only the **bdea**-derived complex is shown in this figure.

$[Fe^{II}S^{Me2}N_4(bdpa)]^+$ is also a pale yellow solid, but it appeared to readily oxidize to the Fe^{III} state when $FeCp_2PF_6$ was added as a chemical oxidant, yielding a burgundy solid with two bands in the absorption spectrum at 415nm and 550nm. The absorption spectrum of $[Fe^{II}S^{Me2}N_4(bdpa)]^+$ is shown below in **Figure 5.07.** It appears from their intensity that the two bands at 415 nm and 550 nm can possibly be assigned to S→Fe charge transfer transitions. However, in order to definitively assign these absorptions, the extinction coefficients need to be determined and resonance Raman studies need to be pursued.

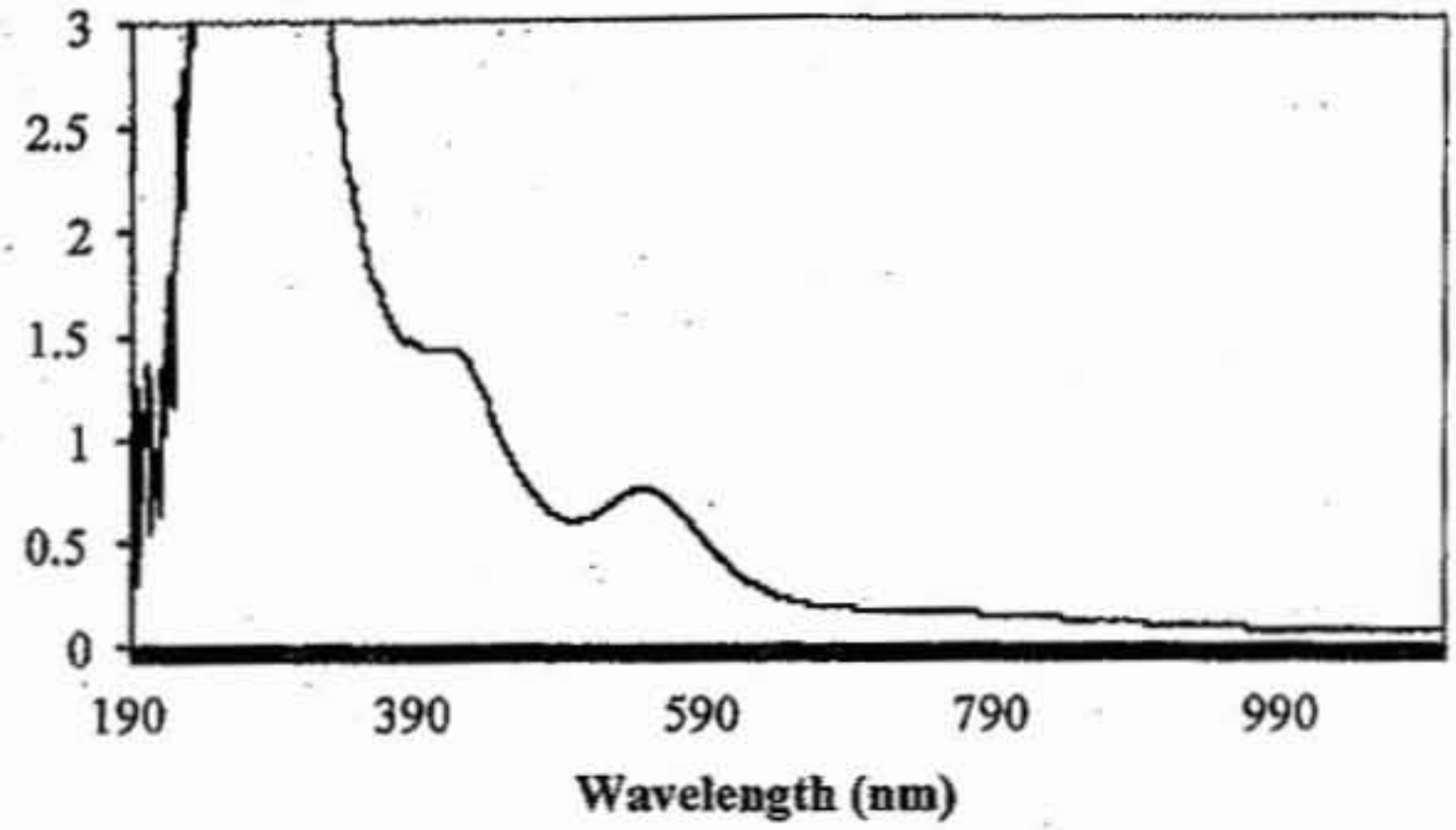

Figure 5.07. The absorption spectrum of the oxidized product when $FeCp_2PF_6$ is added to a solution of $[Fe^{II}S^{Me2}N_4(bdpa)]^+$ in acetonitrile. This is proposed to be the spectrum of $[Fe^{III}S^{Me2}N_4(bdpa)]^+$.

The synthesis of $[Fe^{II}S^{Me2}N_4(bdep)]^+$ yielded pale green crystals which appeared to be quite stable under aerobic conditions for days. Attempts to oxidize this complex via chemical oxidation using $FeCp_2PF_6$ also were unsuccessful. However, preliminary electrochemical studies showed a reversible one-electron redox wave at $E_{1/2}$ = 405 mV vs. SCE, indicating that the ferric state is indeed accessible, perhaps with a stronger chemical oxidant such as $NOBF_4$.

An x-ray structure of $[Fe^{II}S^{Me2}N_4(bdep)]^+$ was obtained. The ORTEP is shown below in **Figure 5.08.** Significant bond lengths and angles are listed in **Table 5.01.**

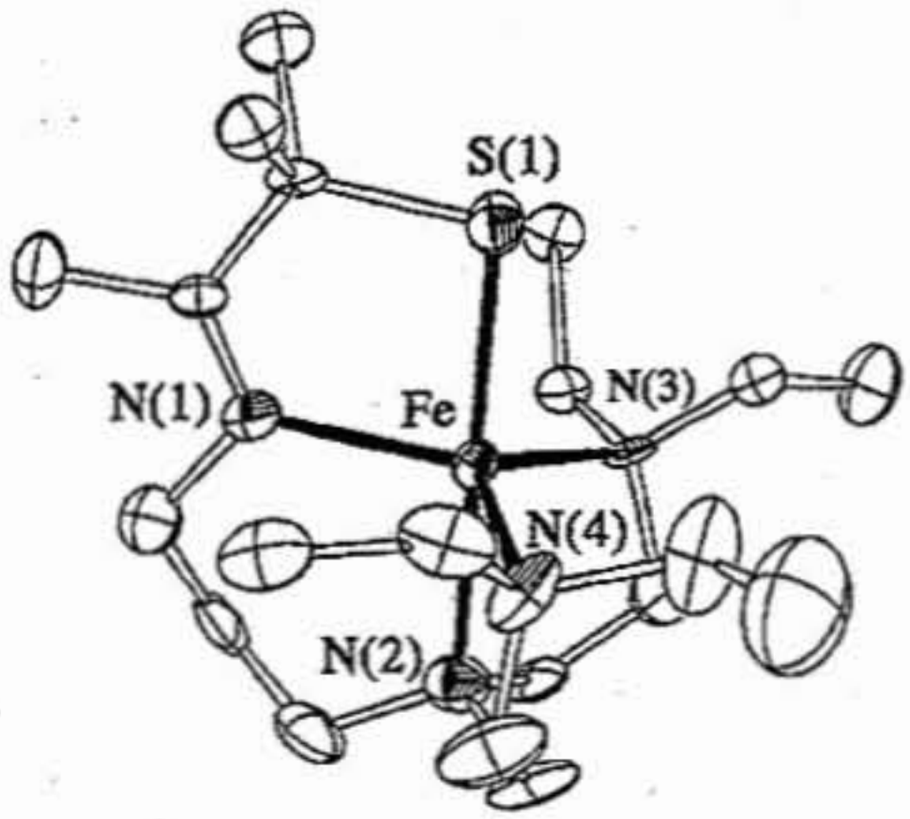

Figure 5.08. The x-ray crystal structure of $[Fe^{II}S^{Me2}N_4(bdpa)]^+$.

Bond lengths (Å)		Bond angles (deg)	
Fe-S(1)	2.305	S(1)-Fe-N(1)	84.9
Fe-N(1)	2.136	S(1)-Fe-N(2)	179.5
Fe-N(2)	2.236	S(1)-Fe-N(3)	99.1
Fe-N(3)	2.265	N(3)-Fe-N(4)	121.4
Fe-N(4)	2.211	N(1)-Fe-N(4)	113.2
		N(1)-Fe-N(3)	123.4

Table 5.01. Selected bond lengths and bond angles of $[Fe^{II}S^{Me2}N_4(bdpa)]^+$.

Synthesis of bis-alkylated analogues of tren-based ligands. Although these tetraalkylated tren-derived ligands displayed interesting properties and reactivities, they were relatively inert to oxidizing substrates. In addition, they did not react with superoxide, and thus were not effective as SOR models. Because of this, designing tren-based ligand systems that were bis-alkylated rather than tetraalkylated became a series of target compounds (**Figure 5.09**). The synthesis of these ligands would also provide an interesting comparison between the effect that the level of alkylation of coordinating

amines and the electronic and reactive properties of the metal center of the respective complexes. Another reason for pursuing these target ligands was because there is undoubtedly a relationship between redox potential of the respective Fe^{II} complexes and the level of alkylation that the coordinating amines possess; increased levels of alkylation correspond with cathodic shifts in redox potentials. This also corresponds with similar reported studies of the alkylation of amine ligand systems.[3,12]

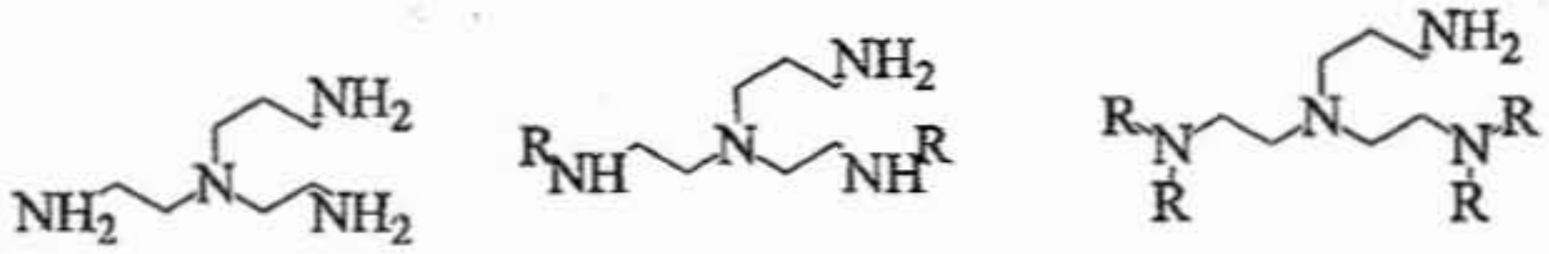

tren | **R2-tren** bis-alkylated tren derivatives | **R4-tren** tetraalkylated tren derivatives

Figure 5.09. The general structures of tren and the desired bis- and tetraalkylated derivatives of tren. These ligands are to be used to stabilize the Fe^{III}-OOH intermediate in the SOR model $[Fe^{II}S^{Me2}N_4(tren)]^+$.

In developing a synthesis for these compounds, several pathways were initiated. The ideal synthesis would involve common intermediates with varied sizes of the alkyl group changed by simply adding a single reagent. Initially, starting with a polyamine such as diethylenetriamine was attempted. Because of the high level of difficulty in synthesizing asymmetric polyamine compounds, a protecting group strategy was initially chosen. However, selectively protecting secondary amines in the presence of primary amines, while being a widely reported method, proved to be very arduous, as separating the multiple byproducts became a significant challenge. Ultimately, the yield obtained for each step was too low to justify continuing in this fashion. Thus, another

methodology was attempted. This new synthetic pathway is shown in **Figure 5.10.** Iminodiacetonitrile was chosen as the starting material because of the difficulty encountered in selectively protecting different amine groups when a polyamine was chosen as the starting material. Using this starting material, the secondary amine could be protected in almost quantitative yields, without the need of complicated purification methods to separate the target compound. Following this, the nitrile arms can easily be reduced using BH_3:THF to afford the respective primary amines easily and efficiently.

Following the reduction of the nitriles to primary amines, the primary amines are then protected with ethyl trifluoroacetate. The trifluoroacetate (TFAc) groups are base-deprotected, as opposed to the refluxing HBr/HOAc deprotection of the tosyl protecting group,. This allows for selective deprotection of the central secondary amine without deprotection of the terminal amines. The TFAc-protected compound was isolated as a pale yellow solid. The following alkylation step shown in Figure 5.10 has not been accomplished yet, and the remainder of the synthesis should be completed in the future. The importance of completing this ligand synthesis would be that it provides a simple pathway in generating numerous novel asymmetric tren derivatives. These ligands would be very useful in determining the effect of alkylation on the reactivity of our SOR models. Asymmetric alkylated derivatives of tren are very uncommon in the literature, as the synthesis of such compounds is very arduous and not trivial by any means.

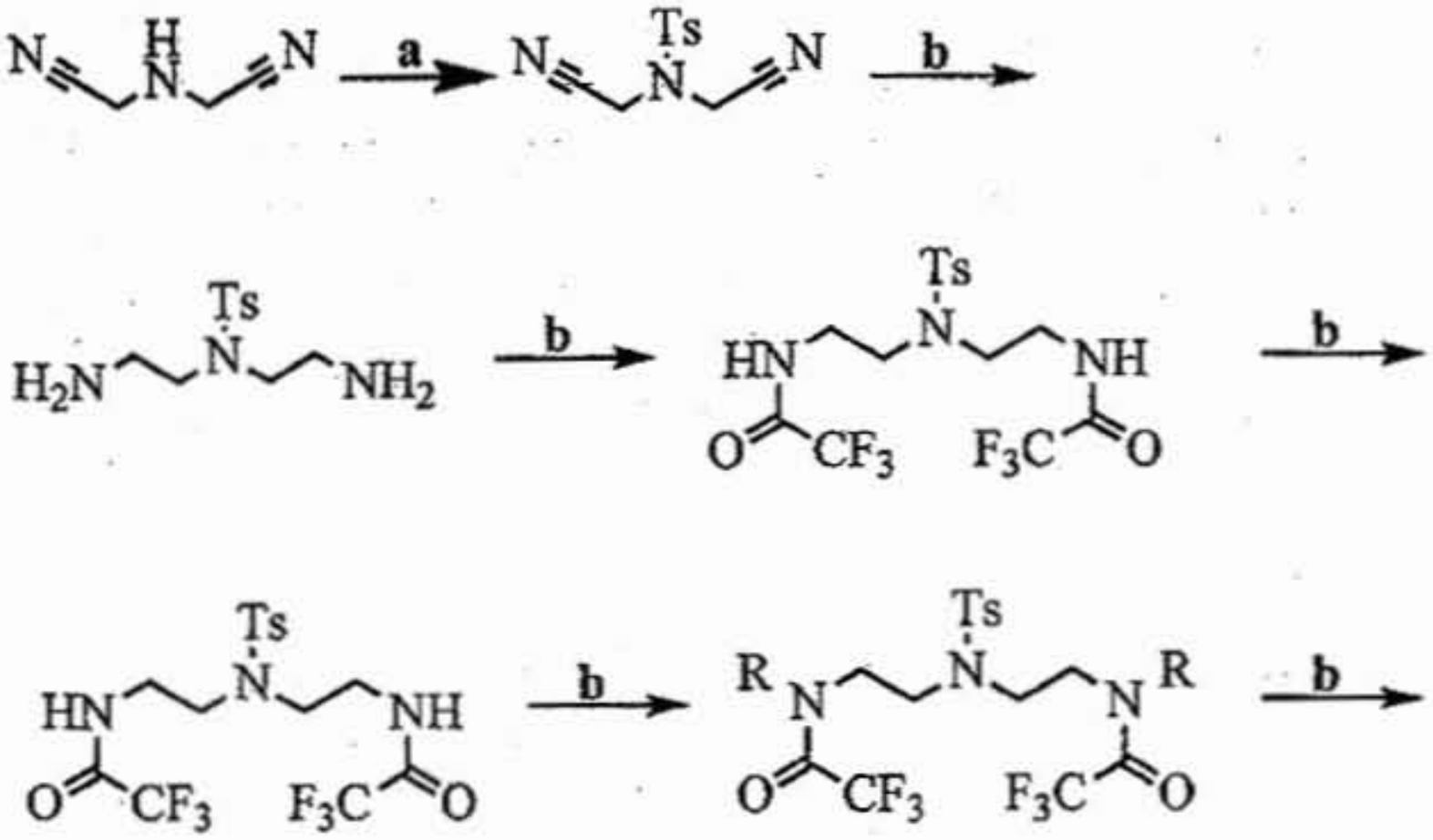

Figure 5.10. The proposed synthesis of bis-alkylated tren-derived ligands. In the scheme, R=alkyl group, i.e. $-CH_3$, CH_2CH_3, etc.

Conclusion. Three new asymmetric tetraalkylated derivatives of the tripodal amine tren have been synthesized using readily available reagents and simple reaction pathways. In addition, preliminary physical and spectroscopic properties of their corresponding Fe-complexes have been obtained and described. It appears that the physical and reactive properties of these alkylated Fe-complexes is significantly altered by the introduction of tertiary amines into the coordination sphere in lieu of the primary amines found in our SOR model $\mathbf{[Fe^{II}S^{Me2}N_4(tren)]^+}$. The preliminary characterization of the new complexes, $\mathbf{[Fe^{II}S^{Me2}N_4(bdpa)]^+}$, $\mathbf{[Fe^{II}S^{Me2}N_4(bdea)]^+}$, and $\mathbf{[Fe^{II}S^{Me2}N_4(bdep)]^+}$, has been reported and corresponds nicely with the reported data for the $\mathbf{[Fe^{II}S^{Me2}N_4(tren^*)]^+}$ complex.

To explain the different reactivies seen with these complexes containing the propylene backbone, as opposed to the ethylene backbone, the additional space and larger bite angle afforded by the larger six-membered chelate from the ligand backbone may allow for the more facile rearrangement of the ethyl groups during oxidation to the ferric state. There is precedence in the literature showing that a slight topological variation caused by stepwise insertion of a CH_2 group into each ligand arm of tren causes significant changes in the chemistry of the ligand.[12]

Chapter 5 – Notes

(1) Fujisawa, K. T., M.; Morooka, Y.; Kitajima *J Am Chem Soc* **1994**, *116*, 12079-12080.

(2) Osako, T.; Nagatomo, S.; Tachi, Y.; Kitagawa, T.; Itoh, S. *Angew Chem Int Ed Engl* **2002**, *41*, 4325-8.

(3) Schatz, M.; Becker, M.; Walter, O.; Liehr, G.; Schindler, S. *Inorg Chim Acta* **2001**, *324*, 173-179.

(4) Theisen, R. M.; Shearer, J.; Kaminsky, W.; Kovacs, J. A. *Inorg Chem* **2004**, *43*, 7682-90.

(5) Simaan, J.; Poussereau, S.; Blondin, G.; Girerd, J.-J.; Defaye, D.; Philouze, C.; Guilhem, J.; Tchertanov, L. *Inorg. Chim. Acta* **2000**, *299*, 221-230.

(6) Meyerstein, D. *Coordination Chemistry Reviews* **1999**, *185-186*, 141-147.

(7) Warden, A.; Graham, B.; Hearn, M. T.; Spiccia, L. *Org Lett* **2001**, *3*, 2855-8.

(8) Clarke, H. T.; Gillespie, H. B.; Weisshaus, S. Z. *J Am Chem Soc* **1933**, *55*, 4571-4587.

(9) Luitjes, H.; Schakel, M.; Klumpp, G. W. *Synthetic Comm.* **1994**, *24*, 2257-2261.

(10) Mosch-Zanetti, N. C.; Kopke, S.; Herbst-Irmer, R.; Hewitt, M. *Inorg Chem* **2002**, *41*, 3513-20.

(11) Song, B.; Reuber, J.; Ochs, C.; Hahn, F. E.; Lugger, T.; Orvig, C. *Inorg Chem* **2001**, *40*, 1527-35.

(12) Ochs, C.; Hahn, F. E.; Lugger, T. *Eur. J. Inorg. Chem.* **2001**, 1279-1285.

List of References

Abreu, I. A.; Saraiva, L. M.; Soares, C. M.; Teixeira, M.; Cabelli, D. E., The mechanism of superoxide scavenging by Archaeoglobus fulgidus neelaredoxin. J Biol Chem 2001, 276, (42), 38995-9001.

Abreu, I. A.; Xavier, A. V.; LeGall, J.; Cabelli, D. E.; Teixeira, M., Superoxide scavenging by neelaredoxin: dismutation and reduction activities in anaerobes. J Biol Inorg Chem 2002, 7, (6), 668-74.

Adam, V.; Royant, A.; Niviere, V.; Molina-Heredia, F. P.; Bourgeois, D., Structure of superoxide reductase bound to ferrocyanide and active site expansion upon X-ray-induced photo-reduction. Structure 2004, 12, (9), 1729-40.

Auchere, F.; Rusnak, F., What is the ultimate fate of superoxide anion in vivo? J Biol Inorg Chem 2002, 7, (6), 664-7.

Balland, V.; Banse, F.; Anxolabehere-Mallart, E.; Ghiladi, M.; Mattioli, T. A.; Philouze, C.; Blondin, G.; Girerd, J. J., Fe(II) and Fe(III) mononuclear complexes with a pentadentate ligand built on the 1,3-diaminopropane unit. Structures and spectroscopic and electrochemical properties. Reaction with H_2O_2. Inorg Chem 2003, 42, (7), 2470-7.

Baran, Y.; Yilmaz, I., Transition Metal Chem 2001, 26, 36-38.

Barefield, E. K.; Wagner, F.; Herlinger, A. W.; Dahl, A. R., Inorg Syntheses, 220-225.

Bernal, I.; Jensen, I. M.; Jensen, K. B.; McKenzie, C. J.; Toftlund, H.; Tuchagues, J.-P., J. Chem. Soc. Dalton Trans. 1995, 3667-3675.

Brandès, S.; C., G.; Denat, F.; Pullumbi, P.; Guilard, R., Bull. Chim. de France 1996, 133, 65-73.

Brines, L. M.; Kovacs, J. A., Understanding the Mechanism of Superoxide Reductase Promoted Reduction of Superoxide. Eur. J. Inorg. Chem 2007, 29-38.

Bukowski, M. R.; Halfen, H. L.; van den Berg, T. A.; Halfen, J. A.; Que, L., Jr., Spin-state rationale for the peroxo-stabilizing role of the thiolate ligand in superoxide reductase. Angew Chem Int Ed Engl 2005, 44, (4), 584-7.

Bukowski, M. R.; Koehntop, K. D.; Stubna, A.; Bominaar, E. L.; Halfen, J. A.; Munck, E.; Nam, W.; Que, L., Jr., A thiolate-ligated nonheme oxoiron(IV) complex relevant to cytochrome P450. Science 2005, 310, (5750), 1000-2.

Chantson, T. E.; Hancock, R. D., Inorg Chim Acta 1995, 230, 165-167.

Clay, M. D.; Jenney, F. E., Jr.; Hagedoorn, P. L.; George, G. N.; Adams, M. W.; Johnson, M. K., Spectroscopic studies of Pyrococcus furiosus superoxide reductase: implications for active-site structures and the catalytic mechanism. J Am Chem Soc 2002, 124, (5), 788-805.

Clay, M. D.; Yang, T. C.; Jenney, F. E., Jr.; Kung, I. Y.; Cosper, C. A.; Krishnan, R.; Kurtz, D. M., Jr.; Adams, M. W.; Hoffman, B. M.; Johnson, M. K., Geometries and electronic structures of cyanide adducts of the non-heme iron active site of superoxide reductases: vibrational and ENDOR studies. Biochemistry 2006, 45, (2), 427-38.

Coelho, A. V.; Matias, P.; Fulop, V.; Thompson, A.; Gonzalez, A.; Carrondo, M. A., J. Biol. Inorg. Chem. 1997, 2, 680-689.

Costas, M.; Mehn, M. P.; Jensen, M. P.; Que, L., Jr., Dioxygen activation at mononuclear nonheme iron active sites: enzymes, models, and intermediates. Chem Rev 2004, 104, (2), 939-86.

Coulter, E. D.; Emerson, J. P.; Jr., D. M. K.; Cabelli, D. E., Superoxide Reactivity of Rubredoxin Oxidoreductase (Desulfoferrodoxin) from Desulfovibrio vulgaris: A Pulse Radiolysis Study. J Am Chem Soc 2000, 122, 11555-11556.

de Visser, S. P., Propene activation by the oxo-iron active species of taurine/alpha-ketoglutarate dioxygenase (TauD) enzyme. How does the catalysis compare to heme-enzymes? J Am Chem Soc 2006, 128, (30), 9813-24.

Dittler-Klingemann, A. M.; Hahn, F. E., Trigonal-Bipyramidal Copper(II) Complexes with Symmetric and Unsymmetric Tripodal Tetramine Ligands. Inorg Chem 1996, 35, 1996-1999.

Dubois, G.; Murphy, A.; Stack, T. D., Simple iron catalyst for terminal alkene epoxidation. Org Lett 2003, 5, (14), 2469-72.

Emerson, J. P.; Cabelli, D. E.; Kurtz, D. M., Jr., An engineered two-iron superoxide reductase lacking the [Fe(SCys)$_4$] site retains its catalytic properties in vitro and in vivo. Proc Natl Acad Sci U S A 2003, 100, (7), 3802-7.

Fiedler, A. T.; Halfen, H. L.; Halfen, J. A.; Brunold, T. C., Synthesis, structure determination, and spectroscopic/computational characterization of a series of Fe(II)-thiolate model complexes: implications for Fe-S bonding in superoxide reductases. J Am Chem Soc 2005, 127, (6), 1675-89.

Fontecave, M.; Pierre, J. L., Iron: metabolism, toxicity and therapy. Biochimie 1993, 75, (9), 767-73.

Fridovich, I., Acc. Chem. Res. 1972, 5, 321-326.

Fridovich, I., Oxygen toxicity: a radical explanation. J Exp Biol 1998, 201, (Pt 8), 1203-9.

Fridovich, I., Superoxide radical and superoxide dismutases. Annu Rev Biochem 1995, 64, 97-112.

Fridovich, I., Superoxide radical: an endogenous toxicant. Annu Rev Pharmacol Toxicol 1983, 23, 239-57.

Fujisawa, K. T., M.; Morooka, Y.; Kitajima, J Am Chem Soc 1994, 116, 12079-12080.

Gagné, R. R.; Ingle, D. M.; Lisensky, G. C., Inorg Chem 1981, 20, 1991-1993.

Grunden, A. M.; Jenney, F. E., Jr.; Ma, K.; Ji, M.; Weinberg, M. V.; Adams, M. W., In vitro reconstitution of an NADPH-dependent superoxide reduction pathway from Pyrococcus furiosus. Appl Environ Microbiol 2005, 71, (3), 1522-30.

Guajardo, R. J.; Chavez, F.; Farinas, E. T.; Mascharak, P. K., J. Am. Chem. Soc. 1995, 117, 3883-3884.

Gupta, M. N.; Roy, I., Enzymes in organic media - Forms, functions and applications. Eur. J. Biochem 2004, 271, 2573-2583.

Halfen, J. A.; Moore, H. L.; Fox, D. C., Synthetic models of the reduced active site of superoxide reductase. Inorg Chem 2002, 41, (15), 3935-43.

Halfen, J. A.; Young, V. G., Jr., Efficient preparation of 1,4,8-trimethylcyclam and its conversion into a thioalkyl-pendant pentadentate chelate. Chem Commun (Camb) 2003, (23), 2894-5.

Hazell, A.; McKenzie, C. J.; Nielsen, L. P.; Schindler, S.; Weitzer, M., Mononuclear non-heme iron(III) peroxide complexes: syntheses, characterisation, mass spectrometric and kinetic studies. J Chem Soc, Dalton Trans 2002, 310-317.

Ho, R. Y. N.; Roelfes, G.; Hermant, R.; Hage, R.; Feringa, B. L.; Que, L. J., Chem. Comm. 1999, 2161-2162.

Hodges, K. D.; Wollman, R. G.; Barefield, E. K.; Hendrickson, D. N., Inorg Chem 1977, 16, (11), 2746-2751.

Horner, O.; Mouesca, J. M.; Oddou, J. L.; Jeandey, C.; Niviere, V.; Mattioli, T. A.; Mathe, C.; Fontecave, M.; Maldivi, P.; Bonville, P.; Halfen, J. A.; Latour, J. M., Mossbauer characterization of an unusual high-spin side-on peroxo-Fe^{3+} species in the active site of superoxide reductase from Desulfoarculus Baarsii. Density functional calculations on related models. Biochemistry 2004, 43, (27), 8815-25.

Imlay, J. A., What biological purpose is served by superoxide reductase? J Biol Inorg Chem 2002, 7, (6), 659-63.

Jenney, F. E., Jr.; Verhagen, M. F.; Cui, X.; Adams, M. W., Anaerobic microbes: oxygen detoxification without superoxide dismutase. Science 1999, 286, (5438), 306-9.

Jensen, M. P.; Lange, S. J.; Mehn, M. P.; Que, E. L.; Que, L., Jr., Biomimetic aryl hydroxylation derived from alkyl hydroperoxide at a nonheme iron center. Evidence for an Fe(IV)=O oxidant. J Am Chem Soc 2003, 125, (8), 2113-28.

Kaizer, J.; Costas, M.; Que, L., Jr., A dramatic push effect on the homolysis of Fe^{III}(OOR) intermediates to form non-heme FeIV=O complexes. Angew Chem Int Ed Engl 2003, 42, (31), 3671-3.

Kehrer, J. P., The Haber-Weiss reaction and mechanisms of toxicity. Toxicology 2000, 149, (1), 43-50.

Kim, S. O.; Sastri, C. V.; Seo, M. S.; Kim, J.; Nam, W., Dioxygen activation and catalytic aerobic oxidation by a mononuclear nonheme iron(II) complex. J Am Chem Soc 2005, 127, (12), 4178-9.

Kitagawa, T.; Dey, A.; Lugo-Mas, P.; Benedict, J. B.; Kaminsky, W.; Solomon, E.; Kovacs, J. A., A functional model for the cysteinate-ligated non-heme iron enzyme superoxide reductase (SOR). J Am Chem Soc 2006, 128, (45), 14448-9.

Klibanov, A. M., Trends Biotechnol. 1997, 15, 97-101.

Klinker, E. J.; Kaizer, J.; Brennessel, W. W.; Woodrum, N. L.; Cramer, C. J.; Que, L., Jr., Structures of nonheme oxoiron(IV) complexes from X-ray crystallography, NMR spectroscopy, and DFT calculations. Angew Chem Int Ed Engl 2005, 44, (24), 3690-4.

Koehntop, K. D.; Rohde, J. U.; Costas, M.; Que, L., Jr., XAS characterization of end-on and side-on peroxoiron(III) complexes of the neutral pentadentate N-donor ligand N-methyl-N,N',N'-tris(2-pyridylmethyl)ethane-1,2-diamine. Dalton Trans 2004, (20), 3191-8.

Kovacs, unpublished results. 2006.

Kovacs, J. A., Biochemistry. How iron activates O_2. Science 2003, 299, (5609), 1024-5.

Kovacs, J. A., Synthetic analogues of cysteinate-ligated non-heme iron and non-corrinoid cobalt enzymes. Chem Rev 2004, 104, (2), 825-48.

Krishnamurthy, D.; Kasper, G. D.; Namuswe, F.; Kerber, W. D.; Narducci Sarjeant, A. A.; Moenne-Loccoz, P.; Goldberg, D. P., A low-spin alkylperoxo-iron(III) complex with weak Fe-O and O-O bonds: implications for the mechanism of superoxide reductase. J Am Chem Soc 2006, 128, (44), 14222-3.

Kurtz, D. M., Jr., Microbial detoxification of superoxide: the non-heme iron reductive paradigm for combating oxidative stress. Acc Chem Res 2004, 37, (11), 902-8.

Kurtz, D. M., Jr.; Coulter, E. D., Chemtracts 2001, 407-433.

Kurtz, D. M., Jr.; Coulter, E. D., The mechanism(s) of superoxide reduction by superoxide reductases in vitro and in vivo. J Biol Inorg Chem 2002, 7, (6), 653-8.

Lanznaster, M.; Hratchian, H. P.; Heeg, M. J.; Hryhorczuk, L. M.; McGarvey, B. R.; Schlegel, H. B.; Verani, C. N., Structural and electronic behavior of unprecedented five-coordinate iron(III) and gallium(III) complexes with a new phenol-rich electroactive ligand. Inorg Chem 2006, 45, (3), 955-7.

Liang, X.; Sadler, P. J., Cyclam complexes and their applications in medicine. Chem Soc Rev 2004, 33, (4), 246-66.

Lim, M. H.; Rohde, J. U.; Stubna, A.; Bukowski, M. R.; Costas, M.; Ho, R. Y.; Munck, E.; Nam, W.; Que, L., Jr., An Fe^{IV}=O complex of a tetradentate tripodal nonheme ligand. Proc Natl Acad Sci U S A 2003, 100, (7), 3665-70.

Lombard, M.; Houee-Levin, C.; Touati, D.; Fontecave, M.; Niviere, V., Superoxide reductase from Desulfoarculus baarsii: reaction mechanism and role of glutamate 47 and lysine 48 in catalysis. Biochemistry 2001, 40, (16), 5032-40.

Lombard, M.; Touati, D.; Fontecave, M.; Niviere, V., Superoxide reductase as a unique defense system against superoxide stress in the microaerophile Treponema pallidum. J Biol Chem 2000, 275, (35), 27021-6.

Lugo-Mas, P., Data obtained by and used with permission.

Lugo-Mas, P.; Dey, A.; Xu, L.; Davin, S. D.; Benedict, J.; Kaminsky, W.; Hodgson, K. O.; Hedman, B.; Solomon, E. I.; Kovacs, J. A., How does single oxygen atom addition affect the properties of an Fe-nitrile hydratase analogue? The compensatory role of the unmodified thiolate. J Am Chem Soc 2006, 128, (34), 11211-21.

Luitjes, H.; Schakel, M.; Klumpp, G. W., N-Lithio-N,N',N", N"-tetramethyldiethylenetriamine and N'-lithio-N,N,N",N"-tetramethyldiethylenetriamine; oxidative coupling of aminomethyllithiom derivatives. Synthetic Comm. 1994, 24, (16), 2257-2261.

MacBeth, C, E.; Golombek, A. P.; Young, V. G., Jr.; Yang, C.; Kuczera, K.; Hendrich, M. P.; Borovik, A. S., O_2 activation by nonheme iron complexes: A monomeric Fe(III)-Oxo complex derived from O2. Science 2000, 289, (5481), 938-41.

Makris, T. M.; von Koenig, K.; Schlichting, I.; Sligar, S. G., The status of high-valent metal oxo complexes in the P450 cytochromes. J Inorg Biochem 2006, 100, (4), 507-18.

Martin, L. Y.; DeHayes, L. J.; Zompa, L. J.; Busch, D. H., J Am Chem Soc 1974, 4046-4048.

Mathe, C.; Mattioli, T. A.; Horner, O.; Lombard, M.; Latour, J. M.; Fontecave, M.; Niviere, V., Identification of iron(III) peroxo species in the active site of the superoxide reductase SOR from Desulfoarculus baarsii. J Am Chem Soc 2002, 124, (18), 4966-7.

Mathe, C.; Niviere, V.; Houee-Levin, C.; Mattioli, T. A., Fe(3+)-eta(2)-peroxo species in superoxide reductase from Treponema pallidum. Comparison with Desulfoarculus baarsii. Biophys Chem 2006, 119, (1), 38-48.

Mathe, C.; Niviere, V.; Mattioli, T. A., Fe^{3+}-hydroxide ligation in the superoxide reductase from Desulfoarculus baarsii is associated with pH dependent spectral changes. J Am Chem Soc 2005, 127, (47), 16436-41.

McCord, J. M., The evolution of free radicals and oxidative stress. Am J Med 2000, 108, (8), 652-9.

McCord, J. M., Iron, free radicals, and oxidative injury. J Nutr 2004, 134, (11), 3171S-3172S.

Meyerstein, D., Are M-N bonds indeed inherently weaker when N is a tertiary rather than a primary or secondary nitrogen atom? Coordination Chemistry Reviews 1999, 185-186, 141-147.

Montellano, P. R. O. d.; Voss, J. J. D., Oxidizing species in the mechanism of cytochrome P450. Nat. Prod. Re. 2002, 19, 477-493.

Mosch-Zanetti, N. C.; Kopke, S.; Herbst-Irmer, R.; Hewitt, M., Unsymmetrical tren-based ligands: synthesis and reactivity of rhenium complexes. Inorg Chem 2002, 41, (13), 3513-20.

Nam, W.; Park, S. E.; Lim, I. K.; Lim, M. H.; Hong, J.; Kim, J., First direct evidence for stereospecific olefin epoxidation and alkane hydroxylation by an oxoiron(IV) porphyrin complex. J Am Chem Soc 2003, 125, (48), 14674-5.

Niviere, V.; Lombard, M.; Fontecave, M.; Houee-Levin, C., Pulse radiolysis studies on superoxide reductase from Treponema pallidum. FEBS Lett 2001, 497, (2-3), 171-3.

Noveron, J. C.; Olmstead, M. M.; Mascharak, P. K., A synthetic analogue of the active site of Fe-containing nitrile hydratase with carboxamido N and thiolato S as donors: synthesis, structure, and reactivities. J Am Chem Soc 2001, 123, (14), 3247-59.

Ochs, C.; Hahn, F. E.; Lugger, T., cis-Octaheddral Nickel(II) Complexes with Symmetric and Unsymmetric Tripodal Tetraamine Ligands. Eur. J. Inorg. Chem. 2001, 1279-1285.

Osako, T.; Nagatomo, S.; Tachi, Y.; Kitagawa, T.; Itoh, S., Low-temperature stopped-flow studies on the reactions of copper(II) complexes and H_2O_2: the first detection of a mononuclear copper(II)-peroxo intermediate. Angew Chem Int Ed Engl 2002, 41, (22), 4325-8.

Otani, H.; Umemoto, M.; Kagawa, K.; Nakamura, Y.; Omoto, K.; Tanaka, K.; Sato, T.; Nonoyama, A.; Kagawa, T., Protection against oxygen-induced reperfusion injury of the isolated canine heart by superoxide dismutase and catalase. J Surg Res 1986, 41, (2), 126-33.

Pallavicini, P. S.; Perotti, A.; Poggi, A.; Seghi, B.; Fabbrizzi, L., J Am Chem Soc 1987, 109, 5139-5144.

Park, M. J.; Lee, J.; Suh, Y.; Kim, J.; Nam, W., Reactivities of mononuclear non-heme iron intermediates including evidence that iron(III)-hydroperoxo species is a sluggish oxidant. J Am Chem Soc 2006, 128, (8), 2630-4.

Patra, A. K.; Afshar, R.; Olmstead, M. M.; Mascharak, P. K., The first non-heme iron(III) complex with a ligated carboxamido group that exhibits photolability of a bound NO ligand. Angew Chem Int Ed Engl 2002, 41, (14), 2512-5.

Pierre, J. L.; Fontecave, M., Iron and activated oxygen species in biology: the basic chemistry. Biometals 1999, 12, (3), 195-9.

Pine, S. H.; Sanchez, B. L., The Formic Acid-Formaldehyde Methylation of Amines. J. Org. Chem. 1971, 36, (6), 829-832.

Pohl, K.; Wieghardt, K.; Wolfgang, K.; Steenken, S., Inorg Chem 1988, 27, (3), 440-447.

Que, L., Jr.; Ho, R. Y., Dioxygen Activation by Enzymes with Mononuclear Non-Heme Iron Active Sites. Chem Rev 1996, 96, (7), 2607-2624.

Que, L., Jr.; Ho, R. Y., Dioxygen Activation by Enzymes with Mononuclear Non-Heme Iron Active Sites. Chem Rev 1996, 96, (7), 2607-2624.

Roelfes, G.; Lubben, M.; Chen, K.; Ho, R. Y.; Meetsma, A.; Genseberger, S.; Hermant, R. M.; Hage, R.; Mandal, S. K.; Young, V. G., Jr.; Zang, Y.; Kooijman, H.; Spek, A. L.; Que, L., Jr.; Feringa, B. L., Iron Chemistry of a Pentadentate Ligand That Generates a Metastable Fe(III)-OOH Intermediate. Inorg Chem 1999, 38, (8), 1929-1936.

Roelfes, G.; Vrajmasu, V.; Chen, K.; Ho, R. Y.; Rohde, J. U.; Zondervan, C.; La Crois, R. M.; Schudde, E. P.; Lutz, M.; Spek, A. L.; Hage, R.; Feringa, B. L.; Munck, E.; Que, L., Jr., End-on and side-on peroxo derivatives of non-heme iron complexes with pentadentate ligands: models for putative intermediates in biological iron/dioxygen chemistry. Inorg Chem 2003, 42, (8), 2639-53.

Rohde, J. U.; In, J. H.; Lim, M. H.; Brennessel, W. W.; Bukowski, M. R.; Stubna, A.; Munck, E.; Nam, W.; Que, L., Jr., Crystallographic and spectroscopic characterization of a nonheme Fe(IV)-O complex. Science 2003, 299, (5609), 1037-9.

Rohde, J. U.; Que, L., Jr., Axial coordination of carboxylate activates the non-heme Fe^{IV}=O unit. Angew Chem Int Ed Engl 2005, 44, (15), 2255-8.

Rowland, J. M.; Olmstead, M.; Mascharak, P. K., Syntheses, structures, and reactivity of low spin iron(III) complexes containing a single carboxamido nitrogen in a [FeN_5L] chromophore. Inorg Chem 2001, 40, (12), 2810-7.

Santagostini, L.; Gullotti, M.; Monzani, E.; Casella, L.; Dillinger, R.; Tuczek, F., Reversible Dioxygen Binding and Phenol Oxygenation in a Tyrosinase Model System. Chem. Eur. J. 2000, 6, (3), 519-522.

Santos-Silva, T.; Trincao, J.; Carvalho, A. L.; Bonifacio, C.; Auchere, F.; Raleiras, P.; Moura, I.; Moura, J. J.; Romao, M. J., The first crystal structure of class III superoxide reductase from Treponema pallidum. J Biol Inorg Chem 2006, 11, (5), 548-58.

Sastri, C. V.; Park, M. J.; Ohta, T.; Jackson, T. A.; Stubna, A.; Seo, M. S.; Lee, J.; Kim, J.; Kitagawa, T.; Munck, E.; Que, L., Jr.; Nam, W., Axial ligand substituted nonheme FeIV=O complexes: observation of near-UV LMCT bands and Fe=O Raman vibrations. J Am Chem Soc 2005, 127, (36), 12494-5.

Sastri, C. V.; Sook Seo, M.; Joo Park, M.; Mook Kim, K.; Nam, W., Formation, stability, and reactivity of a mononuclear nonheme oxoiron(IV) complex in aqueous solution. Chem Commun (Camb) 2005, (11), 1405-7.

Sawyer, D. T.; Valentine, J. S., How Super Is Superoxide? Acc Chem Res 1981, 14, 393-400.

Schatz, M.; Becker, M.; Walter, O.; Liehr, G.; Schindler, S., Reactivity towards dioxygen of a copper(I) complex of tris(2-benzylaminoethyl)amine. Inorg Chim Acta 2001, 324, 173-179.

Selke, M.; Sisemore, M. F.; Ho, R. Y. N.; Wertz, D. L.; Valentine, J. S., Dioxygen activation by iron complexes. The search for reactive intermediates. Journal of Molecular Catalysis A: Chemical 1997, 117, 71-82.

Serres, R. G.; Grapperhaus, C. A.; Bothe, E.; Bill, E.; Weyhermuller, T.; Neese, F.; Wieghardt, K., Structural, spectroscopic, and computational study of an octahedral, non-heme [Fe-NO](6-8) Series: $[Fe(NO)(cyclam\text{-}ac)]^{2+/+/0}$. J Am Chem Soc 2004, 126, (16), 5138-53.

Shaik, S.; Kumar, D.; de Visser, S. P.; Altun, A.; Thiel, W., Theoretical perspective on the structure and mechanism of cytochrome P450 enzymes. Chem Rev 2005, 105, (6), 2279-328.

Shaik, S.; Kumar, D.; de Visser, S. P.; Altun, A.; Thiel, W., Theoretical perspective on the structure and mechanism of cytochrome P450 enzymes. Chem Rev 2005, 105, (6), 2279-328.

Shearer, J.; Fitch, S. B.; Kaminsky, W.; Benedict, J.; Scarrow, R. C.; Kovacs, J. A., How does cyanide inhibit superoxide reductase? Insight from synthetic $Fe^{III}N_4S$ model complexes. Proc Natl Acad Sci U S A 2003, 100, (7), 3671-6.

Shearer, J.; Nehring, J.; Lovell, S.; Kaminsky, W.; Kovacs, J. A., Modeling the reactivity of superoxide reducing metalloenzymes with a nitrogen and sulfur coordinated iron complex. Inorg Chem 2001, 40, (22), 5483-4.

Shearer, J.; Scarrow, R. C.; Kovacs, J. A., Synthetic models for the cysteinate-ligated non-heme iron enzyme superoxide reductase: observation and structural characterization by XAS of an Fe(III)-OOH intermediate. J Am Chem Soc 2002, 124, (39), 11709-17.

Silaghi-Dumitrescu, R.; Silaghi-Dumitrescu, I.; Coulter, E. D.; Kurtz, D. M., Jr., Computational study of the non-heme iron active site in superoxide reductase and its reaction with superoxide. Inorg Chem 2003, 42, (2), 446-56.

Simaan, A. J.; Banse, F.; Girerd, J. J.; Wieghardt, K.; Bill, E., The electronic structure of non-heme iron(III)-hydroperoxo and iron(III)-peroxo model complexes studied by Mossbauer and electron paramagnetic resonance spectroscopies. Inorg Chem 2001, 40, (26), 6538-40.

Stolarczyk, K.; Bilewicz, R.; Siegfried, L.; Kaden, T., Inorg Chim Acta 2003, 00, 1-6.

Szulbinski, W. S.; Busch, D. H., Inorg Chim Acta 1995, 234, 143-148.

Tartaglia, L. A.; Storz, G.; Brodsky, M. H.; Lai, A.; Ames, B. N., Alkyl hydroperoxide reductase from Salmonella typhimurium. Sequence and homology to thioredoxin reductase and other flavoprotein disulfide oxidoreductases. J Biol Chem 1990, 265, (18), 10535-40.

Theisen, R. M.; Kovacs, J. A., Role of protons in superoxide reduction by a superoxide reductase analogue. Inorg Chem 2005, 44, (5), 1169-71.

Theisen, R. M.; Shearer, J.; Kaminsky, W.; Kovacs, J. A., Steric and electronic control over the reactivity of a thiolate-ligated Fe(II) complex with dioxygen and superoxide: reversible mu-oxo dimer formation. Inorg Chem 2004, 43, (24), 7682-90.

Tiago de Oliveira, F.; Chanda, A.; Banerjee, D.; Shan, X.; Mondal, S.; Que, L., Jr.; Bominaar, E. L.; Munck, E.; Collins, T. J., Chemical and spectroscopic evidence for an Fe^{V}-oxo complex. Science 2007, 315, (5813), 835-8.

Tyler, L. A.; Noveron, J. C.; Olmstead, M. M.; Mascharak, P. K., Modulation of the pK(a) of metal-bound water via oxidation of thiolato sulfur in model complexes of Co(III) containing nitrile hydratase: insight into possible effect of cysteine oxidation in Co-nitrile hydratase. Inorg Chem 2003, 42, (18), 5751-61.

van den Berg, T. A.; de Boer, J. W.; Browne, W. R.; Roelfes, G.; Feringa, B. L., Enhanced selectivity in non-heme iron catalysed oxidation of alkanes with peracids: evidence for involvement of Fe(IV)=O species. Chem Commun (Camb) 2004, (22), 2550-1.

Wada, A.; Ogo, S.; Nagatomo, S.; Kitagawa, T.; Watanabe, Y.; Jitsukawa, K.; Masuda, H., Reactivity of hydroperoxide bound to a mononuclear non-heme iron site. Inorg Chem 2002, 41, (4), 616-8.

Weinberg, M. V.; Jenney, F. E., Jr.; Cui, X.; Adams, M. W., Rubrerythrin from the hyperthermophilic archaeon Pyrococcus furiosus is a rubredoxin-dependent, iron-containing peroxidase. J Bacteriol 2004, 186, (23), 7888-95.

Yang, T. C.; McNaughton, R. L.; Clay, M. D.; Jenney, F. E., Jr.; Krishnan, R.; Kurtz, D. M., Jr.; Adams, M. W.; Johnson, M. K.; Hoffman, B. M., Comparing the electronic properties of the low-spin cyano-ferric [$Fe(N_4)(Cys)$] active sites of superoxide reductase and p450cam using ENDOR spectroscopy and DFT calculations. J Am Chem Soc 2006, 128, (51), 16566-78.

Yang, W.; Giandomenico, C. M.; Sartori, M.; Moore, D., Facile N-1 protection of cyclam, cyclen, and 1,4,7-triazacyclononane. Tetrahedron Letters 2003, 44, 2481-2483.

Yeh, A. P.; Hu, Y.; Jenney, F. E., Jr.; Adams, M. W.; Rees, D. C., Structures of the superoxide reductase from Pyrococcus furiosus in the oxidized and reduced states. Biochemistry 2000, 39, (10), 2499-508.

Zang, Y.; Que, L. J., Structure and Reactivity of Fe(II) SAr Complexes: Relevance to the Active Site of Isopenicillin N Synthase. Inorg Chem 1995, 34, 1030-1035.

Zhou, M.; Diwu, Z.; Panchuk-Voloshina, N.; Haugland, R. P., A stable nonfluorescent derivative of resorufin for the fluorometric determination of trace hydrogen peroxide: applications in detecting the activity of phagocyte NADPH oxidase and other oxidases. Anal Biochem 1997, 253, (2), 162-8.

Vita

Terutaka Terence Kitagawa was born on August 18, 1976 in Fremont, California. He performed undergraduate research for Professor Mahdi Abu-Omar from 1998-2000 and earned his Bachelor of Science degree in Chemistry from the University of California at Los Angeles in June 2000. He joined the laboratory of Professor Julie Kovacs at the University of Washington, Department of Chemistry in 2001 to study synthetic modeling of non-heme cysteinate-ligated metalloenzymes. In June 2007, he earned a Doctorate of Philosophy in Chemistry from the Department of Chemistry at the University of Washington. In addition to scientific pursuits, he is an avid enthusiast of cars, music, computers, and sports. He also enjoys spending time with his family and friends, and especially enjoys playing with his brother's Boston Terriers, Leroy and Rollie.